THE UNIVERSITY OF QUEENSLAND

AUSTRALIA

Forming Force Prediction and Process Investigation for Incremental Sheet Forming

Yanle Li

Bachelor of Engineering

A thesis submitted for the degree of Doctor of Philosophy at

The University of Queensland in 2015

School of Mechanical and Mining Engineering

Abstract

Incremental sheet forming (ISF) is a promising manufacturing process in which flat metal sheets are gradually formed into 3D shapes using a generic forming tool. Since the process features benefits of reduced forming forces, enhanced formability and greater process flexibility, it has a great potential to achieve economic payoff for rapid prototyping applications and for small quantity production in various applications. Although substantial research has been performed in the past decades on ISF, there is still a lack of an efficient prediction of forming force to facilitate the production design and optimization of the process. Also, unsatisfactory part quality obtained still hampers its wide use in industrial applications. Therefore, the work presented in this thesis is mainly focused on two aspects of ISF: efficient forming force prediction and process investigation and its improvement.

The first research aspect of this thesis has been focused on the development of an efficient force prediction model that includes the development of both finite element (FE) and analytical models. **(i) FE modelling.** Two types of FE models have been established using an explicit code LS-DYNA to investigate the deformation mechanism in ISF which is the basis for developing the force prediction model as well as further improving the forming process. First, FE models with shell elements for the groove forming process were set up and the strain behaviour and thickness distribution with different tools were evaluated and compared with experimental results. The strain behaviour of elements at different positions has been studied and the maximum strain has been found near the end of the groove corresponding to the failure location. The thickness distributions of the groove formed with different sized tools were predicted and it was found that the groove formed by the 20 mm tool is thinner than that formed by the 30 mm tool. Second, to further investigate different deformation modes and their evolution history in ISF, a FE model with fine solid elements for the cone-forming process has been established. The FE model was verified by experimental work with forming forces to allow a quantitative study of deformation behaviours of stretching, bending and shearing during the process. The evolution history of all the strain components along with the effective strain was presented. Moreover, the characteristic of each strain component and its contribution to the total effective plastic strain during the cone-forming process were investigated in detail. It was confirmed from FE simulations that the deformation mechanism in the ISF process is a combination of shearing, bending and stretching though the quantitative contributions in two directions are varied. **(ii) Force prediction modelling and its validation.** Based on the understanding of the deformation mechanism during the forming process, an efficient analytical model for tangential force prediction has been developed. Initially, deformation modes including shear, bending and stretching were analytically considered separately in the proposed sub-models.

A preliminary combined model has been constructed that can provide a prediction of tangential force with an average error less than 11 % with varying wall angle from 30˚ to 70˚. Subsequently, the force prediction model was further improved to balance the contribution of shear and bending on the total plastic deformation. The enhanced model was successfully validated through a comprehensive experimental campaign with two geometric shapes (truncated cone and pyramid) and various process parameters (step down, wall angle, tool radius and thickness). Finally, the analytical model was further extended to capture the changing of local curvature and wall angle during forming to deal with more complex shapes. The truncated ellipsoidal cup was selected as the target shape which has continuous local curvature and wall angle variations in each contour. It was verified that the extended model is able to provide a reasonably accurate variation of tangential force in each contour compared to experiments.

The second research aspect in this thesis is the process investigation and improvement of forming forces, geometric accuracy, forming efficiency and surface roughness. **(i) Forming forces.** Forming forces have been recorded for forming various shapes including straight groove, truncated cone, truncated pyramid and truncated ellipsoidal cup. The influences of different process parameters (i.e. wall angles, sheet thicknesses, step-down sizes, tool radius, tool-path types and sheet orientation) on forming forces were extensively studied. Particular attention has been paid to the relationship between converted tangential forces and forming parameters for the validation of the analytical model. The steady tangential forces at the second stage of the process demonstrate an increasing trend with the increase of step-down size and wall angle. However, tangential forces vary in a concave manner with the variation of tool diameter from 10 to 30 mm with a minimum occurring between 20-25mm. **(ii) Geometric accuracy.** The effects of various process parameters on geometric accuracy have been investigated by performing a Box-Behnken design of 27 tests that considers four factors at three levels. An empirical model has been developed with the most influential forming parameters and it was concluded that the geometric quality is largely determined by the quadratic effect of wall angle, the linear effect of sheet thickness and the interaction effect of thickness and step down. **(iii) Forming efficiency.** The effects of process parameters (step over (spiral tool path), feed rate, sheet thickness and tool diameter) on forming time have been studied through a Design of experiments (DOE) together with Taguchi method. Energy consumptions during the forming process were calculated based on measured forming forces. It was found that reducing sheet thickness, increasing step-down size with a limited range as well as decreasing the wall angle are effective approaches for energy saving. **(iv) Surface roughness.** The surface topography formed by both sliding and rolling tools were examined through SEM images which showed that a rolling contact condition causes less local damage and scratching of the surface.

Furthermore, an empirical model has been developed to predict the overall roughness of parts formed by ISF using the design of experiments (DOE) and it was found that sheet thickness has the most influential effect on overall surface roughness followed by the step down.

The work in this thesis explores various aspects of ISF research, although the most important contribution is efficient forming force prediction and its validation.

Declaration by author

This thesis is composed of my original work, and contains no material previously published or written by another person except where due reference has been made in the text. I have clearly stated the contribution by others to jointly-authored works that I have included in my thesis.

I have clearly stated the contribution of others to my thesis as a whole, including statistical assistance, survey design, data analysis, significant technical procedures, professional editorial advice, and any other original research work used or reported in my thesis. The content of my thesis is the result of work I have carried out since the commencement of my research higher degree candidature and does not include a substantial part of work that has been submitted to qualify for the award of any other degree or diploma in any university or other tertiary institution. I have clearly stated which parts of my thesis, if any, have been submitted to qualify for another award.

I acknowledge that an electronic copy of my thesis must be lodged with the University Library and, subject to the policy and procedures of The University of Queensland, the thesis be made available for research and study in accordance with the Copyright Act 1968 unless a period of embargo has been approved by the Dean of the Graduate School.

I acknowledge that copyright of all material contained in my thesis resides with the copyright holder(s) of that material. Where appropriate I have obtained copyright permission from the copyright holder to reproduce material in this thesis.

Publications during candidature

Published/submitted papers

1. **Li, Y.L.**, Liu, Z.B., Daniel, W. J. T. and Meehan, P. A. (2014). Simulation and experimental observations of effect of different contact interfaces on the incremental sheet forming process. Materials and Manufacturing Processes 29, 121-128.

2. **Li, Y.L.**, Liu, Z.B., Lu, H.B., Daniel, W. J. T. and Meehan, P. A. (2015). Deformation analysis in single point incremental forming through finite element simulation. To be submitted.

3. **Li, Y.L.**, Liu, Z.B., Lu, H.B., Daniel, W. J. T. and Meehan, P. A. (2014). Experimental study and efficient prediction on forming forces in incremental sheet forming. Advanced Materials Research 939, 313-321.

4. **Li, Y.L.**, Liu, Z.B., Lu, H.B., Daniel, W. J. T., Liu, S. and Meehan, P. A. (2014). Efficient force prediction for incremental sheet forming and experimental validation. The International Journal of Advanced Manufacturing Technology 73 (1-4):571-587.

5. **Li, Y.L.**, Liu, Z.B., Lu, H.B., Daniel, W. J. T. and Meehan, P. A. (2015). Deformation mechanics and efficient force prediction in incremental sheet forming process. Journal of Materials Processing Technology 221, 100-111.

6. Liu, Z.B., **Li, Y.L.** and Meehan, P. A. (2013). Experimental investigation of mechanical properties, formability and force measurement for AA7075-O aluminum alloy sheets formed by incremental forming. International Journal of Precision Engineering and Manufacturing 14, 1891-1899.

7. **Li, Y.L.**, Lu, H.B., Daniel, W. J. T. and Meehan, P. A. (2015) Investigation and optimization of energy consumption and geometric accuracy in the incremental sheet forming process using response surface methodology. The International Journal of Advanced Manufacturing Technology. DOI: 10.1007/s00170-015-6986-5.

8. Lu, H.B., **Li, Y.L.**, Liu, Z.B., Liu, S. and Meehan, P. A. (2014). Study on Step Depth for Part Accuracy Improvement in Incremental Sheet Forming Process. Advanced Materials Research 939, 274-280.

9. Liu, Z.B., **Li, Y.L.**, Daniel, W. J. T. and Meehan, P. A. (2013). Taguchi Optimization of Process Parameters for Forming Time in Incremental Sheet Forming Process. Materials Science Forum 773-774,137-143.

10. Liu, Z.B., Liu, S., **Li, Y.L.** and Meehan, P. A. (2014). Modeling and Optimization of Surface Roughness in Incremental Sheet Forming using a Multi-objective Function. Materials and Manufacturing Processes 29, 808-818.

11. Liu, Z.B., **Li, Y.L.** and Meehan, P. A. (2013). Vertical Wall Formation and Material Flow Control for Incremental Sheet Forming by Revisiting Multistage Deformation Path Strategies. Materials and Manufacturing Processes 28, 562-571.

12. Liu, Z.B., **Li, Y.L.,** Daniel, W. J. T. and Meehan, P. A. (2014). An Analytical Model for Deformation Path Design in Multistage Incremental Sheet Forming Process. Advanced Materials Research 939, 245-252.

13. Liu, Z.B., Daniel, W. J. T., **Li, Y.L.**, Liu, S. and Meehan, P. A. (2014). Multi-pass deformation design for incremental sheet forming: Analytical modeling, finite element analysis and experimental validation. Journal of Materials Processing Technology 214, 620-634.

14. Liu, Z.B., **Li, Y.L.** and Meehan, P. A. (2014). Tool path strategies and deformation analysis in multi-pass incremental sheet forming process. The International Journal of Advanced Manufacturing Technology 75, 395-409.

15. Lu, H.B., Kearney, M., **Li, Y.L.**, Liu, S., Daniel, W. J. T. and Meehan, P. A. (2015). Model predictive control of incremental sheet forming for geometric accuracy improvement. The International Journal of Advanced Manufacturing Technology. Submitted.

16. Daniel, W. J. T., Liu, Z.B., **Li, Y.L.** and Lu, H.B. (2015). Analytical prediction of membrane strains and thinning in incremental forming. Journal of Materials Processing Technology. Submitted.

Conference presentations

1. Li, Y. Simulation and Experimental Observations of Effect of Different Contact Interfaces on the Incremental Sheet Forming Process. The 15th International conference on Advances in Materials & Processing Technologies. Wollongong, NSW, Australia. 23-26 Sep. 2012.

2. Li, Y. Experimental Study and Efficient Prediction on Forming Forces in Incremental Sheet Forming. The 16th International conference on Advances in Materials & Processing Technologies. Taipei, Taiwan. 22-26 Sep. 2013.

3. Li, Y. Investigation on the Effect of Different Contact Interfaces on ISF Process. 2013 Engineering Postgraduate Conference. The University of Queensland. Brisbane, Australia. 3rd June, 2013.

4. Li, Y. Deformation Analysis in Single Point Incremental Forming through Finite Element Simulation. 11th Asia-Pacific Conference on Materials Processing. Auckland, New Zealand. 6-11 July 2014.

Publications included in this thesis

The following publications have been incorporated as Chapter 4.

1. **Li, Y.L.**, Liu, Z.B., Daniel, W. J. T. and Meehan, P. A. (2014). Simulation and experimental observations of effect of different contact interfaces on the incremental sheet forming process. Materials and Manufacturing Processes 29, 121-128.

Contributor	Statement of contribution
Author Y.L. Li (Candidate)	Conception and design (80%) Data analysis and interpretation (70%) Wrote and edited the paper (70%)
Author Z.B. Liu	Conception and design (15%) Data analysis and interpretation (10%)
Author W.J.T. Daniel	Data analysis and interpretation (10%) Wrote and edited the paper (10%)
Author P.A. Meehan	Conception and design (5%) Data analysis and interpretation (10%) Wrote and edited the paper (20%)

2. **Li, Y.L.**, Liu, Z.B., Lu, H.B., Daniel, W. J. T. and Meehan, P. A. (2015). Deformation analysis in single point incremental forming through finite element simulation. To be submitted.

Contributor	Statement of contribution
Author Y.L. Li (Candidate)	Conception and design (70%) Data analysis and interpretation (70%) Wrote and edited the paper (80%)
Author Z.B. Liu	Conception and design (10%) Data analysis and interpretation (5%)
Author H.B. Lu	Data analysis and interpretation (5%) Wrote and edited the paper (5%)
Author W.J.T. Daniel	Conception and design (10%) Data analysis and interpretation (10%) Wrote and edited the paper (5%)

Author P.A. Meehan	Conception and design (10%) Data analysis and interpretation (10%) Wrote and edited the paper (10%)

3. **Li, Y.L.**, Liu, Z.B., Lu, H.B., Daniel, W. J. T. and Meehan, P. A. (2014). Experimental study and efficient prediction on forming forces in incremental sheet forming. Advanced Materials Research 939, 313-321.

Contributor	Statement of contribution
Author Y.L. Li (Candidate)	Conception and design (70%) Data analysis and interpretation (70%) Wrote and edited the paper (80%)
Author Z.B. Liu	Conception and design (10%) Data analysis and interpretation (5%)
Author H.B. Lu	Data analysis and interpretation (5%) Wrote and edited the paper (5%)
Author W.J.T. Daniel	Conception and design (10%) Data analysis and interpretation (10%) Wrote and edited the paper (5%)
Author P.A. Meehan	Conception and design (10%) Data analysis and interpretation (10%) Wrote and edited the paper (10%)

4. **Li, Y.L.**, Liu, Z.B., Lu, H.B., Daniel, W. J. T., Liu, S. and Meehan, P. A. (2014). Efficient force prediction for incremental sheet forming and experimental validation. The International Journal of Advanced Manufacturing Technology 73 (1-4):571-587.

Contributor	Statement of contribution
Author Y.L. Li (Candidate)	Conception and design (70%) Data analysis and interpretation (70%) Wrote and edited the paper (70%)
Author Z.B. Liu	Conception and design (10%) Data analysis and interpretation (5%)
Author H.B. Lu	Data analysis and interpretation (5%) Wrote and edited the paper (5%)

Author W.J.T. Daniel	Conception and design (10%) Data analysis and interpretation (10%) Wrote and edited the paper (5%)
Author S. Liu	Data analysis and interpretation (5%) Wrote and edited the paper (10%)
Author P.A. Meehan	Conception and design (10%) Data analysis and interpretation (5%) Wrote and edited the paper (10%)

5. **Li, Y.L.**, Liu, Z.B., Lu, H.B., Daniel, W. J. T. and Meehan, P. A. (2015). Deformation mechanics and efficient force prediction in incremental sheet forming process. Journal of Materials Processing Technology 221, 100-111.

Contributor	Statement of contribution
Author Y.L. Li (Candidate)	Conception and design (70%) Data analysis and interpretation (70%) Wrote and edited the paper (80%)
Author Z.B. Liu	Conception and design (10%) Data analysis and interpretation (5%)
Author H.B. Lu	Data analysis and interpretation (5%) Wrote and edited the paper (5%)
Author W.J.T. Daniel	Conception and design (10%) Data analysis and interpretation (10%) Wrote and edited the paper (5%)
Author P.A. Meehan	Conception and design (10%) Data analysis and interpretation (10%) Wrote and edited the paper (10%)

6. Liu, Z.B., **Li, Y.L.** and Meehan, P. A. (2013). Experimental investigation of mechanical properties, formability and force measurement for AA7075-O aluminum alloy sheets formed by incremental forming. International Journal of Precision Engineering and Manufacturing 14, 1891-1899.

Contributor	Statement of contribution
Author Z.B. Liu	Conception and design (70%)

	Data analysis and interpretation (50%) Wrote and edited the paper (80%)
Author Y.L. Li (Candidate)	Conception and design (30%) Data analysis and interpretation (40%) Wrote and edited the paper (10%)
Author P.A. Meehan	Data analysis and interpretation (10%) Wrote and edited the paper (10%)

7. **Li, Y.L.**, Lu, H.B., Daniel, W. J. T. and Meehan, P. A. (2015) Investigation and optimization of energy consumption and geometric accuracy in the incremental sheet forming process using response surface methodology. The International Journal of Advanced Manufacturing Technology. DOI: 10.1007/s00170-015-6986-5.

Contributor	Statement of contribution
Author Y.L. Li (Candidate)	Conception and design (70%) Data analysis and interpretation (70%) Wrote and edited the paper (75%)
Author H.B. Lu	Conception and design (10%) Data analysis and interpretation (10%) Wrote and edited the paper (5%)
Author W.J.T. Daniel	Conception and design (10%) Data analysis and interpretation (10%) Wrote and edited the paper (5%)
Author P.A. Meehan	Conception and design (10%) Data analysis and interpretation (10%) Wrote and edited the paper (15%)

8. Lu, H.B., **Li, Y.L.**, Liu, Z.B., Liu, S. and Meehan, P. A. (2014). Study on Step Depth for Part Accuracy Improvement in Incremental Sheet Forming Process. Advanced Materials Research 939, 274-280.

Contributor	Statement of contribution
Author H.B. Lu	Conception and design (60%) Data analysis and interpretation (60%) Wrote and edited the paper (60%)

Author Y.L. Li (Candidate)	Conception and design (20%) Data analysis and interpretation (20%) Wrote and edited the paper (5%)
Author Z.B. Liu	Conception and design (10%) Data analysis and interpretation (5%) Wrote and edited the paper (5%)
Author S. Liu	Data analysis and interpretation (10%) Wrote and edited the paper (10%)
Author P.A. Meehan	Conception and design (10%) Data analysis and interpretation (5%) Wrote and edited the paper (20%)

9. Liu, Z.B., **Li, Y.L.**, Daniel, W. J. T. and Meehan, P. A. (2013). Taguchi Optimization of Process Parameters for Forming Time in Incremental Sheet Forming Process. Materials Science Forum 773-774,137-143.

Contributor	Statement of contribution
Author Z.B. Liu	Conception and design (70%) Data analysis and interpretation (70%) Wrote and edited the paper (70%)
Author Y.L. Li (Candidate)	Conception and design (20%) Data analysis and interpretation (20%) Wrote and edited the paper (5%)
Author W.J.T. Daniel	Data analysis and interpretation (10%) Wrote and edited the paper (5%)
Author P.A. Meehan	Conception and design (10%) Wrote and edited the paper (20%)

10. Liu, Z.B., Liu, S., **Li, Y.L.** and Meehan, P. A. (2014). Modeling and Optimization of Surface Roughness in Incremental Sheet Forming using a Multi-objective Function. Materials and Manufacturing Processes 29, 808-818.

Contributor	Statement of contribution
Author Z.B. Liu	Conception and design (70%) Data analysis and interpretation (70%)

	Wrote and edited the paper (70%)
Author S. Liu	Conception and design (10%) Data analysis and interpretation (20%) Wrote and edited the paper (10%)
Author Y.L. Li (Candidate)	Conception and design (10%) Data analysis and interpretation (10%) Wrote and edited the paper (10%)
Author P.A. Meehan	Conception and design (10%) Wrote and edited the paper (10%)

Contributions by others to the thesis

My principal supervisor Paul Meehan provided extensive assistance with drafting and revision of this thesis so as to contribute to the interpretation. Dr. Bill Daniel has also provided useful comments regarding the development of the analytical model.

Statement of parts of the thesis submitted to qualify for the award of another degree

None.

Acknowledgements

I would like to express my deepest appreciation to my principal supervisor A/Prof Paul Meehan, who led me into this interesting field of research and provide excellent guidance during the course of my candidature. Greatest gratitude is also for my co-supervisor Dr. Bill Daniel, who has spent his entire professional life educating and imparting knowledge to students. Your enlightening guidance and suggestions, especially those regarding the analytical modelling issues are greatly appreciated.

Sincere gratitude is also extended to my milestone review committee members: Dr. Bo Feng, Dr. Zhiqiang Guan, Dr. Michael Bermingham and Dr. Suresh Palanisamy for their valuable comments throughout my PhD study.

I would also like to thank Michael Elford, Geoff Weakley, Sara Eastwood, Gui Wang and Matthew Dargusch for their technical support.

Sincere thank is also given to Dr. Paul Bellette who could always inspire me with useful ideas at the early stage of my research.

I also thank those excellent technical officers: Peter Bleakley, Joy Wang, Doug Malcolm and Graham Ruhle for their assistant for developing the force measurement system.

Special thanks are given to Dr. Zhaobing Liu, Dr. Sheng Liu and Haibo Lu for their extensive discussions and assistance in experimental testing.

The scholarship received from the Chinese Scholarship Council (CSC) and The University of Queensland International Scholarship (UQI) are gratefully acknowledged. I also appreciate the support received from University of Queensland Graduate School International Travel Award (GSITA) for conducting the fruitful research travel in China. I would also like to acknowledge the financial support for the project from the Australian Research Council (ARC), Boeing Research & Technology – Australia (BRTA) and QMI Solutions.

Finally, I greatly acknowledge in particular my parents and families for their continual support, understanding and love over the years. The support and friendship from all my friends are also extremely grateful.

Keywords

Incremental sheet forming, finite element modelling, deformation mechanism, forming force, force prediction, analytical prediction, plastic strain, geometric accuracy, formability, surface roughness

Australian and New Zealand Standard Research Classifications (ANZSRC)

ANZSRC code: 091307, Numerical Modelling and Mechanical Characterisation, 40%
ANZSRC code: 091006, Manufacturing Processes and Technologies, 50%
ANZSRC code: 091399, Mechanical Engineering not elsewhere classified, 10%

Fields of Research (FoR) Classification

FoR code: 0913, Mechanical Engineering, 60%
FoR code: 0910, Manufacturing Engineering, 40%

Table of Contents

List of Figures

List of Tables

List of Abbreviations used in the thesis

2D	Two dimensional
3D	Three dimensional
ADSIF	Accumulative double sided incremental forming
ANOM	Analysis of means
ANOVA	Analysis of variance
CAD	Computer-aided design
CAE	Computer-aided engineering
CAM	Computer-aided manufacturing
CNC	Computer numerically controlled
DOE	Design of experiments
DSIF	Double sided incremental forming
FE	Finite element
FEM	Finite element method
FFLDs	Fracture forming limit diagrams
FLC	Forming limit curve
FLDs	Forming limit diagrams
ISF	Incremental sheet forming
MDF	Medium density fiberboard
MK	Marciniak-Kuczynski
RD	Rolling direction
RSM	Response surface methodology
SEM	Scanning electron microscope
S/N	Signal-to-noise
SPF	Super plastic forming
SPIF	Single point incremental forming
TD	Transverse direction
TPIF	Two point incremental forming
TTS	Through thickness shear

Chapter 1 Introduction

The work presented in this thesis is focused on the development of incremental sheet forming (ISF) technology, mainly including two aspects: mechanics-based forming force prediction and process investigation. The benefit of this research will facilitate the manufacture of complex sheet parts, such as aircraft fairings, vehicle panels and fan blades. This chapter summarises the material presented in the incorporated papers, which form the basis of this PhD thesis. A general introduction with both advantages and limits of current ISF research is provided, followed by the objectives of this thesis.

1.1 Background and Motivation

Sheet metal forming involves a wide range of processes that manufacture parts for a variety of purposes for our modern life. Normally, sheet metal manufacture is mostly performed on a press with two dies. These conventional methods are usually economical and suitable for mass production because the cost of dies and punches can be shared with a large number of products. Nevertheless, the die storage is a problem, such as in the car manufacturing industry, because the parts are large and the product life cycle is relatively long. This leads to long storage times and costs. Recently, with the social and industrial growth, the mass production era has transformed into a quality production era, which largely depends on the small batch production as well as the prototyping of customized design. To compensate cost, time and production, new production methods have been developed. In particular, incremental sheet forming (ISF) which uses a simple tool to form an infinite variety of 3D shapes has gained great attention. In the last two decades, ISF has received increasing interest from both academia and industry due to its reduced forming forces, enhanced formability and greater process flexibility. A brief introduction along with both the advantages and limitations of ISF will be discussed in the following section.

1.2 Incremental Sheet Forming Technology

Incremental Sheet Forming (ISF) technology is an emerging sheet forming process ideal for rapid prototype and small batch production. In an ISF process, a flat metal sheet is gradually formed into the designed 3D shape using Computer Numerical Control (CNC)-controlled generic forming tool. The process is characterized by the fact that at any time only a small part of the product is actually being formed and that area of local deformation is moving over the entire product until the desired geometry is obtained. By using this process, useable parts can be formed directly from CAD data

with a minimum of specialized tooling. Therefore ISF is widely accepted as a promising forming process over conventional processes such as deep drawing and stamping [1, 2] for small batch production and custom manufactured products.

ISF was patented in 1967 by Leszak [3] and was proven to be feasible by Kitazawa et al. [4] in forming rotational symmetric parts using aluminium. The capability study of using an ordinary CNC milling machine instead of a special designed machine-tool apparatus was later performed by Jeswiet [5] and Filice [6]. ISF can be interpreted in different ways as shown in Fig. 1. In general, the forming tool follows the pre-designed tool path to deform the material incrementally along a succession of contours until the desired final shape is obtained.

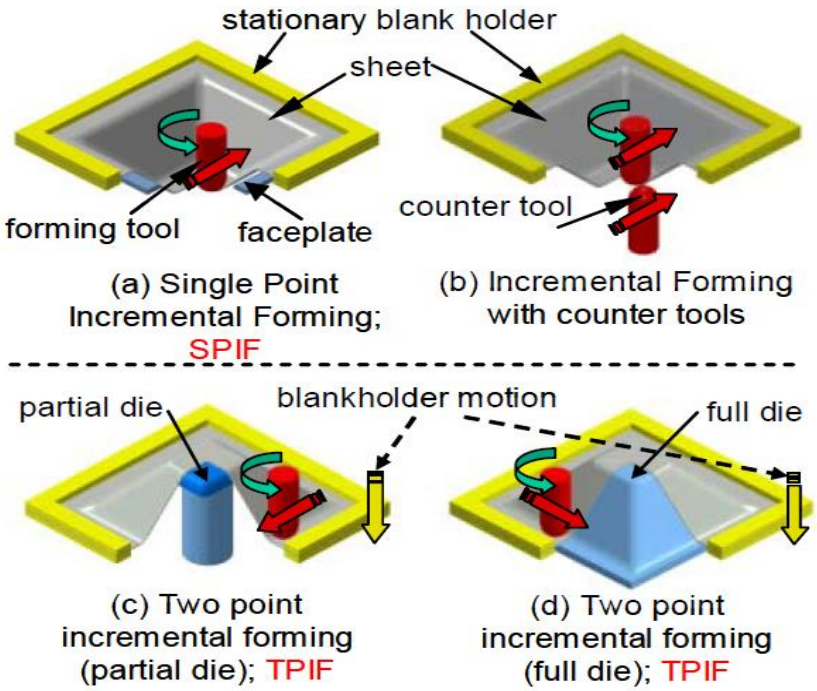

Fig. 1 Four different configurations of ISF process [1].

The configuration shown in Fig. 1(a) belongs to single point incremental forming (SPIF), in which no particular die is needed. The sheet is deformed by the moving tool which is controlled by numerical codes previously designed and imported to the controller. The second one (Fig. 1(b)) shows an incremental forming with two tools on both sides of the material. This was also referred as double sided incremental forming (DSIF) [7]. Since there is no die needed in these two configurations, it is also called a dieless forming process [1, 8]. The other two configurations (Fig. 1(c) and (d)) are classified as two point incremental forming (TPIF) where a partial or full die is placed underneath the material. This is commonly used for complex parts to improve the geometric tolerances with no substantial extra cost as dies can be cheaply manufactured with woods or plastics due to low amplitude forming forces [9]. Recently, to further improve the formability and product quality, assisted forming strategies for ISF has been proposed. In particular, Duflou et al. [10] have

developed a laser-assisted incremental forming process by adding a dynamic heating system. Frictional stir- [11] and electric-assisted [12, 13] incremental forming were also investigated by researchers which were suggested to improve the formability of the process.

The ISF process offers the rapid prototyping advantages of short lead times, high flexibility, high formability and lower cost in small batches for aeronautical, automotive and medical applications. Unlike other fast prototyping technologies which are suited to produce dimensionally accurate but non-functional replicas of parts, ISF can be used to produce functional metal parts suitable for use as prototypes, or even as regular production and service parts. ISF has received great attention particularly in the automotive industry. Fig. 2(a) shows a hood for Honda S800 model car formed with ISF by Amino Corp. and was finally mounted on an existing vehicle. ISF can also be used for additional forming of an existing production panel for low volume production. This allows adding features or styles and sharpening the feature lines for the existing manufactured parts. An example is shown in Fig. 2(b) with logo mark and feature lines formed by ISF. Moreover, ISF is especially favourable to customised products by saving the cost of die fabrication. Fig. 2(c) and (d) present a customised ankle support and a Buddha face formed using ISF technology. Currently, there is an increasing demand to use incremental forming for the frame parts with thick materials as well as thin panels. This is demonstrated by Fig. 2(e) with the successful forming of 4.5 mm thickness material of hot rolled steel.

(a) (b)

(c) (d) (e)

Fig. 2 Applications of ISF: (a) Inner side of a hood for Honda S800 model car [8]; (b) Normal feature lines of TOYOTA iQ compared with sharpen feature line of TOYOTA iQ-GRMN [8]; (c) Customised ankle support [14]; (d) Customised Buddha face (AMINO website); (e) Sample with 4.5 mm thickness material of hot rolled steel [8]

1.2.2 Advantages of ISF

The ISF technology has received increasing attention from both academia and industry due to the following advantages:

- Lower forming forces

  Since only a small area of the part is being deformed at any time during ISF, the required forming forces are greatly reduced. Therefore, it is possible to use material such as plastics or wood for supporting die. Also, this further enhances the forming capacity in terms of both sheet thickness (e.g. 0.1 to 4.0 mm) and also material type (mild steels, aluminium, titanium and even perforated steel mesh). Although forming forces are relatively low, their changing trend was suggested by many researchers [15, 16] as a promising indicator to detect and prevent material fracture and also useful information for on-line control implementation [17, 18]. Therefore, an efficient force prediction model is required for further development of ISF technology.

- Improved formability

  Greater formability is achieved in ISF by incrementally deforming the material to the desired shape. As can be seen in Fig. 3(a), extensive experimental measurements have shown that the forming limit curve for ISF has a negative slope and is much higher than conventional forming. Fig. 3(b) presents a cone shaped flower pot formed using ISF technology. The height of the flower pot is 220 mm and the diameter of leader is only 6 mm. Generally, it is impossible to draw such a shape with conventional stamping as the stretching happens locally at the lead which will result in failure.

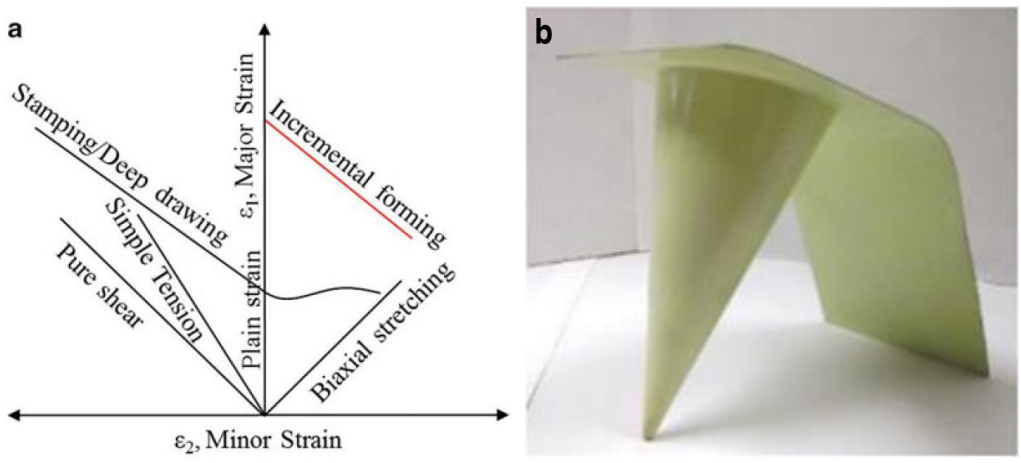

Fig. 3 Improved formability in ISF: (a) Forming limit curve for ISF against conventional forming processes [19] and (b) Flower pot [8]

- Lower die tooling cost

  Depending on the shape of the part, it may be possible to use a partial die or even eliminate the die in ISF. Fig. 4 shows the six different shapes (Cone, Square, Pentagonal, Hexagonal, Octagonal, Dodecagonal) formed by AMINO Corporation [8] using a single blank. The forming die used for these shapes is very simple and only consists of one base plate and six cylindrical posts. The dies can be cheaply made with wood or plastics. For final products with a constant wall angle, it is possible to form these without dies. Moreover, in ISF, a generic forming tool can manufacture an infinite variety of 3D shapes by adopting careful tool path design. These forming tools are also quite simple with different head shapes as shown in Fig. 5. Consequently, the die tooling cost is greatly reduced.

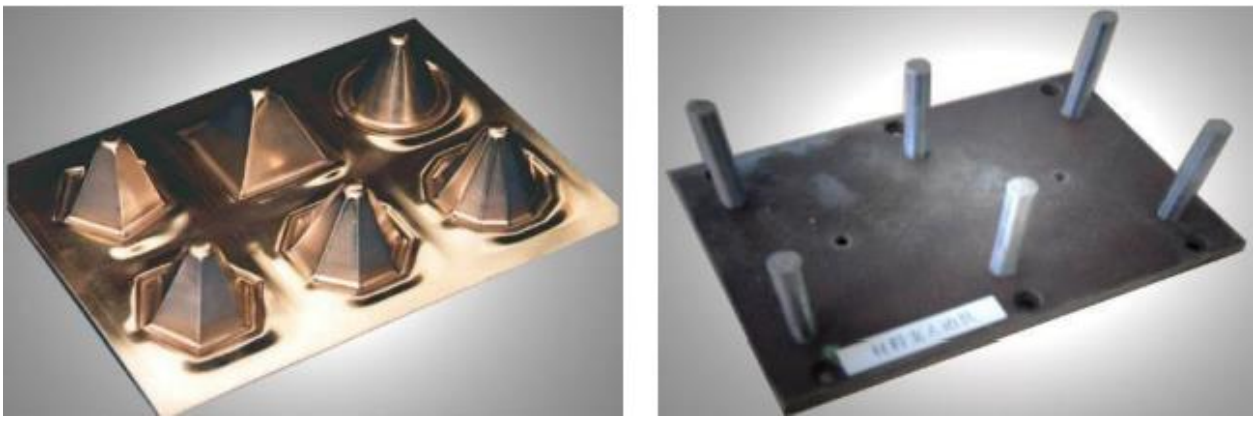

Fig. 4 Variety of pyramid shapes [8]

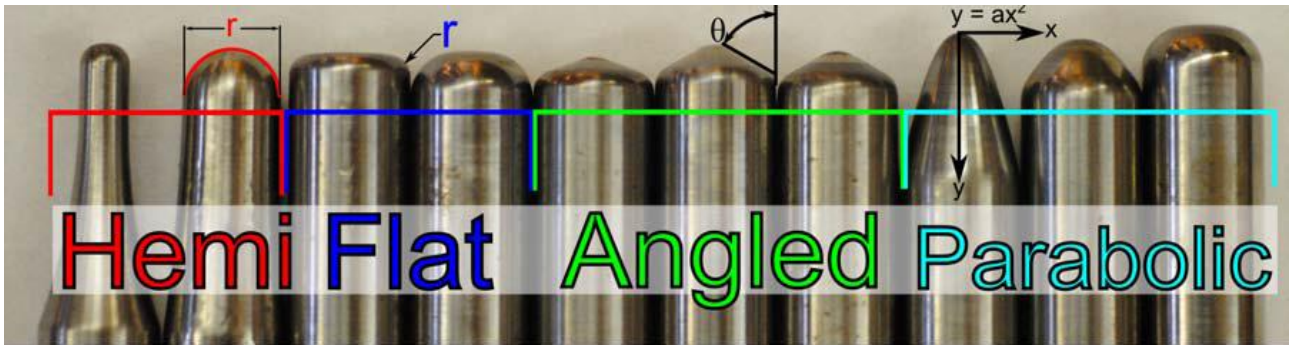

Fig. 5 Variation of forming tool shapes: Hemispherical, Flat, Angled and Parabolic [20]

- Flexible forming facilities

  Generally, the ISF process can be performed by all CNC-controlled three-axis machines, though large working volumes and sufficient stiffness are favourable. Fig. 6 presents some of the commonly used forming machinery for ISF. At the early stage of ISF research, conventional milling machines as shown in Fig. 6(a) were upgraded by adding a material fixture table. Since 2002, AMINO Corporation started to provide specialized equipment dedicated for ISF to industry globally as shown in Fig. 6(b). This equipment features a

pneumatic controlled movable work holder (yellow table in Fig. 6(b)) which can pre-stretch the material towards the final shape during the forming process. An industrial robot can also be used for the ISF process as shown in Fig. 6(c). Some researchers even developed their own ISF machine. Fig. 6(d) shows a prototype fabricated at Northwestern University which focuses on the double sided incremental forming process.

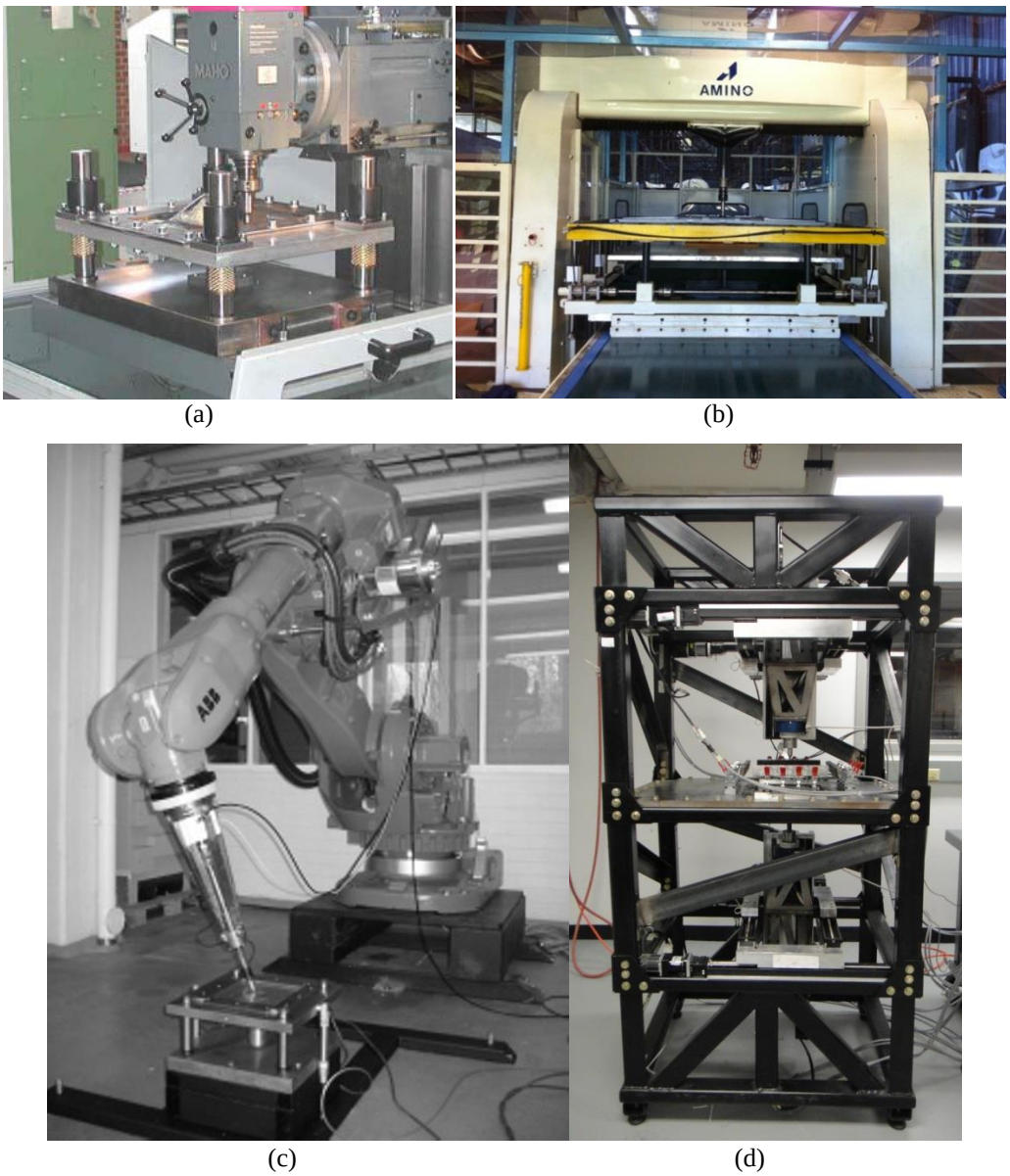

(a) (b)

(c) (d)

Fig. 6 Forming machinery for ISF: (a) Upgraded conventional milling machine for ISF [1]; (b) Dedicated AMINO ISF machine [21]; (c) Robot assisted incremental forming [22]; (d) A prototype double sided incremental forming machine fabricated at Northwestern University [23]

The above advantages have made ISF a strong potential competitor to conventional sheet forming processes. However, there are still some limitations in ISF that inhibit extensive industrial applications, which will be discussed in the following section.

1.2.3 Limitations of ISF

The limitations of ISF are listed and discussed as follows:

- Geometric accuracy: This is one of the dominant limits for the further development and commercialization of the ISF technology. Geometric errors in ISF can be attributed to clamped deviation during forming and unclamped deviation due to residual stresses as well as springback effects.

- Surface finish: This is considered a weak point for ISF products. Surface finish is represented by the large-scale waviness created by the tool path and the small-scale roughness induced by large surface strains. The surface quality is influenced by several process parameters, such as step-down size, tool diameter, sheet thickness, etc.

- Process efficiency: Due to the inherent incremental localized deformation feature, the forming time required to complete the forming process is relatively longer than other processes. Nevertheless, the energy consumption which is influenced by both forming time and working load may be attractive by proper process settings.

- Excessive thinning: The final thickness after deformation is an important indicator to evaluate the product quality, especially with larger wall angles (e.g. 70˚ or more). Excessive thinning narrows the range of geometries that can be produced by ISF.

The above limitations bring some challenges for the further development and commercialisation of ISF, but also motivate the on-going research to promote ISF as a feasible technology on an industrial level. This leads to the determination of the research scope and objectives for this thesis which will be presented next.

1.3 Scope and Objectives of this Thesis

Considering the above limitations, this thesis will focus on two aspects in ISF: efficient forming force prediction based on deformation mechanics and process investigation and its improvement. The specific objectives are proposed as follows:

1. Efficient forming force prediction

   1.1 FE modelling to determine the main deformation mechanism in ISF

To develop FE models to investigate the material deformation behaviour under different forming conditions and clarify the role of stretching, bending and shearing deformation modes in ISF and their contributions to forming forces.

1.2 Analytical modelling for force prediction

a. To develop the efficient mechanics-based models for force prediction in ISF.

b. To validate the proposed efficient force prediction model with comprehensive experimental tests and extend it for more general shapes.

2. Process investigation and its improvement

2.1 To investigate the effects of process parameters (step-down size, wall angle, sheet thickness and tool radius) on forming forces and their evolution trends in ISF.

2.2 To investigate the effects of process parameters on geometric accuracy, forming efficiency (forming time and deformation energy) and surface roughness in ISF and determine their optimal forming settings by performing quantitative design of experiments.

1.4 Thesis Outline

To achieve the specified aims, this thesis is divided into the following chapters:

Chapter 1 briefly introduces the research background, characteristics of ISF and summaries the specific objectives of the research.

Chapter 2 provides a thorough review of the literature of current research activities related to ISF. This includes the knowledge of deformation mechanism, modelling techniques, forming force prediction and also the improvement of product quality. The deficiencies and limitations of these theories/methods are also discussed and the limitations in the literature are then identified which motivate this PhD project.

Chapter 3 generally describes both modelling and experimental methods that have been used to achieve the objectives raised throughout the PhD project.

Chapter 4 presents the research outcomes in the form of a series of publications, which were all completed during the candidature, either as the first author or a co-author, and provide readers with an account for how the research progressed and how the findings of each paper contributes to the

development of the ISF technology. Two papers are incorporated to illustrate the results for deformation mechanism analysis (Obj.1.1). Three papers are grouped to represent the outcomes for forming force study and prediction (Obj.1.2). The remaining papers are appended to demonstrate the research results on investigation into the effects of process parameters on geometric accuracy, forming efficiency and surface finish for ISF (Obj.2).

Chapter 5 summarizes the contributions of this PhD research to the understanding of the deformation mechanism, prediction of forming forces and improvement of product quality for the ISF technology. Potentially fruitful topics for future research are also suggested in this chapter.

Chapter 2 Literature Review

This chapter presents a detailed literature review of the current research relating to forming force prediction and process investigations. The first section provides a review of the fundamental deformation mechanism and formability in ISF. Subsequently, the modelling methods for ISF are reviewed and categorized into two approaches: analytical modelling and finite element modelling. Special interest is given to a critical review regarding the forming forces analysis and prediction during the process. Finally, previous publications related to geometric accuracy, surface finish, and forming efficiency in ISF are reviewed. This leads to a statement of the contributions of this thesis to the ISF technology on both theoretical modelling and experimental investigation.

2.1 Deformation Mechanism and Process Formability

This section firstly presents a comprehensive review of the current status on the understanding of the deformation mechanism in the ISF process. Then, the strategies to characterise the process formability are reviewed along with the current findings on the effects of process parameters on the ISF process.

2.1.1 Deformation mechanism

It has been widely acknowledged that ISF has higher formability compared with other conventional forming processes (such as deep drawing and forging) [24, 25] due to its highly localised plastic deformation. The understanding of the fundamental material deformation and fracture mechanism is of great importance for ISF process design and optimisation in achieving enhanced material formability, geometric accuracy and uniform thickness distribution. In recent years, the deformation mechanics behind ISF has been investigated by many researchers through both theoretical analysis [26, 27] and experimental observations [28, 29], but there still remains a lack of a consistent view on how different process parameters affect the deformation behaviour and thus influence the output qualities. This section provides a comprehensive review of the current status on the understanding of the deformation mechanism in the ISF process.

2.1.1.1 Membrane strain

Several researchers proposed that the dominant deformation mode in ISF process is stretching leading to membrane strain. Silva et al. [26, 27, 30] extensively analysed the single point incremental forming by means of a membrane approach. A closed-form analytical model was firstly

presented which provides insight to the fundamentals behind the fracture of material and the enhanced overall formability of the ISF process. As a result in [26], the membrane analysis of a small plastic zone in rotationally symmetric components was utilized to explain aspects of the formability and damage.

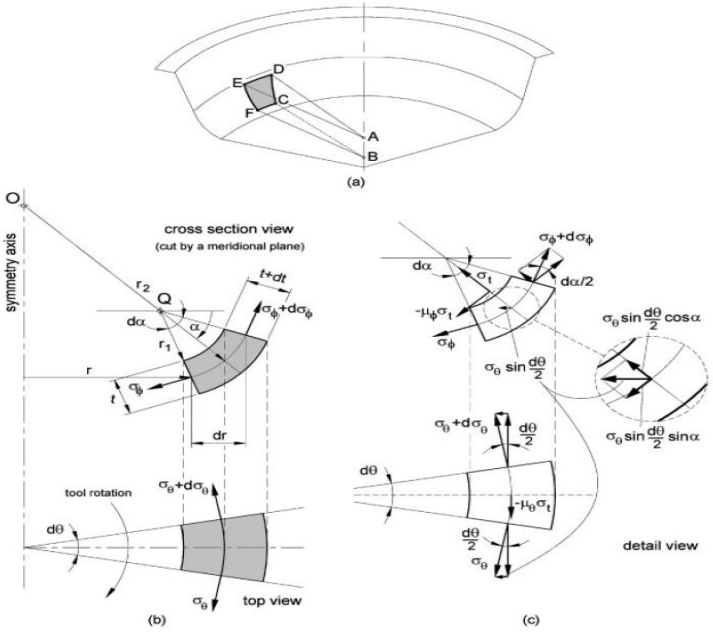

Fig. 7 Rotational symmetric single point incremental forming: (a) schematic representation of the shell element in perspective; (b) top view of the shell element after being cut by an axial meridional plane; (c) detail of the acting stresses [26]

Fig. 7 shows the membrane equilibrium conditions of a local shell element analysed by Silva et al. [30]. To simplify the analysis, bending moments of plastically deforming shells were neglected, and the local cells were assumed to be axisymmetric. Meanwhile, the material was assumed to be rigid-perfectly plastic and isotropic. In this model, the coefficient of friction was defined as $\mu = \sqrt{\mu_{\emptyset}^2 + \mu_{\theta}^2}$, where $\mu_{\emptyset}$ is the meridional component due to the step down movement of the tool, and μ_{θ} is the circumferential feed combined with the rotation of the tool. The equilibrium conditions in three components were analysed according to the schematic represented in Fig. 7. After neglecting higher order terms, the simplified forms of these equations can be deduced as follows:

Circumferential direction

$$d\delta_{\theta} = -\mu_{\theta}\delta_t \frac{rd_{\theta}}{t} \approx -\mu_{\theta}\delta_t \tag{2.1}$$

Thickness direction

$$\frac{\delta_t}{t} + \frac{\delta_{\emptyset}}{r_1} + \frac{\delta_{\theta}}{r_z} = 0 \tag{2.2}$$

Meridional direction

$$\frac{d\delta_{\emptyset}}{dr} + \frac{\delta_{\emptyset} - \delta_{\theta}}{r} + \frac{\mu_{\emptyset}\delta_t}{t\sin\alpha} + \frac{\delta_{\emptyset}}{t}\frac{dt}{dr} = 0 \quad (2.3)$$

where δ_θ , $\delta_\emptyset$ δ_t are the circumferential, meridional and thickness stresses respectively; t is the thickness of the sheet, r is the radial coordinate, r_1 is the radius of curvature of meridian at the element (radius of the SPIF tool), r_z is the radius of the element normal where it cuts the z-axis.

In this model, all possible tool paths were classified into three basic modes of deformation shown in Fig. 8; (a) Flat surfaces under plane strain stretching conditions; (b) Rotationally symmetric surfaces under plane strain stretching conditions; (c) Corners under equal biaxial stretching conditions. Under the geometrical condition of $r_2 = r_1$(see Fig. 7 for definition of these variables), the deformation mode is considered as case (c) of equal biaxial symmetric. While if increase the r_2 until $r_2 \gg r_1$ and $r_2 \gg t$, the deformation mode can be considered as case (b) of plane strain stretching condition. For these three conditions, the states of stress and strain were summarized and compared with those of conventional stamping in Table 1. According to this analysis, the frictional force exerted at the tool-sheet contact interface can be deduced [30] (see equations (22), (26) and (30)). Further, this model also investigated the sheet thinning at the corner radius and the maximum drawing angle which characterized formability of the process.

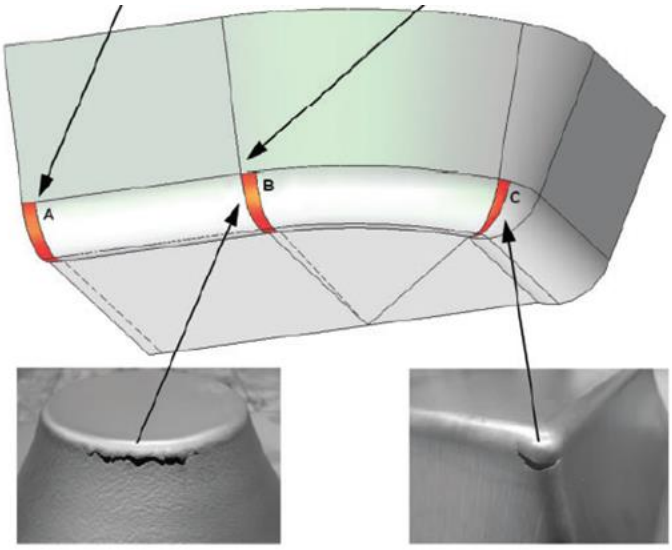

Fig. 8 Instantaneous deformation zone and contact area between forming tool and workpiece during SPIF [30].

Table 1. States of stress and strain that are commonly found in general SPIF processes and conventional stamping [30].

	Assumption	State of strain	State of stress	Hydrostatic stress
SPIF (flat and rotational symmetric surfaces)	Plane strain conditions	$d\varepsilon_\phi = -d\varepsilon_t > 0$ $d\varepsilon_\theta = 0$ $d\varepsilon_t < 0$	$\sigma_\phi = \sigma_1 = \frac{\sigma_Y}{1+t/r_{tool}} > 0$ $\sigma_\theta = \sigma_2 = \frac{1}{2}(\sigma_1 + \sigma_3)$ $\sigma_t = \sigma_3 = -\sigma_Y \frac{t}{r_{tool}+t} < 0$	$\sigma_m = \frac{\sigma_Y}{2}\frac{r_{tool}-t}{r_{tool}+t}$
SPIF (corners)	Equal biaxial stretching	$d\varepsilon_\phi = d\varepsilon_\theta > 0$ $d\varepsilon_t < 0$	$\sigma_\phi = \sigma_\theta = \sigma_1 = \frac{\sigma_Y}{1+2t/r_{tool}} > 0$ $\sigma_t = \sigma_3 = -2\sigma_Y \frac{t}{(r_{tool}+2t)} < 0$	$\sigma_m = \frac{2\sigma_Y}{3}\frac{r_{tool}-t}{r_{tool}+2t}$
Conventional stamping (rotational symmetric surfaces) [**21**]	Equal biaxial stretching	$d\varepsilon_\phi = d\varepsilon_\theta > 0$ $d\varepsilon_t < 0$	$\sigma_\phi = \sigma_\theta = \sigma_1 = \frac{\sigma_Y}{1+t/r_{punch}} > 0$ $\sigma_t = \sigma_3 = -\sigma_Y \frac{t}{(r_{punch}+t)} < 0$	$\sigma_m = \frac{2\sigma_Y}{3}\frac{r_{punch}-t/2}{r_{punch}+t}$

The proposed theoretical framework was confirmed to be capable of addressing the effects of major process parameters and explaining the increased formability of the process. It has been found that necking in SPIF is suppressed, unlike other conventional forming processes. Although the developed analytical model showed a qualitative agreement when compared to its predictive FEM and experimental results, the model used several simplifications, such as neglecting bending effects, assuming axial symmetry, a rigid-perfectly plastic and isotropic material etc., which limits its further applications. Further, this model is developed based on the SPIF configuration which is not suitable for the Two Point Incremental Forming (TPIF) configuration as the TPIF process poses additional contact problems.

2.1.1.2 Shear deformation

Experimental evidences suggest that the through-thickness shear does exist in ISF and might be one of the main causes for the increased forming limit. Allwood et al. [31] presented the existence of through-thickness shear by modelling a novel simplified process named ‘paddle forming’ using the commercial finite element software ABAQUS Explicit. This simplified model allows for characterising the trough-thickness shear in a feasible time. A virtual pin was placed vertically through the workpiece and the deformed location of the pin was tracked over time. It was observed that the pin experienced significant through thickness shear in the forming direction. It was also discussed that the effective stress is lower when no through thickness shear is applied compared with the case with the presence of such shear stress. Therefore, it was concluded that the significant shear parallel to the tool motion occurs and this may explain the improved forming limits of the process.

Jackson and Allwood [28] further experimentally investigated the strain distributions through the thickness along the cross-sectional plane of the specially prepared copper sheets for both SPIF and TPIF configurations. It was claimed that the deformation mechanism for both cases are stretching and shear in the plane perpendicular to the tool direction together with shear in the plane parallel to

the tool direction. It was measured that the shear strain in the tool moving direction is the greatest component of strain. This paper also presents comprehensive discussion on the non-constant distribution of strains and the shear perpendicular to the tool direction.

Mirnia and Dariani [32] analysed the deformation behaviour of a cone-forming process based on the shear deformation assumption using the upper-bound approach. A series of streamlines defined by the Bezier curves along the forming direction were introduced to represent the deformation zone with no flow in the radial direction. This approach was shown to be effective for predicting the tangential forming force and equivalent strain when the deformation at each step is relatively small. However, the errors between measured and predicted tangential forces become considerably high when the step down is large (e.g. $\Delta z > 0.5\,\mathrm{mm}$). This trend suggests that the deformation mechanism is related to the forming process parameters and thus other deformation modes need to be further considered.

Malhotra et al. [33] attempted to predict the occurrence of fracture in SPIF of both a cone and a funnel shapes by combining a damage plasticity model proposed by Xue [34] with finite element analyses. They claimed that the fracture of the material is affected mostly by the through-thickness shear and local bending around the forming tool. Lu et al. [35, 36] further discussed the role of friction and through-thickness shear analytically from the stress state point of view and found that the effect of the through-thickness shear caused by the friction is two-sided. The higher shear stress not only potentially enhances the deformation stability, but also increases the stress triaxiality and reduces the formability at the same time.

Eyckens et al.[37] measured the strain distribution during the deformation process using a stereovision system. It was suggested that the dominant deformation mechanism depends on the selected forming parameters (e.g. wall angle and step-down size). They also studied the strain behaviour through a FE model. It was found that a good qualitative agreement has been obtained for the surface strain but the through-thickness shear was not fully captured. Recently, Smith et al.[38] analysed the deformation mechanics of both single-point and accumulative double-sided incremental forming (ADSIF) processes by FE simulation using LS-DYNA explicit software. The authors concluded that the ADSIF could present greater plastic strains, through-thickness shear strains and greater hydrostatic pressure than in SPIF and suggested this might be one of the reasons for the increased formability in ADSIF.

2.1.1.3 Bending under tension

Emmens and Boogaard [39] performed tensile with bending tests to examine if the bending-under-tension (BUT) can create large uniform strains. The experimental results proved that a low amount of bending is sufficient to allow large uniform strains of the material. However, it was noticed that a too high bending speed will result in a high pulling force leading to a rapid reduction of the maximum elongation. They [40] also summarized that bending under tensile load plays a critical role in the localized deformation of the ISF process. The mechanism of the BUT is based on the fact that the moving tool causes the sheet to be bent and unbent continuously, so it is only validated when the sheet is being bent. The tensile force is resulted from both the stretching strain and the bending strain. However, since the bending-under-tension is a dynamic phenomenon with the moving of the tool, more advanced experimental approaches need to be implemented for providing further investigation.

Fang et al. [41] provided a detailed deformation analysis of SPIF with the consideration of both the bending effect and strain hardening. Several sub-zones were divided from the localized deformation region and the state of stress and strain was investigated through the thickness direction. The proposed analytical model was confirmed by both FE simulation and experimental measurements and the model was shown to explain the enhanced formability and the fracture mechanism in SPIF. The analytical analysis suggested that the deformation takes place not only in the contact zone, but also in the neighbouring wall around the contact zone. In addition, by investigating the hydrostatic stress, it is proved that the fracture tends to occur firstly on the outer side of the wall at the transition area between the contact and non-contact zone. Authors also acknowledged that the proposed model may be only valid for axisymmetric parts or parts with large wall curvature due to the plane strain assumption.

2.1.2 Process formability

Over the recent years, different kinds of studies have been conducted with the emphasis on understanding, assessing and improving the formability in the ISF process. Instead of using the forming limit curves (FLCs) for traditional forming processes, the fracture forming limit curves have to be used to characterise the increased formability in ISF. Alternatively, other formability indicators such as maximum forming angle and fracture depth can be also used to evaluate the maximum formability in ISF.

2.1.2.1 Formability evaluation

Generally, the forming limit curve is defined as a correlation between the major strain ε_1 and minor strain ε_2 in the plane of the sheet metal at the onset of necking failure. These strain values are recorded from a series of experiments under different loading conditions ranging from biaxial tension (stretch forming) to equal tension and compression (deep drawing). The most widely used method of obtaining the FLC is by means of drawing tests of strips with different widths and a hemispherical punch. In the early stage of the development ISF technology, attempts have been made to use the concept of conventional FLCs to evaluate formability limits in SPIF. However, Iseki et al. [42] noticed from the experimental results that ISF allows sheet metal to be stretched much further than that in conventional stamping operations, well beyond the common FLCs. The work performed by Shim and Park [43] also showed that the forming limit diagram in ISF is different from that in conventional forming. It appears to be a straight line with a negative slope in the positive region of the minor strain. Filice et al. [6] argued that this is due to the peculiarity of the loading condition and process mechanics in the ISF process. Plastic deformation ahead of the forming tool is strongly localized and moves progressively along the tool path. As a result, higher strains can be attained in the material before fracture occurs. The experimental tests further revealed that cracks are likely to occur at the corners due to greater deformation than that along part sides. Kim and Park [44] further studied the effect of the process parameters (e.g. tool type, tool size, contact friction and sheet anisotropy) on the formability by experiments and FEM analysis. The straight groove tests have been performed and suggested as an appropriate method to evaluate the effects of process parameters on the formability for aluminium sheet. In this forming test, two characteristics of deformation can be obtained. Biaxial stretching deformation takes place at the starting and ending points of the straight line when the tool moves horizontally. As the forming depth increases, the deformation turns more into biaxial stretching. On the contrary, plane-strain stretching deformation occurs between the starting and ending points. It was found that the formability can be enhanced when a ball tool of 10 mm diameter is used with a small feed rate and a little friction. Additionally, the formability differs according to the direction of the tool movement due to the sheet anisotropy. Further tests were performed to investigate the formability compared to stretching and deep drawing processes for forming complex shapes by Park and Kim [45]. Non-traditional FLCs were used to compare the strains in ISF with those obtained by stretching and deep drawing. They concluded that it is possible to form complicated shapes with sharp corners or edges using TPIF because the plane-strain mode of deformation becomes dominant compared to SPIF.

Filice et al. [6] also demonstrated that the failure strain in ISF significantly exceeds that in conventional forming processes by performing pyramids testing, bi-axial stretching and conical shell testing. This was further studied and confirmed by Silva [30], who concluded that the forming

limit curve in ISF was determined as a straight line with the negative slope positioned on a positive area of the forming limit diagram in the principal strain space. As shown in Fig. 9, the fracture forming limit curve (FFL) is well above the conventional limit curve (labelled FLC) used for stamping and deep drawing processes. Silva et al. [29] revisited the failure mechanics in ISF and provided a much deeper insight on the influence of tool radius. This led to the proposal of a new understanding and assessing on formability limits and formation process of fracture in ISF.

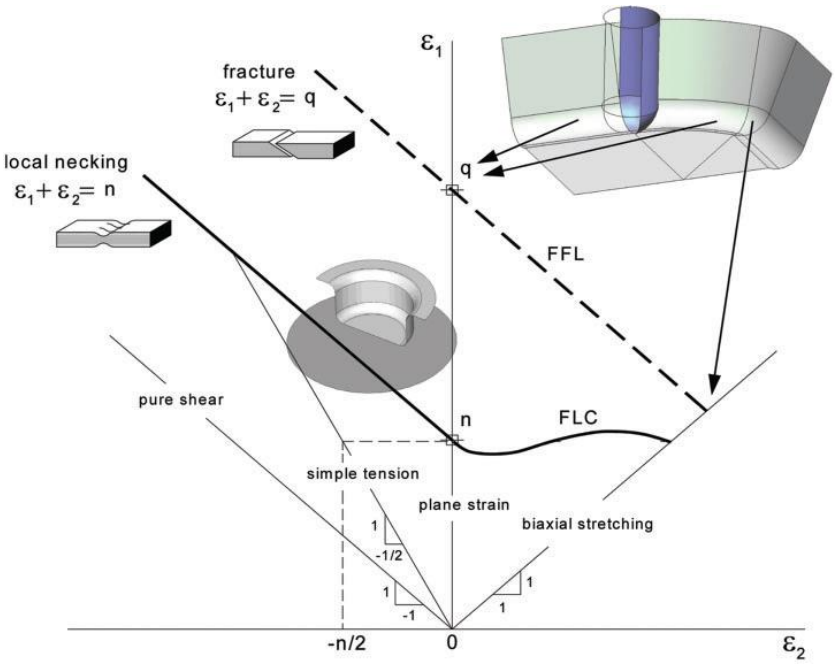

Fig. 9 Schematic representation of the forming limits of SPIF (labelled FFL) against that of conventional stamping and deep-drawing processes (labelled FLC) in the principal strain space ($\varepsilon_1, \varepsilon_2$) [30]

From another point of view, Malhotra et al. [33] explored the unique role of material localization for the enhanced forming limit in SPIF. They combined a fracture model proposed by Xue [34] with finite element analysis to predict material thinning, forming forces and the occurrence of fracture in SPIF. They extensively discussed the effects of five key indicators (i.e. the damage variable, plastic strain, hydrostatic pressure, through-thickness shear and fracture strain) on the occurrence of fracture in SPIF. It was concluded that the fracture in SPIF is determined by both local bending and shear. Detailed investigation confirmed that local bending has greater effect than shear in terms of the contribution towards the increased formability. The combined results of these two deformation modes lead to the earlier fracture of the material sheet on the outer side. In the view of the local nature of the deformation in SPIF, they further proposed a so-called 'noodle' theory, as illustrated in Fig. 10, to explain the increased formability in SPIF. It was shown that the inherently local nature of deformation in SPIF allows the generation of a larger region of unstable deformation. However, this unstable region will not be deformed to fracture as the tool has passed to other regions following the tool path before fracture. These unstable regions play a role of sharing some of the

deformation in the subsequent passes of the tool and argued as the primary reason for the enhanced formability.

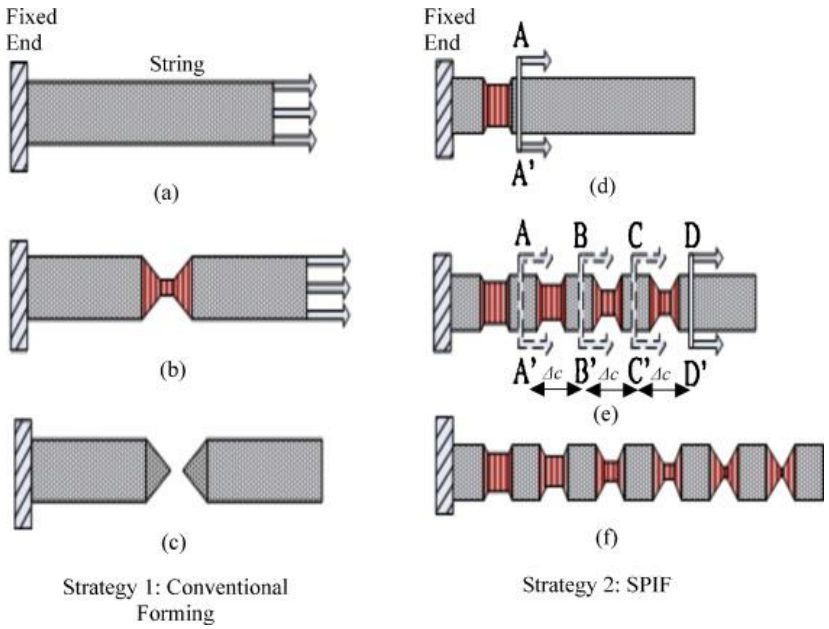

Fig. 10 (a) Stretching the string at the free end. (b) material necking at a single location. (c) fracture at location of material necking. (d) Stretching the string at section A. (e) apply loads at a distance after necking locations. (f) elongation to a greater length without fracture [33].

Although strain analysis is helpful in understanding the mechanics of ISF, the FLCs still have limitations to examine material formability since the process integrating effects of through-thickness shear, bending and cyclic loading [46]. The maximum formable wall angle has been recognized as an indicator for formability by many researchers. Ham and Jeswiet [47] carried out a design of experiments to study the effect of process parameters (material thickness, step size and tool size) on the forming angle. Also, Capece Minutolo et al. [48] successfully evaluated the formability of both truncated pyramids and cones by using the maximum forming wall angle. A set of experiments was designed by Bhattacharya et al. [49] using the Box-Behnken method to study the effect of the process variables on maximum formable angle. It was found that formable angle first increases and then decreases with step down size varying from 0.2 to 0.8 mm. Additionally, Truncated cones with continuously varying wall angle has been used by Fratini et al. [50] and Hussain et al. [51] to reduce the number of experiments required to determine the forming limit.

The fracture depth can also be regarded as another useful geometric formability indictor in ISF. This is more feasible due to the fact that a part with forming angles higher than the critical one can still be formed for a small height. For example, according to Li. et al.[52], the fracture depth for forming a 70˚ conical cone was 23 mm. The fracture depth was used by Fiorentino et al. [53, 54] to evaluate the effect of tool path on the process formability in TPIF with steel sheets. Ambrogio et al.

[55] also evaluated the formability of lightweight alloys by fracture depth in a hot incremental sheet forming process.

2.1.2.2 Effects of process parameters on formability

The effects of main process parameters on the ISF formability have been substantially studied in the literature. Jeswiet et al. [1] reviewed that the formability of the process was influenced by four major parameters: (a) thickness of the metal sheet, (b) vertical step-down size, (c) rotational and feed rate speed, (d) size of the forming tool. The influence of the sheet thickness is commonly explained by the sine law, in which thinning of the material is related to the forming wall angle. The speed of the forming tool is known to influence the formability because it directly affects the frictional conditions at the tool-sheet interface. Smaller radius of the forming tools was claimed to provide better formability due to the concentration of the sheet strains under the forming tool. Larger tool radius tends to distribute the strains over a more extended area and therefore reduces the formability. In terms of step-down size, although Ham and Jeswiet [47] argued that step size does not have significant effect on the formability from their experiments, the general opinion has been that formability decreases with increasing step size (> 0.7 mm) [49]. Experimental work from Li et al. [52] showed that the formability was increased with the increase of step-down size from 0.1 mm to 1 mm. The different observations between this paper and some previous publications are due to two main reasons. First, the investigated range of the step-down size is different. In [52], the step down was set within a small range from 0.1 mm to 1 mm while larger step-down sizes (>0.7 mm) were used in previous published work [49, 56]. Therefore, there is a possibility that the formability could improve with the increase of the step down at small values (<0.7 mm) and then reduce with the further increase of the value of step down. Second, the size of the forming tool used (30 mm in diameter) is larger than most of the forming tools commonly used. The radius of the tool greatly influences the local bending/shearing of the material ahead of the tool as the sheet has to be deformed to conform to the tool surface. Nevertheless, further detailed investigations of the effects of step down and tool size on the formability are essential to clarify this effect.

Petek et al. [57] analysed the influences of the wall angle, tool rotation, vertical step size, tool diameter and the lubrication on the maximal strains of the formed specimens. The measuring circle grid was printed on the specimens before the forming process and then the deformations of the grid were measured by an optical contactless measurement system. It was observed that with higher wall angles, larger deformations can be obtained for the formed part before cracking. Both tool rotation and lubrication have negligible influence on the maximum strains but it was found the surface quality can be improved by rotating the forming tool with lubrication. Larger step size will lead to

higher maximum strains. Finally, it was evidenced that at the same forming depth, a larger value of maximal logarithmic strain can be achieved if a larger tool diameter was used.

Recently, Xu et al. [36] further explored the mechanism and formability variations induced by tool rotation in the SPIF process. The maximum formable wall angle and fracture depth were regarded as the indictor for assessing the formability. First, the effect of tool rotation was investigated through a series of experiments by varying rotation speed from 0 to 7000 rpm. Although the material formability generally improves with the increase of tool rotation speed, four stages were identified depending on different roles of friction and heat during of the forming process. At low tool rotation speed range (0-1000 rpm), friction was found as the dominant factor for formability variation. Nevertheless, the thermal effect on material properties became the most influential factor for formability improvement at high tool rotation speed range (2000-7000 rpm). It was pointed out that the heat generated by friction is enough to activate the dynamic recrystallization of the material when the speed is above 3000 rpm. Moreover, a laser surface textured (LST) forming tool was introduced to investigate its influence on material formability. It is expected that the LST is able to reduce friction at the tool-workpiece interface, thereby reduce the heat generation especially for a high rotation speed. Accordingly, the formability is reduced due to the decreased thermal effect.

2.1.3 Summary

Several methods have been proposed in the literature to analyse the deformation mechanism and explain the increased formability in ISF. The extensive previous research has provided valuable insights of the mechanics in ISF and it is recognized that the process involves a complex combination of deformation modes (shear, bending and stretching). However, current findings are limited and sometimes contradictory which may due to various settings of the process parameters and configurations. The fracture forming limit diagrams, maximum formable wall angle and fracture depth can be applied as effective indictors to evaluate the process formability in ISF.

2.2 Modelling Methods for ISF

Modelling of the ISF process is essential for understanding the deformation behaviour, process investigation and optimisation since it is difficult to reveal the detailed deformation history solely through experimental works due to the highly localized characteristic. In this section, recent developments in the modelling of the ISF process are reviewed from two main perspectives: analytical modelling and finite element (FE) modelling.

2.2.1 Analytical modelling

Analytical study of the process plays a pivotal role in the understanding of fundamentals of the process and the developing of efficient predictive models.

2.2.1.1 The sine law

The sine law is a simple geometrical model for sheet thinning in ISF to predict sheet thickness after deformation. This model was previously used in shear spinning by Avitzur and Yang [58], based on the assumptions that the deformation in shear spinning is (a) a straight projection of the initial blank onto the mandrel, (b) that the through thickness deformation of the sheet is a pure shear deformation, and (c) that volume constancy holds. Fig. 11 depicts the relationship between initial (t_0) and deformed (t_1) sheet thickness for a given wall angle α.

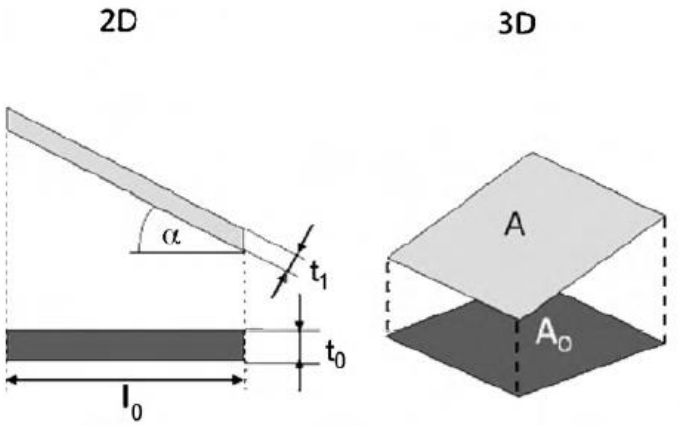

Fig. 11 Illustration of the sine law in 2D and 3D [59].

The following equation can be derived based on the assumptions above,

$$t_1 = t_0 \sin(90^\circ - \alpha) = t_0 \cos \alpha. \tag{2.4}$$

For the non-flat areas, an alternative '3D version' of sine law is more convenient [59]. The surface of the product can be meshed using triangular and quadrilateral elements thereby the thickness can be calculated as a function of the area ratio of the undeformed and deformed elements. This can be expressed as,

$$t_1 = t_0 \frac{A_0}{A}. \tag{2.5}$$

Kim and Yang [24] used the above equation to compute the sheet thinning for two simple shapes, an ellipsoid and a clover cup. A good conformance between calculations and measurements was achieved for areas that have a shallow curvature. Good qualitative agreement with experimental

results were also obtained by Iseki [60]. However, considerable deviations occurred for areas with bending or necking deformation as reported by Young and Jeswiet [61]. To conclude, the sine law provides approximations of sheet thinning for ISF at negligible computational cost, but as a plane strain model it can be applied only when plane strain deformation prevails.

2.2.1.2 Geometrical model based on intermediate shapes

Bambach [59] devised a simplified geometrical model to allow for a more accurate calculation of the sheet thickness after forming, to predict strain states after forming and to visualize the forming kinematics. As discussed above, the sine law only holds where the area is in a plane strain deformation. Instead of using a straight projection between initial and final shapes in sine law, this model is based on the assumption that material points between intermediate stages, proceed along the normal direction of the current surface. A cone with some intermediate stages is shown in Fig. 12.

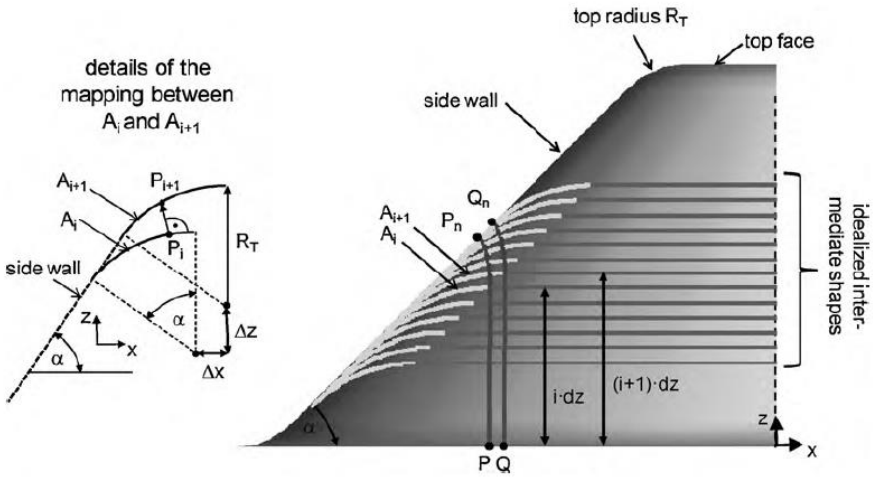

Fig. 12 A cone with some intermediate stages and the trajectories of two adjacent points P and Q [59].

In 2D axisymmetric cases, a first order ordinary differential equation system was developed and expressed by the tool radius R_T and the wall angle α to obtain insight into the material flow. An implementation of the model based on triangular meshes was presented in 3D cases. A new version of the algorithm was developed to calculate the triangulated intermediate stages. The model was used to simulate a pyramidal benchmark part to compare the results with experimental data and the sine law (see Fig. 13). It was concluded that the geometrical model predicts smoother transitions between areas of different inclination, which is more realistic than the abrupt changes predicted by the sine law.

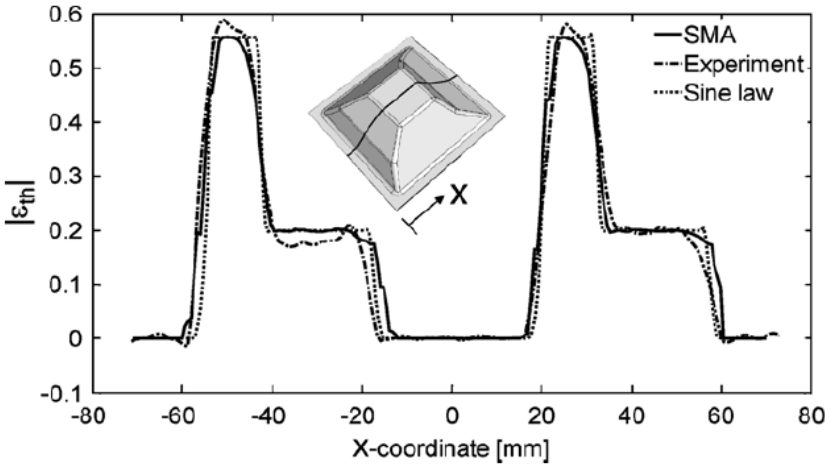

Fig. 13 Comparison of major strains predicted by the simplified modelling approach [59].

However, there are limitations to this model. Material character and friction are not included while bending effects are neglected. As a result, a promising approach to improving this model would be to couple it with a membrane analysis as proposed in [26, 27].

2.2.1.3 Energy-based modelling

The ideal forming theory was proposed by Chung and Richmond [62], in which it was stated that local materials have optimum formability when material elements are prescribed to deform along the minimum plastic work path. A minimum work path is achieved when (a) the principal stretch lines are kept constant with respect to the material during deformation and (b) the ratio of principal true strain rates is constant. The mathematical description of the minimum plastic work path was also derived for forming of membrane sheets under plane-stress conditions. This theory has been implemented to many forming processes by researchers. Ding et.al [63] proposed a new relaxation method to solve the nonlinear problem of predicting the deformed shape due to plastic deformation in roll forming. A small perturbation to each discrete node was applied in order to update the local displacement field, while minimizing plastic work. In chapter 11 of Roll Forming Handbook [64], Kiuchi used the energy method to optimize deformation flow paths by using "shape function" to express the 3D deformed curved surface (DCS) of the strip in order to minimize deformation energy. The shape function can be adjusted by varying a particular factor as shown in Fig. 14. The stress and strain components in the strip, which change as it moves along DCS were analysed using the elastoplastic deformation theory. Chung and Alexandrov [65] reviewed the ideal flow theory, which is the basis of procedures for the direct preliminary design of forming processes involving plastic deformation. The major theoretical base of the ideal forming theory is that material elements are required to deform following the minimum plastic work path, assuming that materials have optimum formability in such paths. Although the reviewed results from [63-65] are based on other

forming processes such as roll forming, these results provide guidelines to model deformation paths based on minimum plastic work for the ISF process.

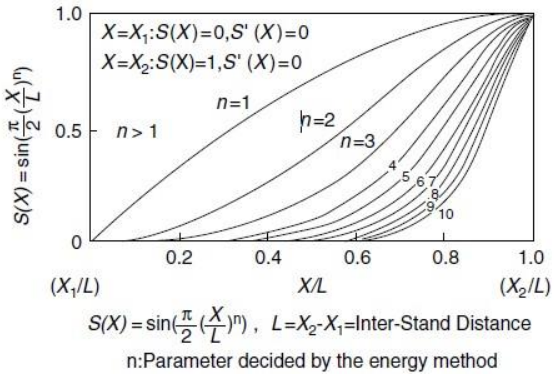

Fig. 14 Calculated curves of shape function '$S(X)$' with different values of parameter 'n' [64].

Raithatha et al. [66] developed a model that is based on the numerical minimization of internal work within the material. In this method, the minimization of plastic work was formulated as a Second Order Cone Programming (SOCP) optimization problem and was solved efficiently using primal dual interior point SOCP algorithms. The results showed that the computing time is 5-9 minutes for a straight line indentation on a sheet with dimensions of 0.1 m×0.1m. However, the reduced computing time was achieved at a loss of model accuracy which results in some fluctuation at the roof of the groove. In this model, only the stretching component of work within the sheet was modelled and was found to be numerically unstable except for very small time increments. To further regulate the simulation, this model was further developed and presented in [67], where the model was improved by incorporating bending work and using finite element discretisation. The modified model showed good geometric agreement compared with measurements from a real product. Nevertheless, the model is not suitable for design and feedback control because the running time was at the same level with the FE model for several hours.

2.2.2 Finite element modelling

The changing contact condition inherent to ISF makes it a highly computational time-consuming process to model with both implicit and explicit FE codes [37]. In order to use FE to understand and explain the temporal deformation mechanics, dedicated strategies for incremental sheet forming simulations need to be developed.

The continuous change of localised plastic deformation and the complex tool path in ISF result in a significant computation time. Therefore, when generic FE codes are being used, a common practice has been to make use of partial FE models which only consider a part of the blank. Henrard et al. [68, 69] modelled a 40˚ pie shape to represent the full cone-forming process. The partial models

were compared to the full models in [70], showing that although the side wall was reproduced well with partial models, significant deviations were observed in the undeformed zone of the sheet. Also, it was suggested that a detailed description of the behaviour occurring across the thickness of the metal sheet is crucial for an accurate force prediction. In partial FE models, non-physical boundary conditions need to be considered, but their exact formulation is of minor consequence on the predicted total deformation [71]. Moreover, Eyckens [72] have developed a model with fine (sub-millimetre) meshing only at the small plastic zone with continuum elements to avoid excessive computation time. In this way, the through-thickness shear was predicted close to experimental results. However, Jackson and Allwood [28] recommended that FE modelling that considers the full tool path should be employed according to the experimental observation that the strains sustained by any given element of material in ISF are not the same at any position.

Lasunon and Knight [73] confirmed that FE modelling can be used to investigate various aspects of ISF processes by validation with experimental testing with truncated pyramids. Yamashita et al. [74] investigated the applicability of the dynamic explicit finite element code DYNA3D for the simulation of an incremental sheet forming process of quadrangular pyramids. The effect of the tool path on deformation behaviour was simulated which showed that the starting position of the forming should be at one of the corners. In this case, the step-pattern deformation at the final product can be considerably mitigated compared with other starting positions. Ma and Mo [75] found that FE modelling based on solid elements is more suitable than shell elements to simulate the SPIF in terms of deformation prediction. Dejardin et al. [76] conducted a numerical analysis using LS-DYNA software to predict the springback effect through the cut rings method. It was found that the finite element model with shell elements is not suitable for all tool path strategies to capture the transverse shear behaviour of the sheet. Further work with FE models using elements able to properly reveal the shear components was suggested.

Regarding the use of material models, Flores et al. [70] showed that the use of an anisotropic yield criterion is not a key factor in terms of the geometric prediction of a cone wall. Also, Ambrogio et al. [77] presented that the sheet material orientation has no substantial effect on the predicted straining history with an anisotropic material constitutive law. In [37], the effect of anisotropy in the FE model constitutive law onto the complete strain history was further explored. It was also concluded that the choice of the anisotropic Hill yield locus has no significant improvement compared to von Mises.

Some other researchers [78, 79] have been focusing on contact optimization in FE simulation. The penalty method has been usually used to deal with contact problems by checking the contact at nodal or integration points. This implies that the force history becomes dependent on the relative position of the tool and also the points where contact is evaluated when the element size is large. Henrard et al. [69] presented a new approach that accounts for contact anywhere inside a small number of elements without using a penalty method. This method is based on a dynamic explicit scheme which has the advantage that no system of equations needs to be solved. The finite element code used was Lagamine that has been developed at the University of Liege for 20 years. The contact algorithm was proven to be more accurate but the computation time was minimal by using a larger element size.

Malhotra et al. [33] developed a finite element model in which a damage plasticity model proposed by Xue [34] was implemented. This model combined the effects of hydrostatic pressure, plastic strain and shear on fracture and it was embedded into a FEA model using a user subroutine in LS-DYNA. A calibration procedure was employed to obtain four material constants used in the material model by tuning the simulated vertical forces and fracture depth to the same as that obtained from experiments of forming a 70˚ cone. The predicted results from the calibrated FE model showed a good agreement with experimental results in terms of vertical forming force, the maximum thinning and the fracture depth. Recently, Smith et al. [38] analysed the deformation mechanics of both single-point and accumulative double-sided incremental forming (ADSIF) process by FE simulation using LS-DYNA explicit software. Solid elements were used in the described FE model to show the evolution history of plastic strain, hydrostatic pressure, and shear strains parallel and perpendicular to tool motion. It was concluded that the ADSIF could present greater plastic strains, through-thickness-shear strains and greater hydrostatic pressure than in SPIF and suggested this might be the reasons for the increased formability in ADSIF.

Unlike the majority of numerical simulations which use the flow rule method to determine the elasto-plastic state of the workpiece. Robert et al. [80] proposed a simplified elasto-plastic scheme based on the incremental deformation theory of plasticity. A brief description of two different principles was given, in which the author pointed out that the classical scheme based on the flow rule requires several iterations for each material point, while the incremental deformation theory of plasticity was considered as an alternative to reduce the CPU time. The results of numerical simulation in ABAQUS explicit, using both plasticity theories, were presented and compared. A significant reduction of calculating time (70%) was achieved for the stretching test of a spherical cup using the new algorithm. However, although it provided a better results for geometry prediction,

only a small (4%) improvement was obtained for simulating incremental forming process where the localization of the contact between the tool and the sheet (high contact non-linearity) are dominant.

2.2.3 Summary

A summary of the characters of the above main predictive models proposed for the ISF are listed in Table 2. Several analytical models are available for efficient estimation of thickness prediction and/or strain calculation, but large deviations could be expected with experimental results. Despite the advances in the finite element analysis for modelling of metal forming processes, existing FE models for the ISF are still computationally inefficient so reducing computational time is still a challenge. Over the past few years, different kinds of customized numerical models have been proposed in the effort to improve computational efficiency with reasonable accuracy.

Table 2. Comparison between different predictive models in ISF.

Model/Paper	Theory/Methodology	Advantages	Limits
The sine law [58]	Straight projection; Volume constancy	Negligible computational cost	Does not hold for a non-plane deformation
Bambach [59]	The deformation between intermediate shapes proceeds along the surface normal direction	Membrane strain and sheet thickness are predicted.	Does not take into account the material behaviour or friction between sheet and tool.
Silva [26]	Membrane analysis	Provides a closed-form analytical model for SPIF	Neglecting bending effects and based on SPIF configuration
Henrard [69]	Contact modelling based on a dynamic explicit time integration scheme	It uses actual location instead of fixed positions(e.g. integration or nodal points); Larger elements can be used.	Simulations were not as accurate as those performed with an implicit strategy; No significant reduction in overall computation time as expected.
Robert [81]	Incremental deformation theory.	Save 70% computing time for deep drawing with accurate results	Time benefit is small (4%) for ISF
Raithatha [67]	Second order cone programming based on minimization of internal work. The rigid perfectly plastic deformation is used	It presents an alternative shell model for incremental deformation.	Longer running time(8 h) compared with LS-DYNA (5.5 h)

2.3 Forming Forces in ISF

Investigation of forming forces in ISF is of great importance since it provides understanding of the deformation mechanics, monitoring of the forming process, failure prediction, and future means of on-line control and optimisation. This section provides a review of studies on the contact conditions and the effects of the process parameters on forming forces in ISF, followed by the current status on forming force prediction and its potential role in the improvement of ISF technology.

2.3.1 Contact conditions in ISF

Johnson [82] categorized contact problems as Non-Conforming Contact Problem (NCCP) and Conforming Contact Problem (CCP). As for NCCP, the contact area is small in comparison with the radius of the object and this is further classified into Hertzian and Non-Hertzian Problems [83]. On the contrary, for CCP, the contact area is large in comparison with the radius of the object. Therefore the contact area is considered not to be flat. Due to the nature of the ISF process, the contact area is relatively large compared to the tool radius. Therefore the contact problem in ISF is considered as a CCP.

2.3.1.1 Surface friction

Hamilton [84] presented that friction in ISF is attributable to three components as shown in Fig. 15: normal indentation, sliding and torsion due to rotation. At first, friction only exists on the projected area of the forming tool perpendicular to the force in basic indentation where normal force, F_n is dominant. When the tool is sliding, both the normal and tangential components of friction are present. Load support with sliding, assuming no tool rotation, would only occur in the leading edge of the tool. In the presence of rotation, the leading edge is constantly changing. However, with constant feed rate, the contact area would be relatively constant. Subsequently a torsion load is created as a combination of rotation and indentation.

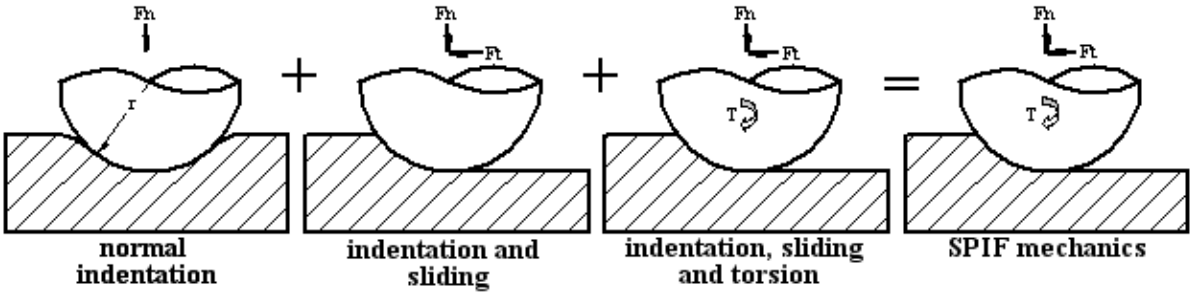

Fig. 15 ISF forming mechanisms [84].

Eyckens et al. [85] experimentally investigated the role of friction in SPIF through forming an aluminium alloy sheet (AA3103-O) into a large wall angle cone with and without the imposed tool rotation. It was observed that the friction hardly affects the force component along the vertical direction (F_z), and along the radial direction (F_r). However, a relatively large difference was observed in the measured tangential force component F_t (along the tool movement direction) whether tool rotation is imposed or not [85].

Hamilton [84] concluded that friction coefficients for the majority of parts formed fell between 0.1 and 0.4. Statistical observations showed that tool size had the largest influence on the coefficient of

friction. The influence of interacting parameters on friction coefficients was represented with response surfaces. From these surfaces, a medium sized tool has the lowest friction in its interaction with every other parameter. Lowest coefficients with thickness were seen when combined with small step size, large tool size, low feed rate, high forming angle and revolution per minute (RPM). For the same thickness with different shapes, lowest friction coefficients were observed when forming pyramids. Therefore, reducing step size and feed rate while increasing RPM, tool size and forming angle will produce low friction coefficients. From a force perspective, each of these parameters either reduces the tangential force or increase the normal force which subsequently reduces the friction coefficient.

2.3.1.2 Contact area

Since the sheet is clamped at its perimeter in ISF, any step down motion will produce three deformation components: indentation, bending and stretching. Hamilton [84] deduced an equation among these three components based on the geometric relationship with an assumption that the contribution of both the bending and indentation components of the step size are equal at a point during forming. Eyckens et al. [86] employed the FE submodelling technique to simulate truncated cone-forming processes with three different scales to evaluate the contact area and the distribution of the contact pressure between sheet and forming tool. Four cases with different forming parameters (i.e. wall angle, tool diameter, scallop height and step size) were simulated and the results suggested that the contact region was made up by two parts. First, the contact with the cone wall which is approximately a line contact at larger wall angles and it dies out at small wall angles. Second, there was also a substantial 'sickle-shape' groove contact at the cone bottom with both small (20˚) and large (60˚) wall angles. It was also observed that the point directly below the tool centre appears not or barely in contact with the sheet.

Based on the observation from the FE simulations, Aerens et al. [87] modelled the contact area by a ribbon of constant width that the contact pressure is approximately uniformly distributed along the ribbon. As shown in Fig. 16, the length of the ribbon in the proposed model relates to three angles: the scallop angle β (depends on step size), the wall angle α and the groove angle γ. The first two angles can be obtained from the process setting parameters while the last angle was modelled empirically as a function of tool diameter according to experimental measurements. Both Hamilton's and Aerens' models present the contact area as a ribbon lying directly in the tool path, therefore the models did not account for tool curvature in the direction of the tool path.

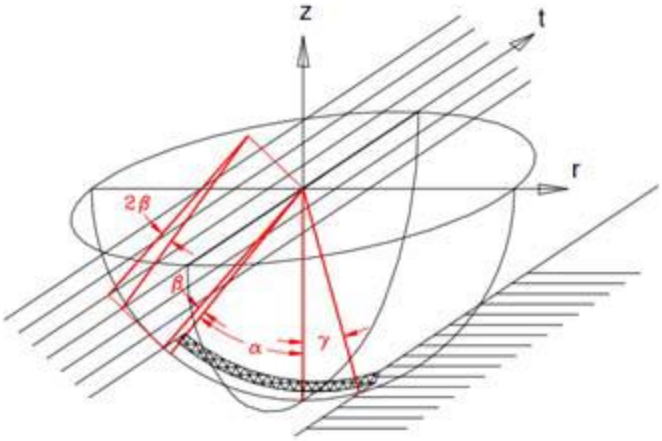

Fig. 16 Contact model proposed by Aerens el al. [87], using to represent wrap around the inside of the tool and the scallop angle due to stepover

Adams [20] firstly introduced a method of calculating the contact area based on direct measurements of the geometry surrounding the contact zone. As shown in Fig. 17 (a), a platinum measurement arm fitted with a point probe was used to take the measurements of the troughs. In this study, a point cloud (Fig. 17 (b)) could be constructed to define the boundaries of the contact patch. Based on a full factorial experimental design with three factors at two levels, an empirical model for contact area was developed considering the effects of tool diameter, wall angle and step size. It was found that, in all cases, the contact area behind the tool was zero or nearly zero, indicating little recovery occurred behind the sheet. Additionally, the diameters of both leading and trailing troughs were larger than the tool that formed them. The vertical step size has the most influential effect on the depth of indentation of the tool below the sheet followed by the wall angle.

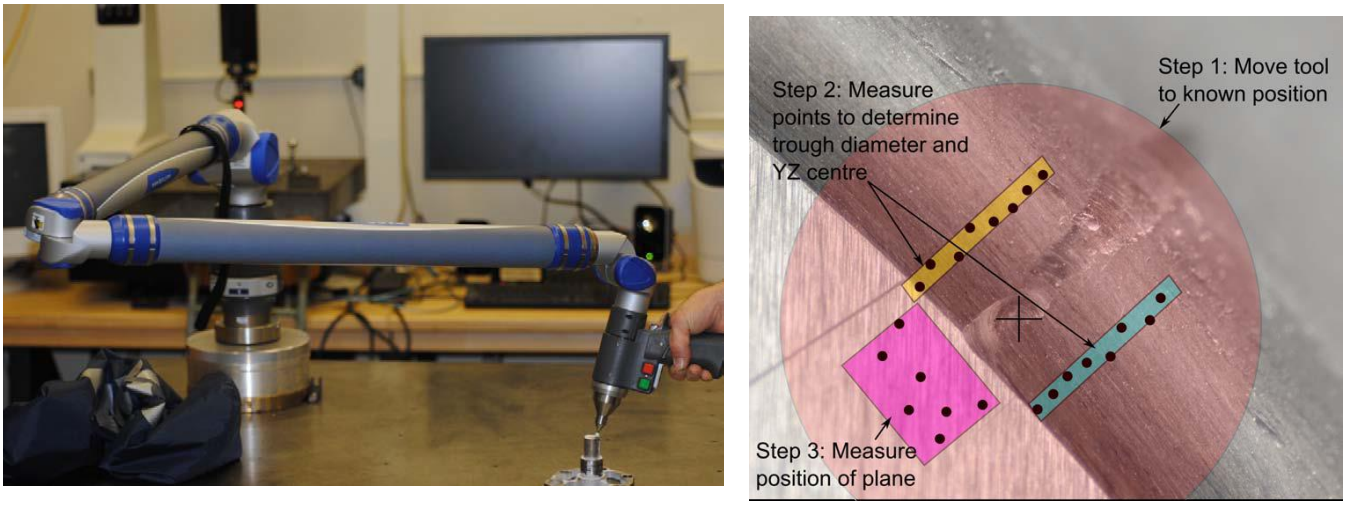

Fig. 17 Measurement method used. Black dots represent approximate location of points measured with the arm. Shaded regions indicate features constructed [20]

2.3.2 Effects of process parameters on forming forces

Forming forces during ISF have been experimentally studied intensively. Minutolo et al. [88], worked on force analysis in a groove test and found that using a tool with a bigger diameter, higher drawing depth, higher forming forces and a different typology of failure can be observed. In 2004, Szekeres [89] designed and successfully manufactured a complete system for measuring, recording and processing the forming forces acting on the sheet metal during ISF, as shown in Fig. 18. This design was based upon other friction measurement work with cantilever beams by Nyahumwa and Jeswiet [90]. They used a spindle mounted cantilever beam with strain gauge Wheatstone bridges, with each bridge designed to measure one of three orthogonal forces: two bending directions, and one axial direction. An advantage of this sensor is that it can be used for friction measurement research. After calibration, the data has been proven to be accurate and it was found that the total force acting on the sheet metal is between 450 to 500N for a part with a wall angle of 40˚. Also, this value seems not to be sensitive to wall angles at a lower range, but differs greatly when the wall angle is close to the maximum capability (e.g. 70˚). In the tested range of feed rate from 60 in/min to 80 in/min, no considerable variation was observed for the total forming force. The author also suggested that the failure during ISF is a predictable phenomenon by monitoring the significant drop of the total force, but no specific criterion was proposed. Szekeres et al. [91] further identified the detailed features of the forming force in ISF using the developed tool with force sensors mounted. It was reported that cracks always occur in the corners when a pyramid is being formed due to the higher strains. Failure in the cone-forming process can be intuitionally predicted by a drop in the total force but this is not readily apparent for the pyramid-forming process. This force measurement system has also been successfully used for measuring the forces in a TPIF configuration [92].

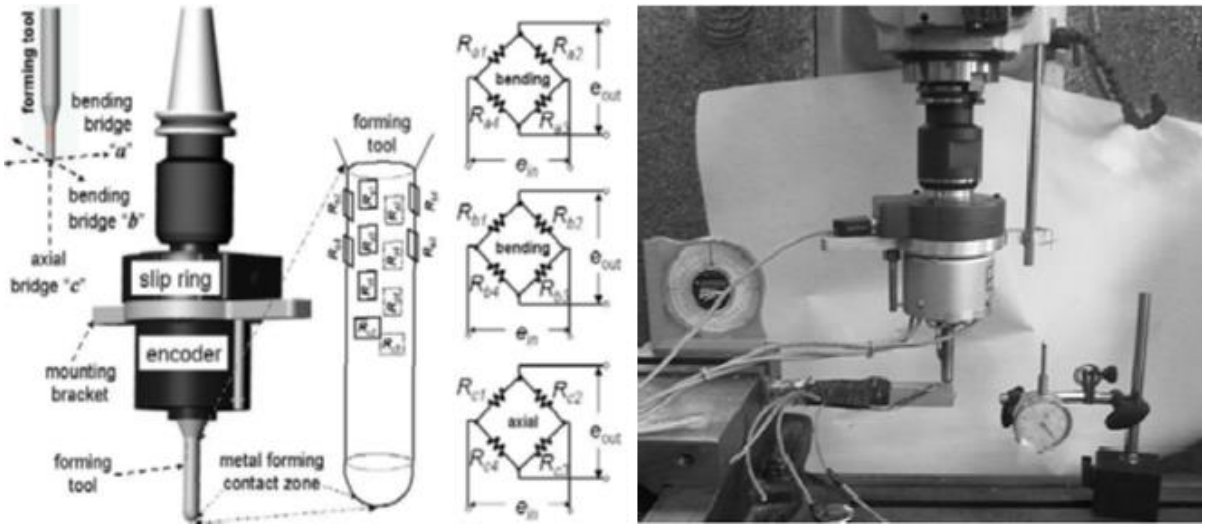

Fig. 18 The Force Sensor as set-up in the CNC Mill and the layout of strain gauges [91, 92]

Duflou et al. [93] presented another experimental platform which is capable of measuring three components of forces during the ISF process to investigate the influence of the three process

parameters on forming forces: the vertical step size, the tool diameter and the wall angle. More detailed results are described in [94] which further considered the effects of the sheet thickness and lubrication. As shown in Fig. 19, experiments were carried out using a 3-axis CNC vertical milling machine and a table type force sensor was mounted between the fixture and the milling machine work platform. The force sensor was a Kistler 9265 force dynamometer and connected to a Kistler 5017A 8-channel charge amplifier for good data recording performance. A series of experiments were performed with Al 3003-O sheet material by varying step size, wall angle, tool diameter and sheet thickness. Conclusions can be drawn from the experimental measurements as follows:

- As step size increases from 0.25 to 1.0 mm, it is apparent that both the magnitude of the peak and average force after the peak rises and fits well as a linear function.
- Similar to the effect of step size, measured forces are also linearly proportional to the tool diameter in the range of 10 to 30 mm.
- In terms of the wall angle, the magnitude of the force needed gradually increases with the increase of wall angle. Significant peaks can be observed for a part with 60˚ wall angle which is suggested as a possible indication of material fracture.
- The sheet thickness is a dominant factor determining the magnitude of the resultant force. The required force was increased from 380 to 1460 N by varying the sheet thickness from 0.85 to 2.0 mm.

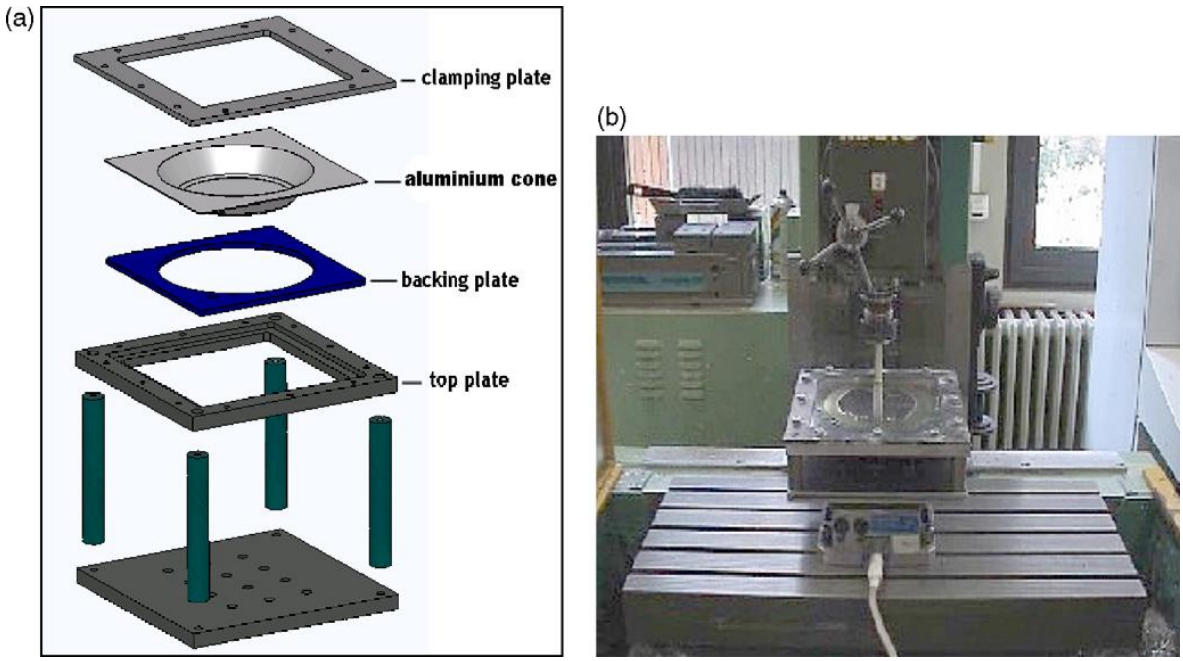

Fig. 19 The experiment setup: (a) exploded view of forming fixture with formed cone; (b) the forming fixture with the force sensor mounted on the machine table [94]

Petek et al. [57] presented experimental equipment for forming force measurement in SPIF. Forming forces were measured using a dynamometer Kistler 9239 and amplified by Kistler 5001 for

analysis. In particular, the impact of the wall angle, tool rotation, vertical step size, tool diameter and lubrication on the magnitude of forming force were presented. It was found that when increasing wall angles, the forming force is progressively enlarged. Both tool rotation and lubrication have no considerable influences on forming forces but have significant influence on the quality of the surface. The increase of the tool diameter and vertical step size resulted in larger forces. The authors [17] also proposed an autonomous on-line system for fracture identification and localization by analysing the reaction force with a skewness function.

Another research group has also conducted intensive experimental work on forming force measurements. Filice et al. [16] worked on force analysis and classified the trends of tangential force into three types: steady state force trends, polynomial force trends and monotonically decreasing force trends. In addition, a statistical analysis was performed based on a proper Design of Experiments (DOE) considering four process parameters at three levels. In particular, the force gradient after the peak was defined and its relation with four process parameters was investigated. It was stated that the force gradient after the peak is highly affected by sheet thickness and wall angle and their interaction, followed by the effects of step size and tool diameter. Ambrogio et al. [15] concluded that the force gradient after the peak can be effectively considered as a critical indicator to detect and prevent workpiece fracture. Moreover, the critical gradient value does not seem to depend on previous process history based on a wide experimental activity. Therefore, forming force is a potential indicator for forming limits identification. Based on the understanding of the effects of each process parameter, a strategy of monitoring and control of force was developed to avoid failure of the produced parts.

2.3.3 Prediction of forming forces

As suggested previously, forming forces in ISF provide further insights into the deformation mechanics, monitoring of the forming process, failure prediction, and a means of on-line control and optimisation, therefore the efficient prediction of forming force would greatly facilitate the advancement of ISF technology.

Although finite element modelling technology has been widely used in the ISF process for geometric prediction, the accurate prediction of forming forces within a reasonable computational time is still a challenge. Flores et al. [70] recommended that the model identification of both yield locus shape and the hardening behaviour is essential for reasonable force prediction from FE models. The mixed hardening model presented better prediction of forces compared to Von Mises or Hill constitutive laws with isotropic hardening. Bouffioux et al. [95] also found that the

conventional methods used to identify material data by a combination of tensile and cyclic shear tests was not adapted to the SPIF process on aluminium alloy AA3103. The 'line test' performed on an ISF machine was proposed to adjust the material parameters and was shown to have better prediction in terms of forming forces. Cerro et al. [96] simulated the SPIF process of a pyramid with a 75˚ wall angle using shell elements and obtained a 5% difference between the maximum values of the measured and calculated vertical forces. Henrard et al. [68] comprehensively compared the prediction accuracy of FE models in terms of forming forces with two different codes (Abaqus and Lagamine) and several constitutive laws (an elastic-plastic law coupled with various hardening models). It was concluded that three factors; the choice of element type, the constitutive law and the identification procedure for material parameters have considerable influence on force prediction. An inverse material identification procedure with line test was a key factor in accurate force modelling in the ISF process. In addition, it was confirmed that the description of the material behaviour through the thickness is also crucial so brick elements were recommended in FE models. In this study, the highest accuracy was attained in the case where brick elements with a fine mesh were used with a material model that combined the isotropic yield locus of von Mises with the mixed isotropic–kinematic hardening model of Voce–Ziegler. However, due to the localized contact condition and long tool path in ISF, force prediction with FE models is significantly time-consuming. Smith et al. [38] reported a simulation time of 24 days for a single point incremental forming process for a truncated cone shape.

Currently, very limited analytical models are available for the efficient prediction of forming forces in ISF although some researchers have attempted to bridge the existing research gap. To overcome the above computational challenges of the FE approach, Iseki [60] derived the forming force for the incremental forming of a pyramid using a simple approximated deformation analysis based on a plane-strain deformation. The proposed numerical model allowed a systematic investigation of the effects of process parameters on the forming force and thickness distribution. However it was only a rough estimation and hasn't been validated by wider experimental results. Raithatha and Duncan [67] developed a model based on numerical minimization of internal work within the material. In this method, the minimization of plastic work was formulated as a Second Order Cone Programming (SOCP) optimization problem. By sacrificing the accuracy, a process of straight line indentation on a sheet with dimensions of 0.1 m × 0.1 m was obtained in 9 minutes. However, the reduced computing time was achieved at a loss of model accuracy which results in considerable fluctuation at the roof of the groove. Moreover, only the stretching component of work within the sheet was modelled and the model was found to be numerically unstable for a full-scale forming process.

Aerens et al. [87] studied the forces in incremental forming of truncated cones with different materials using experimental and statistical analyses. Regression formulae were proposed to predict the triple forming forces including axial, radial, and tangential components at their steady state from input variables including wall angle, initial thickness, tool diameter and step down. In addition, a general model has been presented which can estimate the vertical force component for any material by knowing tensile strength only. Good prediction precision of forming forces was obtained in all tested materials with different working conditions of the cone-forming process. Nevertheless, the proposed model pays little attention to the physical mechanics of the forming process so the contribution to the further optimisation of the process is limited.

More recently, Mirnia an Dariani [32] conducted an upper-bound analysis for a truncated cone-forming process to predict the tangential force using an assumed deformation zone. In this analysis, an assumed deformation zone represented by a series of flow lines was defined and used to calculate the dissipated power. In particular, shear deformation mode is assumed to be the dominant mechanism in the cone-forming process. The influences of four process parameters including step size, sheet thickness, tool diameter and wall angle on the tangential force and the equivalent strain were investigated. It was reported that the forces were in good agreement with experimental results reported by Aerens et al. [87]. However, large errors can be expected for severe deformation conditions (e.g. $\Delta z > 0.5$ mm) and may possibly due to the limit of the pure shearing assumption of plastic deformation. Also, the model needs to be further verified with various geometric shapes.

2.3.4 Summary

It is known that the contact condition in ISF is characterised by its local deformation feature but the determination of the contact area is still not well studied. The effects of process parameters on forming forces in ISF have been studied mainly through experimental approach. General agreement has been achieved regarding the effects of the most critical factors including step size, tool diameter, sheet thickness and wall angle on forming forces, but the physical explanation behind these phenomena need to be further investigated. The above review of recent studies shows that the prediction of forming forces in ISF has been studied either through time-consuming FE simulations or costly trial experimental tests. There is still a lack of analytical analysis to predict forming forces efficiently.

2.4 Other Aspects of ISF

2.4.1 Geometric accuracy

Presently, the geometric accuracy for ISF products is still one of the biggest challenges for both academic researchers and industrial users. Allwood et al. [97] reported that the specification of geometric accuracy from industrial users for metal sheet components are typically within $\pm 0.2\ mm$ over the whole surface of a part, while the geometric error for ISF currently only achieved around $\pm 3\ mm$. They [98] also summarized the geometric accuracy in the ISF process into three definitions, i.e., (a) clamped accuracy, (b) unclamped accuracy, and (c) final accuracy. Research has been mainly aimed at improving the clamped accuracy. Micari et al. [99] further categorized shape accuracy in ISF into three different typologies as shown in Fig. 20: (a) sheet bending close to the major base of the part where plastic deformation starts; (b) sheet springback after lifting the forming tool; and (c) pillow effect on the minor base of the product. The effects of process parameters on geometric error and possible strategies to improve the accuracy are reviewed in this section.

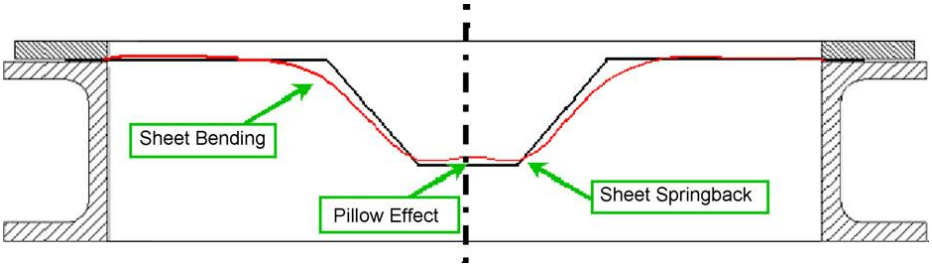

Fig. 20 Geometrical errors during the SPIF process [99]

2.4.1.1 Effects of process parameters on geometric accuracy

The effects of process parameters on geometric accuracy have been investigated through both numerical modelling and experimental methodology. Essa and Hartley [100] investigated the effects of adding a backing plate, a supporting kinematic tool and modifying the final stage of the tool path on the improvement of the geometrical accuracy through a FE model. It was found that the sheet bending near the initial tool contact location can be minimised by the backing plate; the springback can be reduced by the kinematic tool; and the pillow effect can be eliminated by extending the tool path across the base of the sheet.

Guzmán et al. [101] simulated a two-slope SPIF pyramid with two different depths using the FEM to investigate the geometric deviation at the slope transition zone. It was concluded that elastic strains due to structural elastic bending were the main causes of the shape deviations. The localized springback has only minor contribution because no plastic deformation is observed in the angle transition zone. It was recommended that tool path designs could be designed to consider these elastic strains in order to achieve the intended geometry.

Ambrogio et al. [102] statistically analysed the effects of process parameters of tool diameter, step down, wall angle, final product depth and the sheet thickness on geometric accuracy of the formed truncated cone. It was suggested that the geometric error measured at the corner was largely influenced by sheet thickness and total part depth. On the other hand, the pillow effect at the middle of the base was strongly affected by the tool diameter and product height.

Ham [103] performed a Box-Behnken design with 46 experimental tests that considers five factors varied at three levels to study their effects on dimensional accuracy. The five investigated factors include material type, sheet thickness, tool size, step-down size and formed shape. The formed shapes were scanned using a ShapeGrabber® laser scanning system and processed by IMAlign™ software. It was observed that the geometric deviation at the bottom of the formed shape is small compared with the remaining area and the overall geometric error for most of the parts is within 1 mm after a user defined scale. However, only qualitative comparisons were provided based on several contour plots of geometric deviations in this study and further qualitative investigation is required.

2.4.1.2 Strategies to improve geometric accuracy

Current responses to the problem of accuracy in incremental sheet forming can be summarised as the following three main approaches:

a) Additional support

A variety of additional support configurations have been adopted since ISFs inception. Initially, Iseki et al. [42] utilised a stiff backing plate under the undeformed sheet to prevent unwanted bending, and this remains an effective strategy to maintain reasonable geometric accuracy. The use of both male and female dies has shown benefits to capture the detailed features of the product but with the loss of flexibility of the ISF process. To this end, the use of partial die or a static post was recommended by Matsubara [104]. Interestingly, instead of adding extra supporting, Allwood et al. [98] demonstrated an approach to reduce geometric error by introducing partial cut-outs to locally weaken the sheet blank. Although this idea theoretically seems promising, the conducted study showed minor impact on the overall geometrical accuracy. Meier et al. [105, 106] developed the two point incremental forming process with two industrial robots and found that the geometric accuracy could be partially increased by 1 *mm* compared with the single point configuration. It was also pointed that the improvement of the accuracy is limited by the compliance of the robots. Instead of using robots, Malhotra et al. [23] developed a platform which enables double-sided

incremental forming (DSIF). In this configuration, a second tool was used on the opposite side of the sheet, acting as a local support for the forming tool. It was demonstrated that the overall geometry of the components formed with DSIF is much better than that in SPIF by reducing the significant amount of bending at the edges of the component. A substantial improvement of geometric error at the bottom of the formed truncated cones was also achieved.

b) Tool path compensation

Hirt et al. [107] proposed a tool path correction method based on experiments. After measuring the geometric deviation for the first component formed by the regular ISF process, a correction module was applied to the tool path to achieve a specified geometric tolerance. Attanasio et al. [108] conducted a study on tool path optimization in TPIF and concluded that a tool path with a small scallop height and variable step depth sizes contributes to better part quality. Malhotra et al. [23] developed a tool path strategy for DSIF to squeeze the material between the two tools which leads to a faster stabilization of the deformation into a localized zone around the contact point. A significant improvement in the geometry of the formed component wall was obtained from both experiments and FEA. Malhotra et al. [109] also presented an automatic spiral tool path generation algorithm for SPIF, in which the incremental depth is controlled by the geometrical error between the CAD model and formed parts.

Ambrogio et al. [110] performed a robust Taguchi experimental design of ISF with the aim of improving the thickness distribution along with the geometric error by modifying the tool path. In this tool path, an over-slope was applied where the sheet is usually less stretched and a lower angle is imposed where the localized over-thinning usually appears. A FE model was established to simulate and quantify the multi-response optimisation for two considered aims and finally the best process setting for the tool path was provided. Wang and Duncan [111] adopted a closed loop feedback control scheme for generating an optimised tool trajectory. The step depth at each contour for the forming process of a truncated cone was optimised, and a much lower level of geometric error was obtained. However, since current strategies for tool path optimization are mainly based on experimental measurements rather than deformation theory, further investigation on the applicability of current models to different shapes is essential.

c) Multi-stage forming

Recent studies have shown that a multi-stage design is also an effective method to improve the geometric accuracy. Bambach et al. [112] showed that multi-stage forming can be applied to

improve the accuracy of truncated pyramids manufactured by the SPIF process. It was also identified that local elastic deformation and local springback are the main aspects that limit the improvement of geometric accuracy. The results also suggested that the maximum geometric deviations for the formed parts are reduced with an increasing number of forming stages.

2.4.1.3 Summary

Although various strategies have been proposed to improve product accuracy, the geometric accuracy is still a key concern for ISF developers. Use of a simple backing plate can improve the overall geometric accuracy but is not effective for local deviation improvement. Closed loop feedback control by modifying the tool path during the forming process was recommended as a promising strategy to minimise geometric deviations. Although substantial research work has been conducted on the clamped accuracy, the degradation in unclamped and final accuracy due to residual stresses in the sheet has had very little attention in the literature. Therefore, the effects of process parameters on the unclamped accuracy should be further investigated.

2.4.2 Forming efficiency and energy consumption

In recent years, environmental and sustainability concerns for metal forming processes have brought considerable attention in the academic world. As for the ISF process, particular attention is focused on the investigation of the forming efficiency and energy consumption under various process parameters and different machine facilities.

2.4.2.1 Forming efficiency

Due to the long travel of tool movement, forming efficiency (forming time) in ISF is one of the major concerns for practical production. Sarraji et al. [113] studied process forming time in ISF in terms of the effects of four different process parameters (tool diameter, step down size, feed rate and support type). By using Taguchi analysis with design of experiments (DOE) and analysis of variance (ANOVA), the effects of these four process parameters and their combinations were investigated to optimise parameter levels with the aim to minimise forming time. The analysis results showed that the most influential parameter on forming time is step-down size followed by feed rate and then tool diameter.

Ambrogio et al. [114] explored the capability of improving industrial suitability of the ISF process by using very high feed rates to significantly reduce forming time. The effects of high feed rate on formability, surface roughness and geometric accuracy were investigated. It was found that the high

feed rates have no considerable effect on formability and surface roughness compared with other process parameters (e.g. step size and tool diameter). In terms of the geometric accuracy, the effect of the tool feed rate and its interaction with the sheet thickness and the wall angle cannot be ignored. However, it was recommended that the tool feed rate can be increased up two orders of magnitude without relevant reduction in the geometrical precision of the component.

2.4.2.2 Energy consumption

Duflou et al. [115] provided a systematic overview of the energy and resource efficiency improvement methods in the domain of discrete part manufacturing. In terms of the ISF process, three strategies were concluded for reducing the energy usage and improving resource efficiency: (a) redesign of machine tools and selective control, (b) allocating the machine tool at its nominal capacity level and (c) optimising the process parameter settings. Dittrich et al. [116] proposed the concept of exergy analysis (the maximum useful work that can be obtained from a system at a given state in a given environment) in the ISF process and concluded that the exergy of the sheet material contributed a significant fraction to the total exergy input. Also, compared with conventional forming and hydroforming processes, ISF is advantageous for prototyping and small production runs up to 300 parts from an environmental point of view.

Branker et al. [117] firstly analysed the cost, energy and carbon dioxide emissions in a SPIF process for manufacturing a custom designed aluminium hat. By doubling the feed rate and step-down size, as well as using an eco-benign lubricant, it was found that the cost and energy consumed during the process without labour reduced from $4.48 to $4.10 and 4580 kJ to 1420 kJ, respectively. Additionally, a reduction rate of 31% for the embodied CO_2 was recorded due to the increased feed rate and step-down size. After this, they [118] further investigated sustainability issues in SPIF. In particular, the associated CO_2 emissions were estimated using a life cycle analysis (LCA) approach and costs were calculated using a proposed economic model. The model was firstly implemented in a simple bowl study to find the optimum parameters and then these settings were used to improve the process parameters of a more complex hat shape. It was found that the material of the workpiece dominates the embodied CO_2 emissions in the hat forming process.

Ingarao et al. [119] analysed the energy consumption during both the traditional stamping and the ISF process. The focus was to investigate both the efficient use of materials and process energy saving. It was noted that the energy consumption was calculated from the recorded forces in all three orthogonal directions multiplied by the corresponding travel distance of the forming tool in that direction. One conclusion has been drawn that the required deformation energy in the ISF

process is always higher than that for stamping for all the considered cases, although the ISF process allows a certain material saving. Also, it was suggested that the energy reduction could be obtained through varying the material type, part shape as well as thickness. The empirical evidence presented in this paper provides useful comparison guidelines for materials saving and energy consumption but the optimal solution was not discussed. Recently, Ingarao et al. [120] comprehensively analysed and compared the electric energy consumption of the ISF process by using three different machines: a CNC milling machine, a six-axes robot as well as the dedicated AMINO machine. Working cycle time and power studies were conducted for all these three setups. In terms of the effect of material type of the workpiece, no difference in power demand was observed for CNC milling machine but the six-axes robot was proved to be sensitive to the material type. The AMINO setup is the most efficient machine tool in terms of instantaneous power but requires higher total electric energy due to the lower forming speed compared with the six-axes robot. As far as the process parameters are regarded, increasing the feed rate and step-size within the admissible range was recommended as the most effective approach to reduce the energy consumption. In addition, the authors also presented a parametric model to predict the energy consumption for the robot based ISF operations by considering the ultimate tensile strength of the material and the processing time. It should be noted that this model highly depends on the predicting accuracy of the steady vertical force from previous work [87].

Ambrogio et al. [121] compared the power consumption of the SPIF process with two setups: a CNC milling machine and a CNC turning machine. A constant power trend was recorded during the forming step for all the tests due to the fact that loads required to deform the material are much lower than the ones required for the normal operation of machining. It was suggested that the forming time is the dominant factor for energy consumption in the SPIF process. Using the same setup, by reducing the forming time from 144s to 12s, the energy consumption can be effectively reduced from 838 kJ to 103 kJ. Also, a proper selection and use of machine setup could lead to further saving of energy consumption.

Bagudanch et al. [122] studied the effects of process parameters on the energy consumption. A series of experiments were conducted by considering sheet material, step down as well as the tool rotation speed while keeping feed rate as constant. Interestingly, it was concluded that the variation of tool rotation speed is the most significant parameter, followed by the material of the workpiece and step-down size. It was explained that the lower rotation speed greatly reduced the friction between the sheet and the tool and also decreased the processing time since the rotation has to be stopped when the tool descends to the next contour for the machine setup. Unfortunately, the

investigated process parameters were only varied at two levels that should be further extended to provide more comprehensive conclusions.

2.4.2.3 Summary

It is well known that ISF technology is advantageous for its flexibility and greater formability. While at the same time, the actual forming process is time-consuming due to the complex tool path and thus leads to higher energy consumption. It is found that forming time is a dominant factor that determines the consumption of energy while associated CO_2 emissions largely depend on the selection of material of the workpiece. However, there is still a lack of comprehensive research on the simultaneous optimization of energy consumption together with other process quality outputs such as geometric accuracy and surface roughness that takes into account the effects of the most relevant process parameters.

2.4.3 Surface finish

As a critical product quality constraint, surface roughness is regarded as a weak point in ISF. It is of great importance to identify the impact of forming parameters on the surface roughness and optimise the surface finish at the production stage.

Hagan and Jeswiet [123] analysed the influence of several forming variables, such as step-down size and spindle speed, on surface roughness in ISF process. The authors found that the surface finish can be viewed as a resultant of large-scale waviness created by the tool path and small-scale roughness induced by large surface strains. With the decrease of the step-down size, the morphology of surfaces transforms from waviness to strict roughness without waviness.

Powers et al. [124] investigated the surface morphology through a SPIF case analysis. The effect of sheet rolling mark direction on surface topology in SPIF was first studied. The results showed that surface roughness R_z is greater with rolling marks perpendicular to the forming orientation. Lasunon et al. [125] assessed the effects of three process parameters on the surface roughness in SPIF by a factorial design. It was concluded that wall angle and step-down size play an important role on the surface roughness, while feed rate has little effect.

Durante et al. [126] described a model for evaluating the roughness in terms of both amplitude and spacing associated with three parameters: the slope angle, the step-down size and the tool radius. The roughness values R_a, R_z, and the mean spacing between profile peaks were evaluated as the output of the models. The prediction showed that a good agreement can be achieved with an error

below 10% compared with experimental values. Hamilton et al. [84] investigated the influences of tool feed rates and spindle rotation at high speeds during forming on the non-contact side roughness (i.e. orange peel effect). A model for the orange peel prediction in SPIF was established, which provided some guidelines for the improvement of external surface quality by choosing desirable process parameters during forming.

Although some research has been performed on the investigation of effects of process parameters on surface roughness and predictive modelling, little research has been focused on the evaluation of overall surface roughness which considers both internal and external surfaces. In addition, the impact of roll mark orientation of metal sheets on surface roughness should be clarified when the surface roughness measurement is carried out along the step down direction.

2.5 Conclusions

A comprehensive review of the current research in ISF technology, including all the major aspects is provided in this chapter. Research contributions and challenges in each aspect are highlighted based on the relevant studies reported in the literature. First, the foregoing literature research has shown that several different methods have been proposed to analyse the deformation mechanism and explain the increased formability in ISF, but an agreement hasn't been reached regarding the role of different deformation modes under various working conditions. Second, in terms of the modelling methods in ISF, the geometrical model is good for thickness prediction but material behaviour are not taken in to account. FE models can be used to clarify the forming characteristics, predict forming defects, and improve the forming process, but the models are computationally inefficient, costly and slow due to complicated contact problems involved in the ISF process. In addition, it is noticed that despite substantial experimental research into the effects of process parameters on forming forces in ISF, accurate and efficient approaches for predicting forming forces are still lacking. Furthermore, a comprehensive understanding of the how process parameters influence the output qualities (e.g. geometric accuracy, surface finish, forming efficiency, etc.) is still essential to clarify the forming process mechanism and thus optimise the process.

This thesis addresses these limitations by providing comprehensive FE models with fine solid elements, which allows a detailed examination of deformation mechanism in ISF considering different deformation modes including stretching, bending and shearing. In particular, an efficient analytical model for forming force prediction in ISF process is proposed and validated through extensive experimental designs. The detailed experimental investigation is also performed to

understand the forming process mechanism and the effects of process parameters on process formability, forming forces, geometric accuracy, forming time and surface roughness. The corresponding methodologies and results will be provided in the following chapters.

Chapter 3 Methodologies

This chapter summarizes the most important methodologies used in this thesis to achieve the research objectives identified in chapter 1. Section 3.1 introduces theoretical approach for the developing of analytical force prediction models based on the findings of deformation mechanism from FE models. In section 3.2, the facilities and the experimental design methods are described. More detailed information is documented in the incorporated papers in chapter 4.

3.1 Forming Force Prediction (Obj.1)

3.1.1 FE modelling for deformation mechanism investigation

This section briefly introduces the finite element modelling methodology used in this thesis for the incremental sheet forming process. More details can be found in **Papers 1 and 2**. Since the ISF process involves continuously changing of localised plastic deformation as well as large material plastic deformation, the simulation must consider high nonlinearity. LS-DYNA is a general-purpose finite element program capable of simulating complex non-linear problems and can solve dynamic problems which have 3D elastic-plastic large deformation using explicit time integration. Therefore, in the present work, the finite element code of LS-DYNA is used to perform the numerical simulation.

3.1.1.1 Simplified FE model

Groove forming processes with different tool sizes and types were simulated in the developed FE models using LS-DYNA software. The general geometry of the sheet was square with dimension of 300 mm × 300 mm and it was meshed into 1.5 mm × 1.5 mm shell elements which are shown in Fig. 21 (only half of the sheet is presented). To simulate the boundary conditions in the forming process, nodes in all edges were constrained in all degrees of freedom with both displacement and rotation. In these FE models, forming tools were considered as rigid bodies and their boundary conditions that should be followed during the process are given by the path shown in Fig. 22. The sheet was assumed to be isotropic and the plastic property was modelled by means of a power law expression. This expression considers the material hardening with an exponential dependence on strain but neglects the effect of both temperature and strain rate. Material parameters were obtained from published work by M. Durante [88]. The friction coefficient was obtained from experimental measurements of both horizontal and vertical forces as presented in Fig.4 in Paper 1. A value of 0.18 has been assessed and been used in the FE models. Sensitivity study of the value of friction

coefficient has also been performed in the initial stage of the development of the FE model and it was found that the setting of coefficient only have limited effect on the predicted horizontal force.

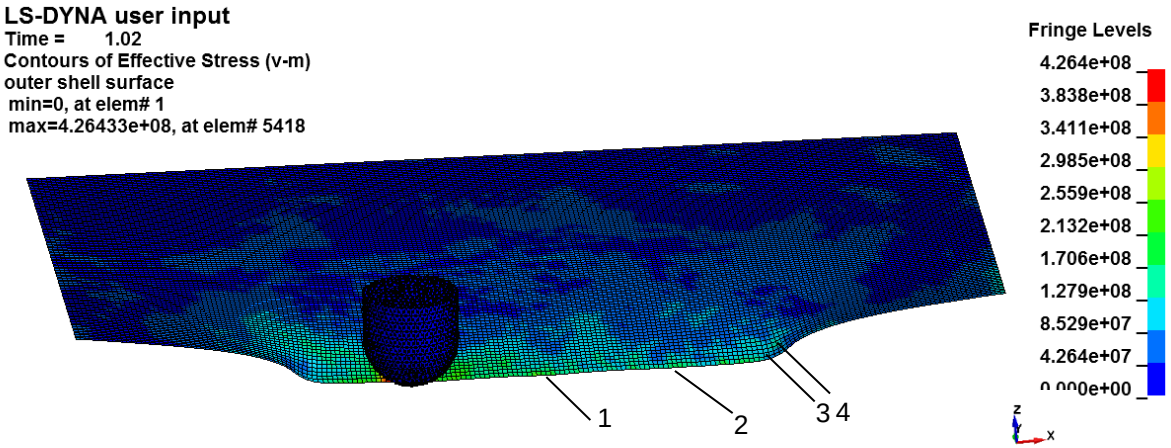

Fig. 21 FE model of the ISF process in LS –DYNA (Reference elements 1-4 marked)

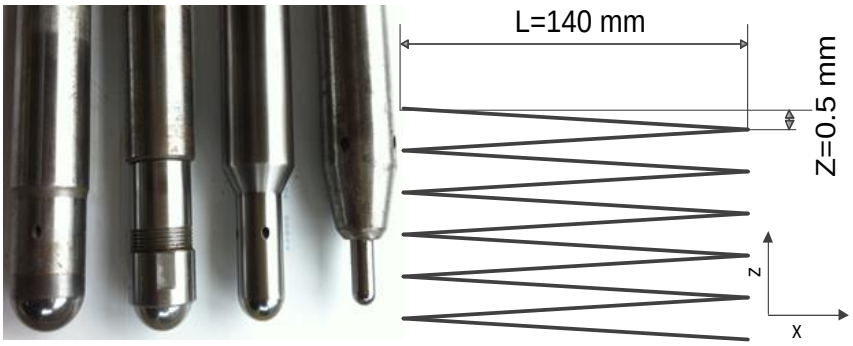

Fig. 22 Four different tools and tool path that were utilised in the experiments

3.1.1.2 Comprehensive FE model

In this comprehensive FE model, the forming tool was also modelled as rigid body and the tool path was predefined using CAM software. As a benchmark study, the forming process of the truncated cone was simulated. During the process, the shape was formed layer by layer with a series of successive contours. To accurately predict the through thickness shear and bending effect of the deformed sheet, the element type of SOLID164 was used in the current model and 5 elements were meshed through the thickness direction. The SOLID164 element is an 8-node brick element and the default one-point integration option was chosen due to savings on computer time and robustness in cases of large deformations. The initial meshing configuration of the metal sheet is shown in Fig. 23 with an enlarged view of the selected small region *d* plotted at the top right corner. Specifically, the sheet was divided into three regions which allow having different meshing of each region. For the region which will be contacting with the tool (region *B*), the elements were arranged with the same size at 1 mm radially and meshed into 400 elements circumferentially which correspond to the size between 0.7 mm to 1.2 mm. Region *A* at the inner base of the cone was meshed freely as the

transition zone towards the centre point of the sheet. For the rest of the sheet out of the contact region, it was meshed with relatively large element size as the deformation in this area is quite small and has little effect on the final results. By using this strategy, the localised deformation in the contact region in both radial and circumferential directions can be captured without much distortion of the elements. As a result, the current meshing is able to increase the localised precision of prediction as well as reduce the computing expenditure. The general geometry of the sheet was square with dimension 300×300 mm and thus it was meshed with 175000 solid elements. In terms of the boundary conditions in the forming process, nodes belong to the four edges of the squared sheet were constrained in all degrees of freedom.

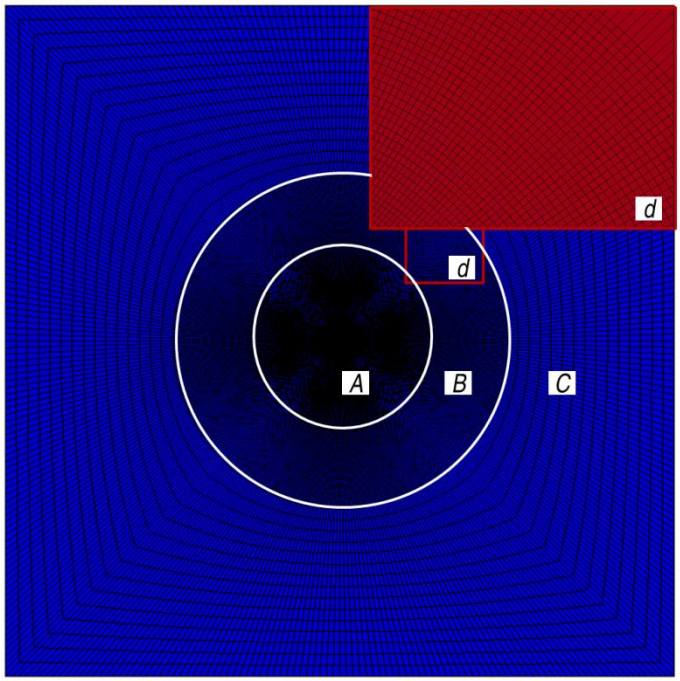

Fig. 23 The initial meshing configuration of the metal sheet with enlarged view at the right top corner

The metal used in the simulation was the aluminium alloy 7075-0 sheet with a thickness of 1.6 mm. It was confirmed from tensile tests that the material can be considered isotropic since deviations of the stress-strain behaviour in different directions (rolling, diagonal and transverse) are small. Therefore, the material could be modelled using Swift's isotropic strain hardening law of $\sigma = K(\varepsilon_0 + \varepsilon)^n$. The detailed mechanical parameters are listed in Table 3. which were determined from previous material tests [21]. Only the data of the stress-strain curve form tensile test before fracture was imported into the LS-DYNA software and the strains beyond the localized point was automatically determined by the LS-DYNA code. In the code, the von Mises (isotropy) yield function was used to determine the plastic flow when the stress is on the yield surface. Based on previous findings, the highest accuracy in FE modelling will be achieved while mixed isotropic–kinematic hardening model of Voce–Ziegler has been selected. But, since this is not the main contribution of this thesis and the limit of the material testing facility, a simple material model was

used in this FE model. In order to improve the simulation efficiency, the virtual forming speed was scaled up by 100 times in which the ratio of the kinetic energy to the total internal energy can be controlled within 1% to ensure a quasi-static forming process.

Table 3. Mechanical properties of Aluminium 7075-O sheets with 1.6 mm thickness

Material	7075-O
Density (t/mm^3)	2.81×10^{-9}
Young's modulus (GPa)	70
Poisson's ratio	0.33
Tensile Yield Strength (MPa)	92
Ultimate Tensile Strength (MPa)	198
Plastic coefficient K	352.58
Hardening exponent n	0.221

3.1.2 Analytical modelling for force prediction

For many metal-working processes, including incremental sheet forming, no exact analytical solutions for the forces to cause unconstrained plastic deformation are available [127]. This is because the exact solutions must be both statically and kinematically admissible which means that the solutions must be geometrically self-consistent as well as satisfying the required stress equilibrium everywhere in the deforming body. To this end, based on previous work by Mirnia and Dariani [128], the upper bound theorem was adopted in the ISF process for force prediction. This theorem states that any estimated load, corresponding to an assumed kinematically admissible displacement field, will be greater than or equal to the real load corresponding to the real displacement field [129]. In this analysis, the strain increments need to satisfy yield criteria and geometric self-consistency but not necessarily satisfy the stress equilibrium. This theorem is based on the principle of maximum work dissipation which states that the real stress field does the most plastic work than any other stress field which conforms to the same yield criterion. Therefore, the estimated force based on the assumed kinematically admissible displacement field by equating the rate of internal energy dissipation to the external forces will be equal to or greater than the actual one. In the analysis, the following assumptions were made: (i) the material is homogeneous and isotropic; (ii) interfaces are frictionless; and (iii) the material is rigid except in the deformation zone. Specifically, the calculation for the prediction of tangential force in a cone-forming process involves the following four steps.

- Define an internal flow field and discretise the deformation zone into smaller regions. A kinematically admissible displacement field of the deformed surface ahead of the forming tool was represented by a series of flow lines with two adjustable parameters M and N.

- Derive the velocity fields for each region from the assumed displacement field based on different plastic deformation conditions.
- Calculate the strain rates and the dissipated power of the forming process under different deformation modes.
- Minimise the dissipated power by varying two parameters in their defined range. Consequently, forming force can be calculated by equating the rate of external work with the rate of internal dissipated power.

Two modules based on different deformation mechanisms (shear and bending with stretching) were included in the proposed model to represent the effects due to the variation of forming parameters. Fig. 24 shows the deformation zone in the ISF process from different viewing aspects. Parameters used for the analytical formulation are defined in Fig. 24 and the similar division of the deformation zone can be found in the published work by [130] and [128]. As presented in the literature review, the model developed by Mirnia and Dariani [128] only considered the dissipated power due to the shear deformation mode and neglected the power caused by bending and stretching. However, the proposed model in this thesis will consider the dissipated power from all the three main deformation modes of shearing, bending and stretching. A kinematically admissible displacement field was assumed for the deformed surface ahead of the forming tool. This deformed surface Zf was represented by a series of flow lines along circumferential direction which can be tailored by adjusting two presupposed parameters M and N.

$$Zf = \begin{Bmatrix} Zf_c(r,\theta) = Z_t & (0 \le \theta \le \theta_c) \\ Zf_t(r,\theta) = S(X) * Z_t & (\theta_c \le \theta \le \theta_t) \\ Zf_s(r,\theta) = S(X) * Z_s & (\theta_t \le \theta \le \theta_s) \end{Bmatrix}. \quad (3.1)$$

Here, Z_t is the geometric function of the tool surface and the boundary position is defined using M and Z_s represents the vertical height of the sheet after the previous pass (refer Fig. 24). $S(X)$ is tentatively designed as two-second order Bezier curves ranging from 0 to 1 which depends on N. More detailed calculation procedure for determining the position of the flow line is given in **Paper 4**. As a result, it is effective to adjust the deformed surface with parameters M and N. However, a velocity discontinuity surface was introduced at the intersecting surface of Zf_t and Zf_s which will result in an extra dissipated power.

The following equations summarized the calculation procedure of dissipated powers due to three different deformation modes and also the velocity discontinuity surface. The dissipated power of the

flow line during the cone forming process based on the shear deformation was integrated using strain rates over the deformed surface as,

$$\dot{w}_f = y_0 \iiint \left(\frac{2}{3}\dot{\varepsilon}_{ij}\dot{\varepsilon}_{ij}\right)^{\frac{1}{2}} dv = \frac{2y_0 t_0}{\sqrt{3}} \iint \left(\dot{\varepsilon}_{\theta z}{}^2 + \dot{\varepsilon}_{rz}{}^2\right)^{\frac{1}{2}} ds, \tag{3.2}$$

The dissipated power due to the discontinuity can be integrated along the discontinuity surface as,

$$\dot{w_{dis}} = \iint k|\Delta v| ds, \tag{3.3}$$

where k is the yield shear stress and related with the average yield strength.

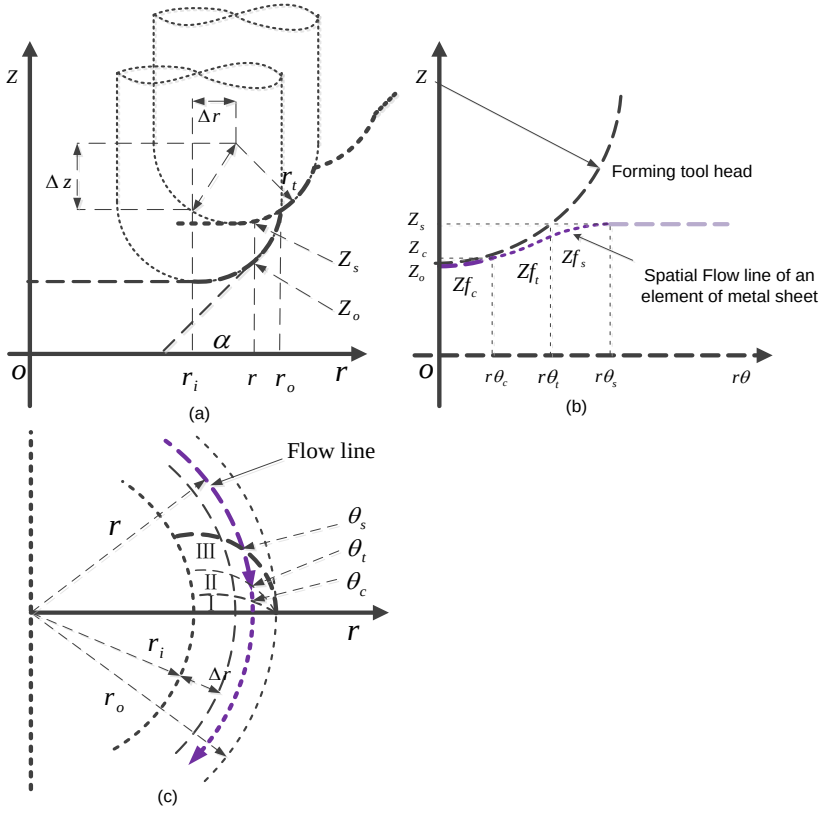

Fig. 24 Deformation zone in the cone forming process: (a) r-z view of the geometrical relations in incremental sheet forming during previous and current path, (b) rθ-z view of a typical flow line for the deformed curved surface along the circumferential direction of the sheet ahead of the tool and (c) r-θ view

Accordingly, the total dissipated power due to shear deformation was obtained as,

$$\dot{w}_{shear} = \dot{w_{dis}} + \dot{w}_f. \tag{3.4}$$

The dissipated power of the deformation zone due to bending and stretching can be determined as,

$$\dot{w}_b = \iint M d\dot{\emptyset}\, ds. \tag{3.5}$$

$$\dot{w}_s = \iint T\varepsilon_a\, \dot{d}l ds = \iint \sigma_a t_0 \varepsilon_a\, \rho_0 d\dot{\emptyset} ds \tag{3.6}$$

where $d\dot{\emptyset}$ is the change rate of the bending angle in the circumferential direction which could be determined by the travelling angle θ in the $\theta - r$ plane (refer [130]). Accordingly, the dissipated power due to bending and stretching is,

$$\dot{w}_{bs} = \dot{w}_b + \dot{w}_s. \tag{3.7}$$

To take into account both shear and bending with stretching deformation, a linear combination of these two modules has been constructed to balance the contribution of shear and bending on the prediction of tangential force,

$$\dot{w}_{total} = \lambda \cdot \min_{0 \le M,N \le 1} \dot{w}_{shear} + (1-\lambda) \cdot \min_{0 \le M,N \le 1} \dot{w}_{bs}. \tag{3.8}$$

The above equation for total dissipated power is a function of two optimizing parameters M and N. By minimising the dissipated power with varying M and N in their defined range (i.e. $0 \le M, N \le 1$), the deformed curved surface for the deformation zone closer to the experiment was obtained. λ is a normalised fraction taking into account parameters of wall angle and step-down size. The purpose of the parameter λ is to weigh the contribution between the shear-based model and the bending-based model and should be varied with different forming configurations. According to the experimental results as well as the mechanics of plastic deformation, an effective way to determine the value of λ can be achieved by,

$$\lambda = \begin{cases} \dfrac{1}{1 + \left(\dfrac{\alpha}{90-\alpha}\right)\left(\dfrac{\Delta z}{1-\Delta z}\right)} & (0 < \Delta z \le 1) \\ 0 & (\Delta z > 1) \end{cases} \tag{3.9}$$

where α and Δz correspond to the algebraic values of the wall angle in degree and step-down size in mm. According to the above equation, the contribution of the shear-based model decreases proportionally with the increase of wall angle and step-down size while the significance of bending and stretching rises with more severe plastic deformation due to larger step-down sizes and higher wall angles. It should be noted that the effect of the sheet thickness on the forming force has been

considered during the calculation of the dissipated power in both sub-models. In particular, it was assumed that the deformation is entirely taken by bending and stretching mode if the step increment is larger than 1 mm. By this modification, the previous model is enhanced for wider working conditions and is also improved in terms of the adaptability that could be further extended for other shapes. Finally, it is reasonably assumed that the rate of plastic work due to the tangential force acting on the forming tool is,

$$\dot{w}_{total} = F_t v_\theta. \tag{3.10}$$

Substituting the average radius of the deformed zone $(r_i + r_o)/2$ to obtain the angular velocity, the tangential force can be expressed as,

$$F_t = \frac{r_i \dot{w}_{total}}{f \cdot (r_i + r_o)/2}. \tag{3.11}$$

where f is the feed rate and r_i and r_o are used to define the deformation zone as shown in Fig. 24.

3.2 Experimental Methodologies for process investigation (Obj.2)

3.2.1 The AMINO DLNC-PC ISF machine

The forming tests were performed on a state-of-the-art machine dedicated for the ISF process designed by AMINO Corporation as shown in Fig. 25. The machine allows mould based forming for a maximum size of 2100 mm×1450 mm×550 mm with a FANUC controller for precise control. The movement of the two horizontal axes (*X* and *Y*) can have a maximum speed of 60 m/min with a repeatability of ± 0.05 mm. The vertical (*Z*) axis is driven by an AC servo motor with the power of 1 kW that allows a maximum acting force of 3 kN. Hemispherical tools with the diameters ranging from 10 mm to 30 mm were used to deform the material. The tip of each tool is tungsten carbide and the body is made of K110 steel which was hardened and tempered to HRC60. The forming tool was set not to rotate in this study for all the tests. The sheet material used in the present study was aluminium alloy 7075-O sheet with different thickness and was cut into 300 mm × 300 mm sized samples.

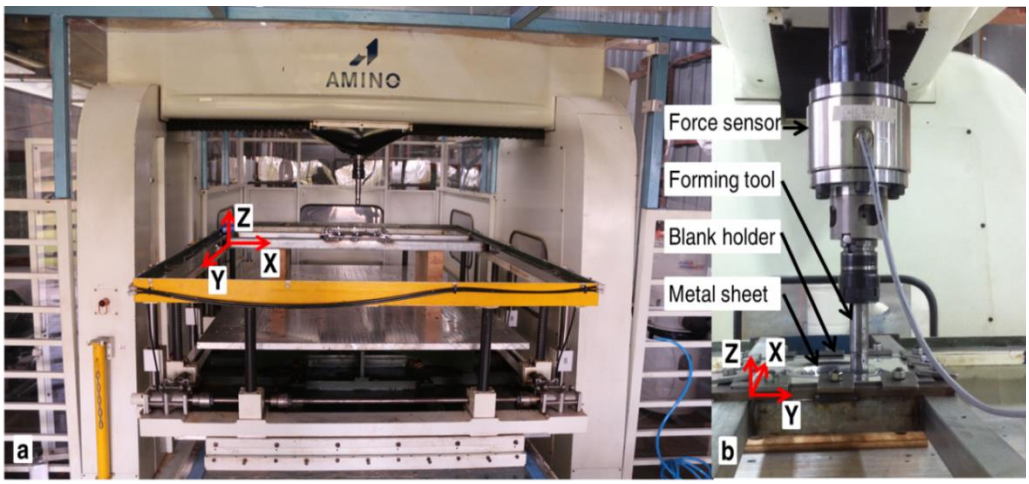

Fig. 25 The AMINO incremental forming machine and the implemented force sensor: (a) front view; (b) side view

3.2.2 Force measurement

3.2.2.1 The strain gauge

In the early stage of the present work, three full Wheatstone bridges configured by four strain gauges have been designed and mounted on a hemispherical tool. The three bridges were designed to measure the three orthogonal forces: two bending directions (F_x and F_y), and one axial direction (F_z) respectively. This configuration can also reject axial strain and compensate the effect of temperature. Those strain gauges were calibrated twice in all three directions by applying a series of known forces. The calibrated system showed a linear relation between strain and output voltage and was applied to record the forming force at the early stage of the research.

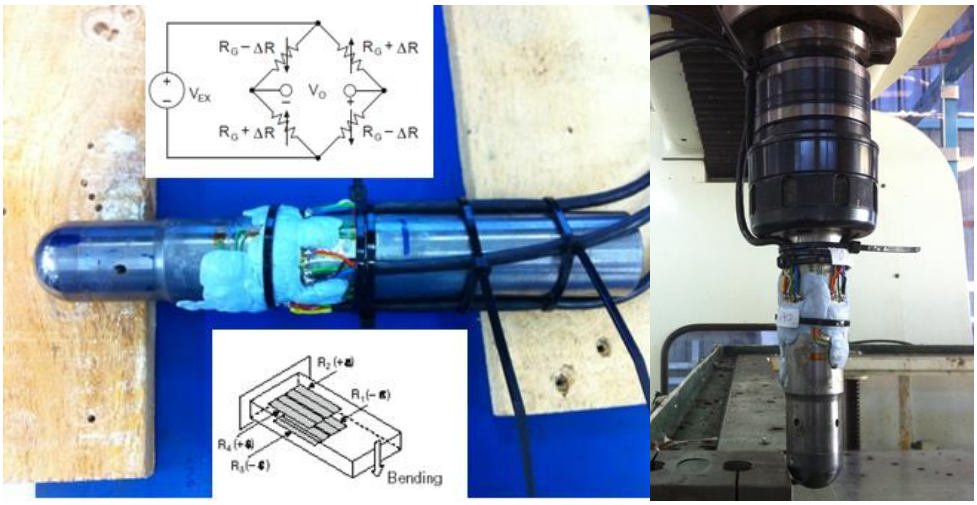

Fig. 26 Connection and mounting of strain gauges

3.2.2.2 The load cell

As shown in Fig. 25 (b), a multiple-axis force sensor K6D175-50 was used to measure the forces between the tool and work piece during the forming process. To alleviate the possible deflection

from other structures, the force sensor was mounted directly between the spindle and the tool holder. The force sensor was manufactured by ME-Meßsysteme GmbH which allows measuring the three orthogonal forces and three torque components at the same time. The 6-channel output signals were recorded with two NI 9237 data loggers and post-processed with the LabVIEW SignalExpress software. This load cell allows replacing the forming tool with different sizes and types.

3.2.3 Tensile test machine

Material property tests were performed to acquire the essential parameters of the aluminium sheets for both FE simulation and analytical modelling. Standard tensile tests were conducted using an INSTRON 5584 universal testing machine equipped with an extensometer with a gauge length of 50 mm (see Fig. 27). Stress and strain can be computed from measurements in a tension test and a stress-strain curve can be approximated by a power-law expression,

$$\sigma = K\varepsilon^n \tag{3.12}$$

From this test, the value of Young's modulus, yield strength, ultimate tensile strength and ultimate elongation can be obtained. These parameters will be used to establish the material model in FE simulation and provide vital information for the judgement and analysis of plastic deformation.

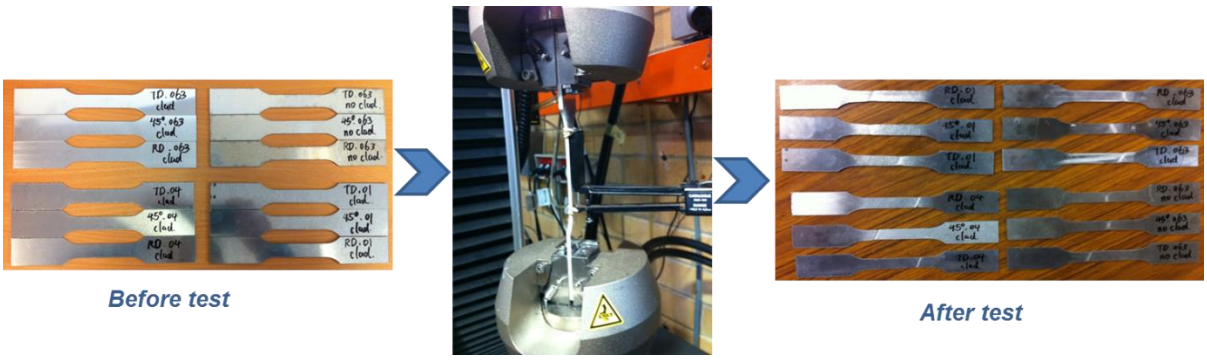

Fig. 27 INSTRON 5584-Standard tensile test machine and samples

3.2.4 Experimental design

3.2.4.1 Taguchi experimental design

The Taguchi method was utilized to design ISF experiments for investigation of the effects of process parameters on forming time. The Taguchi method has been widely used for experiment design which allows reducing the number of tests for optimising purpose through robust design of experiments. The overall objective of the method is to produce high quality product at low cost to the manufacturer. The experimental design proposed by Taguchi involves orthogonal arrays to organize the parameters affecting the process and to define the upper and lower limits of the parameters. Instead of having to conduct all possible combinations like the factorial design, the

Taguchi method tests pairs of combinations. This allows for the collection of the necessary data to determine the most influential factors with a minimum amount of experimentation, thus saving time and resource [131]. The general design steps involved in the Taguchi method in this thesis are as follows:

- Define the process objective or a target value for a performance measure of the process. Forming time was chosen as the target in this design. The deviation in the performance characteristic from the target value was used to define the loss function for the process.
- Determine the design parameters affecting the process. The number of levels that the parameters should be varied must be specified. In this study, four parameters of step over, feed rate, sheet thickness and tool diameter were selected with varying at three levels.
- Create orthogonal arrays for the parameter design indicating the number and conditions for each experiment. A total of 9 experiments have been designed in this case.
- Conduct the experiments indicated in the completed array to collect experimental results.
- Complete data analysis to determine the effect of the different parameters on the performance measure.

3.2.4.2 Box-Behnken design

Box-Behnken design allows efficient estimation of the first- and second-order coefficients between the response and selected factors. Since Box-Behnken designs have fewer design points, they are less expensive to run than other designs with the same number of factors. Hence, a Box-Behnken experimental design was conducted to evaluate the effects of four process parameters (step down, sheet thickness, tool diameter and wall angle) on energy consumption and geometric accuracy. The steps in this research work for the experimental investigation include the following [132]:

- Identifying the important process control variable. In this case, based on previous experimental work, four process parameters of step down, sheet thickness, tool diameter and wall angle were selected as the most relevant factors.
- Finding the upper and lower limits of the control variables. Three levels of each factor were considered and their upper and lower values are set as listed in Table 4.
- Development of the design matrix using Box-Behnken design and conducting the corresponding experiments. A total of 27 experimental tests were designed in the presented study.

Table 4. Process parameters and their levels

Symbols	Factors	Levels			Units
		-1	0	1	

A	Step down	0.5	1.0	2.0	mm
B	Sheet thickness	1.27	1.80	2.54	mm
C	Tool diameter	10	20	30	mm
D	Wall angle	50	60	70	degree

3.2.5 Laser scanner

To evaluate the geometric accuracy, the 3D geometry of formed parts was measured using a noncontact 3D digitiser (VIVID 9i), as shown in Fig. 28. The scanning accuracy is within ±0.05 mm, which is accurate enough for the ISF shape measurement. The VIVID 9i uses the light-stripe method to emit a horizontal stripe light through a cylindrical lens to the object. The reflected light from the object is received by the CCD, and then converted by triangulation into distance information. This process is repeated by scanning the stripe light vertically on the object surface using a Galvano mirror, to obtain a 3D image data of the object. The software of GEOMAGIC Qualify was used to produce 3D geometry data of the scanned shape and analyse the dimensional error between deformed test parts and designed CAD models. Specifically, both produced and designed profiles were given in large sets of points in the same Cartesian coordinate system. In this work, the cross-sectional profile through the pyramid centre and perpendicular to the edges was used to evaluate the geometric accuracy. The deviation in vertical direction (Z) between the designed and fabricated profiles was calculated as the global geometric error for subsequent investigation.

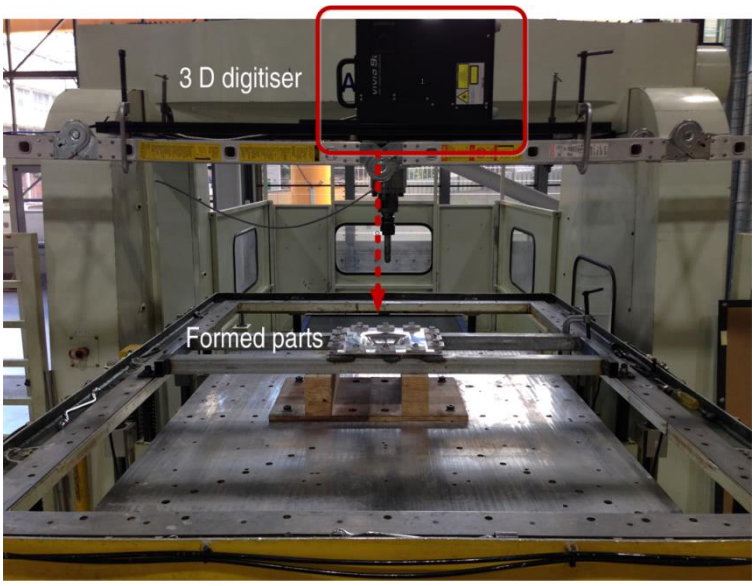

Fig. 28 Set up of the laser scanner

3.2.6 Profilometer

The surface roughness of the formed parts was measured using a portable, self-contained instrument (Taylor-Hobson Surtronic 3+ Profilometer) as shown in Fig. 29. The measurement process was

controlled from a wipe-clean membrane touch key panel, via ‘walk through’ menu selections. This device can be used for horizontal, vertical or inclined surfaces. According to the ISO standard, non-periodic roughness profile evaluation can be conducted with a high-pass Gaussian filter. For the measurement work in this thesis, the sampling length, evaluation length and calculated resolution were set to be 0.8 mm, 4 mm and 0.01 μm, respectively.

Fig. 29 Taylor-Hobson Surtronic 3+ Profilometer

The methodologies for both FE and analytical modelling are firstly provided and then the facilities and experimental design methods are also introduced in this chapter. The associated results are presented in the next chapter.

Chapter 4 Results and Papers

This chapter first provides an overview of the main results that have been achieved for this PhD project, mainly grouped into two aspects according to the proposed objectives. Then, the detailed results are presented as a collection of published/submitted papers.

4.1 Summary of Results for Forming Force Prediction (Obj. 1)

The first part of objective 1of this thesis has been focused on the investigation of the deformation mechanism in ISF which is the basis for developing, the second part, the force prediction model as well as further improving the forming process.

4.1.1 Deformation mechanism investigation

Two types of FE models have been established. **(i) Simplified FE model (Paper 1).** The aim of these FE models is to study the effects of tool type and size on strain behaviour and thickness distribution of the material during the groove forming process. The simulation comparison suggested that the level of strain decreases as the tool size increases. This was explained by the increase of the contact area and deformation zone with larger tools. By checking the strain values of four selected elements, it can be clearly noticed that the strain values of the elements in the middle of the groove keep the same level at each step and the lowest strain values always take place at the very end of the groove. Moreover, it was found that the maximum effective strain occurs before the corner of the groove with a distance of 6 mm. This was confirmed by experimental observation that the crack firstly occurs just prior to the end of the groove. In terms of thickness distribution after forming, it was found that the thickness is greater in the middle and smaller near the ends of the path which can explain why the failure always occurs near the ends. At the same forming depth, the thickness of the groove formed by the 20 mm tool was thinner than that formed by the 30 mm tool, which suggested that failure should occur earlier for the smaller tool. These predicted results for strain and thickness were well corroborated by the experimental tests in this thesis. **(ii) Comprehensive FE model (Paper 2).** A FE model with fine solid elements for truncated cone-forming process has been established to investigate the deformation mechanism. This model allows a quantitative study of the deformation behaviour of stretching, bending and shearing during the ISF process. First, the FE model was verified with experimental work in terms of forming forces. Some of the FE results were summarised in Fig. 30 which compares the strain components for upper, middle and lower elements at section A at the forming depth of 20 mm. It was confirmed that the deformation behaviour in the ISF process is a combination of stretching, bending and shearing. In

addition, the contribution of each strain component to the effective plastic strain during the cone-forming process was discussed. Specifically, the direct strain perpendicular to the tool motion is the major deformation mode in the cone-forming process. This direct strain could be accumulated to a large value while strain in the forming direction only alternates at smaller values. Strain values at both surfaces depend on the bending direction of the sheet. For the material around the bottom of the cone, larger strain values were obtained at the lower surface which is consistent with the experimental observation that cracks tend to occur at the lower surface. Shear strain in the forming direction (ε_{23}) prevails greatly among the three shear components and the maximum value occurred in the middle of the sheet. It was also found that the in-plane shear strain is not negligible, especially at the upper surface. Finally, in the investigated range, larger step-down in the first pass is recommended for the sake of reducing the effective strain and hence enhancing formability. Subsequently, smaller step-down values can be used to improve the geometric accuracy and surface finish. The results highlight that the ISF deformation process is typically a combination of stretching, bending and shearing.

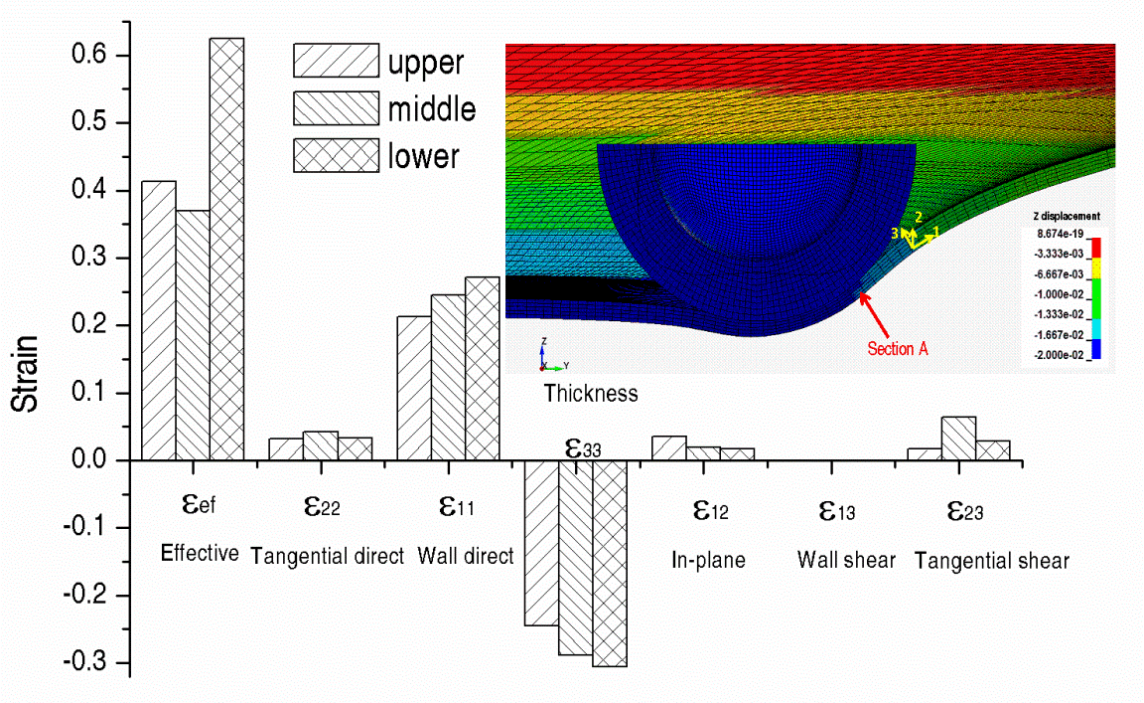

Fig. 30 Strain components for upper, middle and lower elements at section A at the forming depth of 20 mm (**Paper 2**)

4.1.2 Analytical modelling of force prediction

Based on the understanding of the deformation mechanism during the forming process, an efficient analytical model for tangential force prediction has been developed. **(i) Establishment of the analytical model (Papers 3 and 4).** Initially, based on the upper-bound theory, two analytical sub-models have been developed separately to consider both shear and bending with stretching. A deformation zone for the local deformed area ahead of the forming tool has been assumed and

represented by a series of flow lines based on previous research [128]. The shape of the flow line can be adjusted by tuning two parameters *M* and *N* to minimise the dissipated power. In each model, the forming force was calculated by equating the rate of external work with the rate of internal dissipated power based on the assumed deformation mode. The results from each model were analysed separately. The sub-model based on shear deformation can provide good agreement with experimental results for the cases with small step-down sizes (below 0.5 mm). However, with the increase of the step down or wall angle, the difference between analytical and experimental results differs significantly. The predicted forces from the sub-model based on bending with shearing mechanics were also compared with measured results. It was noticed that the predicted tangential values are more accurate for larger step-down sizes. However, the bending model alone cannot accurately predict the force trend across the whole range of wall angles. Therefore, a linear combination of these two modules has been constructed to balance the contribution of shear and bending with stretching on the prediction of tangential force. **(ii) Validation of the force prediction model and its extension (Paper 5).** The proposed force prediction model was validated through a comprehensive experimental campaign with two geometric shapes (truncated cone and truncated pyramid) and various process parameters (step down, wall angle, tool radius and thickness). The measured global forces were firstly converted to the tangential forces and then the steady values in the second phase of the forming process were used for comparisons. In both cases, the predicted forces show good agreements with the experimental results. The validation results with truncated cone shapes are presented in Fig. 31. The prediction provides an accurate result for all the tests except a reasonable deviation (85 N with an error of 12%) for the case with step down of 2 mm. Although the proposed model underestimates tangential force (F_t) slightly with wall angles smaller than 60˚ whereas overestimates it at larger wall angles, the average prediction error can be achieved within 5%. In terms of the effect of tool diameter, the proposed model can correctly reflect the trend of the tangential force with the variation of tool diameter with a deviation less than approximately 10%. Additionally, the proposed analytical model was verified with the truncated pyramid shape. It was found that the relative errors between predicted and measured F_t are less than 15% in most of the cases. Finally, the analytical model was extended to capture the changing of local curvature and wall angle during the forming to address more complex shapes. The truncated ellipsoidal cup was selected as the target shape which has local curvature and wall angle variations in each contour. The extended model is able to predict reasonably accurate tangential force variation in each contour compared to experiments.

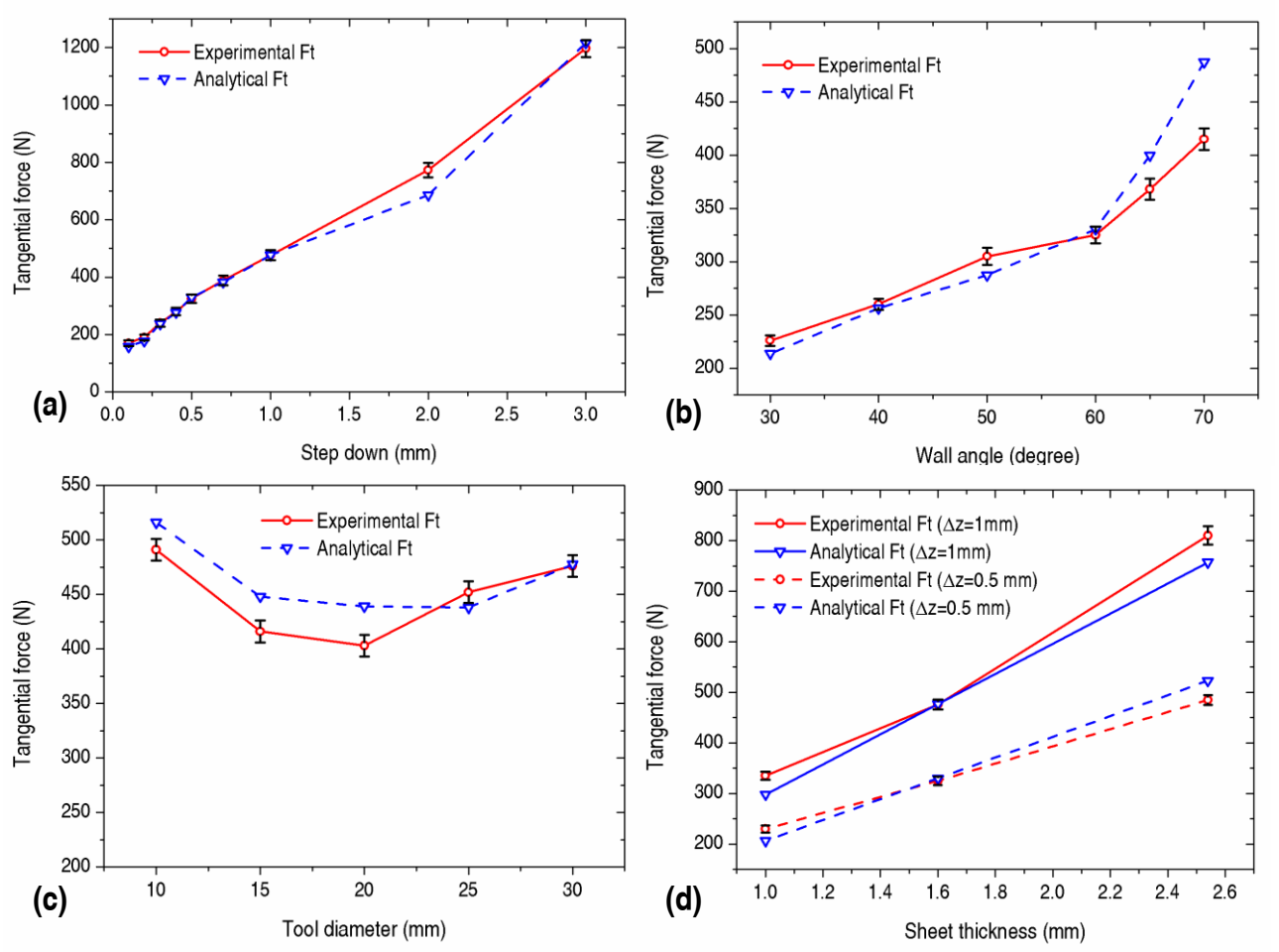

Fig. 31 Comparison between predicted and measured tangential forces for cone-forming process by varying process parameters: (a) step down, (b) wall angle, (c) tool diameter and (d) sheet thickness (**Paper 5**)

4.2 Summary of Results for Process Investigation (Obj. 2)

The second objective of this thesis is the process investigation and improvement of forming forces, geometric accuracy, forming efficiency and surface roughness. **(i) Forming forces (Papers 1, 5 and 6).** First, forming forces have been measured by means of strain gauges during the groove test. Vertical and horizontal forces presented sharper increases at the end of each travel due to the increase of contact area and the impact of the side wall. Forces only showed a slightly growing trend over the central area of the groove. This proved that only localized deformation occurred in the process and thus it is possible to form large and complex shapes without higher forces. Then, a 6-axis load cell was implemented to record the trends of forming forces considering the influence of different wall angles, sheet thicknesses, step-down sizes, tool radius, tool-path types and sheet orientation. It was concluded that the overall trend for all cases may be attributed to the bending effect of the sheet in the early phase of the process and the combined effects of sheet thinning and strain hardening in the second stage of the process. It was observed that the resultant peak forces increase with the increase of wall angle, sheet thickness and step-down size. The slope of force

curve after the peak value can be seen as a forming failure predictor. The influence of sheet orientations on the forming force was first considered in incremental forming. Results have shown that the vertical force was found to be smaller in the sheet orientation 45˚ compared with that in the sheet orientation 0˚ due to the smaller strain hardening exponents in diagonal directions. Particular attention has been paid to the relationship between converted tangential forces and forming parameters for the validation of the analytical model. Steady tangential forces during the second stage of the process demonstrate a growing trend with the increase of step-down size and wall angle. However, the steady tangential forces vary in a concave manner with the variation of tool diameter from 10 to 30 mm with a minimum occurring between 20-25mm. The experimental results also suggested that the increase of tangential force is linearly proportional to the increase of sheet thickness. **(ii) Geometric accuracy (Papers 7 and 8).** A study on the effect of step-down size on geometric accuracy was implemented. It was shown that step-down size can significantly affect the geometric accuracy. Specifically, the geometric accuracy increases when the step-down size is decreased. However, too small a step-down size should also be avoided with regard to the formability as well as forming time. It was clearly suggested that there is an optimum value of step depth in the ISF tool path design; for instance 0.7 mm in this case. A trade-off among geometric accuracy, surface quality, formability and forming time should be made in the design and control of tool paths, which motivates the further research on the design of an advanced ISF control system. Moreover, the geometric accuracy defined as vertical deviations between designed and formed parts has been empirically predicted by quadratic equations giving the influence of the most influential forming parameters. It was concluded that the geometric quality is largely determined by the quadratic effect of wall angle, the linear effect of sheet thickness and the interaction effect of thickness and step down. Decreasing the step-down size was found to be helpful for improving the geometric accuracy. **(iii) Forming efficiency (Papers 7 and 9).** Design of experiments (DOE) together with the Taguchi method was used to investigate the effects of process parameters (step over, feed rate, sheet thickness and tool diameter) on forming time. It was concluded that the most significant process parameter influencing forming time is the step over (spiral tool path) followed by the feed rate. The sheet thickness and tool diameter have little effect on forming time. Furthermore, a Box-Behnken design of 27 tests that considers four factors at three levels was performed. The deformation energy during the forming process for those tests was calculated based on measured forming forces. It was found that the energy consumption heavily depends on the sheet thickness because of higher plastic energy required to deform the material. Increasing step-down size with a limited range as well as decreasing the wall angle is effective to reduce the energy consumption. Finally, the optimal combination of process parameters for simultaneous minimisation of both deformation energy and geometric error has been studied and are shown in Fig.

32 at the vertical lines. A composite desirability of 0.911 can be achieved under the working condition with high step down of 2 mm, low sheet thickness of 1.27 mm, high tool diameter of 30 mm and large wall angle of 70˚. The corresponding deformation energy and global geometric error were predicted to be 2459 J and 0.98 mm, respectively. **(iv) Surface roughness (Papers 1 and 10).** In the groove forming test, the surface topography of parts formed by the hemispherical and ball tools have been scanned by SEM. The result showed that a rolling contact condition causes less local damage and scratching of the surface. Furthermore, the effects of process parameters (step down, sheet thickness, tool diameter and feed rate) on surface roughness have been studied using the design of experiments (DOE) together with response surface methodology (RSM). An empirical model has been developed to predict the overall roughness (tool-sheet non-contact surface and contact surface) of a part formed by ISF. It was found that sheet thickness has the most influential effect on overall surface roughness followed by the step down. An optimal experimental condition was also obtained to achieve a minimum overall surface roughness within the pre-defined range of parameters.

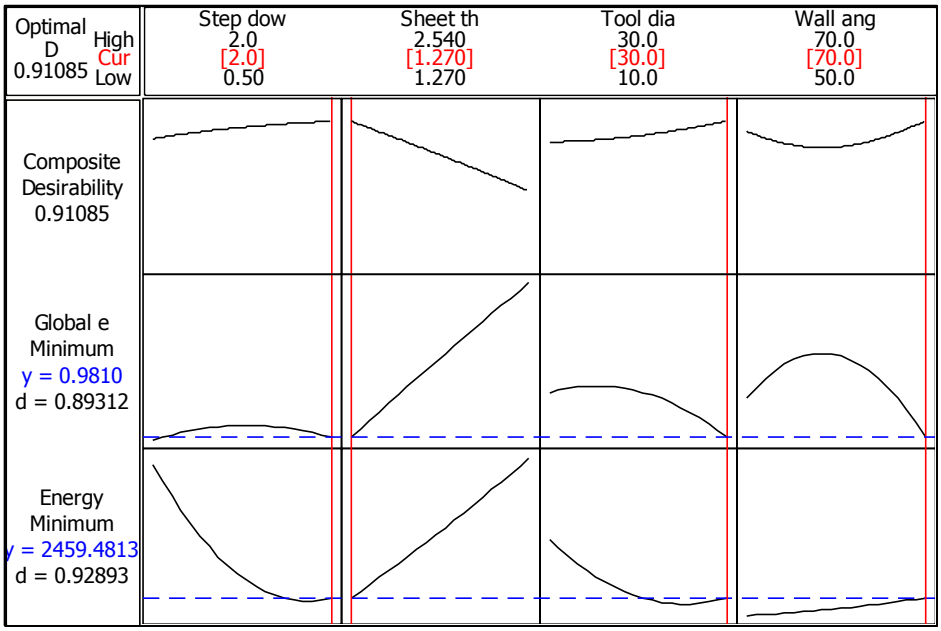

Fig. 32 Multi-response optimisation for both deformation energy and global geometric error (optimal parameters are indicated with vertical lines) (**Paper 7**)

4.3 The Papers

Paper 1

Simulation and experimental observations of effect of different contact interfaces on the incremental sheet forming process

Li, Y.L., Liu, Z.B., Daniel, W. J. T. and Meehan, P. A.

Materials and Manufacturing Processes

2014, Volume: 29, Pages: 121-128.

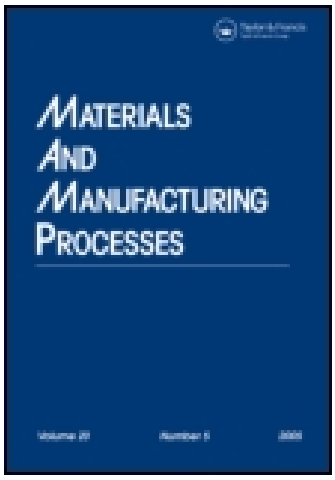

Materials and Manufacturing Processes
Publication details, including instructions for authors and subscription information:
http://www.tandfonline.com/loi/lmmp20

Simulation and Experimental Observations of Effect of Different Contact Interfaces on the Incremental Sheet Forming Process

Yanle Li [a] , Zhaobing Liu [a] , W.J.T.(Bill) Daniel [a] & P. A. Meehan [a]
[a] School of Mechanical & Mining Engineering , The University of Queensland , St Lucia , Brisbane , Australia
Accepted author version posted online: 29 Oct 2013.Published online: 04 Mar 2014.

To cite this article: Yanle Li , Zhaobing Liu , W.J.T.(Bill) Daniel & P. A. Meehan (2014) Simulation and Experimental Observations of Effect of Different Contact Interfaces on the Incremental Sheet Forming Process, Materials and Manufacturing Processes, 29:2, 121-128, DOI: 10.1080/10426914.2013.822977

To link to this article: http://dx.doi.org/10.1080/10426914.2013.822977

Materials and Manufacturing Processes, 29: 121–128, 2014

ISSN: 1042-6914 print/1532-2475 online
DOI: 10.1080/10426914.2013.822977

Taylor & Francis
Taylor & Francis Group

Simulation and Experimental Observations of Effect of Different Contact Interfaces on the Incremental Sheet Forming Process

YANLE LI, ZHAOBING LIU, W.J.T. (BILL) DANIEL, AND P.A. MEEHAN

School of Mechanical & Mining Engineering, The University of Queensland, St Lucia, Brisbane, Australia

Incremental sheet forming (ISF) is a promising forming process perfectly suitable for manufacturing customized products with large plastic deformation by using a simple moving tool. Up to now, however, the effects of contact conditions at the sheet interface are not well understood. The aim of this work is to study the effect of tool type and size on the formability and surface integrity during the forming process. Experimental tests were carried out on aluminum sheets of 7075-O to create a straight groove with four different tools (ϕ 30, ϕ 25.4, ϕ 20 and ϕ 10 mm). One tool tip was fitted with a roller ball (ϕ 25.4 mm) while the other three were sliding tips. The contact force, friction and failure depth were evaluated. A finite element (FE) model of the process was set up in an explicit code LS-DYNA and the strain behavior and thickness distribution with different tools were evaluated and compared with the experimental results. This study provides important insights into the relatively high formability observed in the ISF process. Microscopic observations of the surface topography revealed that a rolling tool tip produced better surface integrity as compared with a sliding tool tip, wherein, distinct scratch patterns in the tool traverse direction were evident.

Keywords Deformation; Forces; Forming; Strain; Stresses.

INTRODUCTION

Incremental sheet forming (ISF) is a promising manufacturing process in which flat metal sheets are gradually formed into 3D shapes using a generic tool stylus only. By using this process, useable parts can be formed directly from computer-aided design (CAD) data with a minimum of specialized tooling; therefore, it has economic benefits for rapid prototyping production and for small quantity applications [1–3].

Over recent years, different kinds of studies have been conducted [2, 4–9] with emphasis on understanding, assessing and improving the formability in this forming process. Among them, straight groove tests have been performed by Kim and Park [10] and suggested as an appropriate method to evaluate the effects of process parameters on the formability for aluminum sheet. In this forming test, two characteristics of deformation can be achieved [10]. One is the deformation condition. Biaxial stretching deformation takes place at the starting and ending points of the straight line when the tool moves horizontally. As the forming depth increases, the deformation turns more into biaxial stretching. On the contrary, plane-strain stretching deformation occurs between the starting and ending points. Another important characteristic of ISF is the higher formability achieved compared with other conventional sheet forming processes. As for deformation mechanics of ISF, stretching rather than vertical shearing appears to be the dominant mode of deformation in ISF according to recent published work by Silva [11] and Allwood [12]. Failure mechanics in ISF [13] were revisited recently and a much deeper insight on the influence of tool radius led to the proposal of a new understanding and assessing on formability limits and formation process of fracture. Minutolo [14], working on force analysis in the groove test, found that using a tool with a bigger diameter and higher drawing depth, higher forming forces and a different typology of failure can be observed. However, comparison between the results using ball (rolling) and hemispherical (sliding) tools were not conducted in this article. Kim [10] concluded that the ball tool is more effective than the hemispherical head tool in terms of formability by simply judging the value of ($\varepsilon_{major}+\varepsilon_{minor}$) [4] after deformation, without comparing the failure depth of two kinds of tools. Durante [15] and Hussain [16], working on the effect of tool/sheet contact conditions on the surface finish of the product, found that the lowest levels of surface roughness were obtained with sphere/sheet contact. Still, surface topography of the forming surface needs to be studied to deepen the knowledge in the effect of different contact conditions on this innovative sheet forming process.

In the present paper, the test to form a straight groove has been carried out and the effect of tool size, tool type and friction between tool and sheet was investigated. One of the few state-of-the-art ISF machines designed by Amino Corporation that allows mold based forming for a maximum

Received February 22, 2013; Accepted June 26, 2013

Address correspondence to Yanle Li, School of Mechanical & Mining Engineering, The University of Queensland, St Lucia, Brisbane, QLD 4072, Australia; E-mail: yanle.li@uq.edu.au.

Color versions of one or more of the figures in the article can be found online at www.tandfonline.com/lmmp.

size 2100 mm × 1450 mm × 550 mm with greater control and quality was used to conduct the forming process. In terms of the sliding conditions, three hemispherical head tools, 30 mm, 20 mm and 10 mm in diameter, have been used. From these experimental tests, the influence of tool sizes on the surface topography and on the value of the failure can be analyzed and revealed. In addition, some failure cases during the process are analyzed to provide experimental evidence on fracture forming limits. A FE model has also been created and utilized to analyze the strain behavior for better understanding the deformation mechanics.

Experimentation and simulation methods

Experiment Setup

The groove forming tests have been performed on a state-of-the-art machine designed dedicated for the ISF process by Amino Corporation which can be numerical controlled by a controller provided by FANUC corporation. Fig. 1 shows a photograph of an experimental test.

Two types of tools; a ball tool and hemispherical head tool as pictured in Fig. 2, have been used in the experiment to produce four different contact interfaces between tool and workpiece. Among them, a ball, with a diameter of 25.4 mm, attached to the end of the ball tool can rotate freely. For the hemispherical tool, the tip is tungsten carbide and the body is made of K110 steel which was hardened and tempered to HRC60. The material used in the present study was aluminum 7075-O sheet of 300 mm × 300 mm in size and 1.016 mm in thickness. Alloy 7075 was one of the most successful Al–Zn–Mg–Cu alloys with high strength and good stress-corrosion cracking resistance and has been widely used for aerospace applications.

In the groove test, metal sheets were fixed along their edges in a special designed frame which mounted on the forming table of the machine; the tool moved back and forth

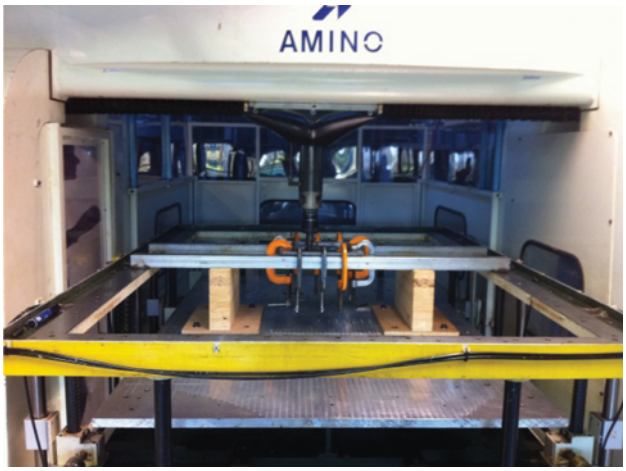

Figure 1.—Incremental sheet forming on Amino machine.

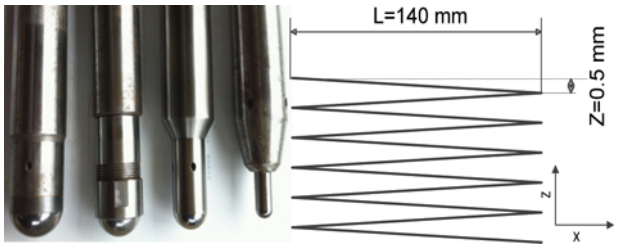

Figure 2.—Four different tools and tool path that were utilized in the experiments.

along a 140 mm long straight path (shown in Fig. 2) with a gradual step down of 0.5 mm in vertical position until a crack was observed. For every test, a feed rate of 1000 mm/min has been set out and a lubricant has been sprayed on the plate to reduce the friction coefficient between tool and sheet surfaces. More detailed configurations for the experimental parameters can be found in Table 1.

Finite Element (FE) Model

By comparing different simulation package and performance [17, 18], DYNA3D, a dynamic explicit FE code, is chosen to simulate the drawing process. It can accurately solve dynamic problems which have 3D elastic–plastic large deformation using explicit time integration. Due to the complexity of the ISF simulation, mass scaling and increasing working speed was essential to reduce computing time with insignificant influence on the simulation results.

The general geometry of the sheet is square with dimension 300 mm × 300 mm and it is meshed into 1.5 mm × 1.5 mm elements which are shown in Fig. 3 (only half of the sheet is presented). To simulate the boundary conditions in the forming process, nodes in all edges are constrained with both displacement and rotation in all degrees of freedom. In the FE model, forming tools are considered as rigid bodies and their boundary conditions that should be followed during the process are given by the path shown in Fig. 2. In the presented FE model, the sheet behavior is assumed to be isotropic and the plastic property is modeled by means of a power law expression. This expression considered the material hardening with an exponential dependence on strain but neglected the effect of both temperature and strain rate to simplify the model. Material parameters were obtained from the work by M. Durante [19] which are shown in Table 2. From our

Table 1.—Experimental parameters design for groove test.

Part No.	Tool size (mm)	Sheet thickness (mm)	Groove length (mm)	Speed (mm/min)
1	30	1.016	140	1000
2	20	1.016	140	1000
3	10	1.016	140	1000
4	25.4(ball)	1.016	140	1000

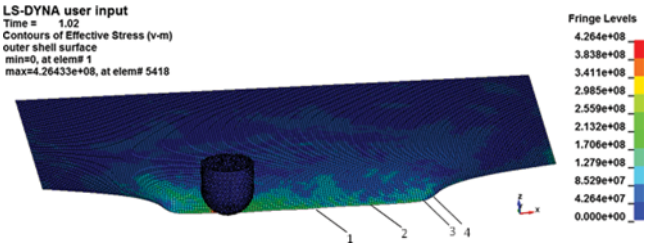

FIGURE 3.—FE model of the ISF process in LS-DYNA. Reference elements 1–4 marked.

experimental work, the friction at the contact surface between tool head and sheet has been assessed and analyzed with a value of 0.18. This value has been used in this FE model (see Fig. 4).

EXPERIMENTATION AND SIMULATION RESULTS

Force Measurement

To better understand the contact mechanics and predict the occurrence of failure, the forces between tool and workpiece have been measured continuously over time during the process. There are several ways to capture the forming force, such as the cantilever sensor designed by Jeswiet [20] and force dynamometer used by Duflou [21]. In the present work, three full Wheatstone bridges have been designed and mounted on the 30 mm hemispherical tool. Each bridge is configured by four strain gauges and designed to measure one of the three orthogonal forces: two bending directions, and one axial direction. Before taking any measurement, the strain gauges were calibrated twice in all three directions by applying a known force to get an accurate result. The calibrated system shows a rather linear relation between strain and output voltage.

The forces measured with this system shown in Fig. 4 are for a 1.016 mm thick 7075-O aluminum sheet. In this test, a groove was formed until it was 25 mm deep when fracture of the aluminum sheet occurred. It can be seen that both vertical and horizontal components experience a sharper increase at the end of each travel and the maximum forces encountered are around $Fv = 2700$ N in the vertical direction and $F_h = 1800$ N in the horizontal direction. These sharper increases are likely due to three main reasons; the increase of the contact area at the end of the groove, the dynamic impact of the side wall and also the large acceleration of the forming tool caused by the sudden change of moving direction. For the steps (vertical depth from 15 mm to 25 mm where failure occurs) which were presented in Fig. 4, only a slight increase from 800 N to 1000 N for the vertical and from 150 N to 200 N for the horizontal component can be found for the nearly steady trend recorded in the middle of each travel. Evaluation of friction coefficients is conducted by calculating the absolute value of the ratios between horizontal and vertical components in the central area of the specimens, which has been widely used by Durante [19] and Hamilton [22]. According to Fig. 4, the absolute value of the ratios shows a slightly growing tendency in the middle area of the groove caused by the continual increase of the groove depth which requires more forces to stretch the sheet during each travel. An average value of 0.18 has been calculated as the average friction coefficient.

TABLE 2.—Mechanical properties for 7075-O aluminum sheet.

Parameters	Value
Sheet thickness (mm)	1.016
Young's modulus (GPa)	75
Yield strength (MPa)	100
Ultimate tensile strength (MPa)	200
Poisson's ratio	0.33
Plastic property	$\sigma = 330\varepsilon^{0.19}$

Failure Depth

Hemispherical head tools of three sizes were used: 10, 20 and 30 mm in diameter. We can obviously see from Fig. 5 that the failure depth is higher with an increase in tool diameter. More specifically, cracking occurs when the forming depth was 16, 21.5 and 25 mm for the tool diameters of 10, 20 and 30 mm with rolling direction (RD), respectively. It is worth noting that all the cracks first occurred near the end of each travelling path: this is due to the fact that these are the regions where the highest amount of deformation, straining and thinning will take place. It appears that there are linear relations between these failure depths and tool diameters in the test coverage. It can be clearly concluded from the

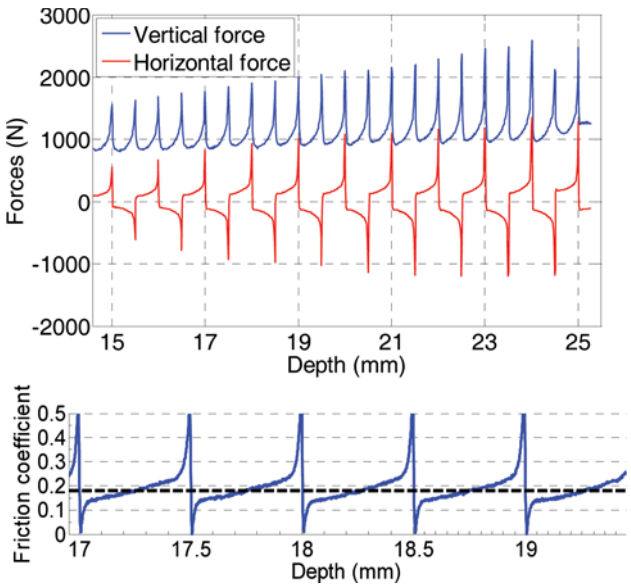

FIGURE 4.—Vertical and horizontal force with a tool of 30 mm in diameter and the absolute value of the ratios between two components.

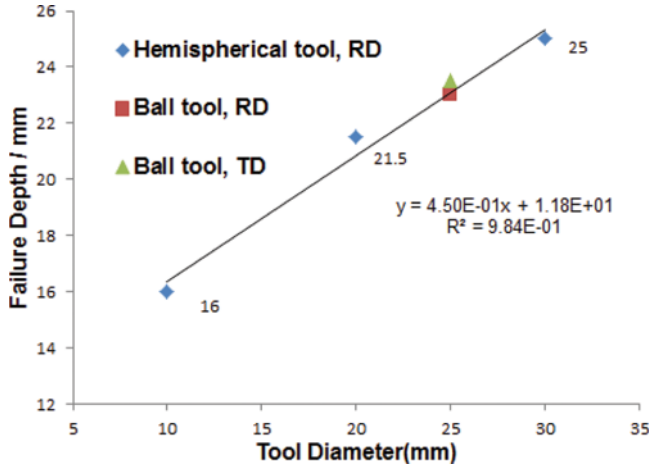

FIGURE 5.—Variations of failure depth of the groove test with tools different in diameter. (RD represents rolling direction and TD for transverse direction).

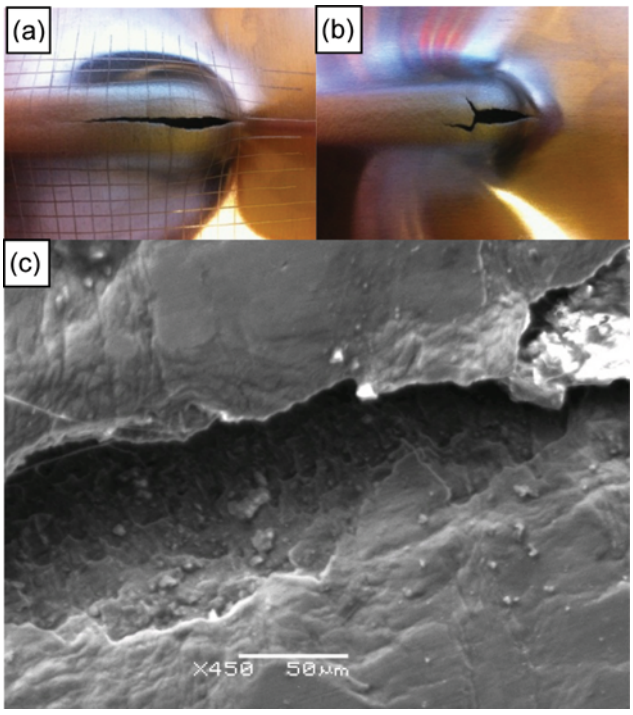

FIGURE 6.—Failure types of sheets formed with different tools. (a) Monodirectional; (b) bidirectional failure; (c) scanning electron micrograph of the onset of fracture and the cross section.

experimental results that the tool diameter should be chosen as large as possible to delay the fracture. These results are consistent with the technical literature [23] in that, with the decrease of the tool diameter, the plastic deformation area also descends but the strain level ascends. The higher level of stresses can explain the early failure with the smaller sized tools.

In terms of the ball tool with a diameter of 25.4 mm, two tests have been performed with the forming direction parallel to ball direction (RD) and transverse direction (TD). The failures of these grooves were recorded at 23 mm and 23.5 mm when the tool was moving along TD and RD, respectively. This phenomenon indicates that a small amount of plane-anisotropy results in the small difference of formability between two directions of the tool.

Figure 6 shows two different failure types at the end of the groove formed by 30 mm large ball tool (a) and hemispherical tool (b), respectively. By checking both macro (Fig. 6(a)) and micro (Fig. 6(c)) structure of the failure point, it is shown that plastic deformation develops by uniform thinning until fracture and in-plane stretching is the principal mode of deformation in this process.

Contact Forces, Strain Behavior and Thickness Distribution in FE Model

To validate the proposed FE model, the simulated contact forces were plotted and compared with experimental data which is shown in Fig. 7. In the FE model, both the tool and the sheet are modeled with the same parameters as in the experimental test (e.g. sheet thickness is 1.016 mm, tool diameter is 30 mm and groove length is 140 mm). From Fig. 7, the predicted forces both in vertical and horizontal components are in reasonable agreement with measured values, except that vertical forces are slightly overestimated and at the end points of the groove sharper force peaks were recorded in the experimental test. The deviation of the modeled and measured force results for the peak values may be due to two main aspects: (1) 7075-O aluminum alloy is strain-rate sensitive and in the case of strain-rate sensitive materials artificially increasing the working speed might adversely affect accuracy of predicted forming forces. In the current model, the forming speed is artificially increased by a time scaling factor of 16.8 to save computing time. (2) Model boundary conditions might not have corresponded to reality. Specifically, there may have been a small amount of sliding between metal sheets and the clamping frame that was not included in the model. It is also possible that dynamic impact of the side wall and acceleration of the forming tool have not been quite accurately modeled. These aspects should be further investigated for developing an accurate force prediction model. However, for the investigation of strain behavior and thickness distribution in this process, the predicted forming forces during the groove forming process are acceptable as conservative measures.

The strain behavior of the sheet was predicted by LS-DYNA. The results of the strain distribution can provide useful information to understand the trend of deformation. To compare the state of the strain for the tool diameter of 30 and 20 mm, the analysis were performed until the forming depth both reached 21 mm.

Figure 8 shows the major strain distribution in the middle of the groove along the longitude direction in which the value of the contacted surface and non-contacted are denoted by upper surface and lower surface, respectively. In this

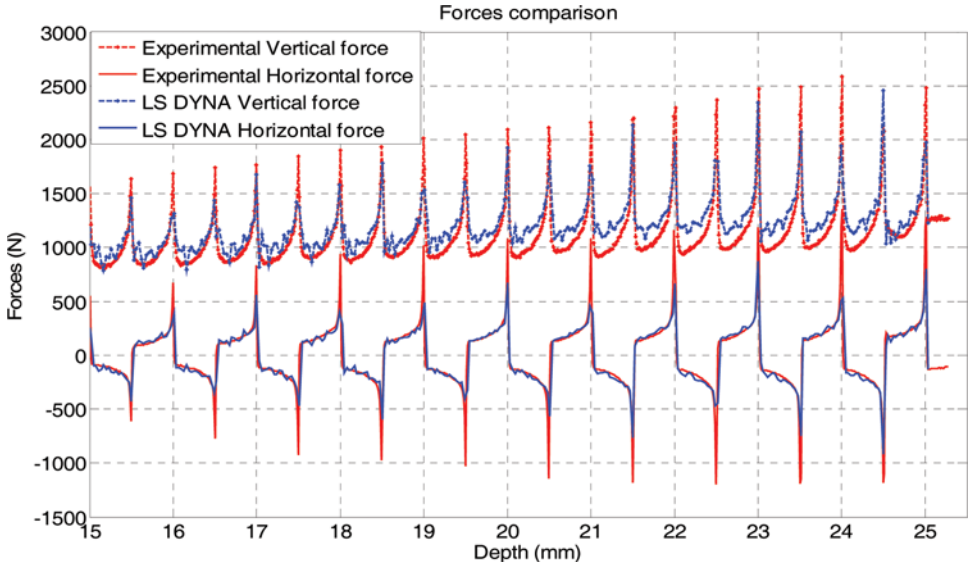

FIGURE 7.—Forces comparison between simulated and experimental results.

figure, the major strain is small in the middle and big at the end of the groove and the major strain on the lower surface is greater than that on the upper surface. It can also be noticed in Fig. 8 that the major strain with the 20 mm tool is greater than that with the tool diameter of 30 mm for both upper surface and lower surface. It suggests that the level of strain decreases as the tool size increases. This could be explained physically by the increase in the contact area and deformation zone. Since the forming limit of the sheet is restricted by the value of strain, earlier occurrence of failure using a smaller tool can be predicted.

To further study the strain behavior and the evolution of the groove, four elements at the bottom of the groove at different places have been selected to compare the strain evolution history in the forming process as shown in Figs. 3, 9 and 10. In the current coordinate system, the origin is defined at the center of the sheet and the tool is travelling along the X-axis from –70 mm to 70 mm while keeping Y as 0. The X-coordinate values of the four selected elements 1, 2, 3 and 4 are 0 mm, 35 mm, 64 mm and 70 mm, respectively (see Figs. 3 and 10). Figure 9 illustrates the strain evolution history of the four elements during the whole forming process which uses a tool with a diameter of 30 mm. It can be clearly noticed that the strain values of the elements (1 and 2) in the middle of the groove keep the same level at each step and the lowest strain values always take place at the very end of the groove (element 4). However, by checking the strain values of each element, it was found that the maximum effective strain occurs before the corner of the groove (element 3) with a distance of 6 mm. The FE modeling results can be confirmed by Fig. 6 which shows that the crack first occurs just prior to the end of the groove.

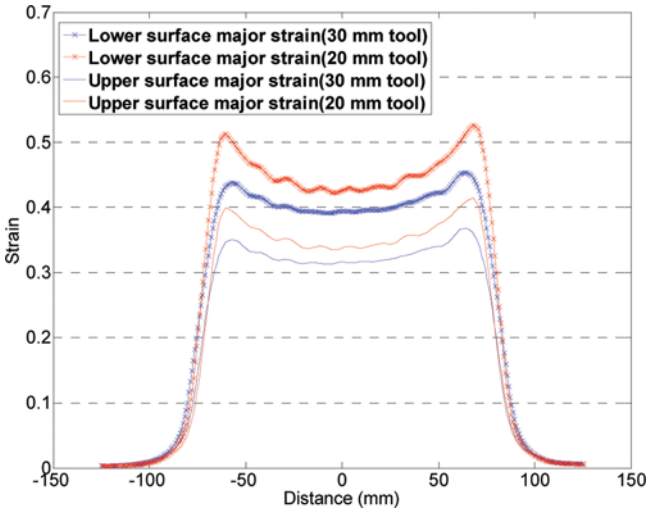

FIGURE 8.—Distributions of major strain predicted by LS-DYNA with different size tools at the depth of 21 mm.

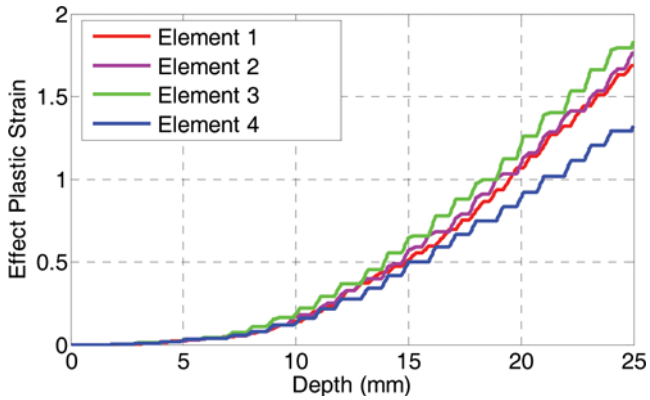

FIGURE 9.—Effective plastic strain evolution of four elements in a groove forming process with 30 mm tool.

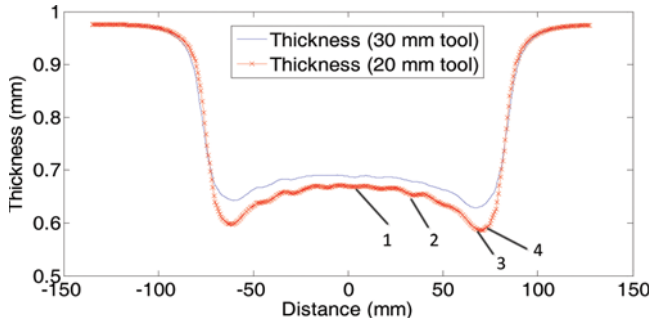

FIGURE 10.—Thickness distributions predicted by LS-DYNA with different size tools. Reference elements 1–4 marked.

Based on the assumption that the metal sheet is incompressible, the large deformation takes place by thinning the sheet. As a result, the thickness distribution is a critical factor to assess the formability and feasibility of a process. The thickness distribution with tools of 30 and 20 mm in diameter are simulated by LS-DYNA and shown in Figure 10. It can be obviously seen that the thickness is greater in the middle and smaller at the ends of the path which can explain why the failure always occurs at the end of the groove. At the same forming depth, the thickness of the groove formed by the 20 mm tool is thinner than that formed by the 30 mm tool, which suggests that failure should occur earlier for the smaller tool. These predicted FE strain and thickness analysis results are well corroborated by the experimental tests performed in the present work.

Surface Topography (SEM)

Figure 11 shows the aluminum sheet surface topography of the grooves produced by hemispherical (a) and ball tools (b) scanned by using JEOL6460 Scanning Electron Microscopy (SEM) with the supply power of 15 KV. The samples were cut into 2 cm squared for SEM observation and no other surface treatment was performed. Compared with sliding contact, the surface damage (striations) of the parts formed under rolling contact appears to be less. Fig. 11 also indicates that many small pits appear on the surface of the aluminum sheet formed with both hemispherical and ball tool. This appears to be due to the coating exfoliating [24] on the sheet.

The border zone between the touched and non-touched area formed by the ball tool are also captured by SEM (Fig. 12). Interesting differences between these two areas can be seen that the surface formed by the ball tool appears smoother than the initial unformed surface. To some extent, it appears that the rolling contact condition can improve the surface topography by flattening the rolling trace initially existing on the sheet surface. However, much more detailed examination should be taken to fully explain this phenomenon.

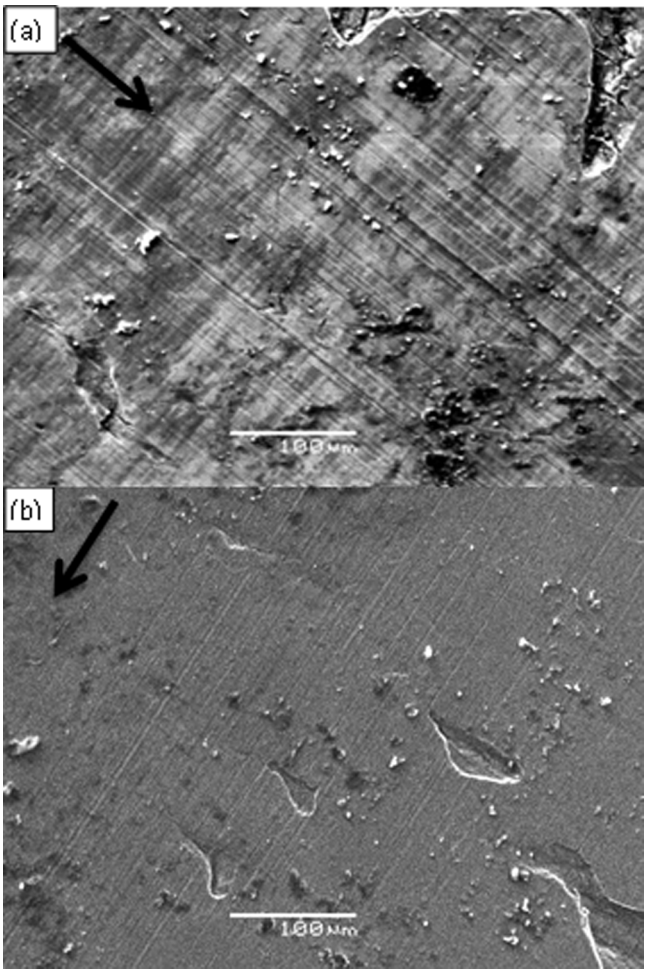

FIGURE 11.—Surface topography examined by SEM for sheets formed with different tools along the directions indicated by arrows: (a) hemispherical tool; (b) ball tool.

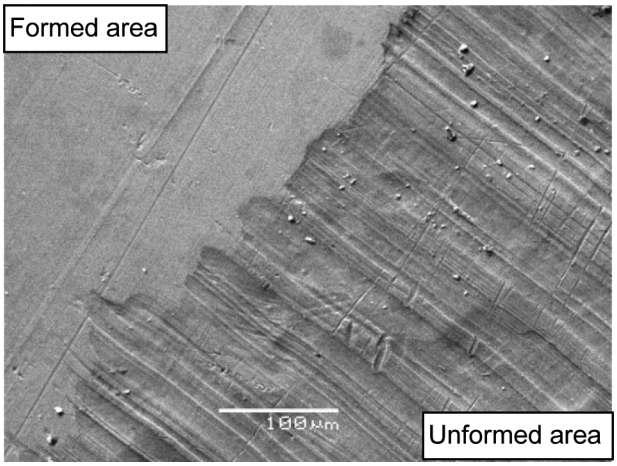

FIGURE 12.—Border zone of the contacted and non-contacted area with ball tool.

Conclusion

Forming forces have been measured by means of strain gauges and provide useful information to monitor and understand the forming process. Even though both vertical and horizontal forces present sharper increases at the end of each travel due to the increase of contact area and impact to the side wall, forces only show a slightly growing trend in the central area of the groove. This information proves that only localized deformation occurred in the process and thus it is possible to form large and complex shapes without higher forces required. By recording the forming depth using three different size tools, an obvious increasing trend in fracture depth was observed with the increase of tool diameter. Therefore, tool diameter should be selected as large as possible to improve formability with the constraints of geometrical complexity. Surface topography of parts formed by the hemispherical and ball tools has been scanned by SEM. The result shows that rolling contact condition causes much less local damage and scratching of the surface. FE analysis is an efficient way to determine the influence of different tool sizes on the strain behavior and thickness distribution, providing how different parameters affect the forming process.

To further compare the effect of contact types, the same size of hemispherical tool (25.4 mm) is being manufactured and would be utilized in future research. Surface roughness is another important parameter to evaluate the output quality of the process and should also be measured in the future.

Acknowledgments

The authors are grateful to Paul Bellette and Peter Bleakley, for their assistance of the initial setup of the experiment test. Revision of the manuscript provided by Dr Prasad Gudimetla is also greatly acknowledged.

Funding

This work is financed by Australian Research Council (ARC) Linkage project which collaborates with QMI Solutions. China Scholarship Council (CSC) is acknowledged for the scholarship support.

References

1. Jeswiet, J., et al., Asymmetric single point incremental forming of sheet metal. *Annals of CIRP—Manufacturing Technology* **2005**, *54*(2), 623–649.
2. Echrif, S.B.M.; Hrairi, M. Research and progress in incremental sheet forming processes. *Materials and Manufacturing Processes* **2011**, *26*(11), 1404–1414.
3. Leacock, A.G.; The future of sheet metal forming research. *Materials and Manufacturing Processes* **2012**, *27*(4), 366–369.
4. Iseki, H.; Kumon, H. Forming limit of incremental sheet metal stretch forming using spherical rollers. *The Japan Society for Technology of Plasticity* **1994**, *35*, 1336.
5. Kim, T.J.; Yang, D.Y. Improvement of formability for the incremental sheet metal forming process. *International Journal of Mechanical Sciences* **2000**, *42*(7), 1271–1286.
6. Sarraji, W.K.H.; Hussain, J.; Ren, W.-X. Experimental investigations on forming time in negative incremental sheet metal forming process. *Materials and Manufacturing Processes* **2011**, *27*(5), 499–506.
7. Hussain, G.; Gao, L.; Hayat, N. Forming parameters and forming defects in incremental forming of an aluminum sheet: correlation, empirical modeling, and optimization: Part A. *Materials and Manufacturing Processes* **2011**, *26*(12), 1546–1553.
8. Banabic, D.; Sester, M.; Influence of material models on the accuracy of the sheet forming simulation. *Materials and Manufacturing Processes* **2012**, *27*(3), 273–277.
9. Silva, M.B.; Martinho, T.M.; Martins, P.A.F. Incremental forming of hole-flanges in polymer sheets. *Materials and Manufacturing Processes* **2013**, *28*(3), 330–335.
10. Kim, Y.H.; Park, J.J. Effect of process parameters on formability in incremental forming of sheet metal. *Journal of Materials Processing Technology* **2002**, *130–131*, 42–46.
11. Silva, M.B., et al. Single-point incremental forming and formability-failure diagrams. *Journal of Strain Analysis for Engineering Design* **2008**, *43*(1), 15–35.
12. Allwood, J.; Shouler, D.; Tekkaya, A.E. The increased forming limits of incremental sheet forming processes. *Key Engineering Materials* **2007**, *344*, 621–628.
13. Silva, M.B., et al. Failure mechanisms in single-point incremental forming of metals. *The International Journal of Advanced Manufacturing Technology* **2011**, *56*(9), 893–903.
14. Minutolo, F.C., et al. Forces analysis in sheet incremental forming and comparison of experimental and simulation results. In *Intelligent Production Machines and Systems-2nd IPROMS Virtual Internationl Conference*, Cardiff, England, July 3–14, 2006.
15. Durante, M.; Formisano, A.; Langella, A. Observations on the influence of tool-sheet contact conditions on an incremental forming process. *Journal of Materials Engineering and Performance* **2011**, *20*(6), 941–946.
16. Hussain, G., et al. Guidelines for tool-size selection for single-point incremental forming of an aerospace alloy. *Materials and Manufacturing Processes* **2012**, *28*(3), 324–329.
17. Vafaeesefat, A. Finite element simulation for blank shape optimization in sheet metal forming. *Materials and Manufacturing Processes* **2011**, *26*(1), 93–98.
18. Cai, G.P.; Zhu, N.Y.; Wen, N. Stress analysis of sheet metal vibration incremental forming. In *Materials Processing Technologies, Pts 1 and 2*; Z.Y. Jiang, X.H. Liu, and J.L. Bu, Eds.; Trans Tech Publications Ltd: Stafa-Zurich, 2011; 166–170.
19. Durante, M., et al. The influence of tool rotation on an incremental forming process. *Journal of Materials Processing Tech* **2009**, *209*(9), 4621–4626.
20. Jeswiet, J.; Alexander Szekeres, J.R.D. Forces in single point and two point incremental forming. *Advanced Materials Research* **2005**, *6–8*, 449–456.
21. Duflou, J.R. Force measurements for single point incremental forming: an experimental study. *Advanced Materials Research* **2005**, *6–8*, 441–448.

22. Hamilton, K.A.S. Friction and external surface roughness in single point incremental forming: a study of surface friction, contact area and the 'orange peel' effect, 2010.
23. Carrino, L.; Giuliano, G.; Strano, M. The effect of the punch radius in dieless incremental forming. In *Intelligent Production Machines and Systems–2nd IPROMS Virtual International Conference*, Cardiff, England, July 3–14, 2006; 204–209.
24. Hou, Y.K., et al. Surface topography evolvement of galvanized steels in sheet metal forming. *Transactions of Nonferrous Metals Society of China* **2009**, *19*(2), 305–310.

4.3 The Papers

Paper 2

Deformation analysis in single point incremental forming through finite element simulation

Li, Y.L., Liu, Z.B., Lu, H.B., Daniel, W. J. T. and Meehan, P. A.

To be submitted

Deformation Analysis in Single Point Incremental Forming through Finite Element Simulation

Yanle Li, Zhaobing Liu, Haibo Lu, Bill Daniel and Paul A. Meehan

School of Mechanical & Mining Engineering, The University of Queensland,
St Lucia, Brisbane, QLD 4072, Australia
e-mail: yanle.li@uq.edu.au, Ph: +61 3365 4115

Abstract

Incremental Sheet forming (ISF) is a promising manufacturing technology in which complex 3D shapes can be formed with one simple tool. Compared to conventional forming processes, for complex shapes, it is more flexible and economical with higher formability and shorter lead time. Therefore, ISF is ideally suitable to rapid prototype and small batch production, especially in the aerospace and biomedical sectors. Over the last decade, although the process has been experimentally studied extensively, the associated deformation mechanics is still unclear and intensive investigation is needed. The purpose of this study is to provide further knowledge of the deformation mechanics of the sheet and clarify the deformation mechanism in a typical cone-forming process through Finite Element (FE) simulation approach. In particular, comprehensive FE models with fine solid elements are utilized which allows the investigation of deformation modes including stretching, bending and shearing. The FE model is firstly validated with experimental results in terms of forming forces and then the evolution history of all the strain components along with the effective strain is presented. The contribution of each strain component to the effective plastic strain during the cone-forming process is discussed. Moreover, the characteristic of each strain component is investigated in detail. It is confirmed from the FE simulation that the deformation modes in the ISF process is a combination of shearing, bending and stretching though the quantitative contributions in each direction are varied. The effect of step-down size on material plastic deformation as well as formability is also investigated.

Keywords:

Incremental sheet forming, Forming force, Formability, Prediction, Shear, Bending

1. Introduction

Incremental sheet forming (ISF) is a flexible, economical low-volume production process which has received much attention in aerospace[1] and biomedical[2] manufacturing sectors over the last two decades. By using this process, complex parts can be formed directly from CAD data with a minimum of specialized tooling. Therefore, it has a high potential for rapid prototyping applications and for small quantity production. Although much research has been performed by researchers in the past few years, there still remains a lack of intensive understanding of the deformation mechanics of the forming process which are critical in optimising the process for better output qualities.

The deformation mechanics behind ISF has been investigated both analytically and experimentally.[3-6] It has been widely accepted that ISF is characterized by higher formability compared with other conventional forming processes.[7, 8] Silva et al.[3-5] extensively analysed the

single point incremental forming by means of a membrane approach. A closed-form analytical model was firstly presented which provides insight to explain the fundamentals behind the fracture of material and the enhanced overall formability of ISF. Lu et al.[9, 10] further discussed the role of friction and through-thickness-shear analytically from the stress state point of view. It was claimed that the effect of through-thickness-shear caused by friction is two-sided. The higher shear stress not only potentially enhances the deformation stability, but also increases the stress triaxiality and reduces the formability at the same time. Although the developed analytical model shows a qualitative agreement when compared to its predictive FEM and experimental results, the model uses some simplifications, such as neglecting bending effects, assuming axial symmetry, rigid-perfectly plastic and isotropic material etc. This limits its further applications. Emmens and Boogaard[11] summarized that bending under tensile load plays a critical role in the localized deformation of ISF process. Unlike the above approach, Mirnia and Darinia[12] analyzed the deformation behavior of a cone-forming process based on the upper bound theory. Despite that shear deformation was assumed as the main deformation mechanism, this approach was shown to be effective for predicting the tangential forming force. Based on Mirnia's work, Li et al.[13] further developed the model to take into account bending and stretching deformation modes and verified the model with experimental tests. However, the contribution between each deformation modes needs to be further investigated and quantified.

The deformation mechanics has been investigated experimentally. Jackson and Allwood[6] experimentally measured the strain distributions through the thickness of the sheets along the cross-sectional plane. It is claimed that the deformation mechanism for ISF is stretching and shear in the plane perpendicular to the tool direction together with shear in the plane parallel to the tool direction. Interestingly, shear strain in the tool moving direction was measured as the greatest strain component. Eyckens et al.[14] measured the strain distribution during the deformation process by a stereovision system. It was suggested that the dominant deformation mechanism depends on the selected forming parameters (e.g. wall angle and step-down size). The author also studied the strain behavior through a FE model. It was found that a good qualitative agreement has been obtained for the surface strain but the through-thickness-shear was not fully captured. However, it is still difficult to reveal the detailed deformation history behind the ISF solely through experimental works due to its highly localised characteristic. Therefore, computer models especially FE technology is widely applied to investigate this process. Despite the advances in the finite element analysis for modelling of metal forming processes and the improvements in computational speed, the numerical simulation of the SPIF process remains a challenging task. The continuous changing localised plastic deformation and the complex tool path result in a significant computation time. Lasunon and Knight[15] confirmed that the FE model can be used to investigate various capabilities of ISF processes by validation with experimental testing with truncated pyramids. Yamashita et al.[16] investigated the applicability of the dynamic explicit finite element code DYNA3D for the simulation of an incremental sheet forming process of quadrangular pyramids. The effect of tool path on deformation behaviour was discovered which shows that the starting forming position should be at one of the corners of the final product. Ma and Mo[17] found that the FE model based on solid elements is more suitable to simulate the SPIF in terms of deformation prediction. Dejardin et al.[18] conducted a numerical analysis using LS-DYNA software to predict the springback effect through the cut rings method. It was found that the finite element model with shell elements is not suitable for all tool path strategies to capture the transverse shear behaviour of the sheet. Future work with a FE model using elements able to properly account for the shear component is

suggested. Recently, Smith et al.[19] analysed the deformation mechanics of both single-point and accumulative double-sided incremental forming (ADSIF) process by FE simulation using LS-DYNA explicit software. Solid elements were used in the described FE model and evolution history to show plastic strain, hydrostatic pressure, and shear strains parallel and perpendicular to tool motion. The authors concluded that the ADSIF could present greater plastic strains, through-thickness-shear strains and greater hydrostatic pressure than in SPIF and suggested this might be the reasons for the increased formability in ADSIF.

Previous FE investigations mostly use shell element considering the reduced computation time, but it is not reasonable to represent the actual deformation mechanism during the forming process. To this end, the purpose of the present work is to develop a comprehensive FE model with fine solid elements and investigate the detailed deformation mechanism during the ISF process. In particular, the evolution history and amplitudes of all the strain components are discussed. Also, deformation modes of shear, bending and stretching are examined. Section 2 briefly presents the modelling and experimental setup for the forming of a truncated cone shape. The validation of the FE model with measured forces is provided in Section 3. Then, the results and the associated discussion are presented in Section 4 followed by the conclusions in Section 5.

2 FE Modelling

As the ISF process involves continuously changing localised plastic deformation as well as large material plastic deformation, the simulation must consider high nonlinearity and large plastic deformation. LS-DYNA is a general-purpose finite element program capable of simulating complex non-linear problems and can accurately solve dynamic problems which have 3D elastic-plastic large deformation using explicit time integration. Therefore, in the present work, the finite element code of LS-DYNA is used to perform the numerical simulation.

In the presented FE model, forming tools are modelled as rigid bodies and the tool path is predefined using CAM software. As a benchmark study, the forming process of the truncated cone is simulated. During the process, the shape is formed layer by layer with a series of successive contours. The vertical distance to the adjacent contour is defined as step-down size Δz. Due to changing contact positions and the three-dimensional tool path, simulations with only a quarter or a half of the whole part are not recommended [6]. Therefore, a fully three-dimensional model needs to be realized. To accurately predict the through thickness shear and bending effect of the deformed sheet, the element type of SOLID164 is used in the current model and 5 elements are meshed through the thickness direction. The SOLID164 element is an 8-node brick element and the default one-point integration option is chosen due to savings on computer time and robustness in cases of large deformations. The initial meshing configuration of the metal sheet is shown in Fig. 1 with an enlarged view of the selected small region *d* plotted at the top right corner. In particular, the sheet is divided into three regions which allow having different meshing of each region. For the region which will be contacting with the tool (region *B*), the elements are arranged with the same size at 1 mm radially and meshed into 400 elements circumferentially which correspond to the size between 0.7 mm to 1.2 mm. Region *A* which is the bottom of the cone is meshed freely as the transition zone to the centre point of the sheet. For the rest of the sheet out of the contact region, it is meshed with relatively large element size as the deformation in this area is quite small and has little effect for the final results. By using this strategy, the localised deformation in the contact region in both radial and circumferential directions can be captured without much distortion of the elements. As a result, the current

meshing is able to increase the localised precision of prediction as well as reduce the computing expenditure. The general geometry of the sheet is square with dimension 300×300 mm and thus it is meshed with 175000 solid elements. In terms of the boundary conditions in the forming process, nodes belong to the four edges of the squared sheet are constrained in all degrees of freedom.

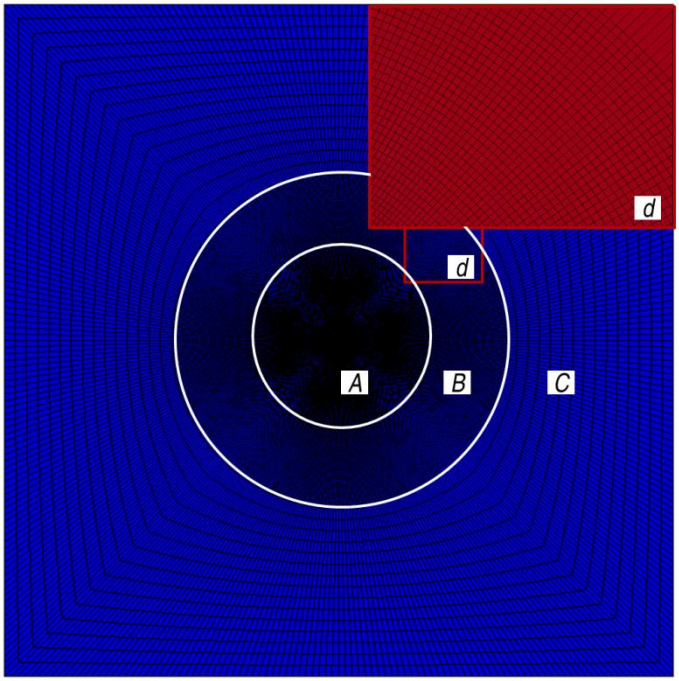

Fig. 1 The initial meshing configuration of the metal sheet with enlarged view at the right top corner.

In the FE model, the sheet behaviour is assumed to be isotropic and the plastic property is modelled using Swift's isotropic strain hardening law of $\bar{\sigma} = K(\varepsilon_0 + \varepsilon)^n$. This material model considers the material hardening with an exponential dependence on strain but neglects the effect of both temperature and strain rate to simplify the model. Tensile tests have been conducted previously [13] for aluminium 7075-O sheets and found that the effect of isotropic is negligible. The values of the mechanical parameters are listed in Table 1. Our previous experimental work [20] suggests a friction coefficient of 0.18 at the contact surface between tool head and metal sheet hence this value was used in the FE model. In order to improve the simulation efficiency, the virtual forming speed is scaled up by 100 times in which the ratio of kinematic energy to total energy can be controlled within a limited value.

Table 1 Mechanical properties of Aluminium 7075-O sheets with 1.6 mm thickness

Material	7075-O
Density (t/mm^3)	2.81×10^{-9}
Young's modulus (GPa)	70
Poisson's ratio	0.33
Tensile Yield Strength (MPa)	92
Ultimate Tensile Strength (MPa)	198
Plastic coefficient K	352.58

Hardening exponent n	0.221

3 Validation of the FE model

The proposed FE model with solid elements is validated by comparing the predicted forming forces with experimental results. In the present work, the forming tests were performed on a state-of-the-art machine dedicated for the ISF process designed by Amino Corporation as shown in Fig. 2. In addition, a multiple-axis force sensor was used to continuously measure the forces between the tool and workpiece during the forming process. The force sensor model K6D175-50 is manufactured by ME-Meßsysteme GmbH which allows measuring the three orthogonal force and three torque components at the same time. As shown in Fig. 2(b), the force sensor is mounted between the spindle and the tool holder to alleviate the indirect impact from other structures. The 6 channel signals are recorded with two NI 9237 data loggers and post-processed with the LabVIEW SignalExpress software. The forces measured with this system shown in Fig. 3 are for a 1.6 mm thick 7075-O aluminium sheet. In this test, as shown in Fig. 2(a1), a truncated cone was formed with a wall angle of 60˚ and step-down size of 0.5 mm at a constant speed of 4000 mm/min.

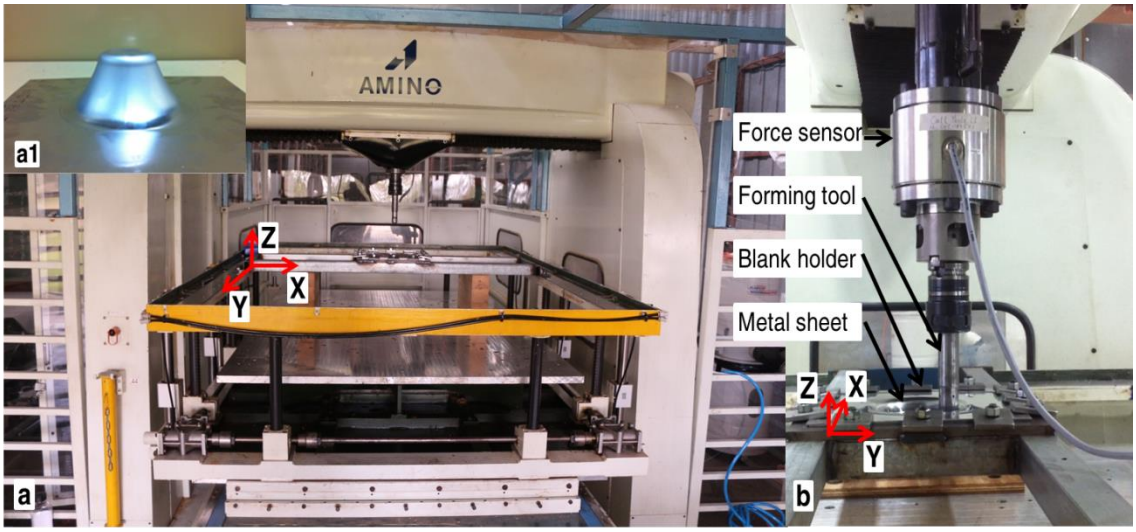

Fig. 2 ISF configuration a) Amino incremental forming machine; a1) a formed truncated cone; b) the implemented force sensor

In Fig. 3 the predicted forming force by the proposed FEM model is compared with the force measured by the force sensor. It can be seen that the predicted forces both in vertical and horizontal components are in good agreement with measured values, except that the vertical force is slightly overestimated at the initial stage of the process. It should be noted that due to the similarity of the two horizontal components (F_x and F_y), only F_x is plotted for comparison. The maximum value of F_x can be considered as the tangential forming force, as it represents the force at 90° where F_y = 0. The same trend can be observed from both experimental and FE simulation results. In one contour, horizontal force F_x changes in a sinusoidal way between their maximum and minimum values due to the current tool position relative to the global absolute axis of the truncated cone. In contrast with the horizontal force, the amplitude of the vertical force increases during the early phase of the process with small fluctuations between each contour and tends to become steady with the further increase of the formed depth. The small deviation of the

modelled and measured force results for the peak values may be due to three reasons: (1) 7075-O aluminium alloy is strain rate sensitive and artificially increasing the working speed might adversely affect the accuracy of predicted forming forces. And (2) although the same tool path trajectory is defined in the FE model, the time increment between two adjacent points is set constant which may result in a slight variation of the forming speed. This is reflected from the offset of the forces obtained from experimental and FE simulation values shown in Fig. 3. (3) Model boundary conditions might not have corresponded to reality. In the simulation, the edges are completely fixed while it may be deflected during actual forming processes. However, for the investigation of strain behaviour and deformation mechanism in this process, the predicted forming forces during the cone-forming process are acceptable as conservative measures; though these aspects could be further investigated for developing an accurate force prediction model.

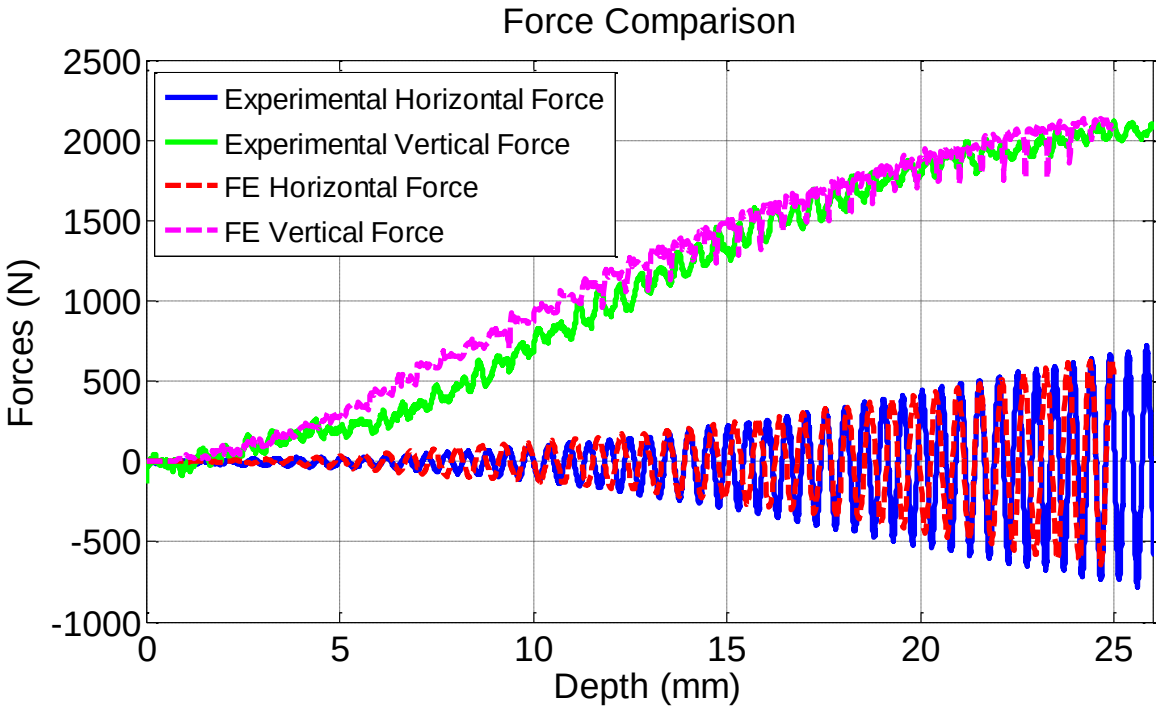

Fig. 3 Force comparison between FE model and experimental results (angle=60, step-down=0.5mm).

4 Results

In order to investigate and quantify the local deformation behaviour in the cone-forming process, 4 distinct sections (1 to 4 from outer to inner as shown in Fig. 4) along the inclined wall are selected. Furthermore, strain values with the variation along thickness direction at each of these sections are also investigated by checking upper element (the side in contact with the forming tool), lower element (the side without contact with the forming tool) and the middle element. It should be noted that the following strain values are presented in the local Cartesian coordinate system as marked in Fig. 4: the direction perpendicular to the tool motion and along the inclined wall is defined as 1 while forming direction (circumferential direction) is defined as 2 and thickness direction as 3. The cross-sectional view of the FE model are presented in the global Cartesian coordinate system as marked at the lower left corner in each figure. In this section, the evolution history of each strain component and their contributions to the effective plastic strain during the cone-forming process with the step-down size of 0.5 mm will be

provided. Since different values of step-down could be used in industrial applications, the effect of step-down size on material plastic deformation as well as formability is also investigated.

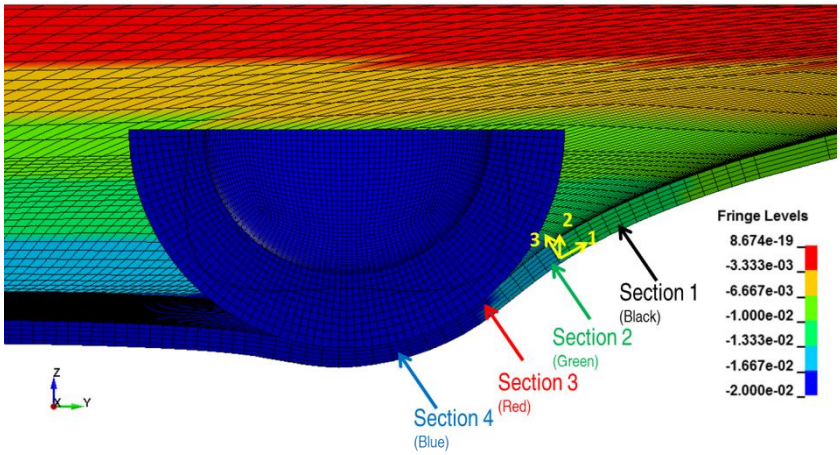

Fig. 4 Four selected critical sections along the cross section to check the strain values

4.1 Evolution history of effective strain

Fig. 5 shows the evolution of effective strain in the cone-forming process simulation for sections 1 to 4, from the outer side (section 1) to the inner side (section 4) of the cone. At each section, the history of effective plastic strain of both upper element and lower element are plotted as a function of the forming depth. The figure shows that the effective strain values for all the elements are increasing continuously with the forming depth for all sections, which reflects the inherent mechanics of incremental forming process. However, the effective plastic strain at sections 1 and 2 are relatively small (less than 0.1) compared with other sections. This may be explained by the fact that these two sections are located close to the outer edge of the cone where no substantial plastic deformation is expected. These already deformed regions would not be further affected by the forming process. It confirms the inherent characteristic of the ISF process that the major deformation of the sheet is localised around the forming tool. For this reason, it can also be noticed that the other two sections (3 and 4) present more severe plastic deformation which correspond to the current local contact zone in the current tool path. Additionally by checking the effective strain value for both sides, an obvious difference can be noticed between upper and lower elements especially for sections 3 and 4. This difference indicates the existence of the bending effect. According to the bending theory[21], with the same thickness, the element with a smaller local radius results in a larger bending strain. In the case of the cone-forming process, the elements at the base corner must have the smallest radius which is represented as section 4 in the presented model. This analysis is consistent with the FE simulation as shown in Fig. 5 that the largest difference of effective strain between upper and lower values occurred at section 4.

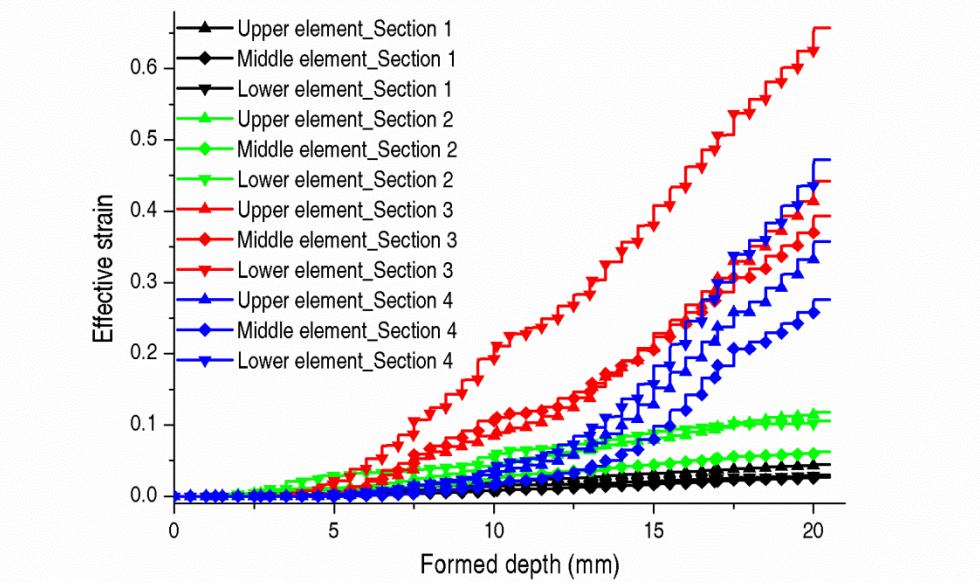

Fig. 5 Plastic strain evolution in cone forming process for upper and lower elements from sections 1 to 4 (as marked in Fig. 4)

4.2 Strain components

Fig. 6 compares the evolution history of 6 strain components along with the plastic effective strain ε_{ef}. It is shown that all the values developed monotonically therefore it is reasonable to analyse the strain composition at a certain point. A column comparison of all 6 strain components and the plastic effective strain for upper, middle and lower elements at section 3 is presented in Fig. 7. These values are obtained when the forming tool is contacting with Section 4 at the depth of 20 mm. In this study, a feature depth of 20 mm was selected due to the following reasons: (a) the long computing time for a deeper cone (110 hrs for the current depth), (b) the selected depth is reasonable to represent the stable deformation process considering the failure depth is only 37 mm in the real experiment and (c) the deformation of the material is localized so the following forming process has limited effect on the deformed part. It is noted that the strain component perpendicular to the forming direction (ε_{11}) dominates the total plastic strain at the picked elements with the highest positive strain. According to the law of volume constancy, the sheet has to be thinned during this process which is clearly confirmed by the negative thickness strain (ε_{33}) in Fig. 6. The thinning in the thickness direction could be considered as a direct indicator for the formability in ISF process since it is suggested that the fracture of sheet comes from the suppression of necking before fracture[22]. Not surprisingly, the strain values in the circumferential direction (ε_{22}) are small compared with the other two orthogonal directions as the deformation in the forming direction is symmetrical and constrained for extension.

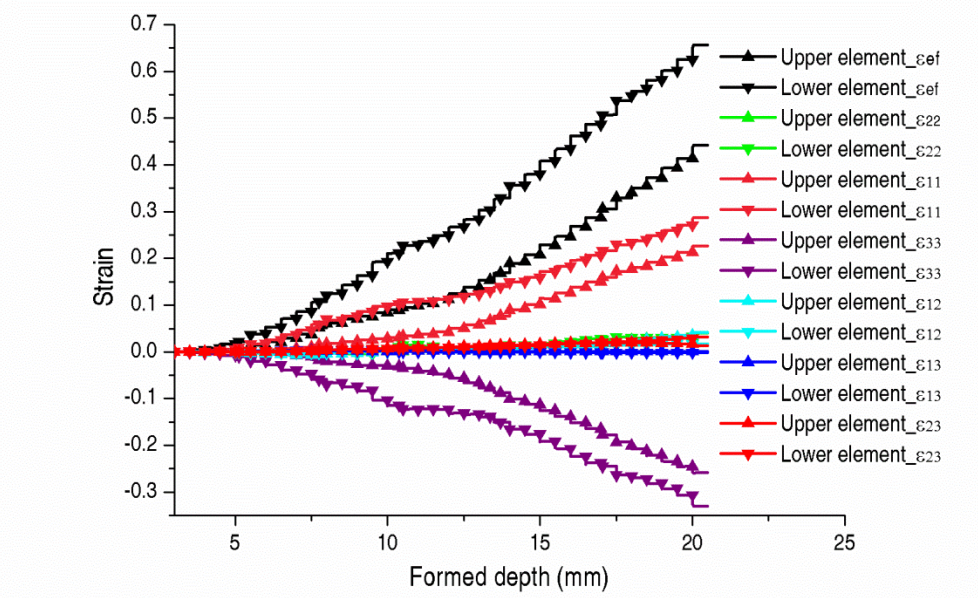

Fig. 6 Evolution history of all strain components at section 3

In contrast, shear strain ε_{23} prevails greatly among the three shear components with negligible ε_{13}. The above results from FE simulation agree with the experimental measurement by Jackson and Allwood[6]. It is also noticed that the strain values are varying through the thickness as shown in Fig. 7. The lower element on the non-contacting surface was deformed with the highest effective strain value which is mainly resultant from large strain ε_{11} and thickness strain ε_{33}. However, the in-plane shear strain ε_{12} takes a significant role as part of the effective strain value at the upper element. The above detailed analysis indicates that the deformation mechanism is different in circumferential and its perpendicular directions. More specifically, the deformation mode in the circumferential (forming) direction is a combination of the transverse shear strain ε_{23} and also a comparable amount of direct strain ε_{22}. However, the direct strain ε_{11} governs the deformation behaviour in the direction perpendicular to the tool motion. This confirms that the formation of the inclined wall is represented by a combination of stretching and bending with substantial transverse shear. The following sections will discuss each strain components individually.

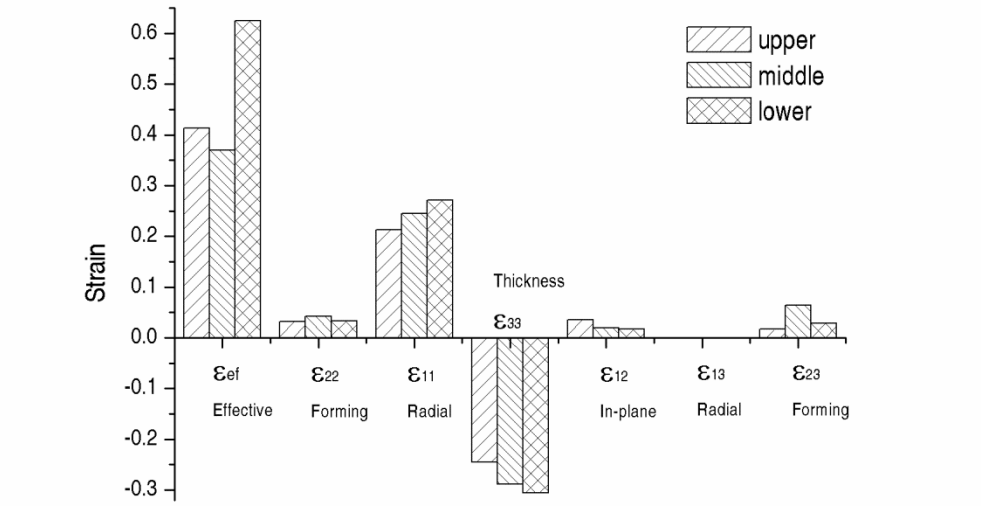

Fig. 7 Strain components for upper, middle and lower elements at section 3 at the forming depth of 20 mm

4.3 Direct strain perpendicular to the forming direction

It was confirmed from earlier discussion that the direct strain perpendicular to the forming direction ε_{11} dominates the magnitude of the plastic strain, therefore, a detailed investigation of ε_{11} is of great importance. Fig. 8 shows the distribution of the direct strain ε_{11} on a cross-section radially during a cone-forming process. It can be clearly seen that a circular deformation band is obtained around the bottom of the cone, which indicates a considerable amount of direct strain is formed. By contrast, there is nearly no plastic strain of ε_{11} at the initial few contours. This is further demonstrated by Fig. 9. In this figure, the amount of ε_{11} for elements at section 1 and 2 are smaller than 0.04 which are insignificant compared with the value of around 0.25 at section 4. In the deformation band, the maximum strain values occurred at the lower surface of the sheet and with an angle α to the axial direction of the forming tool. This is consistent with the basic bending theory that the bending strain is proportional to the distance to the middle surface. For this reason, obvious bending is recorded around this region while the rest of the sheet undergoes uniform direct strain through the thickness. It is also shown that the bending strain (deviation of strain values between upper and lower element) peaks at the forming depth of 10 mm for section 3 when the direct contact level is just above section 3. Similarly, at section 4, the bending strain is building up as the forming tool is currently contacting with this section. Therefore, it is concluded that the bending effect in the direction perpendicular to the tool motion is greatly affected by the contacting of the forming tool. More specifically, the bending strain increases with the approaching of the tool and achieves the maximum value when the region is currently being formed. Then, the bending strain reduces to a steady value after the passing of the forming tool.

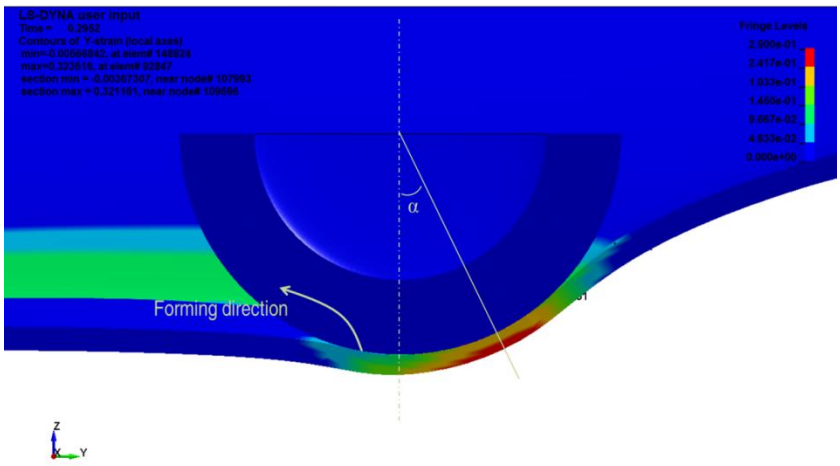

Fig. 8 Direct strain perpendicular to the forming direction (ε_{11}), on a cross-section in ZY plane directly below the tool

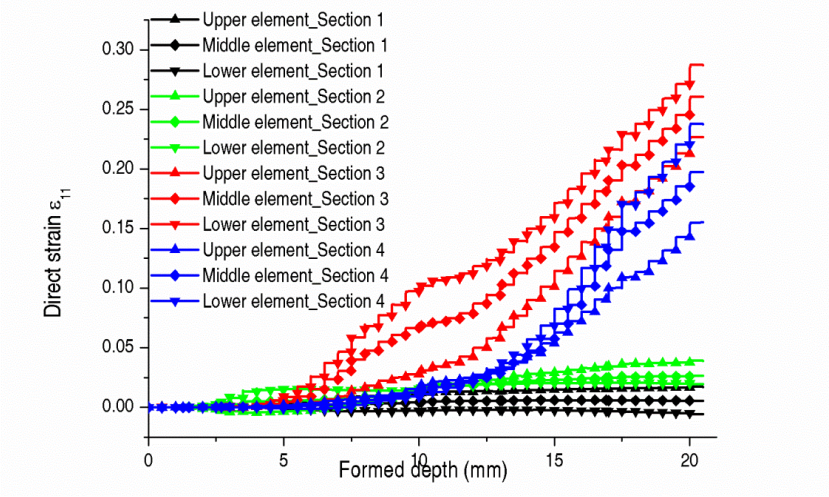

Fig. 9 Evolution of the direct strain perpendicular to tool motion (ε_{11}) of the elements from section 1 to 4

4.4 Direct strain parallel to the forming direction

Fig. 10 shows the distribution of the strain in forming direction (ε_{22}) along a cross-section plane. As indicated by the arrow in the figure, the tool is deforming the sheet leftwards and currently is just above the blue region on the upper surface. Based on the distribution of ε_{22}, the deformation zone around the forming tool can be divided into 3 zones: transition zone, contacting zone and deformed zone. For the elements on the upper surface, they undergo a stretching-compressing-stretching process corresponding to the 3 zones. In the contrast, the elements on the lower surface experience a compressing-stretching-recovering process. As a result, the bending effect is introduced due to the deviation of the strain values between upper and lower elements. Fig. 11 plots the evolution history of the direct strain ε_{22} of the upper, middle and lower elements at section 4. The plot further confirms that the bending effect does exist when the sheet is plastically deformed. However, it is noticed that the bending direction is alternating as the tool passes through the elements.

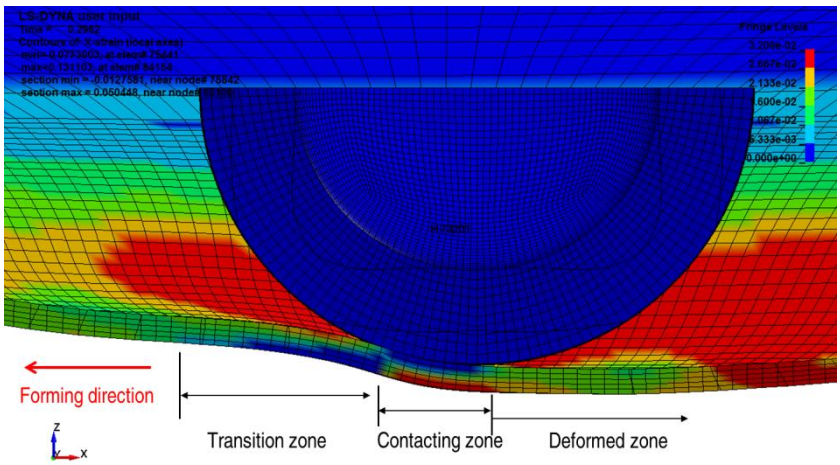

Fig. 10 Direct strain parallel to the forming direction (ε_{22}), on a cross-section in ZX plane directly below the tool

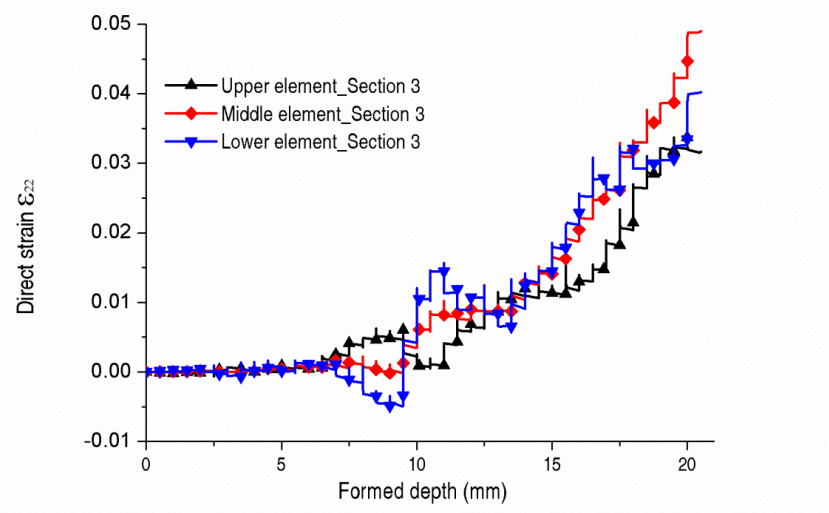

Fig. 11 Evolution of the direct strain (ε_{22}) of the elements at section 4

4.5 Shear strain parallel to forming direction

Fig. 12 presents the magnitude of the shear strain component in forming direction for upper, middle and lower elements for all four selected sections. Similar with the effective plastic strain, the magnitudes of shear strain at sections 1 are small because of the small amount of plastic deformation. However, as deformation accrues much larger values of the shear strain can be obtained at sections 3 and 4. The above observation suggests that the shear strain in the forming direction is proportional to the increase of the plastic strain through the forming process. Additionally, at all of these sections, the magnitudes of the shear strain in the forming direction at upper elements are comparable to that at lower elements whereas the middle elements experience much larger shear deformation. In particular, at the forming depth of 20mm for section 3, the middle element takes on a value of 0.065 which is more than twice that observed in the lower element (0.030). This is clearly illustrated in Fig. 13 where a great deal of transverse shear is elicited in the middle band of the metal sheet after the forming tool passes. This is not surprising if considering the deformation along the circumferential direction as a cantilever beam. It is assumed that the sheet made up of 5 layers is subjected to a transverse vertical loading, so that longitudinal shear stresses must develop to prevent the relative sliding between layers. In this case, there is maximum shear strain at the middle layer, while deformation should be much less at the top and bottom of the sheet because of the loose restraint of the material.

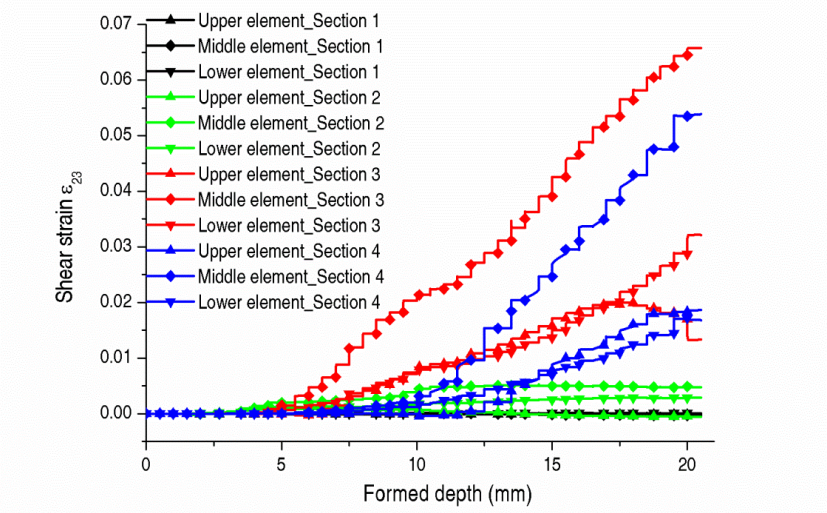

Fig. 12 Shear strain evolution parallel to the forming direction during cone forming process for upper, middle and lower elements from section 1 to 4

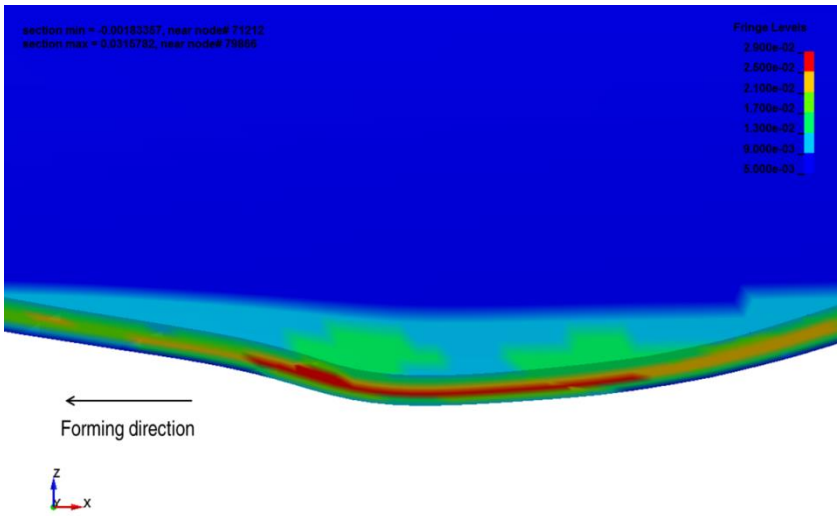

Fig. 13 Distribution of shear strain parallel to the forming direction on a cross-section in ZX plane directly below the tool

4.6 Shear strain perpendicular to forming direction

It should be noted the shear component perpendicular to the forming direction ε_{13} is much smaller than that of shear strain ε_{23}. Nevertheless, it is still beneficial to recognise and understand the evolution pattern of it. Unlike other strain components, as shown in Fig. 14, the evolution history of ε_{13} are not accumulating at section 3 and 4. A peak value is obtained only when the forming tool passing through these sections and then reduces rapidly to zero and negative values. This trend is easily seen from the inspection of the change of the curvature at these sections. At the forming depth of 20 mm, as shown in Fig. 15(a), the maximum positive ε_{13} occurs at section 4 which is currently being deformed where the sheet is bending upwards. Conversely, the maximum negative strain value which is represented by the blue colour takes place at section 2 where the sheet is bending downwards. Due to the symmetric geometry of the truncated cone, a circular band is made up at the same depth with section 2 which can be seen in Fig. 15(b).

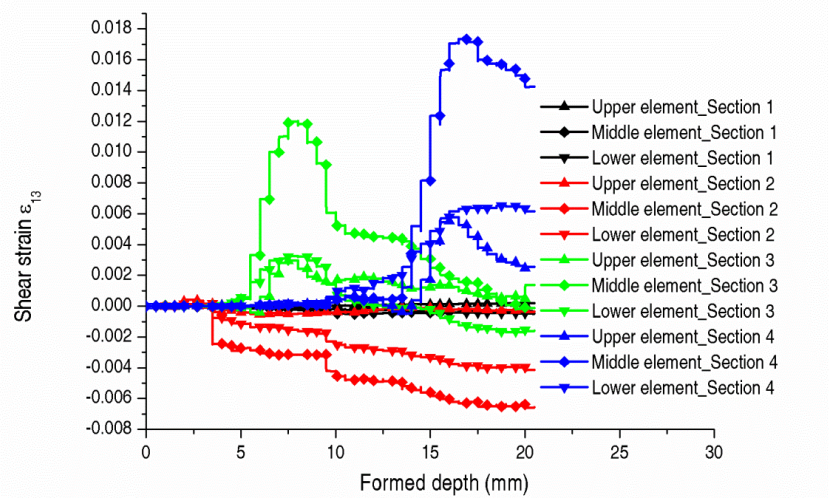

Fig. 14 Shear strain evolution perpendicular to the forming direction during cone forming process for upper, middle and lower elements from section 1 to 4

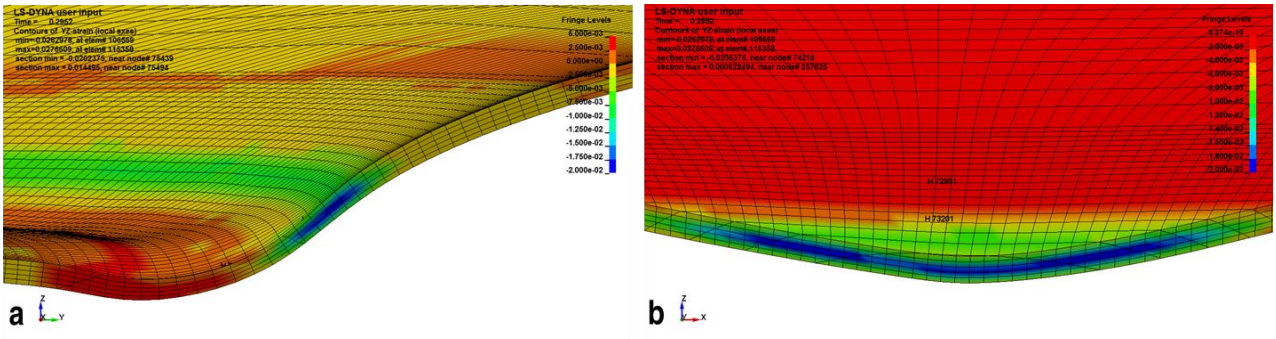

Fig. 15 Distribution of shear strain perpendicular to the forming direction on a cross-section in (a) ZY plane and (b) ZX plane

4.7 Shear strain in the sheet plan

As mentioned in previous section of the present work, the ISF process also produces a considerable amount of in-plane shear strain (ε_{12}). However, this strain component is not well investigated so far. Fig. 16 shows that the tool tends to drag the sheet in the direction of forming, shearing it in-plane, especially at the outside radius of the contact zone when forming a cone. In fact the flat base of the cone being formed has experienced a rigid body rotation about the vertical axis, due to this shearing. This strain is related to the foreshortening of the sheet in the forming direction as it is bent down by the approaching tool. In practice, there is also a significant variation of in-plane shear strain through the thickness due to plate twisting. The evolution history of in-plane shear strain during the cone-forming process for upper, middle and lower elements from section 1 to 4 is shown in Fig. 17.

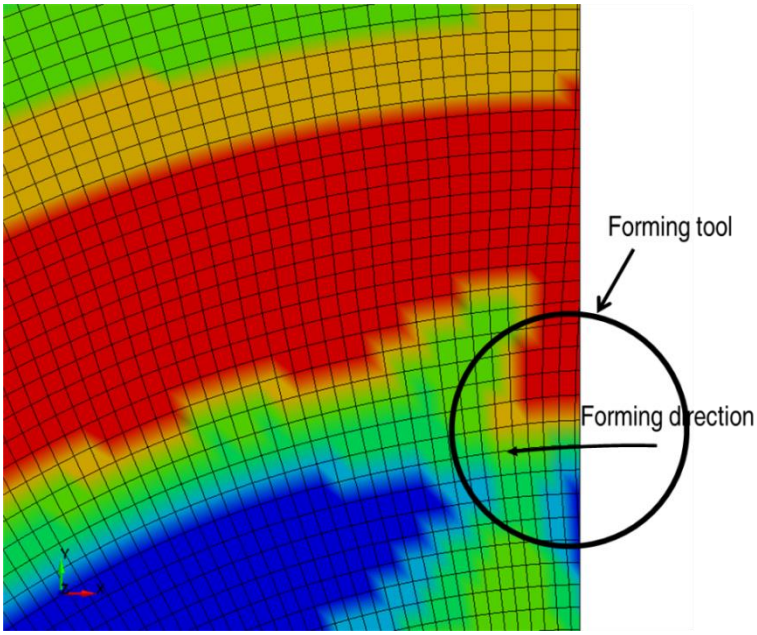

Fig. 16 Distribution of in-plane shear strain from top view

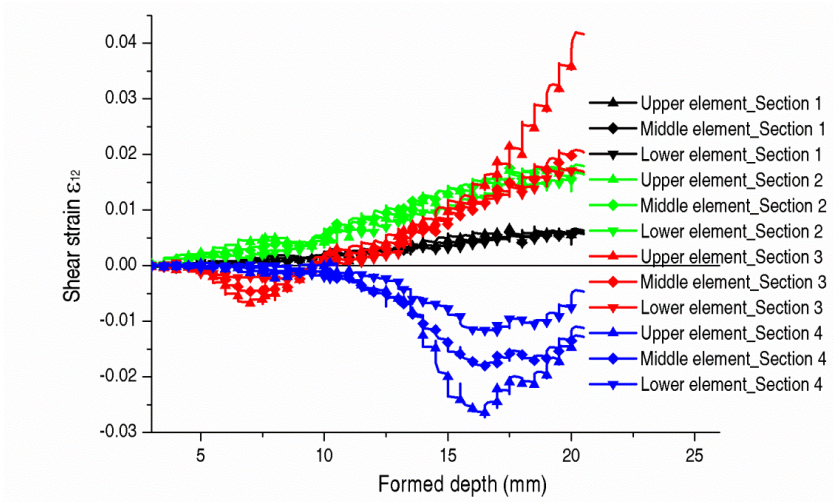

Fig. 17 In-plane shear strain evolution during cone forming process for upper, middle and lower elements from section 1 to 4

4.8 Effect of step-down

The effect of step-down size on the deformation mechanism during the ISF process is also investigated. Four FE simulation cases have been performed with different step-down values from 0.5 mm to 4.0 mm as listed in Table 2. All the simulation cases are successfully reached the designed depth (40 mm) except test 1 in which large hourglass energy was generated due to the severe distortion of the elements. All calculations were carried out by a desktop PC with 8 threads running simultaneously.

Table 2 FE simulation details

Test No.	Wall angle (degree)	Step down (mm)	Sheet thickness (mm)	Tool diameter (mm)	Formed depth (mm)	CPU time (hrs.)

1	60	0.5	1.6	30	20	103
2	60	1	1.6	30	40	200
3	60	2	1.6	30	40	139
4	60	4	1.6	30	40	70

Fig. 18 demonstrates the evolution histories of all strain components for both upper and lower elements at section 3 with the varying of step-down size from 1.0 mm to 4.0 mm. It can be seen that the value of all strain components are continuously increasing with the proceeding of the forming process before contacting with the forming tool and then followed by a steady stage after the forming tool has passed section 3 completely at the forming depth of 25mm. This suggests that the deformation of the material tends to transfer from a distributed deformation to a highly localised deformation under the contact region around the forming tool. At the initial stage, different strain increments are obtained between the neighbouring contours if tool paths with different step-down sizes are adopted. Specifically, as can be seen in Fig. 18, larger strain increments at each step are produced with larger step-down values that are enforced by the forming tool to achieve the same amount of plastic deformation through fewer increments. During the forming process, the relation between strain values of upper and lower elements are inversed for both strain ε_{11} and thickness strain ε_{33}. This is due to the changing of the bending direction in the radial direction of the sheet as the forming tool passes the section.

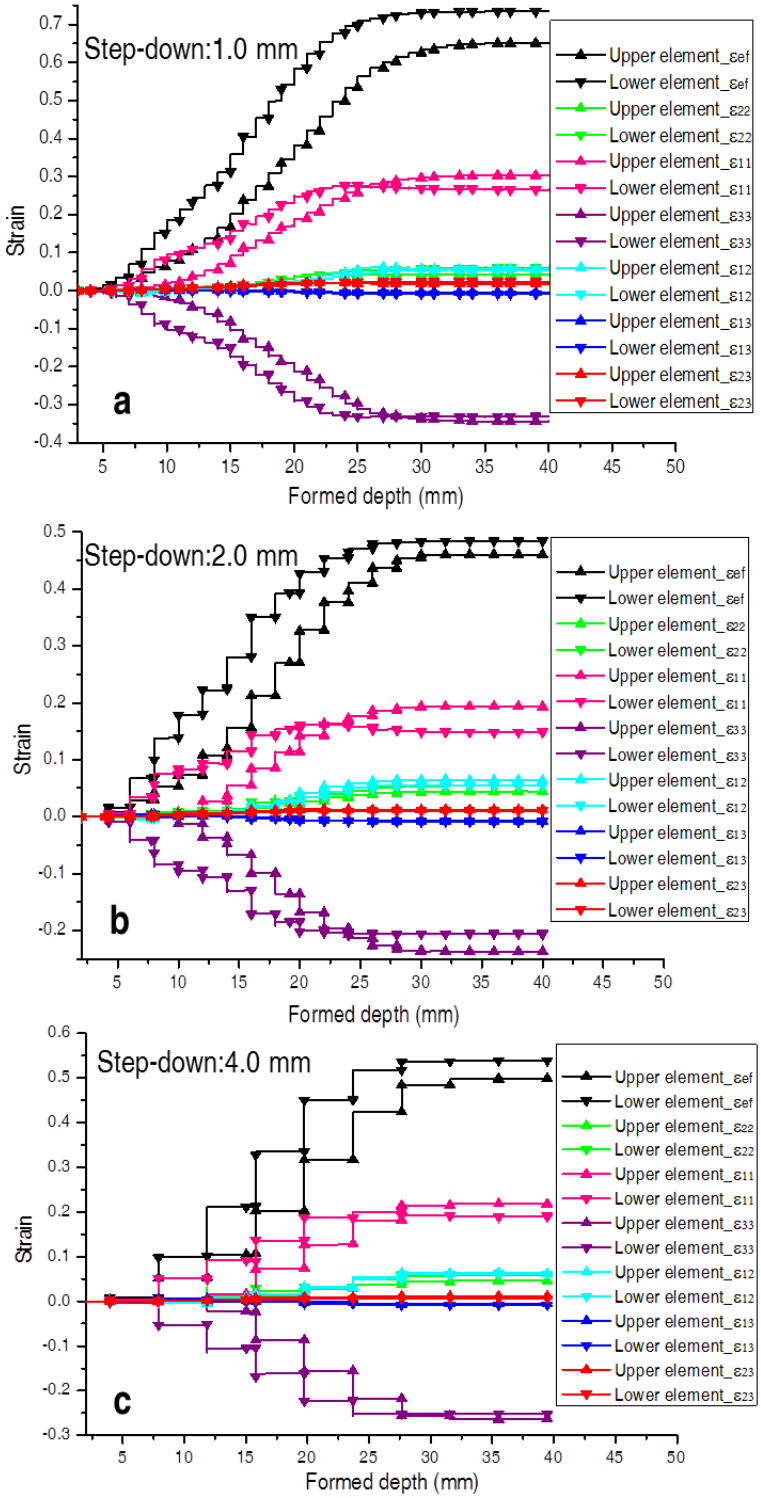

Fig. 18 Strain evolution history with different step-down sizes: a) 1 mm, b) 2 mm and c) 4 mm

Fig. 19 compared the strain values for the middle element at section 3 with four different step-down sizes at the forming depth of 20 mm. It is seen that that the effective plastic strain value decreases with the increase of the step-down up to 2 mm but remains the same level at 4 mm. Similar trends can be observed for the amplitude for all the direct strain components ε_{11}, ε_{22} and

ε_{33} as well as the shear strain ε_{23}. However, the shear strain components ε_{12} and ε_{13} obtained their peak value at the step-down size of 2 mm although amplitudes are small compared with other strain components. This can be due to the fact that smaller step depth size leads to smaller tool contour distance between two neighbouring contours. In the ISF process, material in the contact zone of the metal sheet is deformed by the tool end and is hardened repeatedly after each forming contour. In particular, with small Δz, the amount of already hardened material which is deformed by the forming tool in each pass is higher and may result in more redundant material flow. This leads to a great increase in the contact stress required to reach the target deformation. Consequently, higher total strain values are accumulated in the material with small step-down. Hence, with small step-down size, although the forming forces are small due to the limited strain increment in each step, the final accumulated strain may be large. As a result, the sheet formability will be reduced accordingly. Therefore, small step depth values should be avoided in consideration of the formability. As suggested in the present FE simulation, a step-down size of 2 mm is preferred in consideration of the strain level and formability.

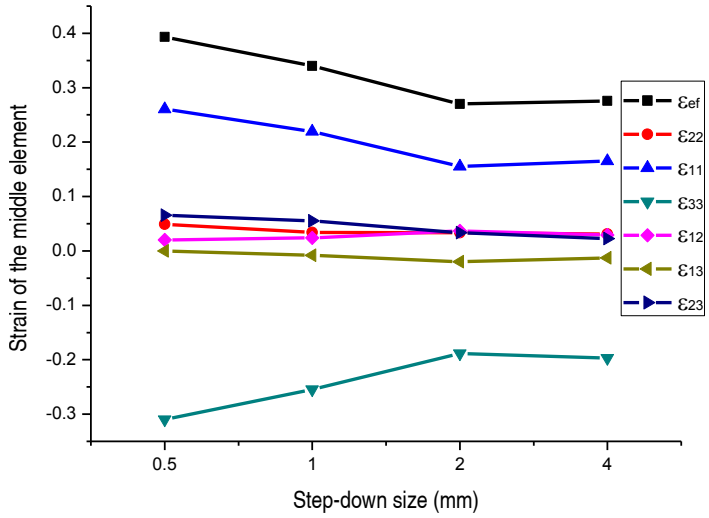

Fig. 19 Comparison of strain values for the middle element at section 3 with four different step-down sizes at the forming depth of 20 mm

5 Conclusions

In the present work, FE models with fine solid elements for truncated the cone-forming process have been established to investigate the deformation mechanism. Firstly, the FE model is verified by experimental work through the comparison of forming forces. It is confirmed from FE simulation that the deformation behaviour in the ISF process is a combination of stretching, bending and shearing. In addition, the contribution of each strain component to the effective plastic strain during cone-forming process is discussed. Specifically, direct strain perpendicular to the tool motion is the major deformation mode in the cone-forming process. This direct strain could be accumulated to a large value while strain in the forming direction only alternates at smaller values. Strain values at both surfaces depend on the bending direction of the sheet. For the material around the bottom of the cone, larger strain values are obtained at the lower surface which is consistent with the experimental observation that cracks tend to occur at the lower

surface. Shear strain in the forming direction (ε_{23}) prevails greatly among the three shear components and the maximum value occurred in the middle of the sheet. It is also found that the in-plane shear strain is not negligible, especially at the upper surface. Finally, it is also found that the selection of step-down size could affect the magnitude of effective strain when the same geometric part is deformed. In the investigated range, larger step-down in the first pass is recommended for the sake of reducing the effective strain and hence enhancing formability. Subsequently, smaller step-down values can be used to improve the geometric accuracy and surface finish.

Acknowledgement

The present work was supported by Australian Research Council (ARC) Linkage project, Boeing Research and Technology Australia and QMI Solutions in Australia. China Scholarship Council (CSC) is also acknowledged for the scholarship support.

References

1. J. Jeswiet, F. Micari, G. Hirt, A. Bramley, J. Duflou and J. Allwood, Annals of CIRP—Manufacturing Technology **54** (2), 623-649 (2005).
2. B. T. Araghi, A. Göttmann, M. Bambach, G. Hirt, G. Bergweiler, J. Diettrich, M. Steiners and A. Saeed-Akbari, Production Engineering **5** (4), 393-404 (2011).
3. M. B. Silva, P. S. Nielsen, N. Bay and P. A. F. Martins, The International Journal of Advanced Manufacturing Technology **56** (9), 893-903 (2011).
4. M. B. Silva, M. Skjoedt, P. A. F. Martins and N. Bay, International Journal of Machine Tools and Manufacture **48** (1), 73-83 (2008).
5. M. B. Silva, M. Skjoedt, A. G. Atkins, N. Bay and P. A. F. Martins, Journal of Strain Analysis for Engineering Design **43** (1), 15-35 (2008).
6. K. Jackson and J. Allwood, Journal of Materials Processing Tech **209** (3), 1158-1174 (2009).
7. T. J. Kim and D. Y. Yang, International Journal of Mechanical Sciences **42** (7), 1271-1286 (2000).
8. J. Jeswiet and D. Young, Proceedings of the Institution of Mechanical Engineers, Part B: Journal of Engineering Manufacture **219** (4), 359-364 (2005).
9. B. Lu, Y. Fang, D. K. Xu, J. Chen, H. Ou, N. H. Moser and J. Cao, International Journal of Machine Tools and Manufacture **85** (0), 14-29 (2014).
10. D. Xu, W. Wu, R. Malhotra, J. Chen, B. Lu and J. Cao, International Journal of Machine Tools and Manufacture **73** (0), 37-46 (2013).
11. W. C. Emmens and A. H. Boogaard, Journal of Materials Processing Tech **209** (8), 3688-3695 (2008).
12. M. J. Mirnia and B. M. Dariani, Proceedings of the Institution of Mechanical Engineers, Part B: Journal of Engineering Manufacture (2012).
13. Y. Li, Z. Liu, H. Lu, W. J. T. Daniel, S. Liu and P. Meehan, The International Journal of Advanced Manufacturing Technology, 1-17 (2014).
14. P. Eyckens, B. Belkassem, C. Henrard, J. Gu, H. Sol, A. M. Habraken, J. R. Duflou, A. Van Bael and P. Van Houtte, International Journal of Material Forming **4** (1), 55-71 (2011).

15. O. Lasunon and W. A. Knight, Proceedings of the Institution of Mechanical Engineers, Part B: Journal of Engineering Manufacture **221** (12), 1725-1732 (2007).

16. M. Yamashita, M. Gotoh and S.-Y. Atsumi, Journal of Materials Processing Technology **199** (1–3), 163-172 (2008).

17. L. W. Ma and J. H. Mo, PROCEEDINGS OF THE INSTITUTION OF MECHANICAL ENGINEERS PART B-JOURNAL OF ENGINEERING MANUFACTURE **222** (3), 373-380 (2008).

18. S. Dejardin, S. Thibaud, J. C. Gelin and G. Michel, Journal of Materials Processing Technology **210** (2), 363-369 (2010).

19. J. Smith, R. Malhotra, W. K. Liu and J. Cao, The International Journal of Advanced Manufacturing Technology, 1-17 (2013).

20. Y. Li, Z. Liu, W. J. T. Daniel and P. A. Meehan, Materials and Manufacturing Processes **29** (2), 121-128 (2013).

21. J. L. Duncan, S. J. Hu and Z. Marciniak, *Mechanics of sheet metal forming*. (Butterworth-Heinemann, Oxford, 2002).

22. L. Montanari, V. A. Cristino, M. B. Silva and P. A. F. Martins, The International Journal of Advanced Manufacturing Technology **69** (5-8), 1175-1183 (2013).

4.3 The Papers

Paper 3

Experimental study and efficient prediction on forming forces in incremental sheet forming

Li, Y.L., Liu, Z.B., Lu, H.B., Daniel, W. J. T. and Meehan, P. A.

Advanced Materials Research

2014, Volume: 939, Pages: 313-321.

Advanced Materials Research Vol. 939 (2014) pp 313-321
Online available since 2014/May/07 at www.scientific.net

doi:10.4028/www.scientific.net/AMR.939.313

Experimental Study and Efficient Prediction on Forming Forces in Incremental Sheet Forming

Yanle Li[1, a], Zhaobing Liu[1, b], Haibo Lu[1, c], W.J.T (Bill) Daniel[1, d] and Paul A. Meehan[1, e]

[1]School of Mechanical & Mining Engineering, University of Queensland, St Lucia, Brisbane, QLD 4072, Australia

[a]yanle.li@uq.edu.au, [b]z.liu7@uq.edu.au, [c]h.lu2@uq.edu.au, [d]billd@uq.edu.au, [e]meehan@uq.edu.au

Keywords: Incremental sheet forming, forming force, formability, prediction

Abstract. Incremental sheet forming (ISF) is a promising forming process in which complex 3D shapes are formed from a sheet of metal using a simple moving tool. The efficient prediction of contact forces in ISF is desirable to monitor the forming process, prevent failure, and implement on-line control and process optimization. However, traditional Finite Element (FE) simulation used for force prediction is significantly time-consuming for complex products. The purpose of this study is to investigate the ISF force prediction and characteristics under different forming conditions and build a potential efficient model.

In the present work, forces during the cone forming process with different wall angles and step down sizes were recorded and compared. Different force trends were identified and discussed with reference to bending and strain hardening mechanics. Influences of different parameters on designated formability were also qualified which should benefit the product design process. An efficient predictive model based on upper-bound approach was applied for force prediction in this case. Predicted tangential forces were then compared with the experimental results showing relatively good agreement. The limits of the proposed model were also identified and the potential of future improvements were suggested.

Introductions

Incremental Sheet Forming (ISF) technology is an emerging forming process ideal for rapid prototype and small batch production. In an ISF process, a flat metal sheet is gradually formed into the designed 3D shape using Computer Numerical Control (CNC)-controlled generic tool stylus. The process is highly flexibility such that complex shapes can be achieved with tool path programming and sometimes with the support of a die. Therefore, ISF was widely accepted as a promising forming process over conventional processes such as deep drawing and stamping [1-3] for small batch production. However, one of the dominant limits for the further development and commercialization of ISF technology is the limited geometrical accuracy of the final shape [4-6]. Although various strategies [7, 8] have been proposed to obtain a better product quality, a systematic understanding of the contact mechanics and further investigation on the forming force are essential to achieve this goal.

In ISF, the blank sheet is incrementally formed to its final shape via a small deformation zone in the vicinity of the forming tool, leading to lower forming forces than traditional processes, such as deep drawing. Additionally, unlike traditional forming processes, the size of the desired part does not affect the forming forces [9]. The characterization and prediction of the forming forces is essential for tool design and to determine the necessary power of the machine. The forming force also provides key insight into the deformation mechanics of the process. Filice and Ambrogio [10, 11] worked on the force measurement and analysis and classified the force trends of tangential force into three types: steady state force trends, polynomial force trends and monotonically decreasing force trends. It was also concluded that the force gradient after the peak can be effectively considered as a critical indicator to detect and prevent workpiece fracture. Therefore, forming force is a potential indicator for forming limits identification. Petek et al. [12] proposed an autonomous on-line system for fracture

identification and localization by analyzing the reaction force with skewness function. Another failure criterion presented by Fiorentino [13] is also based on force monitoring during the forming process. This approach was achieved by comparing the stresses acting on the material calculated from forming forces with the ultimate strength of the material. Additionally, G. Ingarao et al.[14] investigated recorded force data to calculate and evaluate the energy consumption required for the ISF process.

The lack of an efficient predictive force model limits the development of ISF technology in many aspects including on-line control, failure prevention and process optimization. Iseki [15] obtained the forming forces for the incremental forming of a pyramid using an approximated deformation analysis. Aerens et al. [16] studied the incremental forming of truncated cones with different materials using experimental and statistical analyses. They proposed regression formulae to predict the triple forming force components including axial, radial, and tangential components from input variables including wall angle, initial thickness, tool diameter, and vertical pitch. Finally, an approximate formula was deduced for predicting the axial component for forming any material based on the tensile strength only. Unlike other mentioned work for predicting the forming forces acting on the tool, Mirnia [17] proposed a new approach to predict the tangential force on a truncated cone using an assumed deformation zone and the upper-bound analysis. It was reported that the forces were in good agreement with those from the experimental work of Aerens et al.[16]. Nevertheless, this model can only predict tangential force and further experimental validation for different materials is needed.

In this paper, the following research tasks are tackled, and related results are reported:

- An accurate force measurement method was implemented on an ISF CNC machine. The trend of the forming force was identified and analyzed.
- The effects of wall angle and step down size on the forming forces and formability was investigated.
- A potential computationally efficient method to predict forming force for this case was investigated.

Experiments

To facilitate the study of the effect of product geometry and step down size on the forming force and formability, truncated cones with different wall angles are selected as the target shapes.

Equipment Setup. The forming tests have been performed on a state-of-the-art machine designed dedicated for the ISF process by Amino Corporation which can be numerical controlled by a FANUC controller (Fig. 1). The hemispherical tool with a diameter of 30 mm was used to deform the material. The tip of the tool is tungsten carbide and the body is made of K110 steel which was hardened and tempered to HRC60. The sheet material used in the present study was aluminum 7075-O sheet and has been cut into 300 mm × 300 mm in size with 1.016mm in thickness.

The forming forces acting on the forming tool have been measured continuously over time during the process. There are several ways to capture the forming force, such as the cantilever sensor designed by Jeswiet [18] and force dynamometer used by Duflou et al. [19]. In the present work, three full Wheatstone bridges have been designed and mounted on the 30 mm hemispherical tool. Each bridge was configured by four strain gauges and designed to measure one of the three orthogonal forces: two bending directions (F_x and F_y), and one axial direction (F_z). The strain gauges were calibrated twice in all three directions by applying a known force to get an accurate result. The calibrated system shows a rather linear relation between strain and output voltage.

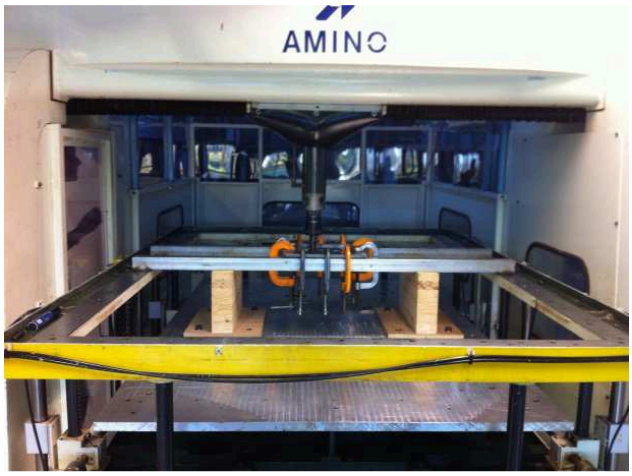

Fig. 1 Incremental sheet forming on Amino machine

Fig. 2 shows the experimental configuration and a case study of a truncated cone formed by Amino CNC machine. The truncated cones are formed in a stepwise way with many contours. The vertical distance between two consecutive contours is defined as step down (Δz). The angle between the deformed sheet to the horizontal plan is defined as wall angle (α).

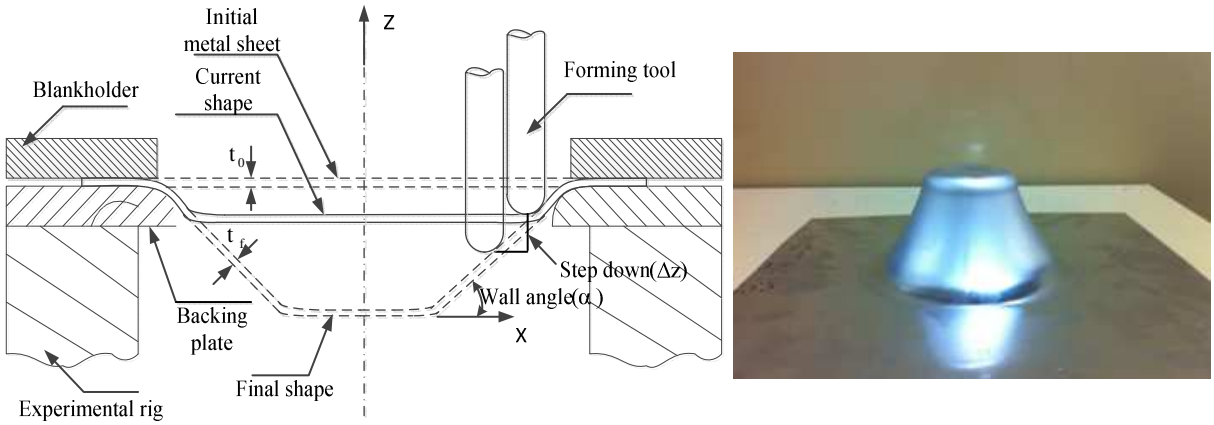

Fig. 2 Sketch of ISF experimental parameters and a case study made from Al 7075 of 1.6 mm in thickness.

Experimental Tests. Lubricant (oil-Shell Tellus Oil 68) was sprayed on the blank before forming to prevent excessive friction. A backing plate was utilized underneath the sheet in order to increase the rigidity between the forming area and sheet flange. The feed rate of forming tool was set to 4000 mm/min. For the tool path strategy, Z-level tool path with different vertical step-down size (Δz, the increment between two successive passes) were utilized. All the cones were designed with the same major diameter of 140 mm and smaller cone height should be defined for smaller inclination of the wall due to the geometric constraint. The tests were conducted until the crack of the sheet and the forming forces for all the three components (F_x, F_y and F_z) were recorded continuously during this process. The detailed tests parameters are listed in Table 1 and Table 2.

Table 1 Experimental design for different wall angles

Wall angle α (Degree)	**Step down Δz (mm)**	**Tool diameter (mm)**	**Thickness (mm)**	**Feed rate (mm/min)**	**Designed height (mm)**
30	0.5	30	1.6	4000	28
40	0.5	30	1.6	4000	40
50	0.5	30	1.6	4000	60
60	0.5	30	1.6	4000	75
62	0.5	30	1.6	4000	75

63	0.5	30	1.6	4000	75
65	0.5	30	1.6	4000	75
70	0.5	30	1.6	4000	75

Table 2 Experimental design for different step down sizes

Wall angle α (Degree)	**Step down Δz (mm)**	**Tool diameter (mm)**	**Thickness (mm)**	**Feed rate (mm/min)**	**Designed height (mm)**
60	0.1	30	1.6	4000	75
60	0.2	30	1.6	4000	75
60	0.3	30	1.6	4000	75
60	0.4	30	1.6	4000	75
60	0.5	30	1.6	4000	75
60	0.7	30	1.6	4000	75
60	1.0	30	1.6	4000	75

Efficient Model for Force Prediction

In this model, the upper-bound approach [17] is used to analysis the deformation behavior and predicts the tangential force of the truncated cone during ISF process. The deformation zone is estimated according to the tool path and tool radius and defined as Bezier curves which can be tailored by adjusting two presupposed parameters. The velocity field and the dissipated power of the process are then expressed with optimizable parameters. Then the tangential force is obtained by minimizing the dissipated power using upper-bound solution according to the assumptions made in literature [17]. This analytical model was recomposed and implemented using MATLAB. In order to confirm the performance of the recomposed efficient MATLAB model, the predicted tangential forces with different forming parameters were compared with the experimental results. The measured forces (F_x and F_y) need to be converted to tangential (F_t) and radial components (F_r) to make sure the comparison is effective. The same methodology presented in [16] are used here to achieve the conversion.

Results and Discussion

Force Trend in ISF. Fig. 3 presents the record of the three components forces all over the process versus time ($\alpha = 60°, \Delta z = 0.5$ mm) with a detailed view in two steady segments on the top. In one cycle, F_x and F_y forces change in a sinusoidal way between their maximum and minimum values due to the current tool position relative to the global absolute axis around a contour of the truncated cone. In contrast with horizontal forces, vertical force only experienced some small fluctuations in the final steps caused by the Z-level tool path. The amplitude of the forces experienced an increasing trend during the first half process and tends to become steady for the rest of the process. This occurs due to a number of reasons. Firstly, the initial increase of the forming forces could be caused by the bending mechanism [11]. Then, with the build-up of the contact area between tool head and the sheet surface, the force required to deform the sheet also increased. Additionally, the following rise can be assigned to the continuous stretching of the material which has been examined by Allwood et al [20]. The stretching would result in the increase of the forming force caused by the strain hardening of the material. However, thinning of the material would reduce the magnitude of the force. Therefore, the later contour loops of the forming force are determined by the combined effects of strain hardening and thinning.

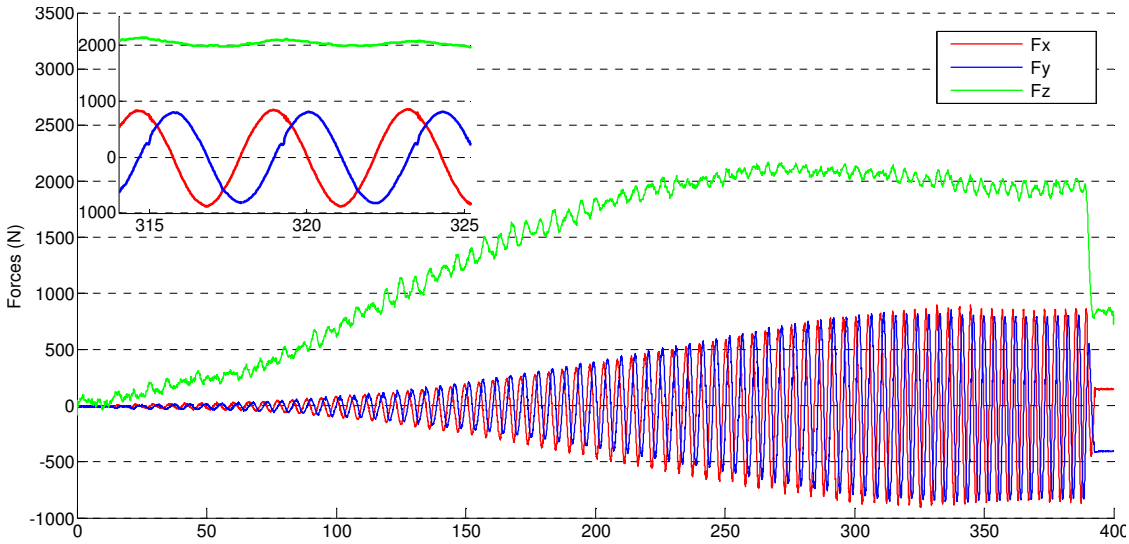

Fig. 3 Three force components (Fx, Fy and Fz) versus forming time and a detailed view for two cycles during forming a cone.

Effect of Wall Angle. To study the effect of wall angles on the forming force, the forming trends of vertical forces at the varying of wall angle from 30 ° to 70 ° are plotted in Fig. 4. For small wall angles under 60°, the vertical forces reach the turning point at the forming depth of around 30 mm and then keep rising slowly until the end of the process. The magnitudes of F_z for these cases at the same depth approximately have the same value. On the contrary, the force trends are recorded in a different fashion for wall angles larger than 60°. The forces quickly register their peak values at a depth of around 12 mm and then decrease monotonically towards process completion/failure. The achievements of steady conditions are delayed with small wall angles. This is because with a smaller wall angle, the sheet undergoes a longer bending mechanism before the occurrence of strain hardening. By carefully checking of these cases, one can concluded that if the material work hardening plays a dominant role to compensate sheet thinning, the force could remain steady and avoid fracture. Otherwise, if thinning prevails, the forces drop quickly which indicates the failure of the material. If appropriate statistical analysis can be performed to calculate the force gradient after peak value, this could possibly be considered as an effective indicator for failure prediction.

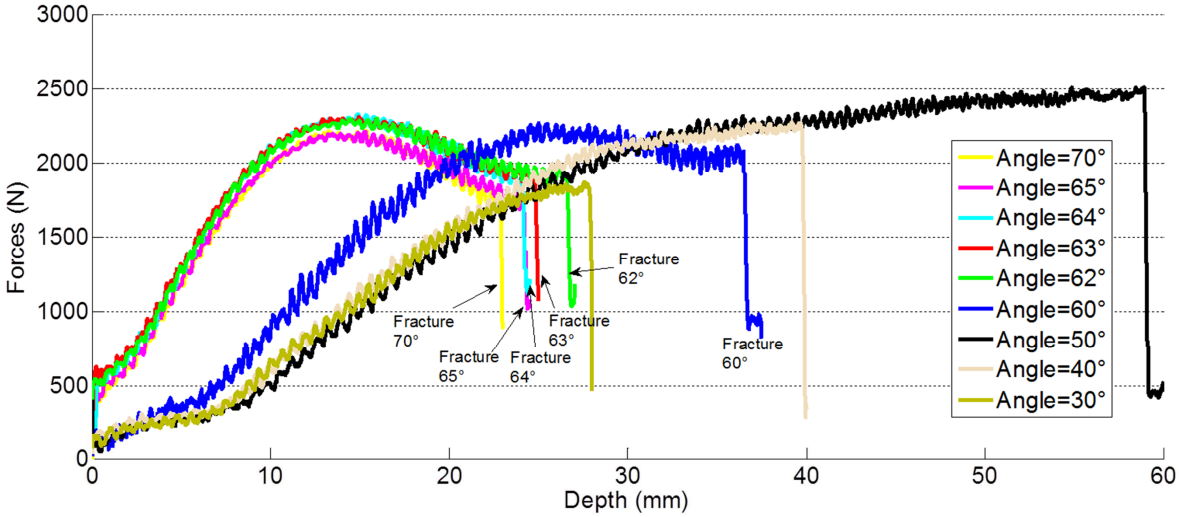

Fig. 4 Vertical force trend with the varying of wall angle (fracture parts are marked).

The variations of the peak values for forces in Y direction (F_{yp}) and vertical direction (F_{zp}) as a function of the wall angle (α) are shown in Fig. 5. It can be seen that with the increase of wall angle from 30º to 70º, F_{zp} has its maximum value when the cone with the angle of 50º is being formed.

Interestingly, if we plot the curve $(\alpha * \cos\alpha)$ scaled by an appropriate factor in the same figure, it can be found that the trend of F_{zp} is similar with curve $(\alpha * \cos\alpha)$. According to the sine law of sheet thinning [21], $\cos\alpha$ is used to calculate the wall thickness of the sheet after deformation. Therefore, it could be inferred that F_{zp} is positive proportional to the inclination of the wall angle and also the thickness of the deformed sheet metal. In the case of the horizontal force F_{yp}, a linear increase can be observed with the increase of wall angle. The equation of the linear regression and its coefficient of determination R^2 are also presented.

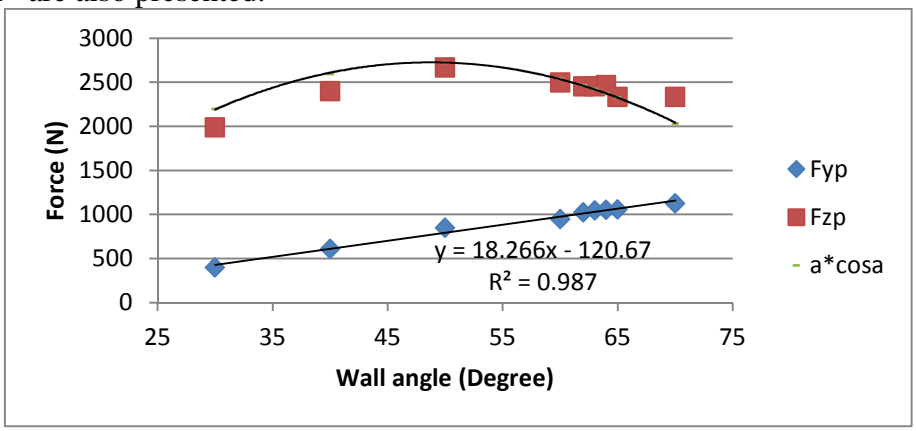

Fig. 5 Variations of forming forces with different wall angles.

The formability of the material can be assessed with various approaches [22, 23]. The traditional way is based on the measurement of the main strain values of a series of parts formed under different deformation conditions. Generally, the definition of forming limits in this way is time consuming and not economical. Moreover, forming limit in ISF would change if different process parameters are used. Therefore, the maximum formable wall angle or forming depth is used directly as an alternative way to evaluate the formability at a given forming condition in the current work. As listed in Table 1, the designed heights of the cones for 30°, 40° and 60° are 28 mm, 40 mm and 60 mm due to the limits of minor diameter, respectively. These three parts are formed successfully without fracture because the thinning of the sheet is relatively light under the forming limit of the material. With the increase of the wall angle from 60° to 70°, the achievable forming depth reduces slightly from 37.5 mm to 23 mm. These tests can provide useful information for preliminary design for the shape to avoid the risk of failure and improve the stability of the final product.

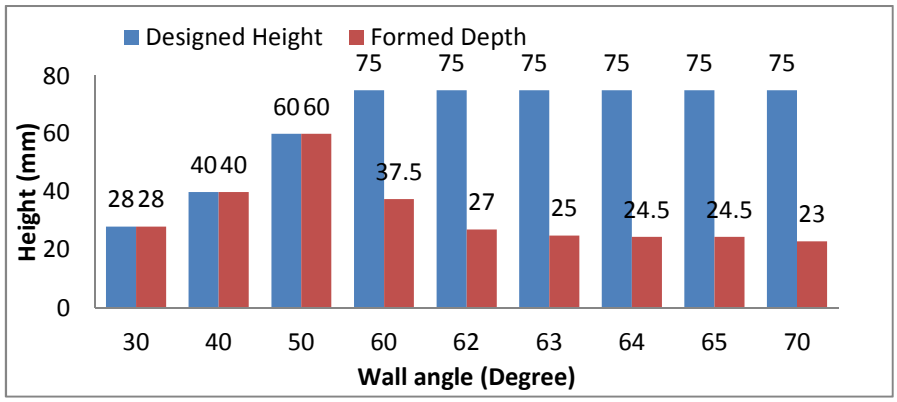

Fig. 6 Formed depth with different wall angles.

Effect of Step Down. A set of experiments has also been performed with different step down sizes (Δz) range from 0.1 mm to 1.0 mm. The evolution histories of the vertical force F_z at the varying of step down sizes are presented in Fig. 7. It can be noticed that at the former stage, the vertical forces for big Δz (0.7 and 1.0 mm) shows smaller values compared with forces with little step down sizes. However, after a depth of 40 mm, the F_z values present a limited decrease and then increase until the

part is successfully formed. From Fig. 7, we can see that only the parts with Δz of 0.7 and 1.0 mm are formed successfully and the facture occurs earlier with lower step down size. This can be explained by the fact that smaller Δz values lead to closer tool punch passes. In particular, with small Δz, the amount of already hardened material which is deformed by the tool punch in each pass is higher; therefore, the stress required for the deformation raises. As a result of the higher stress state induced in the material, the sheet formability is reduced.

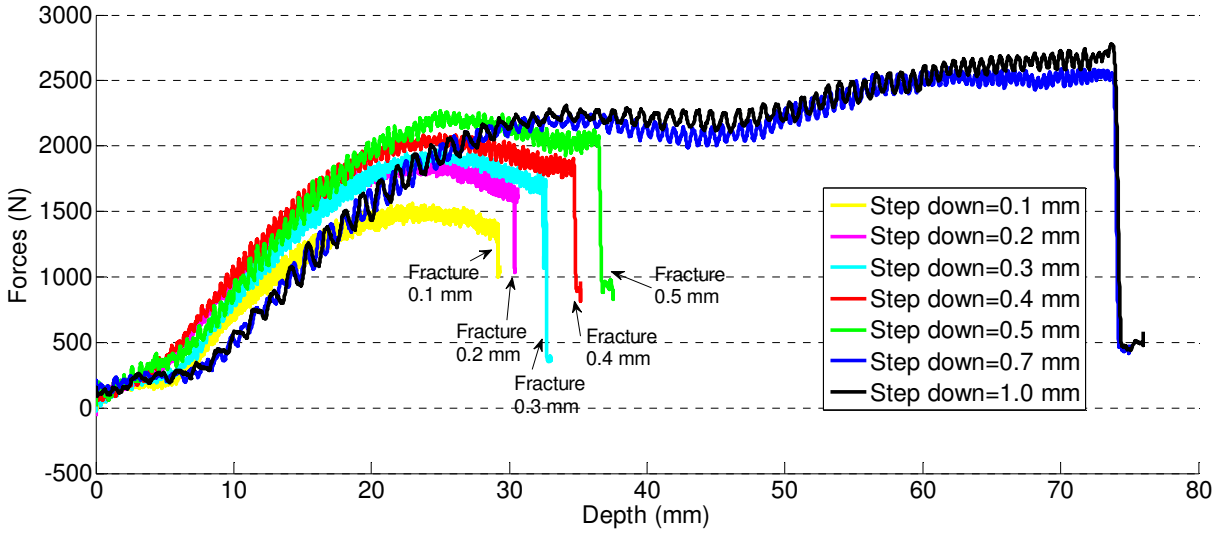

Fig. 7 Vertical force trend with the varying of step down size (fracture parts are marked).

The maximum values of F_{yp} and F_{zp} are plotted in Fig. 8. The figure shows that both F_{yp} and F_{zp} increase with step down size. More specifically, the relation between peak forces and Δz can be approximated as a linear function.

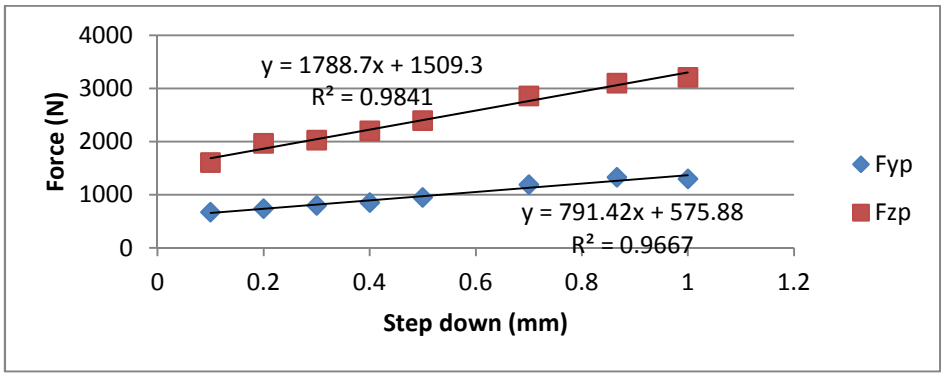

Fig. 8 Variations of forming forces with different step down sizes.

Comparison of the Modeling and Experimental Results

Tangential forces converted from measured results and the predicted values are plotted in Fig. 9. By comparison, the current model can provide good agreement with experimental results for the cases with small step down sizes (below 0.5 mm). The larger deviations for larger step down sizes may be due to the inherent limits existing in the present model. Firstly, the analytical model is based on the assumption that no material flow occurs in the radial direction. Therefore, only transverse shear strains of the deformed elements are considered and no stretching behavior is taken into account along the radial component. However, stretching which causes membrane strain is one of the significant mechanics in some experimental tests [24] and Finite Element simulations [25]. Secondly, the deformation zone is represented by Bezier curves which may be larger than the actual deformed area, resulting in the higher force value. Furthermore, the assumption that the non-contact regions of

the sheet are considered as rigid material may also cause the over prediction of the force. To provide further insight into these above limits, a complete strain analysis of the deformed region which includes membrane strains could be performed.

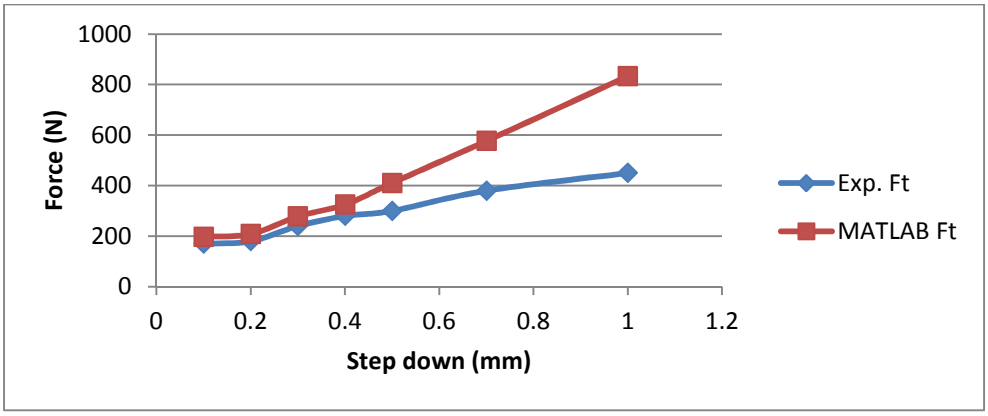

Fig. 9 Comparison between MATLAB model and experimental values.

Conclusion

- Forming forces have been successfully measured on a benchmark ISF case by means of strain gauges and provide useful information to understand the forming process. By analyzing the development of the force, it can be concluded that the forces are attributed to the bending effect of the sheet in the former stage but the combined effects of sheet thinning and strain hardening appear to be important in the second half of the process.
- From the experimental results, by varying wall angles from 30 ° to 70°, the maximum vertical force was observed for the cone with 50° wall angle; while the maximum horizontal forces F_{yp} present a linear growth with the increase of wall angle. Large values of step down size would cause the increase of both vertical and horizontal forces. In the investigated range, a small wall angle and big step down size should be selected to achieve a better formability in terms of forming depth.
- An efficient force prediction model based on upper-bound approach is presented and good agreement is achieved within a limited step down size compared with experimental results. The limitations of the current model are identified for future work.

Acknowledgements: The present work was supported by Australian Research Council (ARC) Linkage project.

References

[1] J. Jeswiet, F. Micari, G. Hirt, A. Bramley, J. Duflou, J. Allwood, Asymmetric single point incremental forming of sheet metal, Annals of CIRP—Manufacturing Technology, 54 (2005) 623-649.
[2] S.B.M. Echrif, M. Hrairi, Research and Progress in Incremental Sheet Forming Processes, Materials and Manufacturing Processes, 26 (2011) 1404-1414.
[3] B.T. Araghi, A. Göttmann, M. Bambach, G. Hirt, G. Bergweiler, J. Diettrich, M. Steiners, A. Saeed-Akbari, Review on the development of a hybrid incremental sheet forming system for small batch sizes and individualized production, Production Engineering, 5 (2011) 393-404.
[4] K. Essa, P. Hartley, An assessment of various process strategies for improving precision in single point incremental forming, International Journal of Material Forming, 4 (2011) 401-412.
[5] F. Micari, G. Ambrogio, L. Filice, Shape and dimensional accuracy in Single Point Incremental Forming: State of the art and future trends, Journal of Materials Processing Technology, 191 (2007) 390-395.

[6] J.R. Duflou, B. Lauwers, J. Verbert, Study on the Achievable Accuracy in Single Point Incremental Forming, in, Springer Berlin Heidelberg, Berlin, Heidelberg, 2007, pp. 251-262.
[7] R. Malhotra, J. Cao, F. Ren, V. Kiridena, Z. Cedric Xia, N.V. Reddy, Improvement of Geometric Accuracy in Incremental Forming by Using a Squeezing Toolpath Strategy With Two Forming Tools, Journal of Manufacturing Science and Engineering, 133 (2011) 61019.
[8] J.R. Duflou, J. Verbert, B. Belkassem, J. Gu, H. Sol, C. Henrard, A.M. Habraken, Process window enhancement for single point incremental forming through multi-step toolpaths, CIRP Annals - Manufacturing Technology, 57 (2008) 253-256.
[9] P.A.F. Martins, N. Bay, M. Skjoedt, M.B. Silva, Theory of single point incremental forming, CIRP Annals - Manufacturing Technology, 57 (2008) 247-252.
[10] L. Filice, G. Ambrogio, F. Micari, On-Line Control of Single Point Incremental Forming Operations through Punch Force Monitoring, CIRP Annals - Manufacturing Technology, 55 (2006) 245-248.
[11] G. Ambrogio, L. Filice, F. Micari, A force measuring based strategy for failure prevention in incremental forming, Journal of Materials Processing Technology, 177 (2006) 413-416.
[12] A. Petek, K. Kuzman, B. Suhač, Autonomous on-line system for fracture identification at incremental sheet forming, CIRP Annals - Manufacturing Technology, 58 (2009) 283-286.
[13] A. Fiorentino, Force-based failure criterion in incremental sheet forming, (2013) 1-7.
[14] G. Ingarao, G. Ambrogio, F. Gagliardi, R. Di Lorenzo, A sustainability point of view on sheet metal forming operations: material wasting and energy consumption in incremental forming and stamping processes, Journal of Cleaner Production, 29–30 (2012) 255-268.
[15] H. Iseki, An approximate deformation analysis and FEM analysis for the incremental bulging of sheet metal using a spherical roller, Journal of Materials Processing Technology, 111 (2001) 150-154.
[16] R. Aerens, P. Eyckens, A. Van Bael, J.R. Duflou, Force prediction for single point incremental forming deduced from experimental and FEM observations, The International Journal of Advanced Manufacturing Technology, 46 (2010) 969-982.
[17] M.J. Mirnia, B.M. Dariani, Analysis of incremental sheet metal forming using the upper-bound approach, Proceedings of the Institution of Mechanical Engineers, Part B: Journal of Engineering Manufacture, (2012).
[18] J.R.D. J. Jeswiet, Alexander Szekeres, Forces in Single Point and Two Point Incremental Forming, Advanced Materials Research, 6-8 (2005) 449-456.
[19] J. Duflou, Y. Tunçkol, A. Szekeres, P. Vanherck, Experimental study on force measurements for single point incremental forming, Journal of Materials Processing Tech, 189 (2007) 65-72.
[20] J. Allwood, D. Shouler, A.E. Tekkaya, The increased forming limits of incremental sheet forming processes, Key Engineering Materials, 344 (2007) 621-628.
[21] B. Avitzur, C.T. Yang, Analysis of Power Spinning of Cones, Journal of Engineering for Industry, 82 (1960) 231.
[22] R. Uppaluri, N. Venkata Reddy, P.M. Dixit, An analytical approach for the prediction of forming limit curves subjected to combined strain paths, International Journal of Mechanical Sciences, 53 (2011) 365-373.
[23] M. Tisza, Preliminary Studies on the determination of FLD for single point incremental sheet metal forming, Key Engineering Materials, 504 (2012) 863-868.
[24] M.B. Silva, P.S. Nielsen, N. Bay, P.A.F. Martins, Failure mechanisms in single-point incremental forming of metals, The International Journal of Advanced Manufacturing Technology, 56 (2011) 893-903.
[25] C. Henrard, Numerical Simulations of the Single Point Incremental Forming Process, in, 2009.

4.3 The Papers

Paper 4

Efficient force prediction for incremental sheet forming and experimental validation

Li, Y.L., Liu, Z.B., Lu, H.B., Daniel, W. J. T., Liu, S. and Meehan, P. A.

The International Journal of Advanced Manufacturing Technology

2014, Volume: 73, Pages: 571-587.

Int J Adv Manuf Technol (2014) 73:571–587
DOI 10.1007/s00170-014-5665-2

ORIGINAL ARTICLE

Efficient force prediction for incremental sheet forming and experimental validation

Yanle Li · Zhaobing Liu · Haibo Lu · W. J. T. (Bill) Daniel · Sheng Liu · Paul A. Meehan

Received: 16 September 2013 / Accepted: 21 January 2014 / Published online: 19 February 2014

Abstract Incremental sheet forming (ISF) has been attractive during the last decades because of its greater flexibility, increased formability and reduced forming forces. However, traditional finite element simulation used for force prediction is significantly time consuming. This study aims to provide an efficient analytical model for tangential force prediction. In the present work, forces during the cone-forming process with different wall angles and step-down sizes are recorded experimentally. Different force trends are identified and discussed with reference to different deformation mechanisms. An efficient model is proposed based on the energy method to study the deformation zone in a cone-forming process. The effects of deformation modes from shear, bending and stretching are taken into account separately by two sub-models. The final predicted tangential forces are compared with the experimental results which show an average error of 6 and 11 % in respect to the variation of step-down size and wall angle in the explored limits, respectively. The proposed model would greatly improve the prediction efficiency of forming force and benefit both the design and forming process.

Keywords Incremental sheet forming · Forming force · Formability · Prediction · Shear · Bending

Nomenclature

t_0	Initial sheet of the metal sheet
Δz	Vertical step-down size of the tool path
A	Wall angle of the cone part
f	Feed rate of the forming tool
r_t	The radius of the forming tool
r_i	The radius of the current tool position
r_o	The outer radius of the deformed zone
r	The radius of the flow line
θ_c, θ_t and θ_s	Dividing angles for the flow line
M and N	Parameters used for optimising dissipated power
Z_t	Vertical position of the tool head surface
Z_s	Vertical position of the sheet after previous tool path
$S(X)$	Shape function
Zf_c, Zf_s and Zf_s	Curve functions for the flow line
v_r, v_θ and v_z	Components of velocity in deforming zone
$\dot{\varepsilon}_{ij}$	Components of strain rates in deforming zone
ε	Plastic strain
y_0	Average yield strength
E_h	Slope of the stress–strain curve
$\dot{w}$	Dissipated power
F_x, F_y and F_z	Force components in global orthogonal Cartesian coordinate system
F_{xp}, F_{yp} and F_{zp}	Peak values of the measured force
Ft	Average value of the converted tangential force at the steady state

Y. Li (✉) · Z. Liu · H. Lu · W. J. T. (B). Daniel · S. Liu · P. A. Meehan
School of Mechanical and Mining Engineering, The University of Queensland, St Lucia, Brisbane, QLD 4072, Australia
e-mail: yanle.li@uq.edu.au

1 Introduction

Incremental sheet forming (ISF) technology is an emerging forming process ideal for rapid prototype and small batch production. In an ISF process, a flat metal sheet is gradually formed into the designed 3D shape using computer numerical control (CNC)-controlled generic tool stylus. The process is highly flexible such that very complex shapes can be achieved with careful tool path programming and sometimes with the

support of a die. Therefore, ISF was widely accepted as a promising forming process over conventional processes such as deep drawing and stamping [1, 2] for small batch production. Emmens et al. [3] comprehensively reviewed the history of the technology of ISF. Three development periods were clarified and an extensive list of patents was provided which directly reflects that ISF has received great attention particularly in the automotive industry. However, one of the dominant limits for the further development and commercialization of ISF technology is the limited geometrical accuracy of the final shape [4]. Essa and Hartley [5] investigated the effects of adding a backing plate, a supporting kinematic tool and modifying the final stage of the tool path on the improvement of the geometrical accuracy through a finite element (FE) model. It was found that the sheet bending near the initial tool contact location was minimised by the backing plate; the springback was reduced by the kinematic tool; and the pillow effect was eliminated by the modified tool path. Although various strategies [6] have been proposed to improve product accuracy, a systematic understanding of the local deformation mechanics and further investigation on the forming force are essential.

Over the past few years, forces during ISF have been intensively studied mainly experimentally due to its possible application in aspects including on-line control, failure prevention and process optimization. Duflou et al. [7] experimentally investigated the relationship of the forming forces with the four selected process parameters: the vertical step-down size, tool diameter, wall angle and the initial sheet thickness. It was concluded that the forming forces will increase with the increase of vertical step-down size, wall angle and sheet thickness. Filice et al. [8] worked on the force analysis and classified the force trends of tangential force into three types: steady-state force trends, polynomial force trends and monotonically decreasing force trends. Ambrogio et al. [9] concluded that the force gradient after the peak can be effectively considered as a critical indicator to detect and prevent workpiece fracture. Therefore, forming force is a potential indicator for forming limits identification. Petek et al. [10] proposed an autonomous on-line system for fracture identification and localization by analysing the reaction force with a skewness function. Another failure criterion presented by Fiorentino [11] is based on force monitoring during the forming process. This approach was achieved by comparing the stresses acting on the material calculated from forming forces with the ultimate strength of the material. Additionally, Ingarao et al. [12] investigated the use of recorded force data to evaluate the energy consumption required for the ISF process, which provides guidance for sustainable development of the process.

Prediction of forming forces in ISF provides understanding of the deformation mechanics, monitoring of the forming process, failure prediction, and a means of on-line control and optimisation. The efficient prediction of the forming force is still one of the main limitations for the further development of ISF technology, although some authors attempted to bridge the existing gap. Even though FE models are commonly used to predict forming force for various forming processes, it is significantly time consuming for the ISF process. This is partly due to the fact that the deformation of the sheet during ISF is localised and continuously changing over the whole process. Smith et al. [13] reported a simulation time of 24 days for a single point incremental forming process for a truncated cone with a major diameter of 45 mm and wall angle of 40°. To overcome the above computational challenges of the FE approach, Raithatha and Duncan [14] developed a new model that is based on the numerical minimization of internal work within the material. In this method, the minimization of plastic work was formulated as a second-order cone programming (SOCP) optimization problem and was solved efficiently using primal dual interior point SOCP algorithms. The results showed that the computing time for a straight line indentation on a sheet with dimensions of 0.1×0.1 m is 5–9 min. However, the reduced computing time was achieved at a loss of model accuracy which results in considerable fluctuation at the roof of the groove. Iseki [15] obtained the forming forces for the incremental forming of a pyramid using an approximated deformation analysis. The analysis was based on a plane-strain deformation model, and the results were validated with experimental values. Aerens et al. [16] studied the incremental forming of truncated cones with different materials using experimental and statistical analyses. Regression formulae were proposed to predict the triple forming forces including axial, radial, and tangential components from input variables including wall angle, initial thickness, tool diameter, and vertical pitch. Finally, an approximate formula was deduced for predicting the axial component for forming any material based on the tensile strength only. Recently, Mirnia and Dariani [17] proposed a new approach to predict the tangential force on a truncated cone using an assumed deformation zone and an upper-bound analysis. It was reported that the forces were in good agreement with those from the experimental work of Aerens et al. [16]. Nevertheless, large errors can be expected for severe deformation conditions (e.g. $\Delta z > 0.5$ mm).

The above review of the recent studies shows that most of the previous work on forming force is investigated experimentally and very few models are available for the efficient prediction of the forming force. Although complex forming processes can be modelled through numerical methods, analytical study of the process still plays a pivotal role in understanding the mechanism of the process and developing efficient predictive modelling. This study will present an analytical method to analyse the deformation of the contact region

and also calculate the required forming force by taking into account two different deformation mechanisms. In particular, the main contributions of this paper are:

- The development and application of two efficient analytical sub-models for tangential force prediction in the ISF process. All three major deformation modes involved in ISF, shear, bending and stretching are taken into account.
- The generalisation and validation of an empirically combined efficient model. A comparison of the results obtained with a very efficient combined model with the experimental values to determine the validity of assumptions for three different deformation mechanisms.
- The experimental investigation and quantification of the effects of wall angle and step-down size on forming force and part formability in terms of failure depth.

To this end, the experimental set up and machine for the cone-forming process is firstly described in Section 2. Subsequently, Section 3 outlines the methodological approach including theoretical justifications and analytical techniques used for the proposed analytical force prediction model. The experimental force results with different forming parameters are then provided in Section 4. This section also provides the results for the tuning and validation of the models to the experimental results. Finally, conclusions and future work are presented in Section 5.

2 Experiments

To facilitate the study of the effect of product geometry and step-down size on the forming force and formability, truncated cones with different wall angles were selected as the target shapes.

2.1 Equipment setup

The forming tests were performed on a state-of-the-art machine dedicated for the multi-point ISF process designed by Amino Corporation as shown in Fig 1. The machine allows mould based forming for a maximum size of 2,100×1,450×550 mm with a FANUC controller for precise control. The movement of the two horizontal axes (X and Y) can have a maximum speed of 60 m/min with a repeatability of ± 0.05 mm. The vertical (Z) axis is driven by an AC servo motor with the power of 1 kW that allows a maximum acting force of 3 kN. The hemispherical tool with a radius of 15 mm was used to deform the material. The tip of the tool is tungsten carbide and the body is made of K110 steel which was hardened and tempered to HRC60. The sheet material used in the present study was aluminium 7,075-O sheet with 1.6 mm in thickness and was cut into 300×300 mm in size.

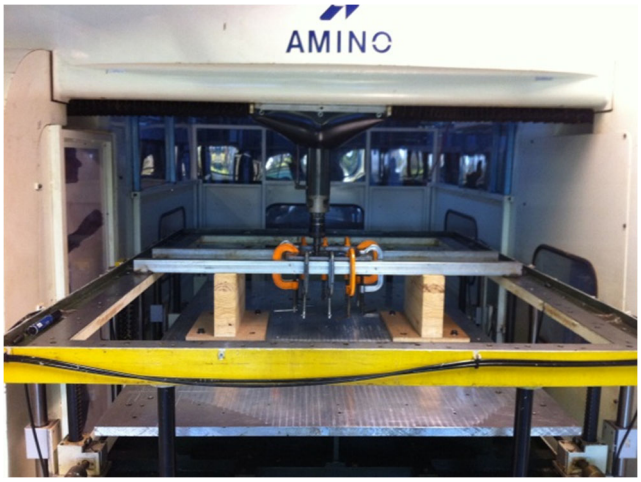

Fig. 1 Incremental sheet forming on amino machine

Figure 2 presents the true stress–strain curves for aluminium 7075-O sheets with 1.6 mm thickness derived from the tensile test for three different directions (rolling, diagonal and transverse). It shows that the deviations of the curves are quite small so the material can be assumed to be isotropic. Similar to r value averaging, the true stress values for three directions can be averaged as,

$$\overline{\sigma} = \frac{\sigma_0 + 2\sigma_{45} + \sigma_{90}}{4} \tag{1}$$

where σ_0, σ_{45} and σ_{90} are the true stress values in rolling, diagonal and transverse direction, respectively. Then the stress–strain relation for the sheet can be fit by the Swift type work hardening power law,

$$\overline{\sigma} = K(\varepsilon_0 + \varepsilon)^n, \tag{2}$$

where ε is the plastic strain; K, ε_0 and n are material parameters listed in Table 1.

The forming forces acting on the forming tool have been measured continuously over time during the process. There are several ways to capture the forming force, such as the cantilever sensor designed by Jeswiet [18] and force dynamometer used by Duflou et al. [7]. In the present work, three full Wheatstone bridges configured by four strain gauges have been designed and mounted on the hemispherical tool. The three bridges were designed to measure the three orthogonal forces: two bending directions (F_x and F_y) and one axial direction (F_z), respectively. Those strain gauges were calibrated twice in all three directions by applying a series of known forces. The calibrated system shows a mostly linear relation between strain and output voltage.

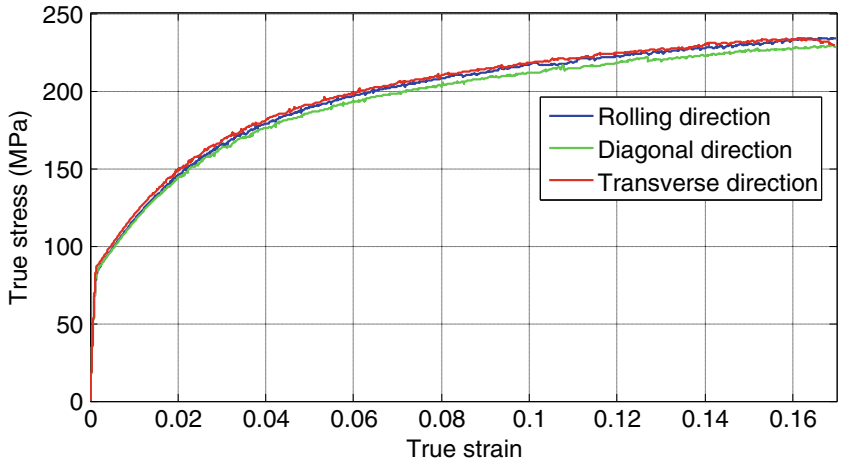

Fig. 2 True stress–strain curves for 7075-O aluminium alloy sheets with 1.6 mm thickness

2.2 Experimental tests

Lubricant (Shell Tellus Oil 68) was sprayed liberally on the blank before forming to prevent excessive friction. A backing plate was placed underneath the sheet in order to increase the rigidity between the forming area and sheet flange. The feed rate of the forming tool was set to 4,000 mm/min. Figure 3 shows the experimental configuration and a case study of a truncated cone formed by Amino CNC machine.

For the tool path strategy, the *Z*-level tool path with different vertical step-down size (Δz, the increment between two successive passes) were utilised so the truncated cones are formed in a stepwise manner with many contours. All the cones were designed with the same major diameter of 140 mm but with a smaller cone height for smaller inclination of the wall due to the geometric constraint. The angle between the deformed sheet to the horizontal plan is defined as wall angle (α). The tests were conducted until fracture and the forming forces for all the three orthogonal components (F_x, F_y and F_z) were recorded continuously during this process. Two sets of experiments have been designed and the detailed process parameters are listed in Tables 2 and 3. Specifically, wall angles of the truncated cone have been set ranging from 30° to 70° while other parameters are constant (i.e. Δz= 0.5 mm, t_0=1.6 mm,f=4,000 mm/minand r_t=15 mm) to investigate the effect of wall angle on forming forces and formability. Similarly, in the second set of experiments, step-down sizes have been designed varying from 0.1 to 1.0 mm, whereas other parameters are fixed to study how step down affects the forming force and formability in the cone-forming process.

Table 1 Mechanical properties of Aluminium 7075-O sheets with 1.6 mm thickness

Material	7075-O
Density (t/mm^3)	2.81×10^{-9}
Young's modulus (GPa)	70
Poisson's ratio	0.33
Tensile Yield Strength (MPa)	92
Ultimate Tensile Strength	198
Plastic coefficient K	352.58
Hardening exponent n	0.221

3 Modelling

In this model, the energy method [19] is used to analyse the deformation behaviour and predict the tangential force of the truncated cone during the ISF process. According to the theory of the energy method, the total power of the plastic deformation should have minimum value. Under this condition, the 3D-deformed shape of the metal sheet and the strain components with minimum dissipated power are recognised as the best approximation for those of actual deformation. This theory is employed to analyse the deformation mechanism and predict the forming force in the ISF process.

A concise block diagram of the procedure to analyse deformation of the deformed curved surface is presented in Fig. 4. Two sub-models based on different deformation mechanisms (shear and bending with stretching) are included in the present model to investigate how the deformation mode is affected by the variation of forming parameters. By making different assumptions of the deformed curved surface, the total dissipated power of the sheet because of the combination of shear, bending and stretching can be calculated and minimised. Once the minimum total power is determined, the detailed information of the deformed zone and tangential force can be calculated.

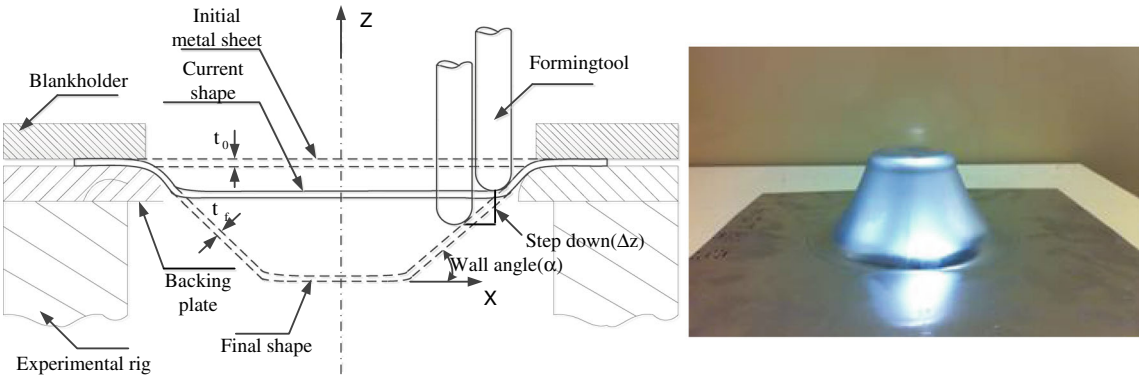

Fig. 3 Sketch of ISF experimental parameters and a case study made from Al 7075-O of 1.6 mm in thickness

The critical task is to construct a proper deformed curved surface for the local deformed area ahead of the forming tool to express the actual deformation. The metal sheet other than the deformed area is assumed rigid. Figure 5 sketches the deformation zone in ISF from different viewing aspects. Parameters used for the analytical formulation are marked in the figure. It is assumed that the deformation area induced by the current tool path is a circle within a radius of $(r_o–r_i)$ ahead of the tool with the same centre of the hemispherical tool; where r_i is the current tool path radius and *ro* is the outer radius of the deformed zone which can be obtained from the geometric relations between the current and previous forming path. Along the circumferential direction, a series of flow lines are assumed to express the surface at the centre of the metal sheet of the deformed sheet.

In the present model, as shown in Fig. 5c, the deformation zone is divided into three regions: I, contact region; II, non-contact region following the height of tool head; and III, non-contact region following the height of the formed sheet. One of the typical flow lines with a radius of r is depicted in Fig. 5b. The flow line is defined as three curves Zf_c,Zf_t and Zf_s which correspond to regions I, II and III, respectively (see Appendix 1 for calculation procedure of three deformation regions). Zf_c has the same geometric function with the tool head surface as it is the region contacting with the tool but the conjunct point with Zf_t is unknown therefore is advisable to be determined as the following equation with an adjustable parameter M,

$$Zf_c(r,\theta) = Z_c = M(Z_s–Z_o) + Z_o, \qquad (0\le M\le 1) \quad (3)$$

where Z_s and Z_o are the vertical position of the sheet formed in previous pass and the tool vertex with the radius of r. To represent the height variation of the non-contact surface of the sheet, a normalised shape function $S(X)$ is introduced. $S(X)$ is tentatively designed as two-second order Bezier curves with the following equation,

$$S(X) = \left\{ \begin{array}{ll} 1-\left(\frac{\theta-\theta_c}{\theta_t-\theta_c}\right)^2(1-N)\left(\frac{r_o-r}{r_o-r_i}\right) & \theta_c\le\theta\le\theta_t \quad 0\le N\le 1 \\ 1-\left(\frac{\theta-\theta_s}{\theta_s-\theta_t}\right)^2(1-N)\left(\frac{r_o-r}{r_o-r_i}\right) & \theta_t\le\theta\le\theta_s \quad 0\le N\le 1 \end{array} \right\} \quad (4)$$

Here, N is another adjustable parameter which can be obtained through the optimisation of the dissipated power. The value of $S(X)$ changes from N to 1 corresponding to the variation of θ and r within their ranges. The calculated shape function $S(X)$ is presented in Fig. 6 with different values of N. As shown in the figure, the pattern of the shape function is significantly affected by the value of N which makes it

Table 2 Experimental design for different wall angles

Wall angle α (deg)	Step-down Δz (mm)	Tool radius (mm)	Thickness (mm)	Feed rate (mm/min)	Designed height (mm)
30	0.5	15	1.6	4,000	28
40	0.5	15	1.6	4,000	40
50	0.5	15	1.6	4,000	60
60	0.5	15	1.6	4,000	75
62	0.5	15	1.6	4,000	75
63	0.5	15	1.6	4,000	75
65	0.5	15	1.6	4,000	75
70	0.5	15	1.6	4,000	75

Table 3 Experimental design for different step-down sizes

Wall angle α (deg)	Step-down Δz (mm)	Tool radius (mm)	Thickness (mm)	Feed rate (mm/min)	Designed height (mm)
60	0.1	15	1.6	4,000	75
60	0.2	15	1.6	4,000	75
60	0.3	15	1.6	4,000	75
60	0.4	15	1.6	4,000	75
60	0.5	15	1.6	4,000	75
60	0.7	15	1.6	4,000	75
60	1.0	15	1.6	4,000	75

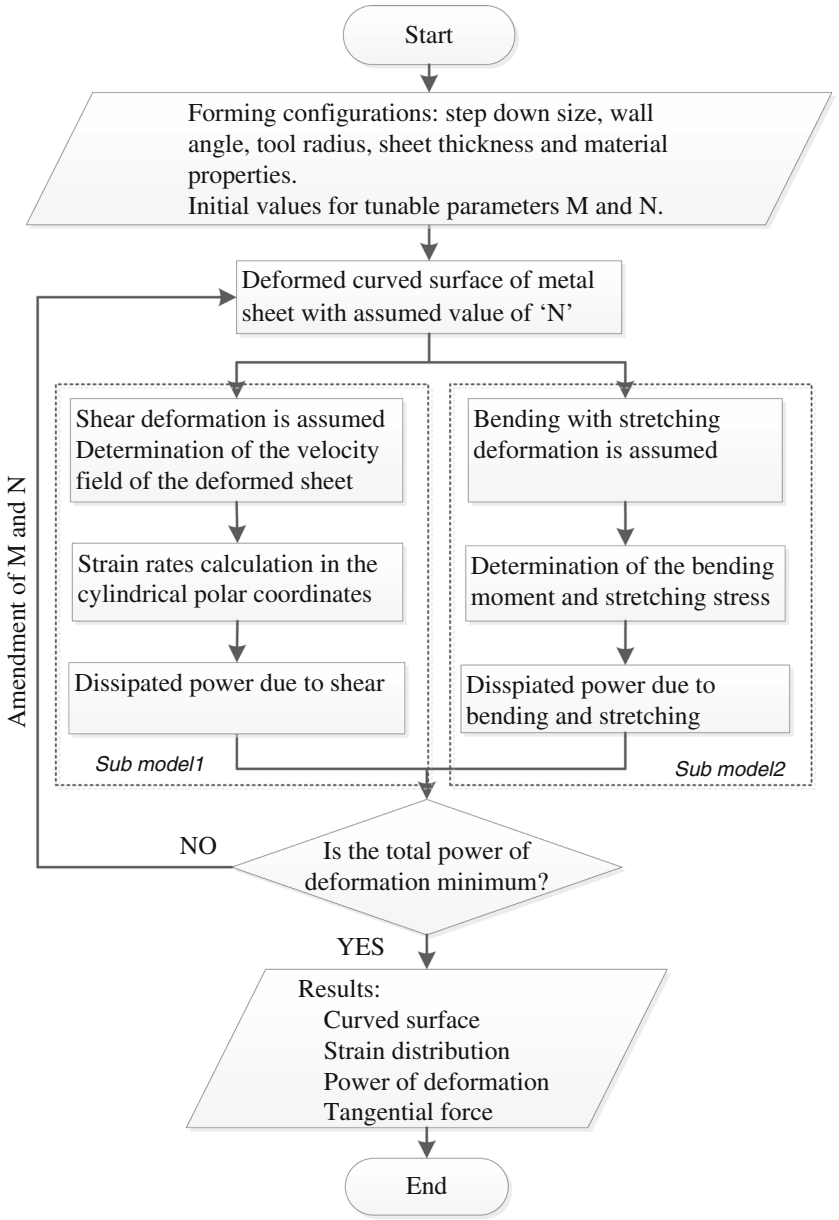

Fig. 4 Block diagram of the procedure to analyse deformation of the deformed curved surface

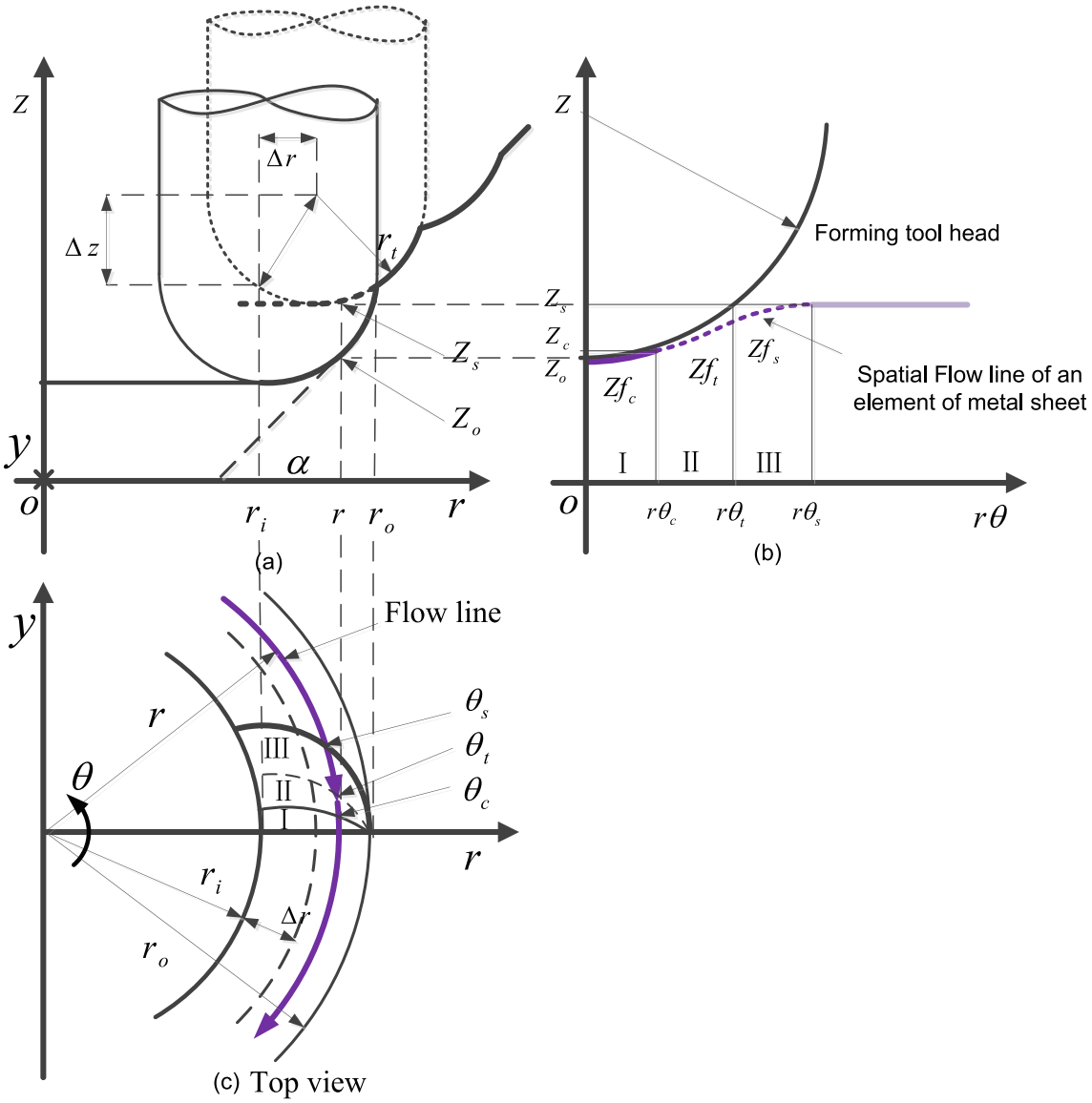

Fig. 5 Deformation zone in the cone-forming process: **a** $r-z$ view of the geometrical relations in incremental sheet forming during previous and current path, **b** $r\theta-z$ view and **c** $r-\theta$ view of a typical flow line for the deformed curved surface along the circumferential direction of the sheet ahead of the tool

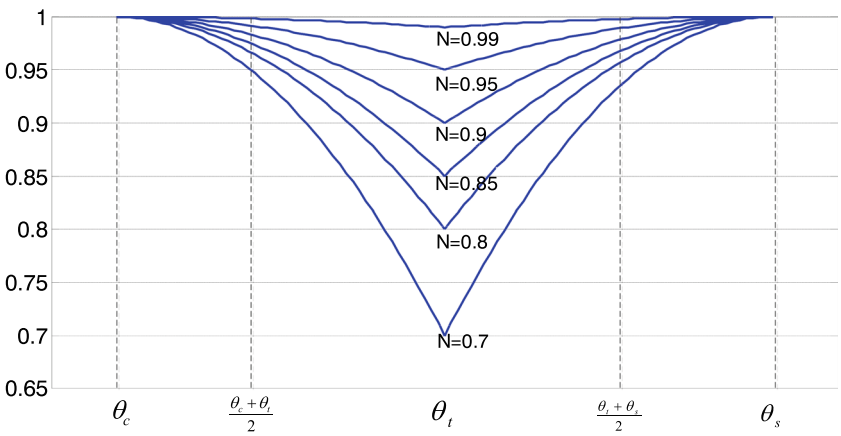

Fig. 6 Calculated curves of shape function $S(X)$ with different values of parameter in N

effective to control the flow line. Another advantage of this definition is to satisfy the boundary condition and also to avoid the velocity discontinuity on the surface with θ_c and θ_s. However, a velocity discontinuity surface is introduced at the intersecting surface of the two shape functions. It should be noted that the dissipated power because of the discontinuity should also be included in subsequent calculation. Using the shape function, the flow line is defined by the following equation,

$$Zf = \left\{ \begin{array}{ll} Zf_c(r,\theta) = Z_t & (0 \le \theta \le \theta_c) \\ Zf_t(r,\theta) = S(X) * Z_t & (\theta_c \le \theta \le \theta_t) \\ Zf_s(r,\theta) = S(X) * Z_s & (\theta_t \le \theta \le \theta_s) \end{array} \right\} \quad (5)$$

Zf_t is defined following on the geometry of the tool surface Z_t, whereas Zf_s is based on the height of the sheet in previous pass (refer Fig. 5 for symbol definition). As a result, the flow line for the deformation zone is successfully defined using two adjustable parameters M and N and can be tailored by adjusting these presupposed parameters. In the following section, the detailed calculation procedure for two sub-models based on the assumed deformation zone and flow line is described.

3.1 Sub-model 1—shear deformation

3.1.1 Velocity field and strain rates

For a flow line at radius r, it only flows in the vertical and the circumferential directions, thus

$$v_r = 0 \quad (6)$$

In the circumferential direction, the sheet metal rotates at an angular velocity f/r_i round the centreline of the cone, thus

$$v_\theta = r\frac{f}{ri} \quad (7)$$

The vertical component can be calculated from the flow line function as,

$$v_z = \frac{\partial Zf}{\partial r}v_r + \frac{\partial Zf}{\partial \theta}\dot{\theta} \quad (8)$$

Therefore, by substituting v_r=0 and $\dot{\theta} = f/r_i$,

$$v_z = \frac{f}{r_i}\frac{\partial Zf}{\partial \theta} \quad (9)$$

The strain rates in the cylindrical polar coordinates are defined as,

$$\begin{array}{lll} \dot{\varepsilon}_{rr} = \dfrac{\partial v_r}{\partial r} & \dot{\varepsilon}_{\theta\theta} = \dfrac{\dot{u}_r}{r} + \dfrac{1}{r}\dfrac{\partial v_\theta}{\partial \theta} & \dot{\varepsilon}_{zz} = \dfrac{\partial v_z}{\partial z} \\ \dot{\varepsilon}_{r\theta} = \dfrac{1}{2}\left(\dfrac{1}{r}\dfrac{\partial v_r}{\partial \theta} + \dfrac{\partial v_\theta}{\partial r} + \dfrac{v_\theta}{r}\right) & \dot{\varepsilon}_{\theta z} = \dfrac{1}{2}\left(\dfrac{\partial v_\theta}{\partial z} + \dfrac{1}{r}\dfrac{\partial v_z}{\partial \theta}\right) & \dot{\varepsilon}_{rz} = \dfrac{1}{2}\left(\dfrac{\partial v_r}{\partial z} + \dfrac{\partial v_z}{\partial r}\right) \end{array} \quad (10)$$

By substituting the velocity field into above equations, the strain rates are obtained as,

$$\dot{\varepsilon}_{\theta z} = \frac{f}{2rr_i}\frac{\partial^2 Zf}{\partial \theta^2} \quad (11)$$

$$\dot{\varepsilon}_{rz} = \frac{f}{2r_i}\frac{\partial^2 Zf}{\partial \theta \partial r} \quad (12)$$

$$\dot{\varepsilon}_{ij} = 0.(\text{for strain rate in other directions}) \quad (13)$$

From the above calculation, it can be noticed that all the strain rate components are equal to zero except the shear components in vertical directions ($\dot{\varepsilon}_{\theta z}$ and $\dot{\varepsilon}_{rz}$). Since the dissipated power is calculated based on the value of strain rates, this sub-model is entirely due to the shear deformation mode.

3.1.2 Dissipated power

As mentioned in the previous section, introduction of the shape function $S(X)$ results in a velocity discontinuity surface at the angle of θ_t. The dissipated power due to the discontinuity can be integrated along the discontinuity surface as,

$$\dot{w}_{\text{dis}} = \iint_{\text{dis}} k|\Delta v|\mathrm{d}s, \quad (14)$$

where k is the yield shear stress and its relation with average yield strength (refer Appendix 2) is express as,

$$k = \frac{y_0}{\sqrt{3}} \quad (15)$$

In the above equation, Δv is the velocity discontinuity in the vertical direction and can be computed in the following equation,

$$\Delta v = \Delta v_z = \frac{f}{r_i}\frac{\partial z f_s}{\partial \theta_{\theta=\theta_t}} - \frac{f}{r_i}\frac{\partial z f_t}{\partial \theta_{\theta=\theta_t}} \quad (16)$$

The dissipated power of the flow line during the cone-forming process, computed using strain rates, neglecting the velocity discontinuity can be expressed as,

$$\dot{w}_f = y_0 \iiint \left(\frac{2}{3}\dot{\varepsilon}_{ij}\dot{\varepsilon}_{ij}\right)^{\frac{1}{2}} \mathrm{d}v = \frac{2y_0 t_0}{\sqrt{3}} \iint \left(\dot{\varepsilon}_{\theta z}{}^2 + \dot{\varepsilon}_{rz}{}^2\right)^{\frac{1}{2}} \mathrm{d}s \tag{17}$$

where t_0 is the initial thickness of the sheet. Accordingly, the total dissipated power due to shear deformation is obtained as,

$$\dot{w}_{\text{shear}} = \dot{w}_{\text{dis}} + \dot{w}_f. \tag{18}$$

The above equation for dissipated power is a function of two optimising parameters M and N. By minimising the dissipated power with varying M and N in their defined range (i.e. $0 \le M,N \le 1$), the deformed curved surface for the deformation zone closer to the experiment is obtained. It is reasonably assumed that the rate of plastic work due to the tangential force acting on the forming tool is,

$$\dot{w}_{\text{shear}} = F_t v_\theta \tag{19}$$

Now, by substituting the average radius of the deformed zone $(r_i+r_o)/2$ into equation (7) to obtain the angular velocity, the tangential force can be expressed as,

$$F_{\text{shear}} = \frac{r_i \dot{w}_{\text{shear}}}{f \cdot (r_i + r_o)/2} \tag{20}$$

3.2 Sub-model 2—bending with stretching

3.2.1 Bending moment and tensile stress

In the current analysis, the dissipated power is minimised through the optimisation of the flow line in the circumferential direction while neglecting the influence along the radial direction. This is based on the following considerations. Firstly, the bending moment and tensile stress could be more sensitive to the shape of the flow line in the forming direction than the radial direction. In addition, in radial direction, the sheet is already curved in the previous pass and the deformed curve is very close to the tool surface so the allowed optimising range is limited. Therefore, the current analysis can increase the calculating efficiency without significant sacrifice in terms of accuracy. Assume the flow line along the circumferential direction is mainly in the deformation mode of bending under stretching. The stress and strain distributions are shown in Fig. 7 in which the range of strain across the thickness is from just below the mid-surface strain ε_{1a}, to just above it. Since the sheet is completely yielded, a strain-hardening effect is assumed for the material sheet as a Swift type of power law. The stress–strain relation is then regarded to be linear across the thickness with constant value of E_h which corresponds to the slope of the stress–strain curve at a local strain value of ε_{1a}. In ISF, the radius of curvature is assumed to be large compared with the thickness, so the bending strain can be approximated as,

$$\varepsilon_b = \ln\left(1 + \frac{y}{\rho_0}\right) = \frac{y}{\rho_0}, \tag{21}$$

where y is the distance to the mid-surface and ρ_0 is the radius of the curved sheet. So the total strain at some distance y from the mid-surface is given by,

$$\varepsilon_1 = \varepsilon_a + \varepsilon_b = \varepsilon_{1a} + \frac{y}{\rho_0} \tag{22}$$

The stress is then given by,

$$\sigma_1 = \sigma_a + E_h \cdot \frac{y}{\rho_0} \tag{23}$$

The moment associated with the stress distribution is then computed as,

$$M = \int_{-t_0/2}^{t_0/2} \left\{\sigma_a + E_h \cdot \frac{y}{\rho_0}\right\} y \mathrm{d}y = \frac{E_h}{\rho_0}\frac{{t_0}^3}{12} \tag{24}$$

Also, the tensile stress is given as,

$$T = \sigma_a t_0 \tag{25}$$

3.2.2 Dissipated power

As shown in Fig. 7a, the local strain along the circumferential direction can be calculated according to Eq. (4) in [20],

$$\varepsilon_{1a} = \frac{dl - d_0}{d_0} = \frac{\rho_0 \mathrm{d}\varnothing - \rho_0 \mathrm{d}\varnothing \cos\varnothing}{\rho_0 \mathrm{d}\varnothing \cos\varnothing} = \frac{1}{\cos\varnothing} - 1 \tag{26}$$

The slope angle of the flow line can be approximated as,

$$\tan\varnothing = \frac{1}{r}\frac{\partial zf}{\partial \theta} \tag{27}$$

The above equation states the relation between the slope angle $\varnothing$ and the tool travelling angle θ, thus the rate of plastic work for the deformation zone due to bending can be given as,

$$\dot{w}_b = \iint M \,\dot{\mathrm{d}}\varnothing \,\mathrm{d}s = \iint \frac{E_h}{\rho_0}\frac{{t_0}^3}{12}\frac{\mathrm{d}\varnothing}{\mathrm{d}\theta}\frac{\mathrm{d}\theta}{\mathrm{d}t}\mathrm{d}s \tag{28}$$

Similarly, the rate of plastic work due to tension stress is,

$$\dot{w}_s = \iint T\varepsilon_a \,\dot{\mathrm{d}}l \,\mathrm{d}s = \iint \sigma_a t_0 \varepsilon_a \rho_0 \,\dot{\mathrm{d}}\varnothing \,\mathrm{d}s = \iint \sigma_a t_0 \varepsilon_a \rho_0 \frac{\mathrm{d}\varnothing}{\mathrm{d}\theta}\frac{\mathrm{d}\theta}{\mathrm{d}t}\mathrm{d}s \tag{29}$$

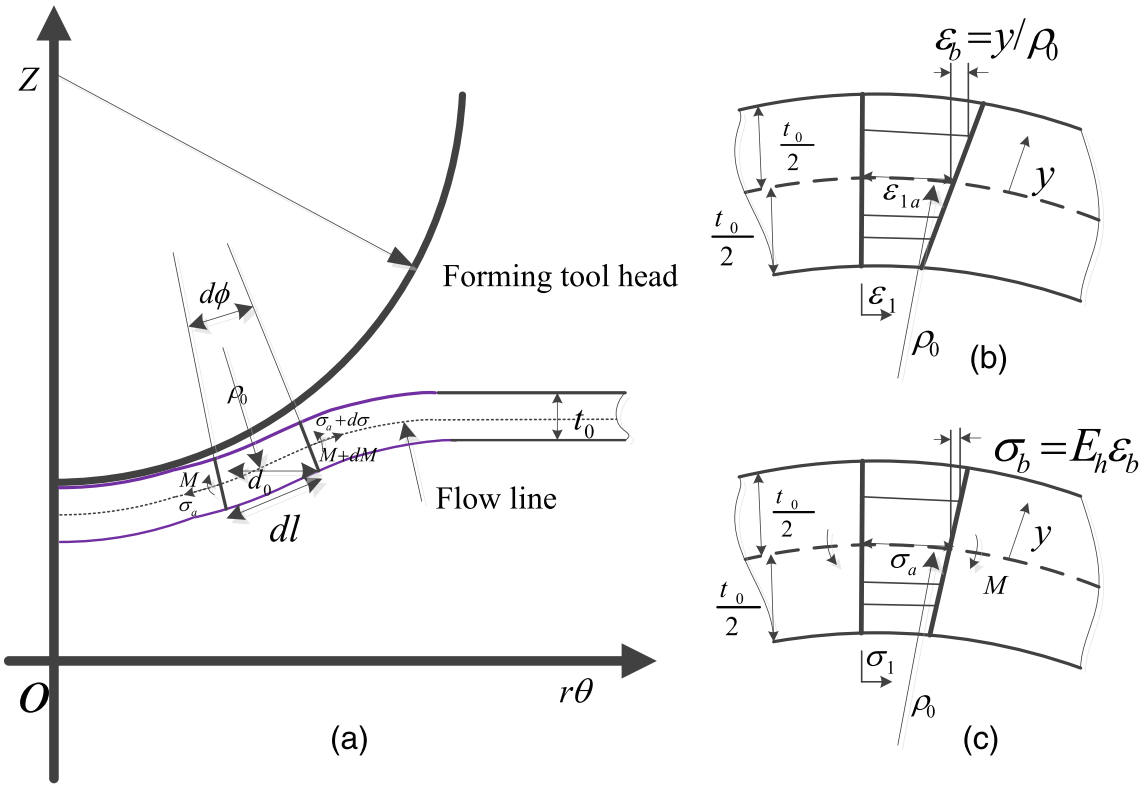

Fig. 7 **a** Deformed diagram showing the range of stress for the sheet bent and stretched to a mid-surface strain of ε_{1a}. **b** The strain distribution when bent over a tool of radius ρ_0 and **c** the stress distribution

Accordingly, the total dissipated power due to bending and stretching is,

$$\dot{w}_{bs} = \dot{w}_b + \dot{w}_s \tag{30}$$

Similar to Eq. (20), the tangential force is computed as,

$$F_{bs} = \frac{r_i \dot{w}_{bs}}{f \cdot (r_i + r_o)/2} \tag{31}$$

4 Results

4.1 Force trend in ISF

Figure 8 presents the record of the three component of force over the process (α=60°, Δz=0.5 mm) versus time with a zoomed view. In one cycle, tangential forces (F_x and F_y) change in a sinusoidal way between their maximum and minimum values due to the current tool position relative to the global absolute axis around a contour of the truncated cone. In contrast with the horizontal forces, the vertical force shows small fluctuations in the final steps caused by the *Z*-level tool path. The amplitude of the forces increases during the early phase of the process and tends to become steady for the rest of the process. This could be due to a number of reasons. Firstly, the initial development of the plastic deformation could result in the rapid increase in forming force according to the characteristic of the stress–strain curve. Previous studies [7, 9] suggest that bending deformation is the most relevant mechanism at this stage. In addition, with the build-up of the contact area between tool head and the sheet surface, the force required to deform the sheet is also increased. Additionally, the increase of the vertical force can be assigned to the continuous deforming of the material which combines bending, shear and stretching mechanisms [21, 22]. The further deformation would result in the increase of the forming force caused by the strain hardening of the material. However, thinning of the material would reduce the magnitude of the force. Therefore, the later contour loops of the forming force are determined by the combined effects of strain hardening and thinning.

4.2 Effect of wall angle

To study the effect of wall angles on the forming force, the vertical forces at wall angles varying from 30° to 70° are

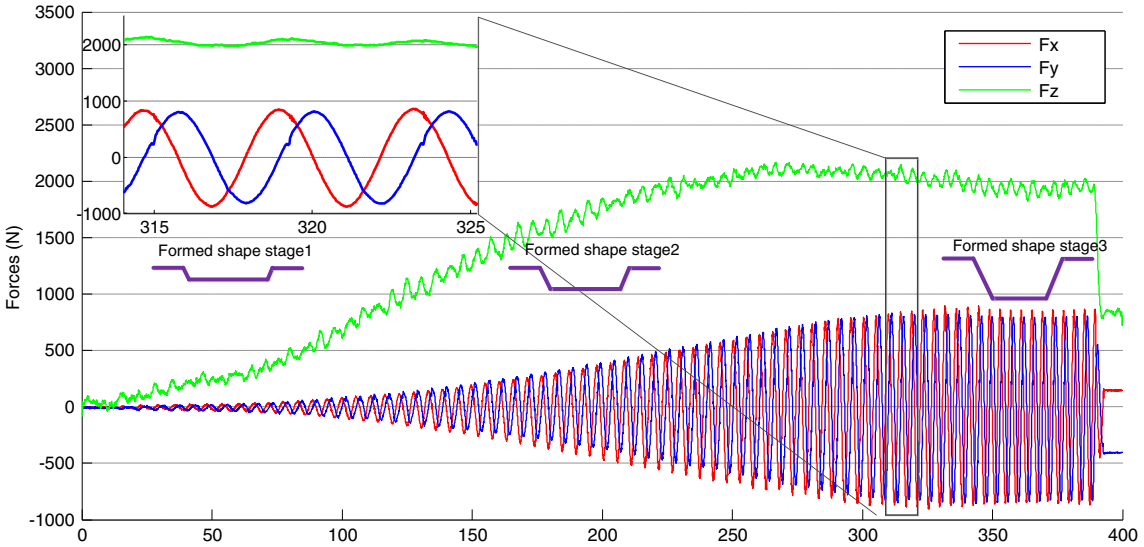

Fig. 8 Three force components (F_x, F_y and F_z) versus forming time and a detailed view for two cycles during forming a cone (with three cross-sectional diagrams of the formed shape)

plotted in Fig. 9. For small wall angles under 60°, the vertical forces reach the turning point at the forming depth of around 30 mm and then keep rising slowly until the end of the process. The magnitudes of F_z for these cases at the same depth approximately have the same value. On the contrary, the force trends are recorded in a different fashion for wall angles larger than 60°. The forces quickly register their peak values at a depth of around 12 mm and then decrease monotonically towards process completion/failure. The achievements of steady conditions are delayed with small wall angles. This is because with a smaller wall angle, the sheet undergoes a longer bending process before the occurrence of strain hardening. It appears that the increase of F_z is caused by work hardening, while the decrease is due to the material thinning. From Fig. 9, it is demonstrated that a decrease of F_z is only found in cases with fracture. Therefore, if the material work hardening plays a dominant role to compensate sheet thinning, the force could remain steady and avoid fracture. Otherwise, if thinning prevails, the forces drop quickly which indicates the failure of the material. If appropriate statistical analysis can be performed to calculate the force gradient after the peak value, this could possibly be considered as an

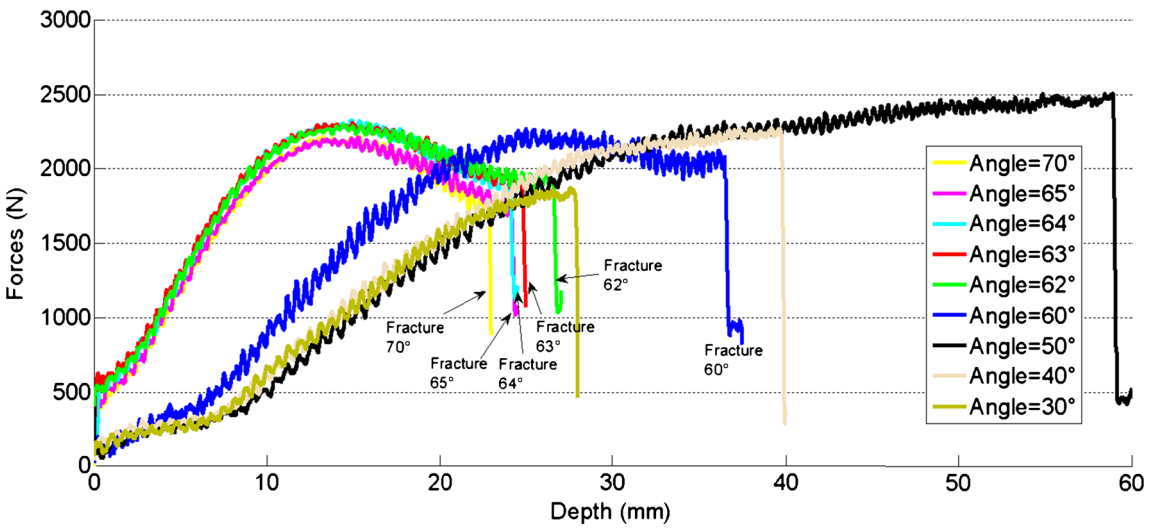

Fig. 9 Vertical force trend with the varying of wall angle (fracture parts are marked)

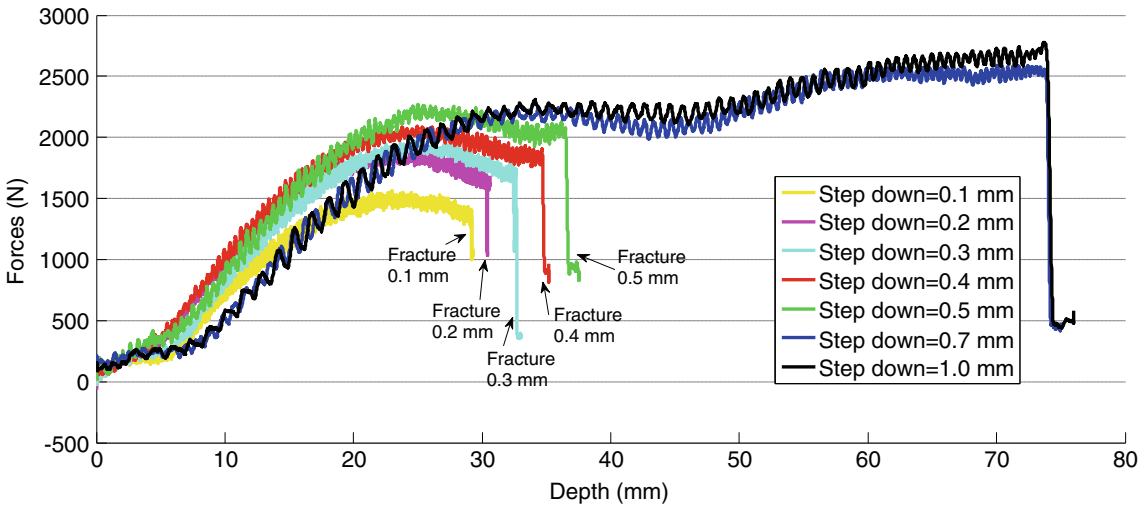

Fig. 10 Vertical force trend with the varying of step-down size (fracture parts are marked)

effective indicator for failure prediction. As listed in Table 2, the designed heights of the cones for 30°, 40° and 60° are 28, 40 and 60 mm because of the limits of minor diameter, respectively. These three parts are formed successfully without fracture because the thinning of the sheet is under the forming limit of the material. With the increase of the wall angle from 60° to 70°, the formability in terms of the achieved forming depth, as marked in Fig. 9 reduces slightly from 37.5 to 23 mm. According to the sine law ($t=t_0*\sin(90-\alpha)$) [23] which is based on the constancy of volume, the sheet thickness after deformation is decreases as wall angle increases. The literature also indicates that the local thinning determines the formability of the ISF process. Therefore, at the same forming depth, the thinning ratio of the material is higher for the parts with larger wall angle, resulting in a lower formability.

4.3 Effect of step down

A set of experiments has also been performed with different step-down sizes (Δz) ranging from 0.1 to 1.0 mm. The evolution histories of the vertical force F_z at the varying of step-down sizes are presented in Fig. 10. It can be noticed that at the former stage with depth from 0 to 20 mm, the vertical forces for large Δz (0.7 and 1.0 mm) show smaller values compared with forces with small step-down sizes. However, after a depth of 40 mm, the F_z values present a limited decrease and then increase until the part is successfully formed. It can also be seen from Fig. 10 that only the parts with Δz of 0.7 and 1.0 mm are formed successfully and the fracture occurs with smaller step-down size. This can be explained by the fact that smaller Δz leads to more tool contact overlaps. In particular, with small Δz, the

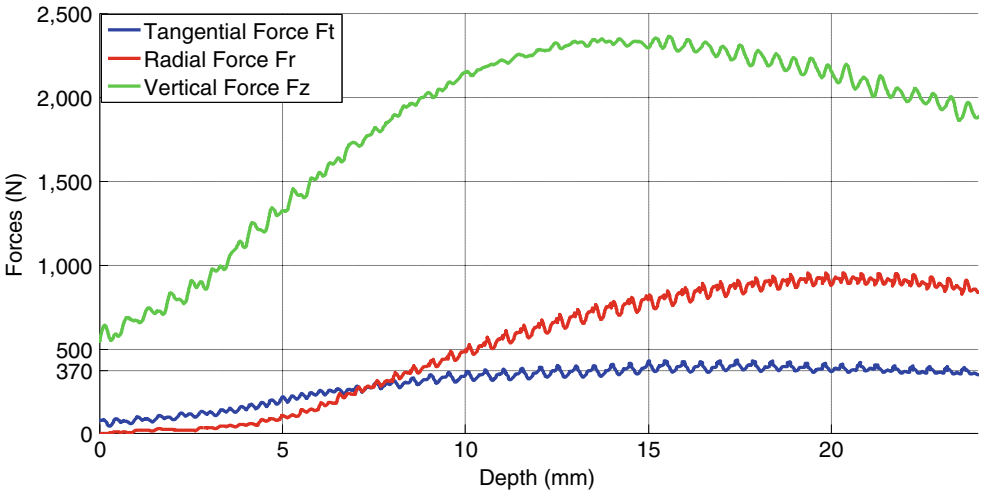

Fig. 11 Transposed tangential and radial forces versus forming depth for a cone with angle of 65°

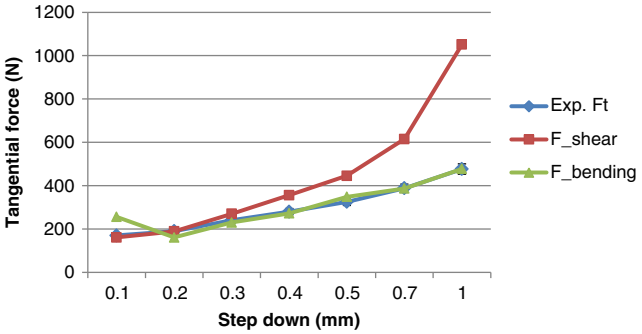

Fig. 12 Predicated tangential forces for two sub-models compared with experimental values with different step-down sizes (other parameters as standard setting: α=60°,r_t=15 mm, t_0=1.6 mm)

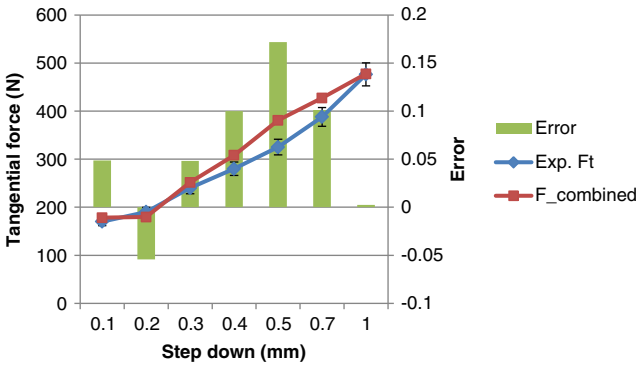

Fig. 14 Errors between predicted and measured tangential forces with different step-down sizes

percentage of overlap between consecutive tool paths is higher which means the portion of hardened material deformed by the tool in each pass is larger. Therefore, the stress required for the deformation rises. As a result of the higher stress state induced in the material, the sheet formability is reduced while the required forming force is increased.

4.4 Comparison of the modelling and experimental results

Force components in vertical and global X and Y directions have been compared and analysed in previous sections. However, to better understand the mechanism of the deformation process and to make a comparison with the proposed model, forces in tangential direction are critical. Therefore, the horizontal forces (F_x and F_y) need to be converted to tangential (F_t) and radial components (F_r) to ensure the comparison is effective. The same methodology presented in [16] is used to determine the converted tangential and radial forces and the results for a 65° cone-forming process are plotted in Fig. 11. It is shown that the tangential force increases gradually until the forming depth of 10 mm and then reaches the steady state for the rest of the forming cycles where the forces remain reasonably constant. The average tangential force value in the steady state is recorded and used to compare with the proposed analytical model.

In order to validate the proposed efficient analytical model, the predicted tangential forces with different forming parameters were compared with the experimental results. Figure 12 presents the comparison of predicted tangential forces and experimentally measured values with variation of step-down size from 0.1 to 1 mm. By comparison, the sub-model 1 based on shear deformation can provide good agreement with experimental results for the cases with small step-down sizes (below 0.5 mm). With the increase of the step down, the difference between analytical and experimental results increases accordingly. Additionally, for step down larger than 0.5 mm, the error becomes significantly high. A similar error trend can be noticed for the tangential force prediction for sub-model 1 with the increase of wall angle values as shown in Fig. 13. The larger deviations for large step-down sizes as well as large wall angles may be due

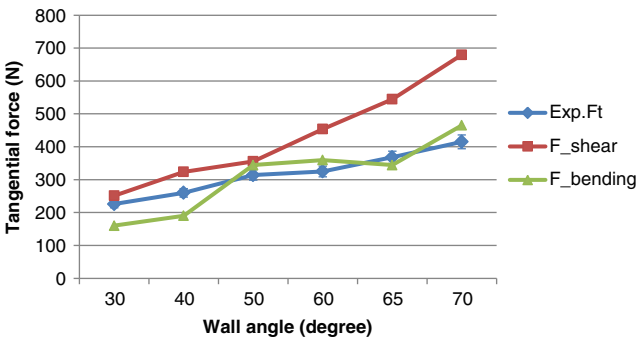

Fig. 13 Predicated tangential forces for two sub-models compared with experimental values with different wall angles (other parameters as standard setting: α=60°,r_t=15 mm, t_0=1.6 mm)

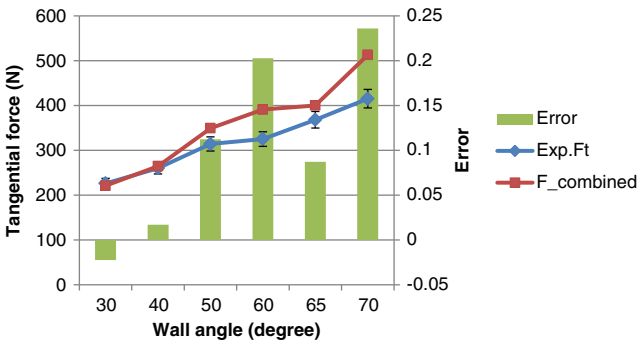

Fig. 15 Errors between predicted and measured tangential forces with different wall angles

to the following inherent limits of the deformation mechanics. Firstly, the sub-model 1 is based on the assumption that no material flow is taken into account in the radial direction. Therefore, the calculated dissipated power is totally due to the shear strain rates of the deformed elements. However, bending and stretching which cause plastic strains are also evident in some experimental tests [24] and FE simulations [22]. Secondly, with a large-step depth, the deformation zone which is represented by Bezier curves may contribute to a more severe deformation compared with that of the actual deformed area, resulting in the higher force value. Furthermore, the assumption that the non-contact regions of the sheet are considered as rigid material may also cause the over prediction of the force.

To provide further insight into these above limits, a sub-model 2 which takes into account bending and stretching effects was established. The predicted forces using the sub-model 2 are also compared with measured results in Figs. 12 and 13. It is noticed that the bending based prediction of tangential values is more accurate for larger step-down sizes. However, as shown in Fig. 13, the bending model alone cannot accurately predict the force trend across the range of wall angles. Therefore, a linear combination of these two sub-models has been constructed to balance the contribution of shear and bending on the prediction of tangential force,

$$F_{\text{combined}} = \lambda F_{\text{shear}} + (1-\lambda) F_{bs} \tag{32}$$

where F_{shear} and F_{bs} are the predicted tangential force due to shear and bending deformation mechanism, respectively; λ is a normalised fraction taking into account parameters of wall angle and step-down size. The purpose of the parameter λ is to balance the contribution between the shear based model and the bending based model to provide a more accurate prediction of the tangential force. The shear-based model depends on λ and the bending-based model depends on $(1-\lambda)$ as given in Eq. (32). According to the experimental results as well as the mechanics of plastic deformation, the parameter λ has to meet the following requirements,

- The parameter of λ should be dimensionless,
- The value of λ should range from 0 to 1 in the experiments,
- The value of λ should decrease with the increase of wall angle,
- The value of λ should decrease with the increase of step-down size.

Considering the above conditions, an effective way to determine the value of λ can be achieved empirically by,

$$\lambda = \frac{\left(1-\frac{\alpha}{90^\circ}\right)\left(1-\frac{\Delta z}{\Delta z_{\max}}\right)}{\left(1-\frac{\alpha}{90^\circ}\right)\left(1-\frac{\Delta z}{\Delta z_{\max}}\right)+\frac{\alpha}{90^\circ}\frac{\Delta z}{\Delta z_{\max}}} = \frac{(90^\circ-\alpha)(\Delta z_{\max}-\Delta z)}{(90^\circ-\alpha)(\Delta z_{\max}-\Delta z)+\alpha\Delta z}. \quad (0 < \Delta z \leq 1) \tag{33}$$

where α and Δz correspond to the values of wall angle and step-down size. The explored maximum step down $\Delta z_{\max}$ in this study is 1 mm. According to the above equation, the contribution of the shear based model decreases proportionally with the increase of wall angle and step-down size while the significance of bending and stretching rises with more severe plastic deformation due to larger step-down sizes and higher wall angles The choice of model for λ could be explained more deeply in future research to obtain model based prediction.

Figures 14 and 15 present the comparison between the predicted and experimental values of tangential forces with different configurations. The average error for the combined model is only 6 and 11 % in respect to the variation of step-down size and wall angle, respectively. As the prediction can be performed within only several minutes using the proposed model, it would greatly improve the prediction efficiency of forming force.

5 Conclusions

In the present work, experimental measurement on forming forces in the truncated cone-forming process was conducted and the trend of forming force was also analysed. Efficient analytical models for tangential force prediction were proposed and validated through experimental data. The following was concluded.

- Forming forces have been successfully measured on a benchmark ISF case by means of strain gauges and provide useful information to understand the relationship

between the force and other forming parameters. It is concluded that the force trend may attributed to the bending effect of the sheet in the early phase of the process and the combined effects of sheet thinning and strain hardening in the second stage of the process.

- From the experimental results, tangential forces are nearly constant during the second stage of the process and the steady values demonstrate a growing trend with the increase of step-down size and wall angle. In the investigated range, a reasonably large step-down size should be selected to achieve a better formability in terms of forming depth.
- Major deformation modes including shear, bending and stretching are analytically considered in the proposed sub-models. The results from each model were analysed separately which suggest that the deformation mechanism in ISF is a combination of shear, bending and stretching.
- An empirical combined model has been constructed which can provide the prediction of tangential force with an average error less than 11 % for the experimental conditions employed in this study. The current work will be helpful to provide an efficient method for tangential force prediction.

The current model is based on the tool path for the cone-forming process. Nevertheless, it can be expected that using a modification of the presented model, tangential forces for different part geometries can be obtained as well. As the empirical relationship given herein for the two sub-models is valid for the experimental conditions employed in this study, a general empirical model able to predict forming force for any process design needs to be investigated under a wider range of process conditions.

Acknowledgements The present work was supported by Australian Research Council (ARC) Linkage project, Boeing Research and Technology Australia and QMI Solutions in Australia. China Scholarship Council (CSC) is also acknowledged for the scholarship support.

Appendix 1

Calculation of critical angles

As we can see from Fig. 16, the deformation zone which is being formed in current path can be divided into six regions. In radial direction, the deformation zone is divided into two parts by the radius of (r_i+Δr). In circumferential direction, three critical angles (θ_c, θ_t and θ_t) are used to define the assumed flow line. In Fig. 16, we can see that regions Ia, IIa and IIIa are undeformed areas during last pass so these are flat before the current forming pass, whereas regions Ib, IIb and IIIb are previously deformed in the last forming pass. Vertical positions for the sheet before the current forming pass are,

$$Z_{sa} = Z_t + \Delta z \qquad (r_i \le r \le r_i + \Delta r) \tag{34}$$

$$Z_{sb} = Z_t + \Delta z + r_t - \sqrt{r_t^2 - (r - r_i - \Delta z \tan(90 - \alpha))^2} \qquad (r_i + \Delta r \le r \le r_o) \tag{35}$$

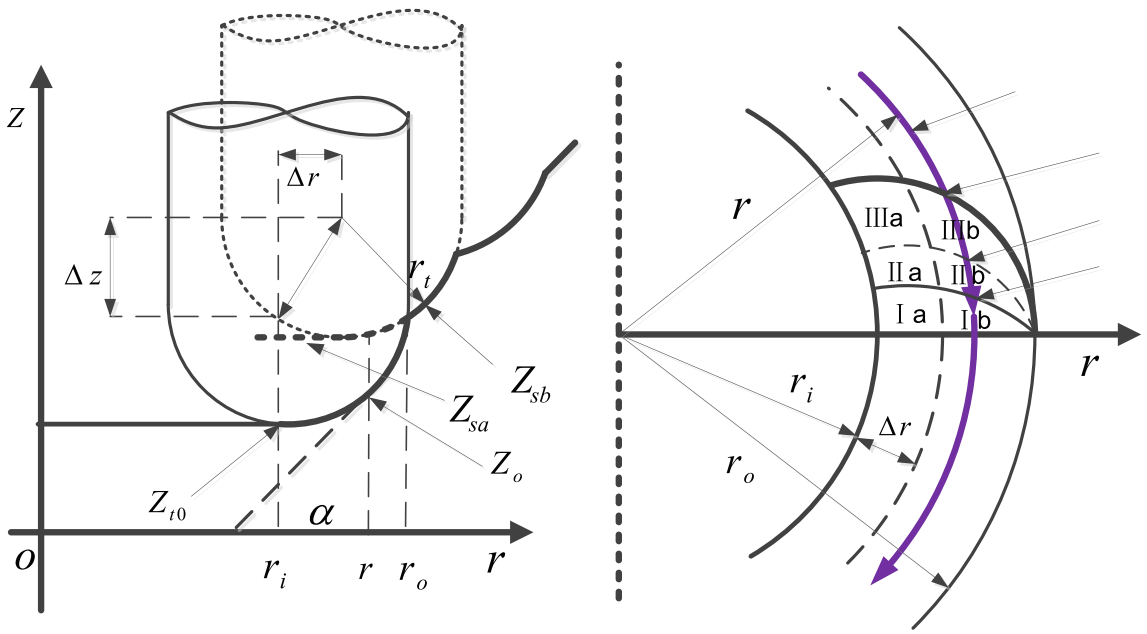

Fig. 16 Divided deformation zone in the cone-forming process

a) Calculation of θ_c

As previously defined, Z_c is the conjunct point for curve Zf_c and tool head surface, so θ_{ca} is calculated by solving the following two equations,

$$\begin{cases} Z_c = M(Z_{s1}-Z_o)+Z_o \\ Z_c = Z_{t0}+r_t-\sqrt{r_t{}^2-(r\cos\theta-r_i)^2-(r\sin\theta)^2} \end{cases} \tag{36}$$

According to the geometric relations of the tool head, we have,

$$\begin{cases} Z_o = Z_{t0}+(r_t-r_{tc}) \\ r_{tc} = \sqrt{r_t{}^2-(r-r_i)^2} \end{cases} \tag{37}$$

The contact angle θ_{ca} can be solved from Eqs. (37) and (38) gives

$$\theta_{ca} = \cos^{-1}\frac{\left(\sqrt{r_t{}^2-(r-r_i)^2}-M(Z_{sa}-Z_o)\right)^2-r_t{}^2+r^2+r_i{}^2}{2rr_i} \tag{38}$$

Similarly, the contact angle θ_{cb} which separates regions Ib and IIb can be solved as,

$$\theta_{cb} = \cos^{-1}\frac{\left(\sqrt{r_t{}^2-(r-r_i)^2}-M(Z_{sb}-Z_o)\right)^2-r_t{}^2+r^2+r_i{}^2}{2rr_i} \tag{39}$$

b) Calculation of θ_t

When $r_i \le r \le r_i+\Delta r$, θ_{ta} is calculated to define regions IIa and IIIa,

$$\begin{cases} Z_{ta} = Z_{t0}+\Delta z \\ Z_t = Z_{t0}+r_t-\sqrt{r_t{}^2-(r\cos\theta-r_i)^2-(r\sin\theta)^2} \end{cases} \tag{40}$$

Let Z_{ta} equals Z_t, the angle θ_{ta} can be solved as,

$$\theta_{ta} = \cos^{-1}\frac{(r_t-\Delta z)^2-r_t{}^2+r^2+r_i{}^2}{2rr_i} \tag{41}$$

Similarly, for calculation of θ_{tb}, we have

$$\begin{cases} Z_{tb} = Z_{t0}+\Delta z+r_t-\sqrt{r_t{}^2-(r-r_i-\Delta z\tan(90-\alpha))^2} \\ Z_t = Z_{t0}+r_t-\sqrt{r_t{}^2-(r\cos\theta-r_i)^2-(r\sin\theta)^2} \end{cases} \tag{42}$$

$$\theta_{tb} = \cos^{-1}\frac{\left(\sqrt{r_t{}^2-(r-r_i-d_z\tan(90-\alpha))^2}-\Delta z\right)^2-r_t{}^2+r^2+r_i{}^2}{2rr_i} \tag{43}$$

c) Calculation of θ_s

The deformation zone is assumed to be a circle with the radius of r_o-r_i, so the following equations set can be given as,

$$\begin{cases} X^2+Y^2 = r^2 \\ (X-r_i)^2+Y^2 = (r_o-r_i)^2 \end{cases} \tag{44}$$

The angle θ_s can be solved as,

$$\theta_s = \sin^{-1}\frac{Y}{r} \tag{45}$$

Appendix 2

Calculation of average yield strength and equivalent strain

For each of the six regions, do the integral for equivalent strain. Take region Ia for example,

$$\bar{\varepsilon}_{I\alpha} = \iint_0^{\theta_{ca}}\frac{2}{\sqrt{3}}\left(\varepsilon_{\theta z}{}^2+\varepsilon_{rz}{}^2\right)\mathrm{d}\theta\mathrm{d}r \tag{46}$$

On the velocity discontinuity surface,

$$\bar{\varepsilon}_{\mathrm{dis}a} = \frac{2}{\sqrt{3}}\varepsilon_{\theta z} = \frac{1}{\sqrt{3}}\frac{|\Delta v|}{v_\theta}. \tag{47}$$

The average equivalent strain is given as,

$$\bar{\varepsilon}_{\mathrm{avg}} = \frac{\bar{\varepsilon}_{\mathrm{total}}}{r_o-r_i} = \frac{\bar{\varepsilon}_{\mathrm{Ia}}+\bar{\varepsilon}_{\mathrm{Ib}}+\bar{\varepsilon}_{\mathrm{II}\alpha}+\bar{\varepsilon}_{\mathrm{IIb}}+\bar{\varepsilon}_{\mathrm{III}\alpha}+\bar{\varepsilon}_{\mathrm{III}b}+\bar{\varepsilon}_{\mathrm{dis}a}+\bar{\varepsilon}_{\mathrm{dis}b}}{r_o-r_i} \tag{48}$$

By assuming the swift type work hardening law $\sigma_{eq}=K(\varepsilon_0+\varepsilon)^n$ for a sheet metal, the average yield strength is obtained as,

$$y_0 = \frac{\int_0^{\bar{\varepsilon}_{\mathrm{avg}}}\sigma_{eq}\mathrm{d}\varepsilon}{\int_0^{\bar{\varepsilon}_{\mathrm{avg}}}\mathrm{d}\varepsilon}, \tag{49}$$

where ε is the plastic strain. Also, K,n and ε_0 are the material parameters.

References

1. Jeswiet J, Micari F, Hirt G, Bramley A, Duflou J, Allwood J (2005) Asymmetric single point incremental forming of sheet metal. Ann CIRP—Manuf Technol 54(2):623–649
2. Echrif SBM, Hrairi M (2011) Research and progress in incremental sheet forming processes. Mater Manuf Processes 26(11):1404–1414. doi:10.1080/10426914.2010.544817

3. Emmens WC, Sebastiani G, van den Boogaard AH (2010) The technology of incremental sheet forming—a brief review of the history. J Mater Process Technol 210(8):981–997. doi:10.1016/j.jmatprotec.2010.02.014
4. Micari F, Ambrogio G, Filice L (2007) Shape and dimensional accuracy in single point incremental forming: state of the art and future trends. J Mater Process Technol 191(1–3):390–395. doi:10.1016/j.jmatprotec.2007.03.066
5. Essa K, Hartley P (2011) An assessment of various process strategies for improving precision in single point incremental forming. Int J Mater Form 4(4):401–412. doi:10.1007/s12289-010-1004-9
6. Duflou JR, Verbert J, Belkassem B, Gu J, Sol H, Henrard C, Habraken AM (2008) Process window enhancement for single point incremental forming through multi-step toolpaths. CIRP Ann- Manuf Technol 57(1):253–256. doi:10.1016/j.cirp.2008.03.030
7. Duflou J, Tunçkol Y, Szekeres A, Vanherck P (2007) Experimental study on force measurements for single point incremental forming. J Mater Process Tech 189(1):65–72
8. Filice L, Ambrogio G, Micari F (2006) On-line control of single point incremental forming operations through punch force monitoring. CIRP Ann—Manuf Technol 55(1):245–248
9. Ambrogio G, Filice L, Micari F (2006) A force measuring based strategy for failure prevention in incremental forming. J Mater Process Technol 177(1–3):413–416
10. Petek A, Kuzman K, Suhač B (2009) Autonomous on-line system for fracture identification at incremental sheet forming. CIRP Ann - Manuf Technol 58(1):283–286. doi:10.1016/j.cirp.2009.03.092
11. Fiorentino A (2013) Force-based failure criterion in incremental sheet forming. Int J Adv Manuf Technol 68(1–4):557–563. doi:10.1007/s00170-013-4777-4
12. Ingarao G, Ambrogio G, Gagliardi F, Di Lorenzo R (2012) A sustainability point of view on sheet metal forming operations: material wasting and energy consumption in incremental forming and stamping processes. J Cleaner Prod 29–30(0):255–268. doi:10.1016/j.jclepro.2012.01.012
13. Malhotra R, Xue L, Belytschko T, Cao J (2012) Mechanics of fracture in single point incremental forming. J Mater Process Technol 212(7):1573–1590
14. Raithatha A, Duncan S (2009) Rigid plastic model of incremental sheet deformation using second-order cone programming. Int J Numer Methods Eng 78(8):955–979
15. Iseki H (2001) An approximate deformation analysis and FEM analysis for the incremental bulging of sheet metal using a spherical roller. J Mater Process Technol 111(1):150–154
16. Aerens R, Eyckens P, Van Bael A, Duflou JR (2010) Force prediction for single point incremental forming deduced from experimental and FEM observations. Int J Adv Manuf Technol 46(9):969–982
17. Mirnia MJ, Dariani BM (2012) Analysis of incremental sheet metal forming using the upper-bound approach. Proceedings of the Institution of Mechanical Engineers, Part B: Journal of Engineering Manufacture
18. Jeswiet J, Duflou JR, Szekeres A (2005) Forces in single point and two point incremental forming. Adv Mater Res 6–8:449–456
19. Halmos GT (2006) Roll forming handbook, vol 67, Book, Whole. CRC/Taylor & Francis, Boca Raton
20. Wang G, Ohtsubo H, Arita K (1998) Large deflection of a rigid-plastic circular plate pressed by a sphere. J Appl Mech 65(2):533–535. doi:10.1115/1.2789089
21. Allwood J, Shouler D, Tekkaya AE (2007) The increased forming limits of incremental sheet forming processes. Key Eng Mater 344:621–628
22. Smith J, Malhotra R, Liu WK, Cao J (2013) Deformation mechanics in single-point and accumulative double-sided incremental forming. The International Journal of Advanced Manufacturing Technology:1–17. doi:10.1007/s00170-013-5053-3
23. Avitzur B, Yang CT (1960) Analysis of power spinning of cones. J Eng Ind 82(3):231. doi:10.1115/1.3663052
24. Silva MB, Nielsen PS, Bay N, Martins PAF (2011) Failure mechanisms in single-point incremental forming of metals. Int J Adv Manuf Technol 56(9):893–903. doi:10.1007/s00170-011-3254-1

Int J Adv Manuf Technol (2014) 73:589
DOI 10.1007/s00170-014-5893-5

ERRATUM

Erratum to: Efficient force prediction for incremental sheet forming and experimental validation

Yanle Li · Zhaobing Liu · Haibo Lu · W. J. T. (Bill) Daniel · Sheng Liu · Paul A. Meehan

Published online: 9 May 2014

Erratum to: Int J Adv Manuf Technol
DOI: 10.1007/s00170-014-5665-2

The first sentence in section 3 needs to be changed into:

In this model, the energy method [19] and upper bound theory [17] are used to analyse the deformation behaviour and predict the tangential force of the truncated cone during the ISF process.

The division of deformation zone in Figures 5 and 16 referred to Figure 2 in [17].

References

17. Mirnia MJ, Dariani BM (2012) Analysis of incremental sheet metal forming using the upper-bound approach. Proceedings of the Institution of Mechanical Engineers, Part B: Journal of Engineering Manufacture
19. Halmos GT (2006) Roll forming handbook, vol 67, Book, Whole. CRC/Taylor & Francis, Boca Raton

The online version of the original article can be found at doi:10.1007/s00170-014-5665-2.

Y. Li (✉) · Z. Liu · H. Lu · W. J. T. (B). Daniel · S. Liu · P. A. Meehan
School of Mechanical and Mining Engineering, The University of Queensland, St Lucia, Brisbane, QLD 4072, Australia
e-mail: yanle.li@uq.edu.au

4.3 The Papers

Paper 5

Deformation mechanics and efficient force prediction in incremental sheet forming process

Li, Y.L., Liu, Z.B., Lu, H.B., Daniel, W. J. T. and Meehan, P. A.

Journal of Materials Processing Technology

2015, Volume: 221, Pages: 100-111.

Journal of Materials Processing Technology 221 (2015) 100–111

Contents lists available at ScienceDirect

Journal of Materials Processing Technology

journal homepage: www.elsevier.com/locate/jmatprotec

Deformation mechanics and efficient force prediction in single point incremental forming

Yanle Li*, William J.T. Daniel, Zhaobing Liu, Haibo Lu, Paul A. Meehan

School of Mechanical & Mining Engineering, The University of Queensland, St Lucia, Brisbane 4072, QLD, Australia

ARTICLE INFO

Article history:
Received 25 August 2014
Received in revised form
23 November 2014
Accepted 7 February 2015
Available online 16 February 2015

Keywords:
Incremental sheet forming
Forming force
Deformation mechanics
Prediction
Shear
Bending

ABSTRACT

Incremental sheet forming (ISF) is a promising forming process which is able to deform a flat sheet into a complex 3D shape by using a generic moving tool. The flexibility, increased formability and the reduced forming force make the ISF process ideal for rapid prototype and small batch production. However, the effective production design and optimization in ISF require the efficient prediction of forming force, especially the tangential force which is the actual force component that does plastic work during the forming process. In this paper, in order to investigate the deformation mechanism in the ISF process, a comprehensive finite element (FE) model for the cone-forming process with fine solid elements is established which allows the quantitative study of the deformation behavior of stretching, bending and shearing during the process. Based on such analysis, an efficient model for tangential force prediction is deduced analytically in which all these three deformation modes are considered. In particular, the contribution from each deformation mode is related to the variation of forming parameters. Additionally, the proposed efficient model is comprehensively validated with both truncated cone and pyramid shapes by varying four forming parameters (i.e. step down, wall angle, tool radius and sheet thickness). In both cases, the predicted forces show good agreements with the experimental results. Furthermore, the proposed model is generalized to deal with more complex shapes (e.g. ellipsoidal cup). It is found that the trend of tangential force could be properly represented by the change of the curvature of the formed part. Considering the proposed model can be solved within only several minutes, it will guide the forming process and shorten the lead time.

1. Introduction

Incremental sheet forming (ISF) is an extremely flexible process using a single generic tool for an infinite variety of shapes with great potential for production of short runs of new or replacements parts. By using this process, useable parts can be formed directly from CAD data with a minimum of specialized tooling; therefore, it has a high potential and economic payoff for rapid prototyping and small quantity production for various applications. In the early stage of the ISF technology, Allwood et al. (2005) performed a structured search which identified the potential applications; Ambrogio et al. (2005) successfully produced a customized ankle support with good dimensional accuracy; Micari et al. (2007) demonstrated that ISF can be used for manufacturing automotive body parts. However, the further development and commercialization of ISF is presently inhibited by a lack of understanding in the deformation mechanics. In particular, a model-based efficient prediction of forming force is critical to improve the production efficiency as it provides monitoring of the forming process, failure prediction, and a future means of on-line control and optimization.

Over the last decade, the deformation mechanics behind ISF is investigated both analytically and experimentally. Silva et al. (2008) extensively analyzed the single-point incremental forming by considering membrane strains. A closed-form analytical model is first presented which provides insight to explain the fundamentals behind the fracture of material and the enhanced overall formability of ISF. Emmens and Boogaard (2008) summarized that bending under tensile load plays a critical role in the localized deformation of the ISF process. Additionally, using finite element (FE) simulation, Smith et al. (2013) demonstrated the deformation mechanics in single point incremental forming and compared with that in accumulative double-sided incremental forming process. Lu et al. (2014) further discussed the role of friction and through-thickness-shear analytically from the stress state point of view. It was claimed that through-thickness-shear caused by friction results in contrary effects on deformation stability and formability. Through

* Corresponding author. Tel.: +61 3365 4115.
E-mail addresses: yanle.li@uq.edu.au, kuge0501@126.com (Y. Li).

http://dx.doi.org/10.1016/j.jmatprotec.2015.02.009
0924-0136/

experimental measurements, Jackson and Allwood (2009) found that the deformation mechanism in ISF is a combination of stretching and shear in the plane perpendicular to the tool motion but shear in the tool direction. However, Eyckens et al. (2011) suggested that the dominant deformation mechanism depends on the selected forming parameters (e.g. wall angle, step-down size and spindle rotation speed).

On the one hand, forming forces during ISF have been experimentally studied intensively. Duflou et al. (2007) concluded that the forming forces are increased with the increase of vertical step down size, wall angle and sheet thickness. Filice et al. (2006) worked on the force analysis and classified the force trends of tangential force into three types: steady state force trends, polynomial force trends and monotonically decreasing force trends. Ambrogio et al. (2006) found that the force gradient after the peak can be effectively considered as a critical indicator to detect and prevent work piece fracture. Filice et al. (2006) considered forming force as an indicator to realize the on-line control and optimization. Petek et al. (2009) proposed an autonomous on-line system for fracture identification and localization by analyzing the reaction force with a skewness function. Another failure criterion presented by Fiorentino (2013) is also based on force monitoring during the forming process. Additionally, Ingarao et al. (2012) evaluated the energy consumption required for the ISF process according to the measured force data, which provides guidance for sustainable development of the process. However, very limited analytical models are available for the efficient prediction of forming forces in ISF although some researchers have attempted to bridge this gap. Due to the localized contact condition and long tool path in ISF, force prediction with FE models is significantly time-consuming, although it is commonly used for various forming processes. Smith et al. (2013) reported a simulation time of 24 days for a single point incremental forming process for a truncated cone shape. To overcome the above computational challenges of the FE approach, Iseki (2001) obtained the forming forces for the incremental forming of a pyramid using a simple approximated deformation analysis based on a plane-strain deformation. Raithatha and Duncan (2009) developed a model based on the numerical minimization of internal work within the material. In this method, the minimization of plastic work was formulated as a Second Order Cone Programming (SOCP) optimization problem. By sacrificing the accuracy, a process of straight line indentation on a sheet with dimensions of 0.1 m × 0.1 m is achieved in 9 min. Aerens et al. (2010) studied the incremental forming of truncated cones with different materials using experimental and statistical analyses. Regression formulae were proposed to predict the triple forming forces including axial, radial, and tangential components from input variables including wall angle, initial thickness, tool diameter, and vertical pitch. In particular, the tangential force is the actual force component that does plastic work during the forming process, so it is more closely related to the deformation mechanism of the process. Also, the prediction of the tangential component could contribute as a pathway for the extensive investigation of both vertical and radial components. In addition, although the value of the tangential force tends to be small compared with vertical force, the trend of the tangential force might be used as an important potential indicator for preventing material failure and to hence enhance the surface quality. Recently, Mirnia and Dariani (2012) conducted an upper-bound analysis to predict the tangential force on a truncated cone-forming process using an assumed deformation zone. It was reported that the forces were in good agreement with those from the experimental work of Aerens et al. (2010). Nevertheless, large errors can be expected for severe deformation conditions (e.g. $\Delta z > 0.5$ mm) and possibly due to the pure shearing assumption of plastic deformation.

Li et al. (2014b) have proposed a preliminary efficient force prediction model with validation by forming of truncated cone shapes. Even though the model shows great potential to deal with various process parameters, it uses empirical coefficients to combine different deformation modes that require further quantitative investigation and experimental validation. Additionally, a generalized model that can be used in any user-defined shapes is required. In particular, this paper will focus on the further extension and validation of the efficient force prediction model. The main contributions of this paper to the field are:

- It is clarified that the deformation mechanics in the cone-forming ISF process involves shearing, stretching and bending through a FE simulation.
- An efficient tangential force prediction model is proposed which takes into account the above three deformation modes. The model is comprehensively validated with two benchmark shapes (truncated cone and pyramid) with varying forming parameters including step-down size, wall angle, tool diameter and sheet thickness.
- The proposed model is successfully extended and validated for a more complex shape (i.e. ellipsoidal cup) by considering the change of local curvature. This will provide a valuable contribution towards the future investigation for the force prediction of general shapes.

2. FE model for deformation analysis

The understanding of the deformation mechanism in ISF is fundamental for the establishment of the analytical model for the prediction of forming force. However, it is difficult to reveal the detailed deformation history behind the ISF solely through experimental works due to its highly localized characteristic. Specifically, FE simulations can allow individual quantitative investigations of stretching, bending and shearing strains which are difficult to achieve using an experimental approach. Another benefit of FE simulations is that working parameters can be efficiently adjusted without any considerable economic cost. Therefore, computer models especially FE technology is widely applied to investigate this process. In particular, the explicit FE code of LS-DYNA is used in the present study due to its great performance to solve dynamic problems with large plastic deformation.

2.1. FE modelling

In the presented FE model, the forming tool is considered as a rigid body and its movement follows the same tool path as in the actual forming process which was designed using CAM software. As shown in Fig. 1 (revised from Silva et al., 2008), the truncated cone is formed in a stepwise way with a series of contours. The vertical distance between each neighbouring contour is defined as step-down size Δz and the angle between the deformed sheet to the horizontal plane is defined as wall angle α.

To accurately predict the through thickness shear and bending effect of the deformed sheet, the element type of SOLID164 is used in the current model and five elements are meshed through the thickness direction. The initial meshing configuration of the metal sheet is shown in Fig. 2 with an enlarged view of the selected small region *d* plotted at the top right corner. In particular, for the region which will be contacting with the tool (region *B*), the elements are arranged with the size equal to 1 mm radially and meshed into 400 elements circumferentially which correspond to the size between 0.7 mm to 1.2 mm. The general geometry of the sheet is square with dimension 300 mm × 300 mm and thus it is meshed with 175,000 solid elements. In terms of the boundary conditions in the forming process, nodes belong to the four edges of the squared sheet are constrained in all degrees of freedom.

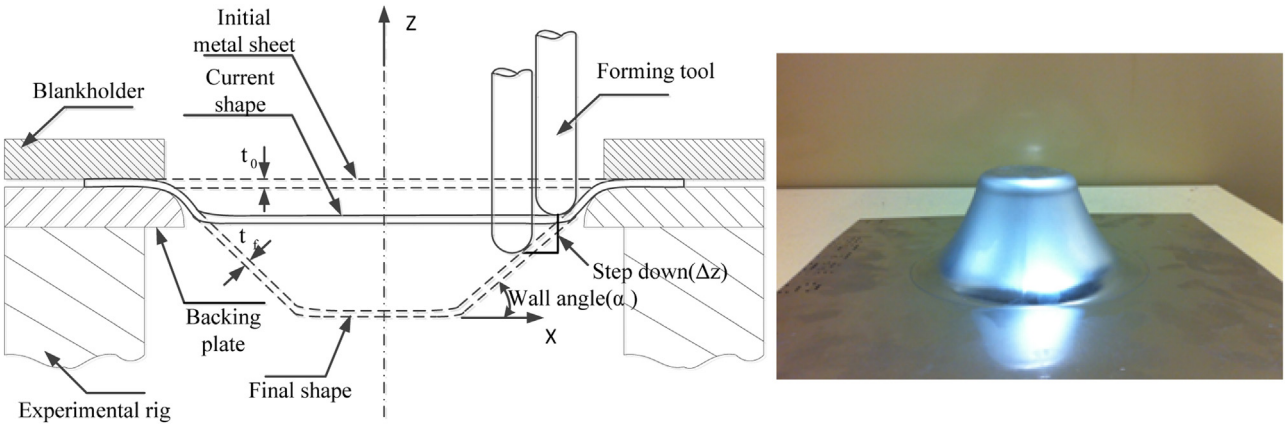

Fig. 1. Sketch of ISF experimental parameters and a case study made from Al 7075 of 1.6 mm in thickness (refer to Silva et al., 2008).

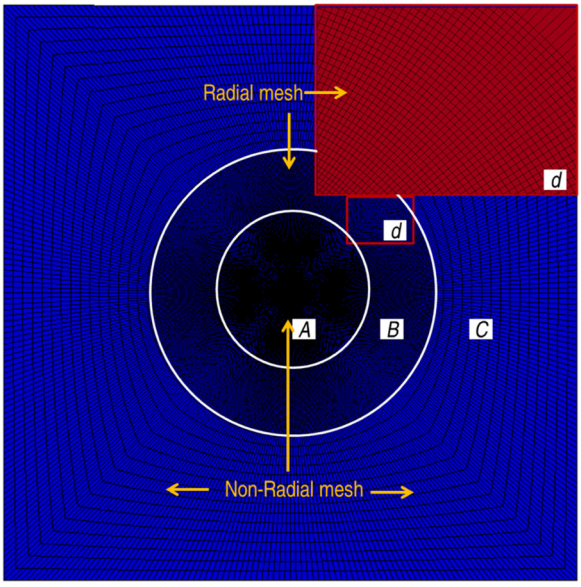

Fig. 2. The initial meshing configuration of the metal sheet with an enlarged view at the right top corner.

The metal used is the aluminum alloy 7075-O sheet with a thickness of 1.6 mm. It is confirmed from tensile tests that the material can be considered isotropic since deviations of the stress–strain behavior in different directions (rolling, diagonal and transverse) are small. Therefore, the material could be modeled using Swift's isotropic strain hardening law of $\sigma = K(\varepsilon_0 + \varepsilon)^n$. The detailed mechanical parameters are listed in Table 1 which were determined from previous material testing in Liu et al. (2013). From our previous experimental work, Li et al. (2014a), the friction at the contact surface between tool head and sheet has been assessed with a value of 0.18. This value has been used in this FE model. In order to improve the simulation efficiency, the virtual forming speed is scaled up by 100 times in which the ratio of the kinetic energy to the total internal energy can be controlled within 1% to ensure a quasi-static forming process.

Table 1
Mechanical properties of Aluminium 7075-O sheets with 1.6 mm thickness.

Material	7075-O
Density (t/mm^{-3})	2.81×10^{-9}
Young's modulus (GPa)	70
Poisson's ratio	0.33
Tensile yield strength (MPa)	92
Ultimate tensile strength (MPa)	198
Plastic coefficient K	352.58
Hardening exponent n	0.221

2.2. FE simulation results

Fig. 3 shows the deformed sheet on a cross-section perpendicular to the forming direction as well as the top view from the FE simulation. The displacement of elements in the vertical direction (Z) is presented with colored contours. In particular, strain components at the Section A are selected to have further investigation as the forming tool has already passed this section and reached a relatively steady state. Despite the fact that the maximum forming force occurs during contacting with elements, it is hard to observe the strain behavior of elements as it undergoes a transition period. Due to the inherent localized feature of ISF, the strain state of the

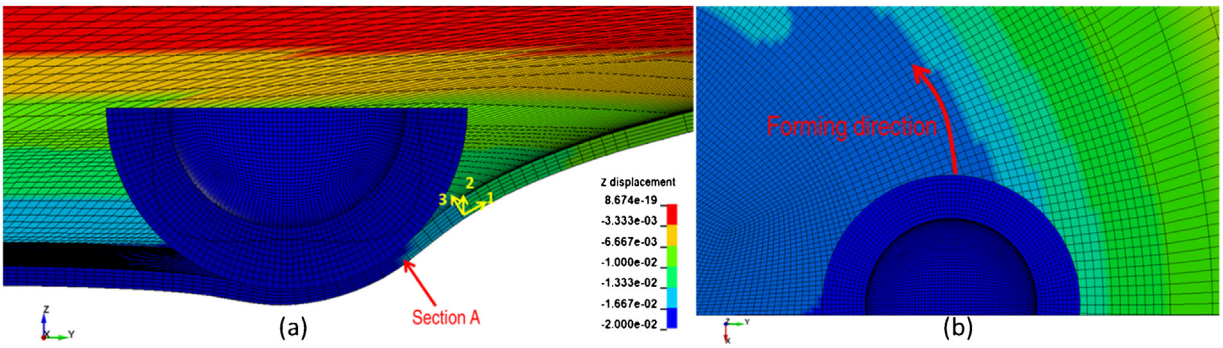

Fig. 3. Deformed sheet in the FE model: (a) cross-sectional view perpendicular to the forming direction and (b) top view.

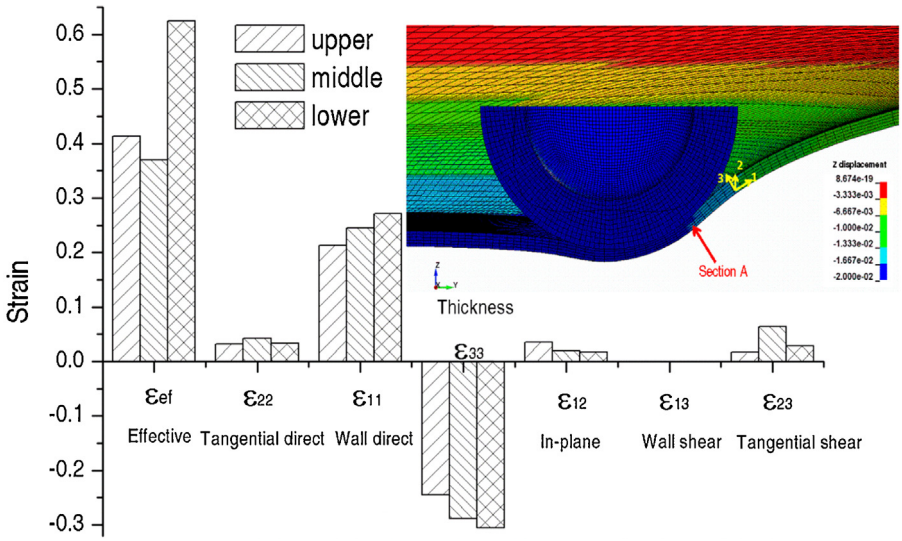

Fig. 4. Strain components for upper, middle and lower elements at Section A at the forming depth of 20 mm.

deformed elements will not be considerable affected by the following move of the forming tool. Furthermore, strain values along thickness direction are also investigated by checking upper element (the side in contact with the forming tool), lower element (the side without contact with the forming tool) and the middle element. It should be noted that the following strain values are presented in the local Cartesian coordinate system as marked in Fig. 3: the direction perpendicular to the tool motion and along the inclined wall is defined as 1 while forming direction (tangential direction) is defined as 2 and thickness direction as 3.

Since the strain components in ISF were developed incrementally, it is reasonable to analyze these values at a certain depth for comparison purpose. Such a comparison is presented in Fig. 4 as a bar graph for upper, middle and lower elements at Section A. These values are obtained when the forming tool is at the depth of 20 mm. It is noted that the strain component perpendicular to the forming direction and along the inclined wall (ε_{11} wall strain) dominates the total plastic strain at the selected elements with the highest positive strain. According to the law of volume constancy, the sheet has to be thinned during this process which is clearly confirmed by the negative thickness strain (ε_{33}) in Fig. 4. Not surprisingly, the direct strain values in the forming direction (ε_{22}) are small compared with the other two orthogonal directions as the deformation in this direction is symmetrical and constrained for extension. In contrast, shear strain in the forming direction ε_{23} prevails greatly among the three shear components, whereas the value of ε_{13} is negligible. The above results from FE simulation agree with the experimental measurement by Jackson and Allwood (2009). It is also noticed that the strain values are varying through the thickness as shown in Fig. 4. The lower element on the non-contacting surface was deformed with the highest effective strain value which is mainly resulted from the large strain ε_{11} and thickness strain ε_{33}. It should be noticed that the in-plane shear strain ε_{12} takes a non-negligible role to contribute to the substantial effective strain value especially for the upper element. The above detailed analysis indicates that the deformation mechanism is different between the forming and its perpendicular directions. More specifically, the deformation mode in the circumferential direction is a combination of the transverse shear strain ε_{23} and also a comparable amount of direct strain ε_{22}. However, the direct strain ε_{11} governs the deformation behavior in the direction perpendicular to the tool motion. This confirms that the formation of the inclined wall is represented by a combination of stretching and bending effect with non-negligible transverse shear in the current cone shape.

3. Analytical model for force prediction

For many metal-working processes, including incremental sheet forming, no exact analytical solutions for the forces to cause unconstrained plastic deformation are available as claimed by Hosford and Caddell (2007). This is because the exact solutions must be both statically and kinematically admissible which means that the solutions must be geometrically self-consistent as well as satisfying the required stress equilibrium everywhere in the deforming body. To this end, based on previous work by Mirnia and Dariani (2012), the upper bound theorem stated in Johnson and Mellor (1983) is adopted in the ISF process. This analysis is based on satisfying yield criteria and geometric self-consistency but not necessarily satisfying the stress equilibrium. According to the principle of maximum work dissipation, in a given set of strain increment field, the plastic work due to the true increment is greater than the same strain increment by any other distribution of stresses which conforms to the same yield criterion. Therefore, the estimated force based on the upper-bound theorem by equating the rate of internal energy dissipation to the external forces will equal or be greater than the actual one. In the analysis, the following assumptions have to be made: (i) the material is homogeneous and isotropic; (ii) interfaces are frictionless; and (iii) the material is rigid except in the deformation zone. To summarize, the calculation involves the following four steps for the prediction of tangential force in a cone-forming process.

1. Define an internal flow field and discretise the deformation zone into smaller regions. A kinematically admissible displacement field of the deformed surface ahead of the forming tool is represented by two adjustable parameters *M* and *N*.
2. Derive the velocity fields for each region from the assumed displacement field based on different plastic deformation conditions.
3. Calculate the strain rates and the dissipated power of the forming process due to different deformation modes.
4. Minimize the dissipated power by varying two parameters in their defined range. Consequently, forming force can be calculated by equating the rate of external work with the rate of internal dissipated power.

Two modules based on different deformation mechanisms (shear and bending with stretching) are included in the proposed

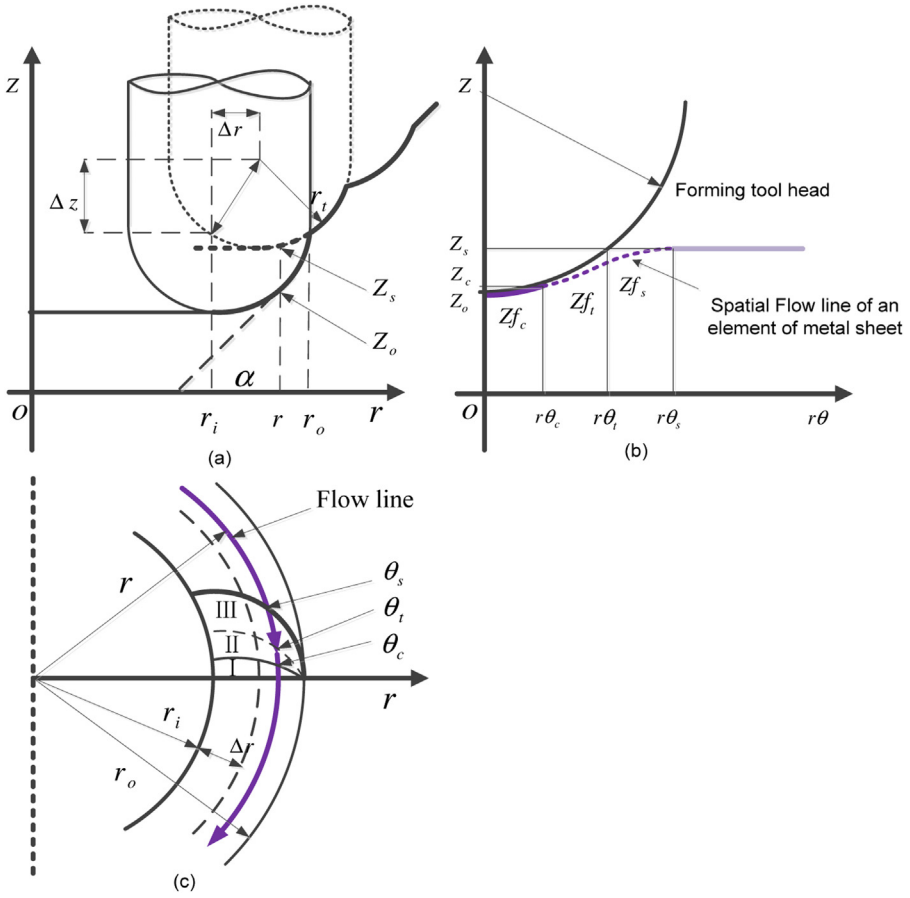

Fig. 5. Deformation zone in the cone forming process: (a) r–z view of the geometrical relations in incremental sheet forming during previous and current path, (b) $r\theta - z$ view of a typical flow line for the deformed curved surface along the circumferential direction of the sheet ahead of the tool and (c) $r - \theta$ view.

model to represent the effects due to the variation of forming parameters. Fig. 5 shows the deformation zone in the ISF process from different viewing aspects. Parameters used for the analytical formulation are defined in Fig. 5 and the similar division of the deformation zone could be found in the published work by Li et al. (2014b) and Mirnia and Dariani (2012). A kinematically admissible displacement field is assumed for the deformed surface ahead of the forming tool. This deformed surface Zf is represented by a series of flow lines along circumferential direction which can be tailored by adjusting two presupposed parameters M and N.

$$Zf = \begin{cases} Zf_c\left(r,\theta\right) = Z_t & \left(0 \le \theta \le \theta_c\right) \\ Zf_t\left(r,\theta\right) = S(X) \times Z_t & \left(\theta_c \le \theta \le \theta_t\right) \\ Zf_s\left(r,\theta\right) = S(X) \times Z_s & \left(\theta_t \le \theta \le \theta_s\right) \end{cases}. \tag{1}$$

Here Z_t is the geometric function of the tool surface and the boundary position is defined using M and Z_s represents the vertical height of the sheet after the previous pass (refer Fig. 5). $S(X)$ is tentatively designed as two-second order Bezier curves ranging from 0 to 1 which depends on N. More detailed calculation procedure for determining the position of the flow line is given in Appendix A. As a result, it is effective to adjust the deformed surface with parameters M and N. However, a velocity discontinuity surface is introduced at the intersecting surface of Zf_t and Zf_s which will result in extra dissipated power.

The following equations summarized the published work, Li et al. (2014b), regarding the calculation of dissipated powers due to three different deformation modes and also the velocity discontinuity surface. The dissipated power of the flow line during the cone forming process based on the shear deformation is integrated using strain rates over the deformed surface as

$$\dot{w}_f = y_0 \iiint \left(\frac{2}{3}\dot{\varepsilon}_{ij}\dot{\varepsilon}_{ij}\right)^{\frac{1}{2}} \mathrm{d}v = \frac{2y_0 t_0}{\sqrt{3}} \iint \left(\dot{\varepsilon}_{\theta z}^2 + \dot{\varepsilon}_{rz}^2\right)^{\frac{1}{2}} \mathrm{d}s, \tag{2}$$

The dissipated power due to the discontinuity can be integrated along the discontinuity surface as

$$\dot{w}_{\mathrm{dis}} = \iint k\left|\Delta v\right| \mathrm{d}s, \tag{3}$$

Accordingly, the total dissipated power due to shear deformation is obtained as

$$\dot{w}_{\mathrm{shear}} = \dot{w}_{\mathrm{dis}} + \dot{w}_f \tag{4}$$

The dissipated power of the deformation zone due to bending and stretching can be determined as

$$\dot{w}_b = \iint M\dot{\mathrm{d}}\phi \mathrm{d}s. \tag{5}$$

$$\dot{w}_s = \iint T\varepsilon_a \dot{\mathrm{d}}l\, \mathrm{d}s = \iint \sigma_a t_0 \varepsilon_a \rho_0 \dot{\mathrm{d}}\emptyset\, \mathrm{d}s \tag{6}$$

where $\dot{\mathrm{d}}\emptyset$ is the change rate of the bending angle in the circumferential direction which could be determined by the travelling angle θ in the $\theta - r$ plane (refer to Li et al., 2014b). Accordingly, the dissipated power due to bending and stretching is

$$\dot{w}_{bs} = \dot{w}_b + \dot{w}_s. \tag{7}$$

To take into account both shear and bending with stretching deformation, a linear combination of these two modules has been constructed to balance the contribution of shear and bending on the prediction of tangential force,

$$\dot{w}_{\text{total}} = \lambda \times \min_{0\le M,N\le 1} \dot{w}_{\text{shear}} + (1-\lambda) \times \min_{0\le M,N\le 1} \dot{w}_{bs}. \quad (8)$$

The above equation for total dissipated power is a function of two optimizing parameters M and N. By minimizing the dissipated power with varying M and N in their defined range (i.e. $0 \le M, N \le 1$), the deformed curved surface for the deformation zone closer to the experiment is obtained. λ is a normalised fraction taking into account parameters of wall angle and step-down size. The purpose of the parameter λ is to weigh the contribution between the shear based model and the bending based model and should be varied with different forming configurations. According to the experimental results as well as the mechanics of plastic deformation, an effective way to determine the value of λ can be achieved by

$$\lambda = \begin{cases} \dfrac{1}{1+\left(\dfrac{\alpha}{90-\alpha}\right)\left(\dfrac{\Delta z}{1-\Delta z}\right)} & (0 < \Delta z \le 1) \\ 0 & (\Delta z > 1) \end{cases} \quad (9)$$

where α and Δz correspond to the algebraic values of the wall angle in degree and step-down size in mm. According to the above equation, the contribution of the shear based model decreases proportionally with the increase of wall angle and step-down size while the significance of bending and stretching rises with more severe plastic deformation due to larger step-down sizes and higher wall angles. It should be noted that the effect of the sheet thickness on the forming force has been considered during the calculation of the dissipated power in both sub-models. In particular, it is assumed that the deformation is entirely taken by bending and stretching modes if the step increment is larger than 1 mm. By this modification, the previous model is enhanced for wider working conditions and is also improved in terms of the adaptability that could be further extended for other shapes. The choice of λ for the combined model will be further discussed in the next section based on the experimental data. Finally, it is reasonably assumed that the rate of plastic work due to the tangential force acting on the forming tool is

$$\dot{w}_{\text{total}} = F_t v_\theta. \quad (10)$$

Substituting the average radius of the deformed zone $(r_i + r_o)/2$ to obtain the angular velocity, the tangential force can be expressed as

$$F_t = \frac{r_i \dot{w}_{\text{total}}}{f \times (r_i + r_o)/2}. \quad (11)$$

4. Experimental validation

To investigate the effects of various forming parameters on the forming forces with different geometries and also the validation of the proposed efficient force prediction model, two shapes of truncated cone and truncated pyramid are selected as the target shapes.

4.1. Experimental setup

The forming tests were performed on a state-of-the-art DLNC-PC (Dieless Numerical Control-PC model) machine dedicated for the ISF process designed by the AMINO® Corporation (Fig. 6(a)). The machine allows a maximum workspace of 2100 mm × 1450 mm × 550 mm to be formed. The movement of the two horizontal axes (X and Y) can have a maximum speed of 60 m/min with a repeatability of ±0.05 mm. The Vertical (Z) axis is driven by an AC servo motor with the power of 1 kW that allows a maximum acting force of 3 kN. Hemispherical tools with diameter values from 10 to 30 mm were used to deform the material. The tip of the tool is tungsten carbide and the body is made of K110 steel which was hardened and tempered to HRC60. The forming tool was set not to rotate in this study for all the tests. The material used in the present study is aluminum 7075-O sheet with various thickness and were cut into 300 mm × 300 mm sized samples.

Before forming, the sheet was clamped on the frame with 12 evenly distributed blank holders. During the forming process, the forming tool is numerically controlled by a FANUC controller which follows the previously designed tool path. The contact between forming tool and metal sheet is lubricated by Shell Tellus Oil 68 to reduce friction and avoid excessive wear of the tool surface. Since the purpose of the current tests is to provide experimental force data for the validation of the proposed analytical model, the forming forces acting on the forming tool have been measured continuously. As shown in Fig. 6(b), a multiple-axis force sensor K6D175-50 was used to measure the forces between the tool and work piece during the forming process. To alleviate the possible deflection from other structures, the force sensor is mounted directly between the spindle and the tool holder. The force sensor is manufactured by ME-Meßsysteme GmbH which allows measuring the three orthogonal forces and three torque components at the same time. The 6-channel output signals are recorded with two NI 9237 data loggers and post-processed with the LabVIEW SignalExpress software.

4.2. Experimental design

In this section, validation of the proposed analytical model is carried out through two benchmark shapes; the truncated cone and truncated pyramid. In particular, during the cone-forming process, four process parameters including step-down size, wall angle, tool diameter and sheet thickness are selected and varied for a comprehensive validation. Additionally, the analytical model is further validated with the experimental results from the forming of truncated pyramids with different step-down size and sheet thickness. A full list of testing parameters for the truncated cone shape is presented in Table 2. Specifically, the effect of wall angle is investigated through tests 1 to 8 by varying wall angle from 30° to 70°. In tests 9 to 17, the Δz is set from 0.1 mm to a large value up to 3 mm to have a full range validation. The effects of tool diameter and sheet thickness are also investigated through tests 18 to 26. All the cones are designed with the same major diameter of 140 mm and a depth of 75 mm (except for tests 1–3 due to the geometric conflict). The successfully formed depths before crack of the material are also recorded in the last column.

For the truncated pyramid shape, the effect of step-down size and sheet thickness are investigated. The wall angle and tool diameter are set at constant values of 55° and 30 mm, respectively. Table 3 summarizes the detailed forming parameters for the pyramid-forming testing.

4.3. Model validation with truncated cone

In the current experimental setup, the forming forces are measured in the Global Cartesian coordinates system which is marked in Fig. 6, so forces need to be converted into tangential and radial directions to make a comparison. The same method presented in Aerens et al. (2010) is used in the current work and the converted forces for a cone with an angle of 65° with a step down of 0.5 mm is shown in Fig. 7. It is observed that the tangential force increases gradually during the early phase of the process and becomes steady for the rest of the process. This steady force is recorded to make comparison with the predicted results calculated with the same

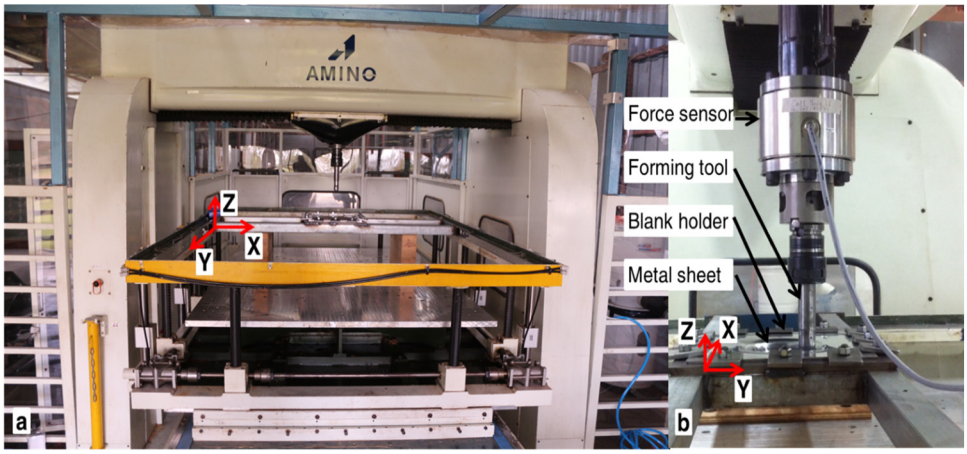

Fig. 6. AMINO incremental forming machine and the implemented force sensor: (a) front view; (b) detailed side view.

parameters presented in Tables 2 and 3 and the model presented in Section 3.

4.3.1. Effect of step-down size

To have a comprehensive assessment of the proposed model, four processing parameters are investigated individually. Previous studies (Aerens et al., 2010; Li et al., 2014c) show that forming forces in the ISF process are largely affected by the value of step-down size. Therefore, it is of great importance to verify that the analytical model is capable of predicting the trend as well as the magnitude accurately for a variation of step down. Fig. 8 presents the comparison between the predicted and measured tangential forces with different step-down sizes ranging from 0.1 mm to 3 mm. It is observed that the prediction provides an accurate result for all the tests except a reasonable deviation (85 N with an error of 12%) for the case with step down of 2 mm. As incorporated in the combined model, the final result is a combination of two sub-models which based on different deformation mechanisms. It is suggested that the

Table 2
Experimental design for truncated cone.

Test no.	Wall angle α (°)	Step down Δz (mm)	Tool diameter (mm)	Thickness (mm)	Feed rate (mm/min)	Designed depth (mm)	Formed depth (mm)
1	30	0.5	30	1.6	4000	28	28
2	40	0.5	30	1.6	4000	40	40
3	50	0.5	30	1.6	4000	60	60
4	60	0.5	30	1.6	4000	75	37.5
5	62	0.5	30	1.6	4000	75	27
6	63	0.5	30	1.6	4000	75	25
7	65	0.5	30	1.6	4000	75	24.5
8	70	0.5	30	1.6	4000	75	23
9	60	0.1	30	1.6	4000	75	29.3
10	60	0.2	30	1.6	4000	75	29.8
11	60	0.3	30	1.6	4000	75	33
12	60	0.4	30	1.6	4000	75	35.2
13	60	0.5	30	1.6	4000	75	37.5
14	60	0.7	30	1.6	4000	75	75
15	60	1.0	30	1.6	4000	75	75
16	60	2	30	1.6	4000	75	75
17	60	3	30	1.6	4000	75	75
18	60	1	10	1.6	4000	75	75
19	60	1	15	1.6	4000	75	75
20	60	1	20	1.6	4000	75	75
21	60	1	25	1.6	4000	75	75
23	60	0.5	30	1	4000	75	35
24	60	0.5	30	2.54	4000	75	75
25	60	1	30	1	4000	75	50
26	60	1	30	2.54	4000	75	75

Table 3
Experimental design for truncated pyramid.

Test no.	Wall angle α (°)	Step down Δz (mm)	Tool diameter (mm)	Thickness (mm)	Feed rate (mm/min)	Designed depth (mm)
1	55	0.5	30	1.02	4000	65
2	55	1	30	1.02	4000	65
3	55	1.5	30	1.02	4000	65
4	55	0.5	30	1.6	4000	65
5	55	1	30	1.6	4000	65
6	55	1.5	30	1.6	4000	65
7	55	0.5	30	2.54	4000	65
8	55	1	30	2.54	4000	65
9	55	1.5	30	2.54	4000	65

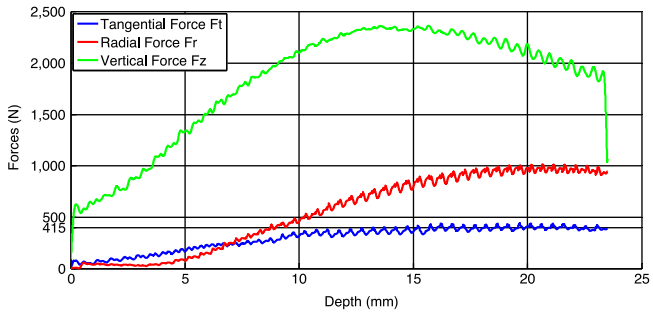

Fig. 7. Converted tangential and radial forces versus forming depth for a cone with an angle of 65° (case 8 in Table 2).

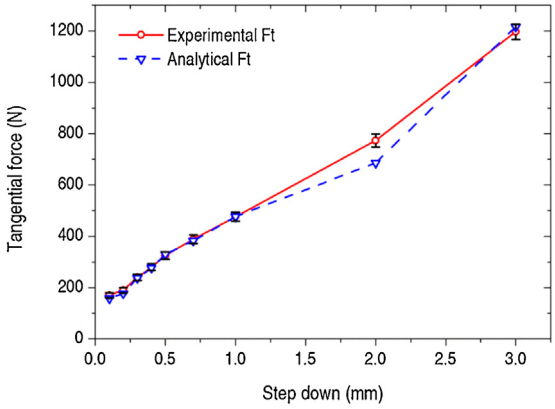

Fig. 8. Comparison between predicted and measured tangential forces with different step-down sizes (r_t = 15 mm, t_0 = 1.6 mm, α = 60°).

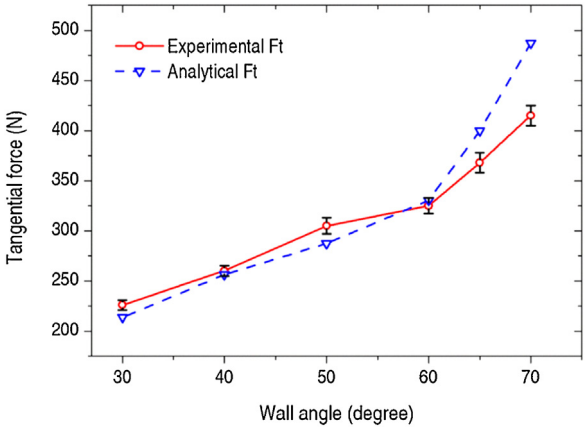

Fig. 9. Comparison between predicted and measured tangential forces with different wall angles (r_t = 15 mm, t_0 = 1.6 mm, Δz = 0.5 mm).

shear deformation could be more significant with small step-down size (i.e. $\Delta z \leq 0.5$ mm), while bending and stretching deformation modes are shown to be dominant when large increments of plastic deformation involves.

4.3.2. Effect of wall angle

The effect of wall angle on the tangential force is also investigated with the range from 30° to 70°. Similar with the effect of step down, the tangential force increases with the increase of wall angle. Comparison between predicted and measured tangential forces with different wall angles is illustrated in Fig. 9. It can be observed that the proposed model underestimates F_t slightly with wall angles smaller than 60° whereas overestimates it at larger wall angles. Specifically, for wall angles below 65°, the average

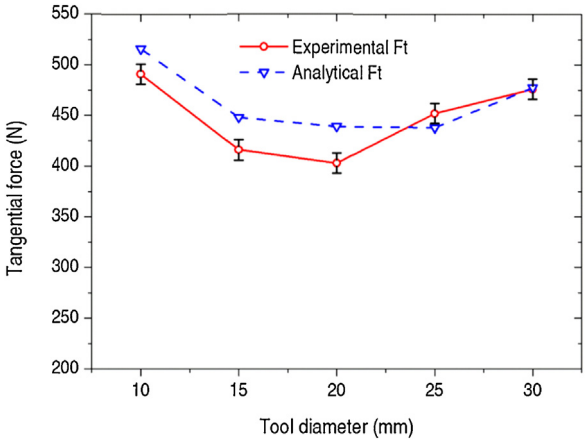

Fig. 10. Comparison between predicted and measured tangential forces with different tool diameter (Δz = 1.0 mm, t_0 = 1.6 mm, α = 60°).

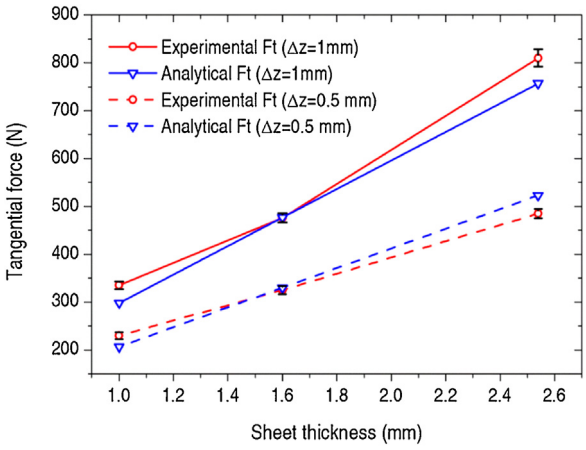

Fig. 11. Comparison between predicted and measured tangential forces with different sheet thickness and step down sizes (r_t = 15 mm, α = 60°).

prediction error could be achieved within 5%. While with the wall angle of 70°, which is close to the maximum formable angle of the material, the effect of strain hardening is more significant which may not be effectively represented by a conventional simplified material constitutive model; therefore, a larger error of 17% with 80 N was obtained.

4.3.3. Effect of tool diameter

Forming tools with different diameter are used in the cone-forming process and the converted tangential forces are shown in Fig. 10. Interestingly, there is a valley effect of the tangential force with the variation of tool diameter from 15 to 30 mm. In the experiments, the minimum force is achieved with a tool diameter of 20 mm and the maximum force occurs for 30 mm. The prediction shows the same trend although the minimum force occurs with the 25 mm tool. Overall, the proposed model reflects the trend of the tangential force with the variation of tool diameter with a deviation less than approximately 10%.

4.3.4. Effect of sheet thickness

In the ISF process, it could be assumed that the tangential force is linearly proportional to the sheet thickness according to Mirnia and Dariani (2012). This assumption is also confirmed by the present experimental work with the forming of the truncated cone. The relations between tangential force and sheet thickness are plotted in Fig. 11 with step-down size of 0.5 and 1 mm. The predicted forces

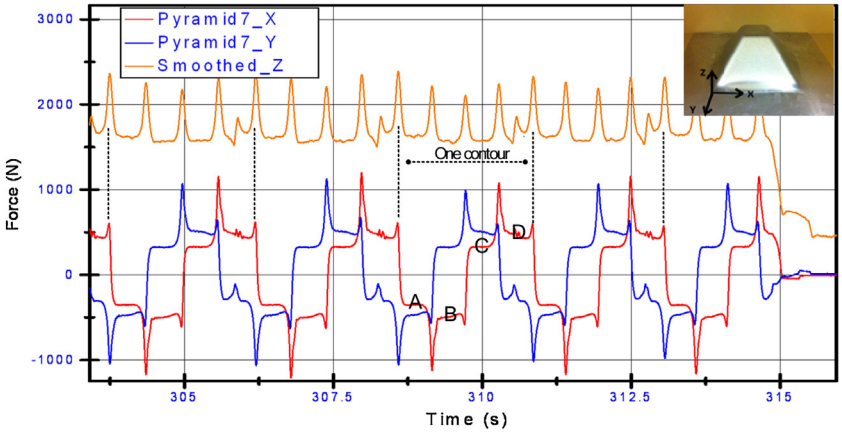

Fig. 12. Three force components in the forming of a truncated pyramid.

based on this analysis are also compared with experimental results. As shown in Fig. 11, in both cases, the predicted forces are in good agreement with the experiments. In particular, a maximum deviation value of 50 N was obtained when forming a 2.54 mm thick material with a step down size of 1 mm.

4.4. Model validation with truncated pyramid

Additionally, the proposed analytical model is verified with the truncated pyramid shape. A typical force trend during the forming of a truncated pyramid is plotted in Fig. 12. It is noticed that there are four stages during each contour which reflects the four sides of the pyramid. Specifically, during one contour as indicated in Fig. 12, the forming force in global *X* direction undergoes four stages: *A, B, C* and *D*. After the detailed verification of the force variation, it is confirmed that the absolute lower values as marked with stages *A* and *C* correspond to tangential forces. A sample of the formed truncated pyramid is also presented. 9 tests have been performed according to the experimental design in Table 3.

Fig. 13 compares the predicted tangential forces with the experimental values for all the 9 tests. It is shown that, for the experimental results, the tangential force rises with the increase of the step-down size for all the sheets with different thickness. In particular, it is shown that the step down size has more effect on the force when the thickness is larger. It is also confirmed that a larger tangential force is required to deform the thicker sheet. These phenomena are successfully reflected for the tangential forces obtained from the proposed analytical model. As shown in Fig. 13, the relative error between predicted and measured F_t is less than 15% in most of the cases.

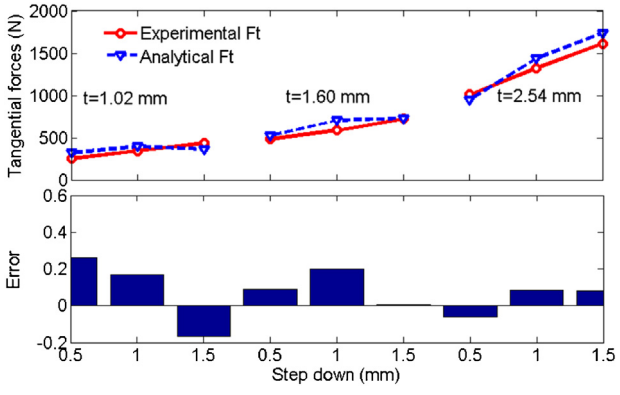

Fig. 13. Comparison between predicted and measured tangential forces with different sheet thickness and step down sizes for the forming of truncated pyramids (r_t = 15 mm, α = 55°).

5. Model extension

The force prediction model is further generalized to more complex shapes, where wall angle and local radius become a variable rather than a constant. The truncated ellipsoidal cup is designed as a general shape to evaluate the generalized capacity of the analytical model as well as to reveal the fundamental deformation mechanics in the ISF process. The inherent geometric characteristics of this shape make it an ideal benchmark for this process. At a certain contour, both the local radius and wall angle are changing with the moving of the forming tool which is not represented in the previous two shapes. The detailed trend will be discussed in the following section. The studied ellipsoidal cup can be described with an analytical equation by,

$$\frac{x^2}{a^2}+\frac{y^2}{b^2}+\frac{z^2}{c^2}=1. \tag{12}$$

The ellipsoidal cup can also be written as a parametric equation by

$$\begin{aligned} x &= a\cos u\sin v \\ y &= b\sin u\sin v \\ z &= c\cos v \end{aligned} \tag{13}$$

where a = 75 mm, b = 45 mm, c = 60 mm, and $u \in [0, 2\pi]$ and $v \in [0, \pi]$. To ensure the successful forming of the ellipsoidal cup, only a part of the shape will be formed due to the following considerations. First, due to the limitation of formability, the region with excessive wall angles should be avoided. Also, as the forming tool will be contacting with the inner surface, the inner local radius of the shape should be larger than the tool radius to avoid geometric conflict. As a result, the ellipsoidal shape has been truncated between the planes of $z = -20$ and $z = -50$ and the detailed dimensions are shown in Fig. 14. Two tests with different step-down sizes are designed for this shape as listed in Table 4.

Fig. 15 plots the experimentally measured forces of 3 orthogonal directions for the last ten forming contours with a step down of 1 mm. During this period, it can be seen that forces have reached a relative steady state with the same pattern and magnitude for each contour. Specifically, the forces in the horizontal plane (F_x and F_y) present a symmetric pattern about zero. During the forming between points *a* and *c* (refer to Fig. 14), both magnitudes of horizontal forces experienced a sinusoidal-like decrease-increase changing process. F_x drops sharply to zero and then reaches the negative peak value at the point of *c*. However, F_y hasn't decreased

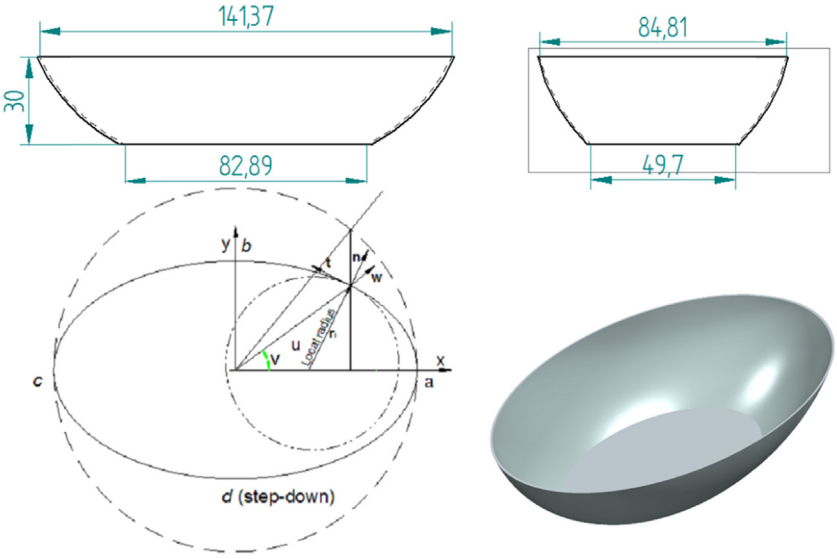

Fig. 14. Dimensions of the truncated ellipsoidal cup and the sketch of an ellipsoidal contour.

Table 4
Experimental design for truncated ellipsoidal cup.

Test no.	Step down Δz (mm)	Tool diameter (mm)	Thickness (mm)	Feed rate (mm/min)	Designed depth (mm)
1	0.5	30	1.6	4000	30
2	1	30	1.6	4000	30

to zero until reaching the point of *c*. In terms of vertical force F_z, it only fluctuates over a limited range during each loop of the forming process and the steady value is recorded as 2100 N.

The tangential force F_t is obtained using the similar conversion method mentioned in the cone-forming process. Fig. 16 plots the converted tangential force during two contours of a forming case with an ellipsoidal cup. Unlike the previous results for both truncated cone and pyramid, the tangential force is not steady within one contour but changing with a regular pattern. Specifically, the lowest tangential force occurs before the end points of the long axis (points *a* and *c* in Fig. 14), and then increases to the peak value at a certain point (where angle *u* is about 30°) before dropping continuously to the smallest value before point *c*. This trend is also presented in the other half of the ellipse except for a sudden dip resulting from the step-down movement of the forming tool.

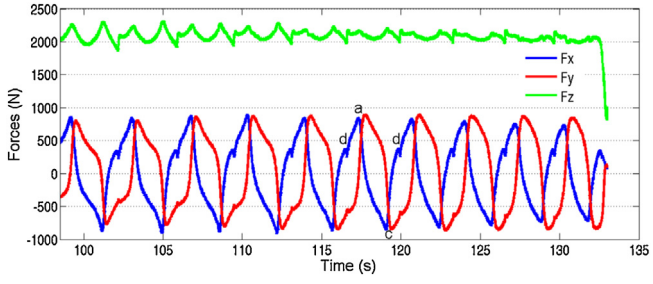

Fig. 15. Force trend during the forming of ellipsoidal cup ($\Delta z = 1$ mm, $t = 1.6$ mm).

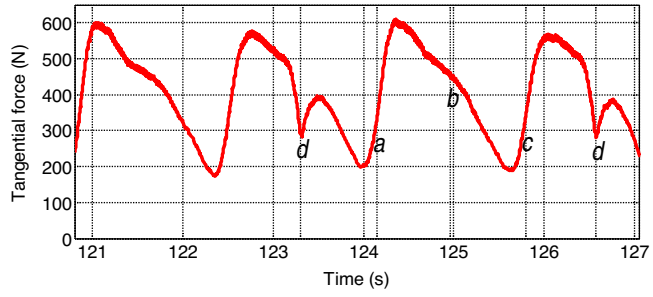

Fig. 16. Converted tangential force from experimental tests for ellipsoidal cup with a step-down size of 1 mm.

As discussed previously, in the ellipsoidal cup-forming process, both the local radius and wall angle are constantly changing over time. As a result, the metal sheet undergoes an additional twisting deformation. Therefore, the model has to be generalized by taking into account these effects. Accordingly, at a particular point during ellipsoidal cup-forming process as marked in Fig. 14, the twist in the local coordinates (*ntw*) is given by Timoshenko and Woinowsky-Krieger (1959),

$$\frac{1}{T_{nt}} = \frac{\partial^2 w}{\partial n \partial t} = \frac{\partial \frac{\partial w}{\partial n}}{\partial t} = \frac{\partial \alpha}{\partial t}, \tag{14}$$

where *w* is the displacement normal to the mid-surface of the plate and *t*,*n* are defined as the forming and normal direction, respectively. α is the wall angle in the normal direction at a particular point on the contour and its variation is shown in Fig. 17. It is noted from the above equation that the change rate of wall angle along the tangential direction can be treated as an indicator to reflect the effect of twisting. The twist does plastic work and therefore affects the forming force. This can be taken into account empirically by modifying the analytical model with the effect of change rate of wall angle and local radius r_l as follows:

$$F_{t\_new} = \left(1 + 2r_l \frac{\partial \alpha}{\partial t}\right) \times F_t = \left(1 + 2\frac{\partial \alpha}{\partial u}\right) \times F_t \tag{15}$$

where F_t is the predicted value from original combined model and a scaled factor of 2 is used to rectify the amplitude of the variation. $\partial\alpha/\partial u$ represents the rate of change of wall angle over the angle *u* defined in Eq. (13) and its variation during one contour is demonstrated in Fig. 17. Note this modification is not in conflict

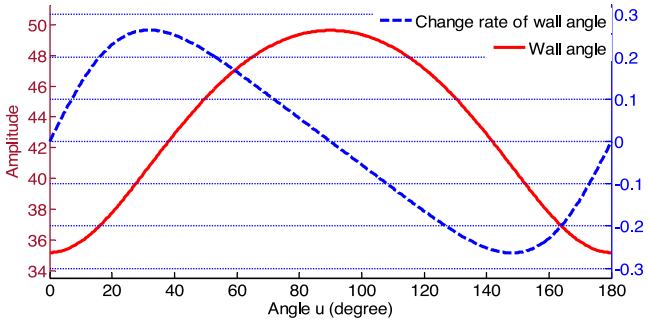

Fig. 17. The variations of the wall angle and its change rate over angle *u*.

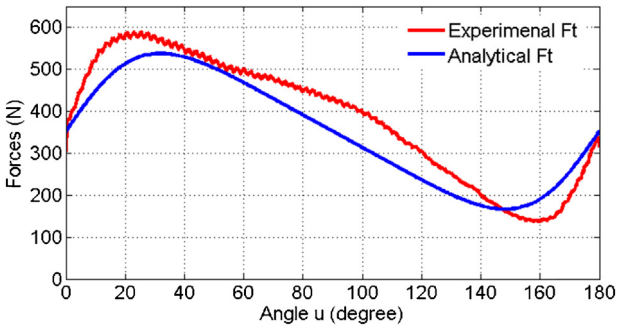

Fig. 18. Predicted tangential force for ellipsoidal cup with a step-down size of 1 mm.

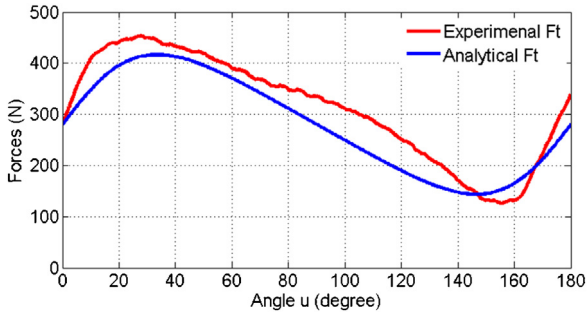

Fig. 19. Predicted tangential force for ellipsoidal cup with a step-down size of 0.5 mm.

with verification for the truncated cone and pyramid in which the wall angle at each step is constant so the change rate is zero.

The predicted tangential forces are compared with the converted one in Figs. 18 and 19 with step-down size of 1 mm and 0.5 mm, respectively. It is observed that the predicted values are in good agreement with the experimental results and deviations are also within a reasonable range. In particular, the positions of both maximum and minimum values are correctly predicted and also the overall amplitude during the whole contour is reasonably represented. Further study is necessary to develop a less empirical model.

The above results reflect that the extended model has been validated through a specific shape but it is still limited by the integrity of experimental tests. Since it has been clearly demonstrated that the trend of the measured tangential force is closely related to the feature of the local geometry, further in-depth theoretical justification of the effect of twisting on the plastic dissipated power could be incorporated into the model as a potential approach to mitigate such a limitation. As discussed, the choice of an ellipsoidal cup shape is due to the continuous variation of both wall angle and local radius during one contour. In addition, the available symbolic expression of the geometry further allows an efficient verification procedure for the empirical correlation. Although the shape of an ellipsoidal cup may be still considered as an extension of truncated cone and pyramid, the current model provides valuable foundation for future investigation towards more general shapes. Another suggestion for the future work is to investigate the influence of the material type on the tangential force, using the proposed model.

6. Conclusions

In the present work, a comprehensive FE model with fine solid elements is established and deformation behaviors of typical elements after deformation are analyzed. These provide further insights into the deformation mechanism and more evidence for the derivation of the analytical model. Based on the deformation analysis, an efficient tangential force prediction model is deduced which considers main deformation modes including shearing, stretching and bending. In particular, the contribution from each deformation mode is related to the variation of forming parameters. Additionally, comprehensive experimental tests with shapes of truncated cone, truncated pyramid by varying the critical forming parameters are conducted to investigate the effects of process parameters on forming forces. The predicted tangential forces from the proposed model are then compared with those experimental results and good agreements are obtained. Finally, the analytical model is further extended to investigate its potential capacity to handle complex geometries (e.g. ellipsoidal cup). The conclusions can be summarized as follows:

- It is confirmed from FE simulation that the deformation in ISF process is a combination of shearing, bending and stretching. Specifically, direct strain in perpendicular to the forming direction (ε_{11}) is the major deformation mode in the cone-forming process. The strain ε_{11} could be accumulated to a large value while strain in the forming direction only alternates at smaller values. Shear strain in the forming direction (ε_{23}) prevails greatly among the three shear components and the maximum value occurred at the middle of the sheet. It is also found that the in-plane shear strain is not negligible, especially at the upper surface.
- The proposed force prediction model is validated through a comprehensive experimental campaign with two geometric shapes (truncated cone and truncated pyramid) and various process parameters (step down, wall angle, tool radius and thickness). It is concluded that the tangential force increases with the increase of step-down, wall angle and sheet thickness. However, the tangential force varies in a concave manner with the variation of tool diameter from 10 to 30 mm with a minimum occurring between 20 and 25 mm.
- The proposed analytical model is further extended to capture the changing of local curvature and wall angle during forming to address more complex shapes. The truncated ellipsoidal cup is selected as the target shape which has local curvature and wall angle variations in each contour. The modified model is able to predict reasonably accurate tangential force variation in each contour compared to experiments.

It is also worthwhile to point out that the current analytical model has its limitations and future work is needed to extend its adaptability. The combined model is semi-analytical and there is still uncertainty as to the type of deformation mode that is dominant in the ISF process under different forming configurations. As a further contribution, the extended model shows great potential towards dealing with more complex geometries, although further theoretical justification is essential. Considering the proposed model can be efficiently solved within several minutes, the further

development of this model will greatly facilitate the production design and optimization process in ISF.

Acknowledgements

The present work was supported by Australian Research Council (ARC) Linkage project (LP100200689), Boeing Research and Technology Australia and QMI Solutions in Australia. China Scholarship Council (CSC) is also acknowledged for the scholarship support.

Appendix A

In the present model, as shown in Fig. 5(c), the deformation zone is divided into three regions: I contact region, II non-contact region following the height of tool head and III non-contact region following the height of the formed sheet. One of the typical flow lines with a radius of r is depicted in Fig. 5(b). The flow line is defined as three curves Zf_c, f_t and Zf_s which correspond to region I, II and III, respectively. Zf_c has the same geometric function with the tool head surface as it is the region contacting with the tool but the conjunct point with Zf_t is unknown therefore is advisable to be determined as the following equation with an adjustable parameter M,

$$Zf_c\left(r,\theta\right) = Z_c = M\left(Z_s - Z_o\right) + Z_o, \qquad (0 \le M \le 1) \tag{A1}$$

where Z_s and Z_o are the vertical position of the sheet formed in previous pass and the tool vertex with the radius of r. To represent the height variation of the non-contact surface of the sheet, a normalized shape function $S(X)$ is introduced. $S(X)$ is tentatively designed as 2 s order Bezier curves with the following equation,

$$S(X) = \left\{ \begin{array}{ll} 1 - \left(\dfrac{\theta - \theta_c}{\theta_t - \theta_c}\right)^2 (1-N)\left(\dfrac{r_o - r}{r_o - r_i}\right) & \theta_c \le \theta \le \theta_t \quad 0 \le N \le 1 \\ 1 - \left(\dfrac{\theta - \theta_s}{\theta_s - \theta_t}\right)^2 (1-N)\left(\dfrac{r_o - r}{r_o - r_i}\right) & \theta_t \le \theta \le \theta_s \quad 0 \le N \le 1 \end{array} \right\}. \tag{A2}$$

here N is another adjustable parameter which can be obtained through the optimisation of the dissipated power. The value of $S(X)$ changes from N to 1 corresponding to the variation of θ and r within their ranges.

References

Aerens, R., Eyckens, P., Van Bael, A., Duflou, J.R., 2010. Force prediction for single point incremental forming deduced from experimental and FEM observations. Int. J. Adv. Manuf. Technol. 46, 969–982.
Allwood, J.M., King, G.P.F., Duflou, J., 2005. A structured search for applications of the incremental sheet-forming process by product segmentation. Proc. Inst. Mech. Eng. Part B J. Eng. Manuf. 219, 239–244.
Ambrogio, G., De Napoli, L., Filice, L., Gagliardi, F., Muzzupappa, M., 2005. Application of incremental forming process for high customised medical product manufacturing. J. Mater. Process. Technol. 162–163, 156–162.
Ambrogio, G., Filice, L., Micari, F., 2006. A force measuring based strategy for failure prevention in incremental forming. J. Mater. Process. Technol. 177, 413–416.
Duflou, J., Tunçkol, Y., Szekeres, A., Vanherck, P., 2007. Experimental study on force measurements for single point incremental forming. J. Mater. Process. Technol. 189, 65–72.
Emmens, W.C., Boogaard, A.H., 2008. An overview of stabilizing deformation mechanisms in incremental sheet forming. J. Mater. Process. Technol. 209, 3688–3695.
Eyckens, P., Belkassem, B., Henrard, C., Gu, J., Sol, H., Habraken, A.M., Duflou, J.R., Van Bael, A., Van Houtte, P., 2011. Strain evolution in the single point incremental forming process: digital image correlation measurement and finite element prediction. Int. J. Mater. Form. 4, 55–71.
Filice, L., Ambrogio, G., Micari, F., 2006. On-line control of single point incremental forming operations through punch force monitoring. CIRP Ann. Manuf. Technol. 55, 245–248.
Fiorentino, A., 2013. Force-based failure criterion in incremental sheet forming. Int. J. Adv. Manuf. Technol. 68, 557–563.
Hosford, W., Caddell, R., 2007. Metal Forming: Mechanics and Metallurgy. Cambridge University Press, Cambridge.
Ingarao, G., Ambrogio, G., Gagliardi, F., Di Lorenzo, R., 2012. A sustainability point of view on sheet metal forming operations: material wasting and energy consumption in incremental forming and stamping processes. J. Cleaner Prod. 29–30, 255–268.
Iseki, H., 2001. An approximate deformation analysis and FEM analysis for the incremental bulging of sheet metal using a spherical roller. J. Mater. Process. Technol. 111, 150–154.
Jackson, K., Allwood, J., 2009. The mechanics of incremental sheet forming. J. Mater. Process. Technol. 209, 1158–1174.
Johnson, W., Mellor, P.B., 1983. In: Horwood, E. (Ed.), Engineering Plasticity. Ellis Horwood Limited, Van Nostrand Reinhold (UK) Ltd., New York, Chichester, West Sussex, England.
Li, Y., Liu, Z., Daniel, W.J.T., Meehan, P.A., 2014a. Simulation and experimental observations of effect of different contact interfaces on the incremental sheet forming process. Mater. Manuf. Processes 29, 121–128.
Li, Y., Liu, Z., Lu, H., Daniel, W.J.T., Liu, S., Meehan, P., 2014b. Efficient force prediction for incremental sheet forming and experimental validation. Int. J. Adv. Manuf. Technol. 73, 571–587.
Li, Y., Liu, Z., Lu, H., Daniel, W.J.T., Meehan, P.A., 2014c. Experimental study and efficient prediction on forming forces in incremental sheet forming. Adv. Mater. Res. 939, 313–321.
Liu, Z., Li, Y., Meehan, P., 2013. Experimental investigation of mechanical properties, formability and force measurement for AA7075-O aluminum alloy sheets formed by incremental forming. Int. J. Precis. Eng. Manuf. 14, 1891–1899.
Lu, B., Fang, Y., Xu, D.K., Chen, J., Ou, H., Moser, N.H., Cao, J., 2014. Mechanism investigation of friction-related effects in single point incremental forming using a developed oblique roller-ball tool. Int. J. Mach. Tools Manuf. 85, 14–29.
Micari, M.G., Duflou, J., Shirvani, B., Clarke, R., Di Lorenzo, R., Fratini, L., 2007. Incremental forming process for the accomplishment of automotive details. Key Eng. Mater. 344, 559–566.
Mirnia, M.J., Dariani, B.M., 2012. Analysis of incremental sheet metal forming using the upper-bound approach. Proc. Inst. Mech. Eng. Part B J. Eng. Manuf. 226, 1309–1320.
Petek, A., Kuzman, K., Suhač, B., 2009. Autonomous on-line system for fracture identification at incremental sheet forming. CIRP Ann. Manuf. Technol. 58, 283–286.
Raithatha, A., Duncan, S., 2009. Rigid plastic model of incremental sheet deformation using second-order cone programming. Int. J. Numer. Methods Eng. 78, 955–979.
Silva, M.B., Skjoedt, M., Martins, P.A.F., Bay, N., 2008. Revisiting the fundamentals of single point incremental forming by means of membrane analysis. Int. J. Mach. Tools Manuf. 48, 73–83.
Smith, J., Malhotra, R., Liu, W.K., Cao, J., 2013. Deformation mechanics in single-point and accumulative double-sided incremental forming. Int. J. Adv. Manuf. Technol. 69, 1185–1201.
Timoshenko, S., Woinowsky-Krieger, S., 1959. Theory of Plates and Shells. McGraw-Hill, New York, US.

4.3 The Papers

Paper 6

Experimental investigation of mechanical properties, formability and force measurement for AA7075-O aluminum alloy sheets formed by incremental forming

Liu, Z.B., **Li, Y.L.** and Meehan, P. A.

International Journal of Precision Engineering and Manufacturing

2013, Volume: 14, Pages: 1981-1989.

DOI: 10.1007/s12541-013-0255-z

Experimental Investigation of Mechanical Properties, Formability and Force Measurement for AA7075-O Aluminum Alloy Sheets Formed by Incremental Forming

Zhaobing Liu[1,#], Yanle Li[1], and Paul Anthony Meehan[1]

1 School of Mechanical and Mining Engineering, The University of Queensland, Brisbane St Lucia, QLD 4072, Australia
Corresponding Author / E-mail: z.liu7@uq.edu.au, TEL: +61-7-336-53885, FAX: +61-7-336-54799

KEYWORDS: Incremental sheet forming, Mechanical properties, Aluminum 7075-O, Formability, Force measurement

Incremental sheet forming (ISF) has demonstrated its high potential to shape complex three-dimensional components without using specific tooling, thus enabling product customization, cost reduction and efficiencies. This paper presents an experimental campaign to investigate AA7075-O aluminum alloy sheet forming using single point incremental forming (SPIF) technology and understand the forming process mechanism. Firstly, tensile tests were carried out to characterize the mechanical properties of AA7075-O sheets with three different thicknesses. Then, the effects of tool path types with different incremental steps on the maximum part draw angle and the successful part height were evaluated to clarify the formability. Additionally, a fracture forming limit diagram was developed to give the design limits for strain. Finally, the trends in forming forces were analyzed considering the influence of different draw angles, sheet thicknesses, step-down sizes and sheet orientations. Experimental results showed that formability is affected by the part draw angle and incremental steps of the tool path. However, the likelihood of successful forming also depends on other geometrical design parameters such as the part height. In addition, the influences of process parameters on tool forces provide further insights into the deformation mechanics of AA7075-O sheets. The slope of the force curve after the peak value can be identified as a forming failure prediction indicator regardless of the tool path types when using a truncated cone as a benchmark. Also the influence of sheet orientations on forming forces was investigated in SPIF. The vertical forming force is found to be smaller in a sheet orientation 45 to the rolling direction than that of a sheet orientation 0 for three different sheet thicknesses.

Manuscript received: January 25, 2013 / Accepted: September 14, 2013

1. Introduction

The 7xxx series aluminum alloys have been widely utilized as structural materials due to their attractive comprehensive properties, such as low density, high strength, ductility, toughness and resistance to fatigue.[1-3] The 7075 aluminum alloy is one of the highest strength alloys and is typically used as aircraft structures. The 7075 aluminum alloy sheets, in O temper condition, have practical and wide industrial application due to their higher formability compared with the other temper conditions. For many applications, AA7075-O sheets are required to deform in various kinds of 3D shells. In industry, the cost of forming is high for processes such as deep drawing or stamping where specialized tooling is needed for a specific 3D designed shape. However, applications in fields such as rapid prototyping and customized products require small-batch production, so the high cost tooling is disadvantageous. The inception of incremental sheet forming (ISF) has provided a solution, which is quite flexible, suitable for small-batch production, and no high-cost tooling is required.[4-16] The development of ISF began in the 1990s in Japan.[4] Since then, this technology has gained great attention in Europe and North America, and many efforts have been made to push it towards industrial applications.[9] Basically, there are two variations of incremental sheet forming, single point incremental forming (SPIF) and two point incremental forming (TPIF). In single point incremental forming, the tool deforms the sheet metal into the concave shape without any dies while in two point incremental forming, the tool moves on the convex sheet surface with a positive die. The blank holder is moved by the hydraulic actuator in order to firmly maintain the sheet metal in the proper working position.

Comprehensive reviews have been provided on the development of ISF in the past decades.[9,10] It is noted that the tool path defines the component geometry. So, the influence of different tool paths with

different incremental steps on formability is worth further investigating. Filice et al. discussed the material formability in incremental forming, in which a spiral tool path was proposed to form a truncated cone shape.[11] They concluded that incremental forming is characterized by local stretching deformation mechanics which determines a linear forming limit curve with a negative slope in the first quadrant. Young et al. pointed out that the maximum draw angle for SPIF could be defined to evaluate part formability.[12] Experimental tests were performed to determine specific values for two kinds of aluminum alloys (3003-O and 5754-O). Durante et al. preformed experimental campaigns to deform AA7075-T0 sheets.[13] They found that formability decreases with the increase of tool diameter and the angular step, which is evaluated by measuring the maximum forming angle for truncated cones. However, the comparison between two kinds of tool paths (spiral and z-level) with different incremental steps has not been made in terms of formability.

Forming force is one of the important quantities required to understand the deformation mechanics in ISF. Duflou et al. investigated the influence of four process parameters (vertical step size, tool diameter, geometrical wall angle and sheet thickness) as well as the lubrication and the geometry of the part on the forming forces.[14] It was concluded that within the explored limits, vertical step size has the least significant impact and can therefore be increased without great penalty, in favor of lower part production times. Jackson et al. compared the forming forces between sandwich panel incremental forming and aluminum incremental forming.[15] The influence of tool radius and vertical pitch on tool force was highlighted. They concluded that vertical force increases approximately linearly with tool radius for both materials. Jeswiet et al. found that tool force usually evolves to a peak value and then stabilizes to a steady state when manufacturing a part with a constant wall angle.[16]

The scope of this paper is mainly focused on incremental forming of AA7075-O aluminum sheets. Uniaxial tensile tests were performed on AA7075-O sheets with three different thicknesses to characterize some basic material properties. Then, two aspects are investigated in this paper. Firstly, formability has been evaluated in order to clarify the influence of different kinds of tool paths with different incremental steps. The maximum draw angle can be seen as a simple formability indicator. However, the likelihood of successful forming also depends on other geometric design parameters such as the part height. A safety formability region is given in view of different tool paths and incremental steps. Moreover, the fracture forming limit diagram is derived to further characterize the material formability. Secondly, the influences of process parameters on tool forces have been revisited to give further insights into the deformation mechanics of AA7075-O sheets. In particular, the influence of sheet orientations on forming forces has been considered for the first time in this study.

2. Material Characterization and Mechanical Behavior

In this section, AA7075 O-temper aluminum alloy sheets were investigated with three different thicknesses (1.02 mm, 1.60 mm and 2.54 mm). The chemical composition for AA7075-O sheets is presented in Table 1. In order to obtain the mechanical properties, uniaxial tension tests were performed on samples which have been cut in the directions of 0°, 45° and 90° with respect to the rolling direction. The dimensions of the specimen shape are shown in Fig. 1. The tensile tests were carried out using INSTRON 5584 universal testing machine equipped by extensometer with a gauge length of 50 mm, see Fig. 2.

Through the tensile tests, the basic mechanical properties such as yield stress, ultimate tensile strength for different directions were obtained as presented in Table 2.

The material flow behavior, in the sheet plane, was characterized on the base of the true stress-true strain curves for three orientations in 0°, 45° and 90° with respect to the rolling direction. They are presented in Figs. 3~5. Through these curves, certain anisotropic flow behavior in the sheet plane for each thickness is revealed. It is shown that anisotropy

Table 1 Chemical composition (% wt) for AA7075-O aluminum alloy sheets

Si	Fe	Cu	Mn	Mg	Cr	Zn	Ti	Al
0.08	0.12	1.7	0.01	2.5	0.19	5.7	0.04	Balance

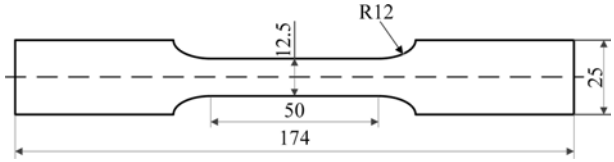

Fig. 1 Specimen shape for uniaxial tensile test (Unit: mm)

Fig. 2 INSTRON 5584 universal testing machine

Table 2 Mechanical properties for AA7075-O aluminum alloy sheets with three different thicknesses

Material	Orientation	Y	UTS	El	E
1.02 mm	Rolling (0°)	88	190	17	69
	Diagonal (45°)	88	191	18	71
	Transverse (90°)	91	192	14	70
1.60 mm	Rolling (0°)	91	199	20	70
	Diagonal (45°)	91	196	22	69
	Transverse (90°)	94	202	19	70
2.54 mm	Rolling (0°)	93	190	19	70
	Diagonal (45°)	95	200	22	70
	Transverse (90°)	97	203	21	72

Note: Y is yield stress at 0.2% yield [MPa], UTS is ultimate tensile strength [MPa], El is elongation [%] and E is young's modulus [Gpa].

becomes a little more obvious as the sheet thickness increases. But, overall, it represents a rather weak anisotropic behavior for the investigated sheets. The true stress-true strain curves can be fit by the Hollomon power law

$$\sigma = K\varepsilon^n \quad (1)$$

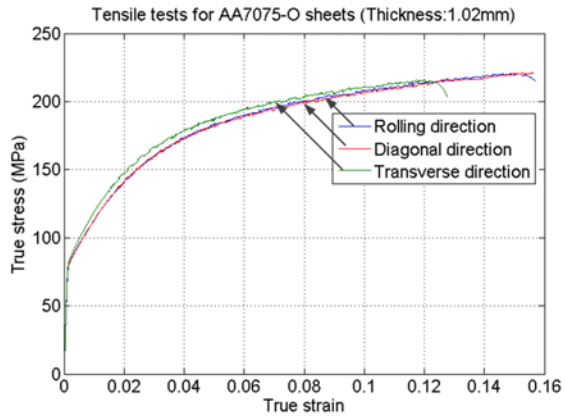

Fig. 3 True stress-true strain curves for AA7075-O aluminum alloy sheets with 1.02 mm thickness

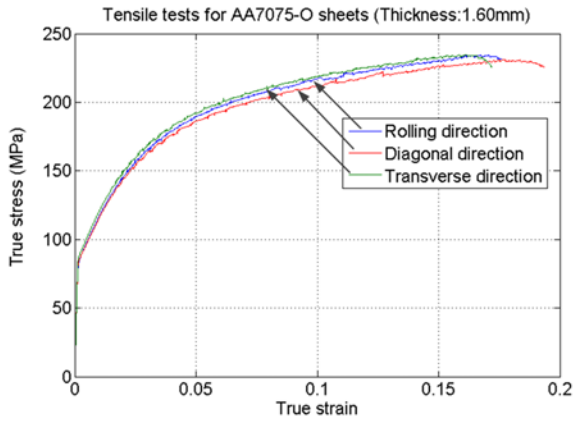

Fig. 4 True stress-true strain curves for AA7075-O aluminum alloy sheets with 1.60 mm thickness

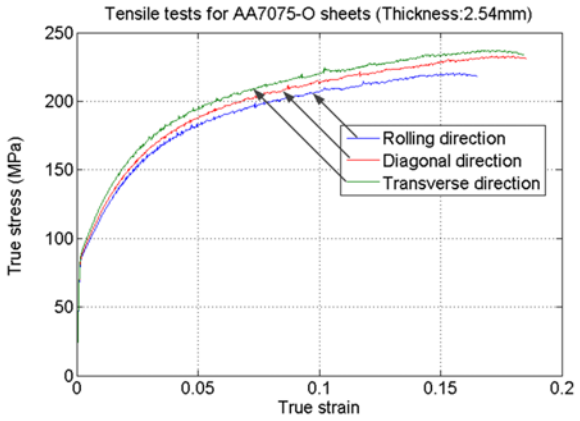

Fig. 5 True stress-true strain curves for AA7075-O aluminum alloy sheets with 2.54 mm thickness

where K is the strength coefficient and n is the strain-hardening (or work-hardening) exponent. The corresponding parameters are presented in Table 3.

3. Formability

In ISF, the formability is much higher than the conventional forming processes such as deep drawing and stamping. In many ISF research papers,[9,12,13] the draw angle can be seen as a formability indicator, because this quantity has a close relationship with the sine law which is widely used to estimate the thickness distribution as a plane strain model. In this section, the maximum draw angle is used as an indicator to estimate the formability of AA7075-O sheets with 1.6 mm thickness considering the influence of different tool paths with different incremental steps. A truncated cone is selected as the benchmark as

Table 3 Strength coefficient K and strain-hardening exponent n for AA7075-O sheets with three different thicknesses

Material	Orientation	K	n
1.02 mm	Rolling (0°)	351.2	0.2301
	Diagonal (45°)	349.5	0.2294
	Transverse (90°)	361.3	0.2300
1.60 mm	Rolling (0°)	361.2	0.2276
	Diagonal (45°)	343.9	0.2176
	Transverse (90°)	361.3	0.2224
2.54 mm	Rolling (0°)	341.2	0.2202
	Diagonal (45°)	349.4	0.2181
	Transverse (90°)	353.4	0.2190

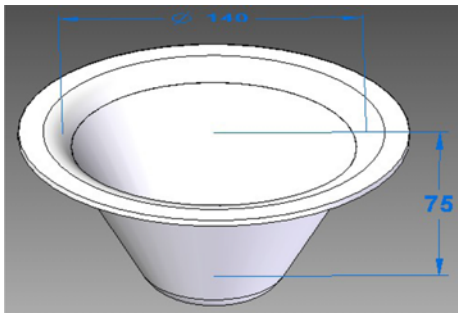

Fig. 6 Benchmark-a truncated cone

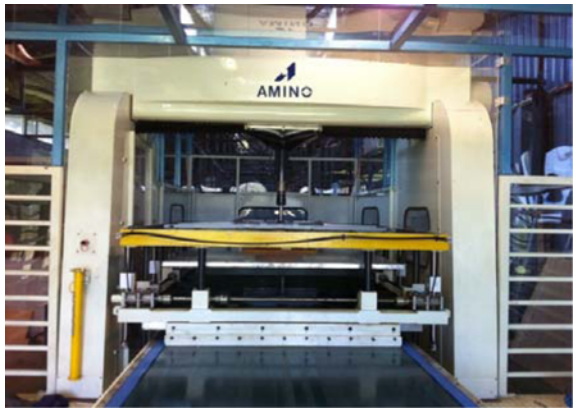

Fig. 7 The Amino ISF machine used for experiments

shown in Fig. 6. The size of AA7075-O sheet is 300 mm×300 mm. The tool radius is 15 mm and feed rate was set to 4000 mm/min. In order to increase the rigidity between the forming area and the sheet flange, a backing plate is utilized underneath the sheet metal. Before forming, lubricant oil-Shell Tellus Oil 68 was sprayed on the blank. The tool paths were generated by Siemens NX 7.0. Fig. 7 shows the Amino ISF machine used for the experiments.

Fig. 8 shows the details of incremental forming and the illustration of incremental steps. It is noted that step over is the adjustable quantity to generate the spiral tool path in Siemens NX software. For the investigated truncated cone with the constant draw angle, step over and step down are directly related based on simple trigonometric relationship. In order to make comparison clear, step over is used here to generate two kinds of tool paths (spiral and z-level) to control the downward movement of the forming tool and investigate their influence on formability. The spiral tool path in Fig. 9(a) is continuous with an incremental descent of the tool distributed over the entire surface of a part, which can be adjusted by changing the step over. The advantage of this tool path is that no marks occur at step down. Z-level tool path in Fig. 9(b) is defined by fixed vertical increments between consecutive discrete contours. Previous studies[9] have shown that for a z-level tool path, deformation is biaxial at the starting and end points of each contour, and is close to plane strain in between. It has been observed that the tendency for fracture at the start and end points of each contour is higher as compared with when the rest of the contour is being formed. Compared with the spiral tool path, the z-level tool path can leave stretch marks at the transition points between layers and create force peaks. It is noted that tool path defines the forming geometry. So, is there any difference in formability when different tool paths are adopted to deform the same part? How is the formability affected by different incremental steps of tool paths? These questions will be answered based on experimental tests in the following discussion.

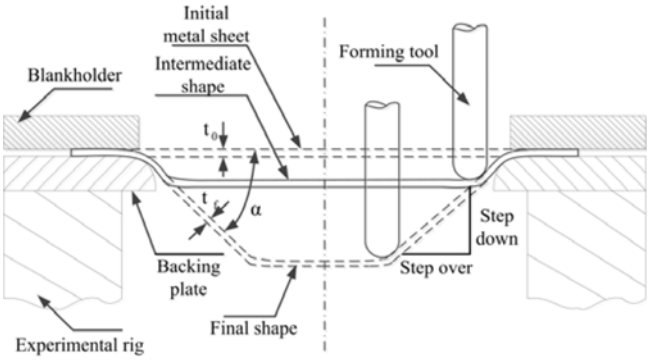

Fig. 8 Details of incremental forming and illustration of incremental steps (step over and step down)

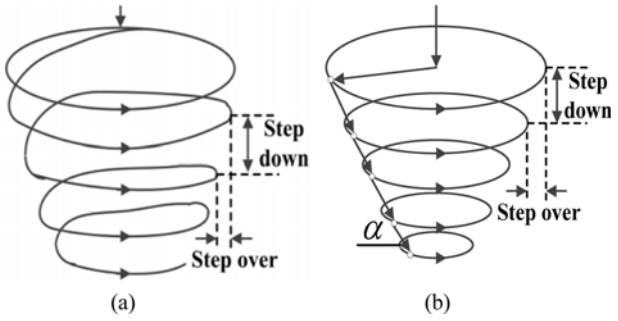

Fig. 9 Design of tool paths to test formability for truncated cones: (a) spiral tool path and (b) z-level tool path (α is the draw angle)

3.1 Influence of tool path and step-down size on formability

In the first test, in order to investigate the influence of the spiral tool path and the z-level tool path on formability, step over was set to be a constant value 0.5 mm for both tool paths. A series of truncated cones were formed with draw angles 60°, 61°, 62°, 63°, 64°, 65° and 70° to evaluate the formability. The experimental results are presented in Fig. 10. It can be seen that under the same step-over size, there is no noticeable difference on formability between the spiral tool path and the z-level tool path. Formability is greatly affected by the draw angle of the truncated cone. However, the likelihood of successful forming also depends on the cone height. As can be seen, draw angles 62° and 63° are the formability boundary for successful forming of the truncated cone. Taking the cone height into consideration, a safety formability region is identified as shown in Fig. 10. Areas A+B are the safety formability zone for the spiral path compared with the area B for the z-level path.

In the second test, emphasis is laid on evaluating the influence of the z-level tool path with different incremental steps on formability. The experimental results are shown in Fig. 11. It is concluded that formability is higher for a larger step over (0.5 mm as compared to 0.2 mm) based on the experimental results. However, because only two step-down sizes were tested, more tests involving a wide range of step down sizes need to be performed to further demonstrate this conclusion in the future. In addition, a safety formability region is drawn in Fig. 11. The area B is the safety formability zone for z-level tool path with 0.2 mm step-over size. The area A shows the quantitative formability difference between 0.5 mm step-over size and 0.2 mm step-over size for the z-level tool path. Fig. 12 summarizes the comparison of effects of spiral and z-level tool paths with different incremental steps on formability.

3.2 Fracture forming limit diagram

In order to further investigate the formability, fracture forming limit

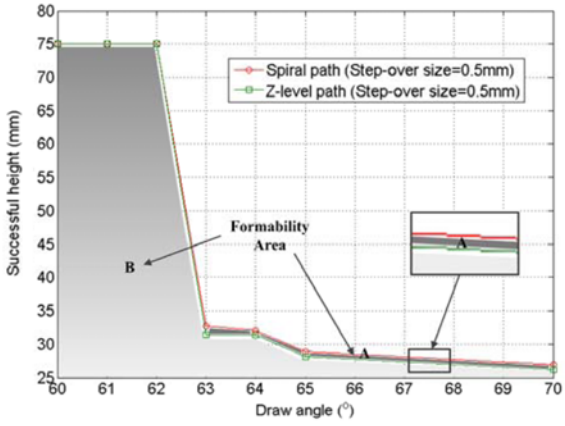

Fig. 10 Influence of spiral and z-level tool paths on formability vs the draw angle α

diagram was obtained as shown in Fig. 13. The results were obtained by measuring the experimental strains at several places along the crack for truncated cones with different draw angles in the case of z-level path with 0.2 mm step-over size. To measure the strains after deformation, circles with 5.5 mm initial diameter were drawn on the surface of the sheets before forming using 0.5-mm-thick oil-based blue pen. The line pitch was 0.5 mm and was already included in the size of the initial diameter of the circle. The size of the major and minor axis of the ellipses after the plastic deformation of the circles was measured and calculated based on the in-plane surface strains directly from

$$\varepsilon_1 = \ln\left(\frac{Y}{D}\right) \tag{2}$$

$$\varepsilon_2 = \ln\left(\frac{X}{D}\right) \tag{3}$$

where D is the initial diameter of the circle and X and Y are the corresponding measured major and minor axis of the ellipse.

As seen in Fig. 13, the measured major true strain for crack failure lies between 0.68 and 0.92 defining a fracture band for major true strain. The process designer can acquire an insight from this result and increase the product formability by properly choosing process parameters such as larger incremental step in the beginning of forming or choosing multi-stage deformation path design.

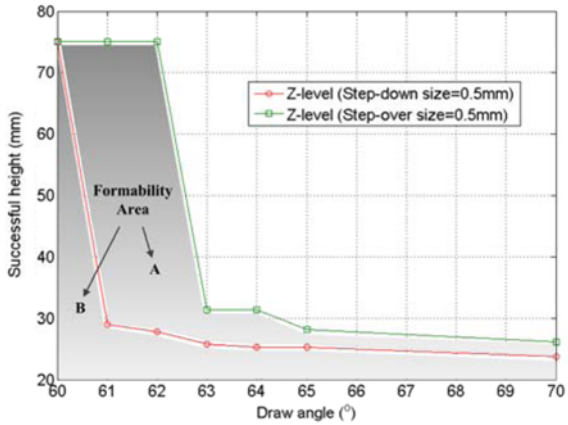

Fig. 11 Influence of the z-level tool path with different incremental steps on formability vs the draw angle α

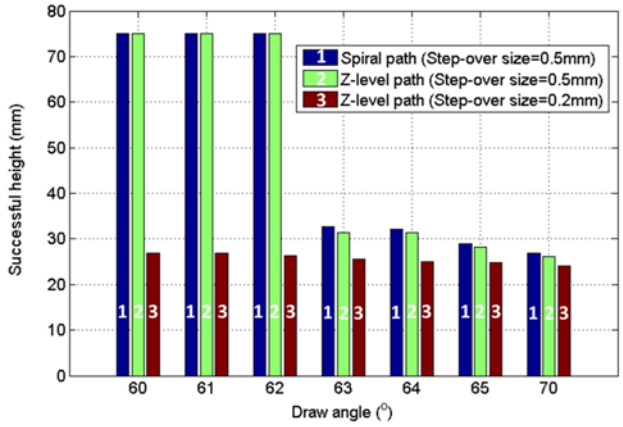

Fig. 12 The comparison of effects of spiral and z-level tool paths with incremental steps on formability vs the draw angle α

4. Force Measurement

It is noted that the investigation of forming forces is one of the most important aspects to understand the deformation mechanism of ISF. Previous studies have mainly focused on the influences of process parameters on tool forces. In this section, emphasis is laid on the analysis of mechanics of forming AA7075-O sheets with three thicknesses (1.02 mm, 1.60 mm and 2.54 mm) through the force measurement. Forming forces are evaluated from three characteristics: (1) the influence of the draw angle and the tool path on resultant forming forces, (2) the influence of the sheet thickness and the step-down size of z-level tool path on forming forces, (3) the influence of sheet orientations on forming forces. It is worth noting that the third aspect has not been considered before in ISF.

In this study, the force measurement was implemented using a specially designed sensor mounted on a forming tool with 30 mm diameter as seen in Fig. 14, which has three full Wheatstone bridges. Each bridge is configured by four strain gauges and designed to measure one of the three orthogonal forces: two bending directions, and one axial direction. Before taking any measurements, the strain gauges were calibrated twice in all three directions by applying a known force. The calibrated system shows an approximate linear relation between strain and output voltage. During the forming process, strains transmitted from the sensor were first input into the NI USB-9237 (Bridge and Strain Measurement Module), which provides a USB interface for four channels of 24-bit half/full-bridge analog input, and then connected to the laptop computer in order to record the strain signals using NI LabVIEW software. Finally, the recorded strains were converted to 3-axis forces according to the calibration relation between forces and corresponding strains.

4.1 Influence of draw angle and tool path on forming forces

The influence of the part draw angle and the type of tool path on resultant forming forces was compared by forming truncated cones

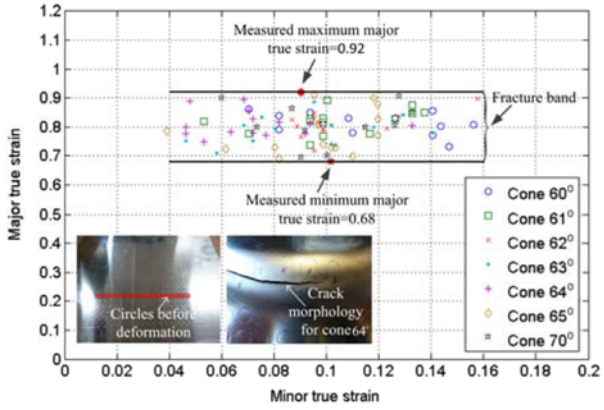

Fig. 13 Fracture forming limit diagram-experimental strains for truncated cones with different draw angles (z-level path with 0.2 mm step-over size) - The solid points correspond to maximum and minimum major true strains

with different draw angles (60°, 65° and 70°). AA7075-O sheet with 1.6 mm thickness was selected and the other experimental configuration is the same as described in the previous section. Fig. 15 shows the evolution of resultant forming forces with different draw angles for the spiral tool path. Different draw angles influence the formability. Only the truncated cone with the draw angle 60° was successfully formed. In this case, the trend of resultant force with forming time goes up first and then reaches a force peak and slightly decreases. After that the force increases again until the forming is finished. For the truncated cones with draw angles 65° and 70°, cracks happen before the forming goal is achieved. In these two cases, the resultant forces show the same trend as the case with the draw angle 60° in the initial stage (below 300 s). However, when the cracks appear, the forces drop down quickly. The crack for the draw angle 70° case happens earlier than the case with the draw angle 65°. In addition, as the draw angle increases, the peak force also increases in the initial stage.

Fig. 16 represents the evolution of resultant forming forces with different draw angles for the z-level tool path. Overall, the trend of resultant forming forces in Fig. 16 is quite similar to the force trend in Fig. 15. However, the maximum resultant forces in Fig. 16 are higher than those in Fig. 15 in the case with the same draw angle. In addition, the oscillation of the forces in Fig. 16 is more severe than the situations in Fig. 15. The reason is that the z-level tool path is not a continuous tool path. Large force peaks will occur at the transition points between two consecutive contours. Conversely, the spiral tool path is a continuous one and no transition points are involved, so the force evolution is smoother.

A geometry that is about to fail will experience an obvious force peak followed by a drop trend in force magnitude and then will develop fractures before achieving a minimum force level and slowly increasing again.[14] Therefore, the slope of the force curve after the peak value may be seen as a forming failure prediction indicator. Some results have been obtained for AA3003-O sheets with the 1.2 mm thickness.[14] In this study, the similar results have also been observed in terms of force slopes after peak values when using both spiral path and z-level path, seen in Figs. 15 and 16. Fig. 17 shows the calculated results of slopes for force curves after peak values for 1.6 mm thick AA7075-O sheets. It is noted that the slope decreases as the draw angle increases, which is in agreement with the previous results[14] regardless of the types of the tool paths.

4.2 Influence of sheet thickness and step-down size of z-level tool path on forming forces

In this section, the influence of the sheet thickness and the step-down size of z-level tool path on forming forces was compared by

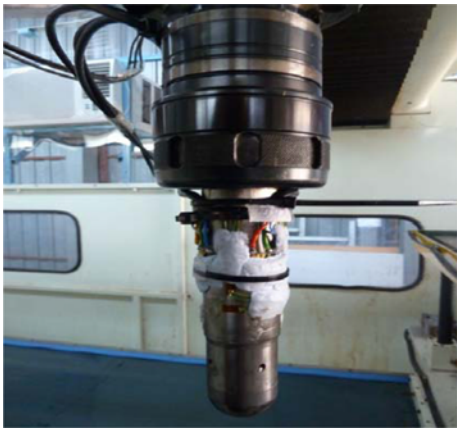

Fig. 14 Sensor for the force measurement

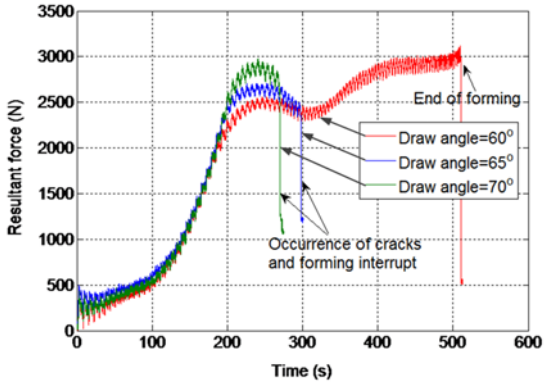

Fig 15 Influence of three different draw angles on resultant forces with 1.6 mm sheet thickness, spiral tool path with 0.5 mm step-over size and 15 mm tool radius for AA 7075-O sheets (Cracks happen in the cases with draw angles 65° and 70°)

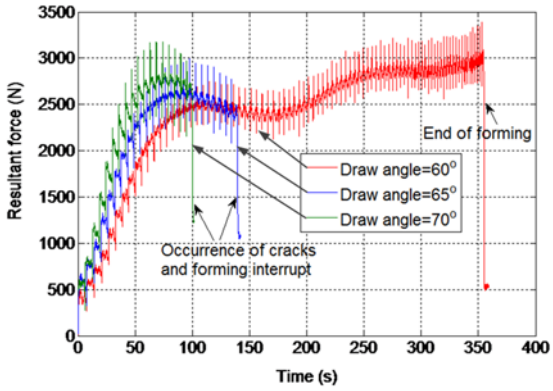

Fig. 16 Influence of three different draw angles on resultant forces with 1.6 mm sheet thickness, z-level tool path with 0.5 mm step-over size and 15 mm tool radius for AA 7075-O sheets (Cracks happen in the cases with draw angles 65° and 70°)

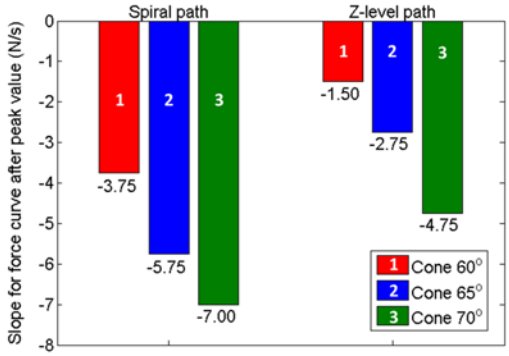

Fig. 17 Slopes for force curves after force peak values for both spiral and z-level tool paths

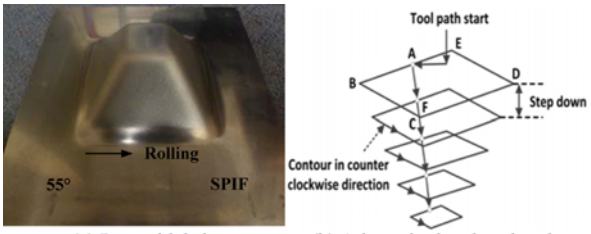

(a) Pyramidal shape (b) Adopted z-level tool path

Fig. 18 Investigated benchmark shape and z-level tool path: (a) pyramidal shape (b) z-level tool path

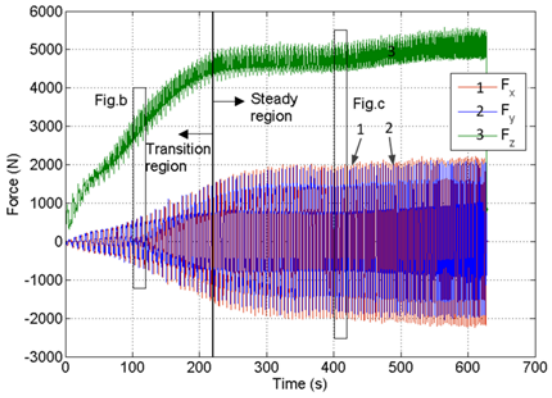

(a) The whole forming process with three-axis forces

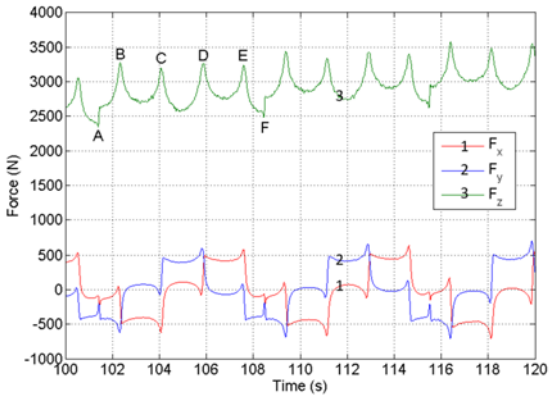

(b) One typical lap within a small time period in transition region

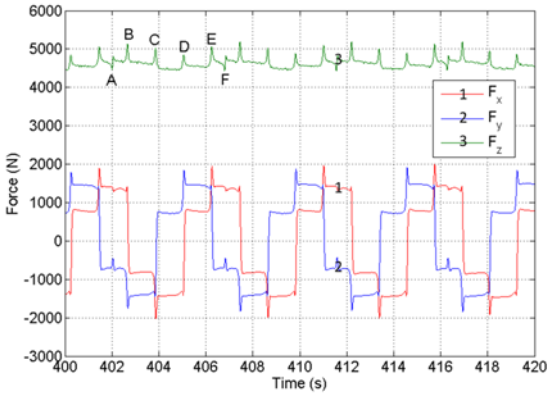

(c) One typical lap within a small time period in the steady region

Fig. 19 Three-axis forces for the truncated pyramid of draw angle 55° with 2.54 mm sheet thickness, z-level tool path with 0.5 mm step-down size and 15 mm tool radius for AA 7075-O sheets: (a) the whole forming process (b) one small time period with one typical lap in transition region (c) one small time period with one typical lap in steady region

forming pyramids using nine combinations of three sheet thicknesses (1.02 mm, 1.60 mm and 2.54 mm) and three step-down sizes (0.5 mm, 1.0 mm and 1.5 mm). Those pyramids, as shown in Fig. 18a, had a constant draw angle of 55° and a major base area of 140 mm×140 mm. The size of sheet metal is 300 mm×300 mm and a square backing plate is utilized to increase rigidity between forming area and undeformed area. Other experimental parameters are the same as described in the previous sections. The tool movement can be described corresponding to points A-F shown in Fig. 18b. Firstly, the tool moves in the vertical direction with the desired pitch. Then, it moves along square path in the same direction. Once this square movement is finished, the tool moves and penetrates the sheet along the part surface and begins the next square movement.

Fig. 19(a) shows a time evolution of three-axial forces for a truncated pyramid of draw angle 55° with 2.54 mm sheet thickness and 0.5 mm step-down size. In all nine experiments, the shape of these curves is quite similar. So, the analysis is only focused on one case. The three-axial forces increase over the first initial period (approximate 220 s) and then the vertical force stabilizes to a relatively steady state. For x-axial and y-axial forces, they evolve in a periodic way but with almost the same amplitude. Fig. 19(b) shows a typical lap within a small time period in the transition region. As can be seen, points B, C, D and E are corresponding to four corners of the pyramid illustrated in Fig. 18(b). In the typical lap, four peaks of the vertical force can be observed corresponding to the four corners B, C, D and E. The trend of three-axis forming forces in the steady region in Fig. 19(c) is quite similar to that in the transition region.

In order to compare all nine experiments, the maximum vertical forming force was plotted against the sheet thickness and the step-down size for each of the nine experiments on AA7075-O sheets in Fig. 20. Fig. 20(a) shows that the maximum vertical forming force increases in an approximately linear way with the sheet thickness. It also shows that the maximum vertical forming force increases as the step-down size increases. Fig. 20(b) represents the magnitude comparison of the maximum vertical forces in nine experiments. In these nine experiments, the biggest maximum vertical force is 6792.4 N with 2.54 mm thickness and 1.5 mm step-down size, which is a little more than twice that of the maximum vertical force (3038.8 N) in the case with 1.02 mm thickness and 1.5 mm step-down size. The similar trends can be also found in other cases. The explanation for this phenomenon would be that more deformation energy is required to deform thicker sheets. In addition, with bigger step-down size, more material is deformed in one step and more deformation energy is needed as well.

4.3 Influence of sheet orientation on vertical forming forces

In this section, emphasis is laid on the influence of sheet orientation on vertical forming forces. The sheet was arranged at two orientations 0° and 45° by rotating the rolling direction when clamping the sheet. Fig. 21 shows the forming results with different sheet orientations.

Fig. 22 shows the vertical forming forces for sheet orientations 0° and 45° with 0.5 mm step-down size and 15 mm tool radius for three thicknesses. It is obvious that the vertical forces in the sheet orientation 45° are smaller than those in the sheet orientation 0° regardless of sheet thicknesses. This is due to the influence of different strain-hardening exponents in different orientations. The strain-hardening exponent is a

very significant parameter for sheet metal forming process.[17] The higher its value, the greater will be the resistance of the material and the greater the absorption of strain, but the more force will be required to deform the material. Based on the calculated strain-hardening exponents with three directions for three different sheet thicknesses, the strain-hardening exponents in diagonal directions are smaller than those in rolling and transverse directions. This illustrates the reason why vertical forces in sheet orientation 45° are found to be smaller than those in the sheet orientation 0°.

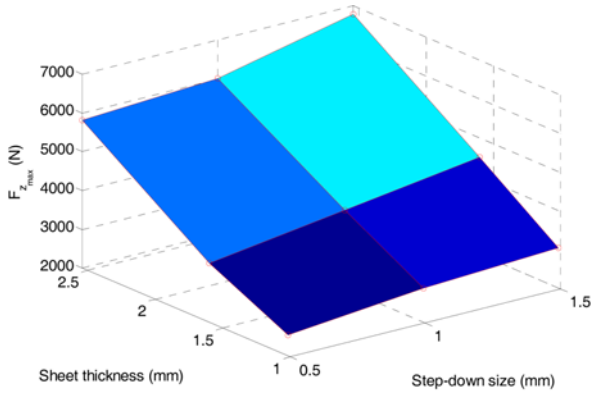

(a) The relationship of the sheet thickness and the step-down size with the maximum vertical forces

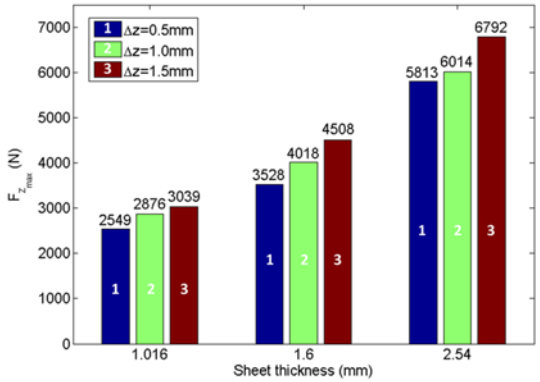

(b) The magnitude comparison of the maximum vertical forces in nine experiments

Fig. 20 The influence of sheet thickness and step-down size on vertical forming force of truncated pyramid with 55° draw angle in SPIF: (a) the relationship of sheet thickness and step-down size with maximum vertical forces (b) the comparison of the maximum vertical forces in nine experiments

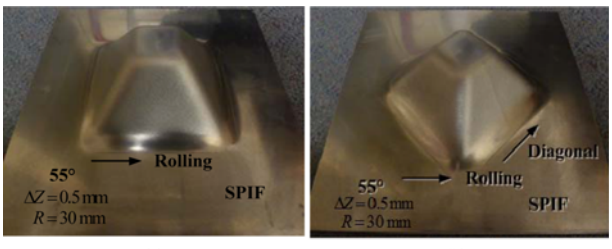

(a) (b)

Fig. 21 Forming results with different sheet orientations (a) 0 degree (b) 45 degree

5. Conclusions

In this study, an experimental campaign has been carried out to deform AA7075-O aluminum alloy sheets by incremental forming. Basic material properties have been acquired to clarify the material behavior using tensile tests. Formability and forming forces are evaluated to understand the forming process mechanism. Some conclusions can be drawn as follows:

(1) The phenomenon of anisotropy increases as the sheet thickness increases. The strain-hardening exponent in diagonal direction is smaller than that in rolling direction and transverse direction for all three thicknesses.

(2) In terms of formability, spiral and z-level tool paths have no significant difference when forming the same part. For the z-level tool path, formability can increase as step-over (or step-down) size increases (0.2 mm vs 0.5 mm). However, more tests involving a wide range of step-over (step-down) sizes need to be performed to further demonstrate this conclusion in the future.

(3) The maximum draw angle can be considered as a formability indicator, but other geometrical design parameters, such as the part height, also play a role on formability. A safety formability zone has been given for the truncated cone forming. Furthermore, a fracture forming limit diagram has been derived to characterize the material formability. A fracture band was obtained with maximum major true strain (0.92) and minimum major true strain (0.68).

(4) For spiral and z-level tool paths, the overall trend of resultant force is similar. However, the evolution force curve for the spiral tool path is smoother than that for the z-level tool path. In addition, the slope of force curve after peak value can be seen as a forming failure prediction indicator. The slope decreases as the draw angle increases. This provides an approach to on-line control and failure detection of incremental forming.

(5) The maximum vertical force increases as the step-down size increases. In addition, the maximum vertical force increases in an approximately linear way with the increase in the sheet thickness. This is expected due to greater deformation forces. The measured biggest vertical force is 6792.4 N with 2.54 mm sheet thickness and 1.5 mm step-down size.

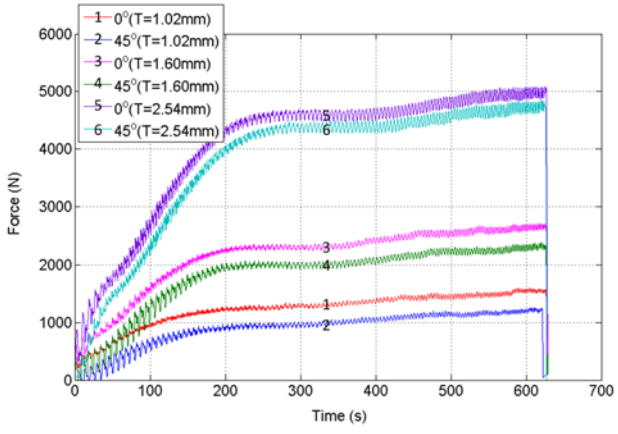

Fig. 22 Vertical forming forces for two sheet orientations (0 degree and 45 degree) with 0.5 mm step-down size and 15 mm tool radius for AA 7075-O sheet (T = thickness)

(6) The influence of sheet orientations on the forming force is first considered in incremental forming. Results have shown that the vertical force is found to be smaller in the sheet orientation 45° compared with that in the sheet orientation 0° due to the smaller strain-hardening exponents in diagonal directions.

This study provides a further insight into how to successfully deform 7075-O aluminum sheets into a 3D shell product by ISF. The process formability is not only affected by geometrical parameters (draw angle and part height), but also by different tool paths and incremental step-down sizes. In addition, forming force, as a process quantity, can be monitored to develop a closed-loop on-line control and failure detection system for product quality improvement. Vertical forming forces can be noticeably reduced when forming a part along the sheet diagonal direction due to the smaller strain-hardening exponent.

ACKNOWLEDGEMENT

This research was supported by the ARC Linkage Program, Boeing Research and Technology Australia and QMI Solutions in Australia. The authors are specifically grateful for the insights and assistance from Michael Elford BRTA and Sara Eastwood QMI.

REFERENCES

1. Tajally, M. and Emadoddin, E., "Mechanical and anisotropic behaviours of 7075 aluminum alloy sheets," Materials and Design, Vol. 32, No. 3, pp. 1594-1599, 2011.
2. Molladavoudi, H. R. and Djavanroodi, F., "Experimental study of thickness reduction effects on mechanical properties and spinning accuracy of aluminum 7075-O, during flow forming," International Journal of Advanced Manufacturing Technology, Vol. 52, No. 9-12, pp. 949-957, 2011.
3. Rikhtegar, F. and Ketabchi, M., "Investigation of mechanical properties of 7075 Al alloy formed by forward thixoextrusion process," Materials and Design, Vol. 31, No. 8, pp. 3943-3948, 2010.
4. Kitazawa, K., Wakabayashi, A., and Murata, K., "Metal flow phenomena in computerized numerically controlled incremental stretch-expanding of aluminum sheets," Japanese Journal of Institute of Light Metals, Vol. 46, No. 2, pp. 65-70, 1996.
5. Liu, Z. B., Li, Y. L., and Meehan, P. A., "Vertical wall formation and material flow control for incremental sheet forming by revisiting multistage deformation path strategies," Materials and Manufacturing Processes, Vol. 28, No. 5, pp. 562-571, 2013.
6. Manco, L., Filice, L., and Ambrogio, G., "Analysis of the thickness distribution varying tool trajectory in single-point incremental forming," Proc. of the Institution of Mechanical Engineers Part B: Journal of Engineering Manufacture, Vol. 225, No. 3, pp. 348-356, 2011.
7. Centeno, G., Silva, M. B., Cristino, V. A. M., Vallellano, C., and Martins, P. A. F., "Hole-flanging by incremental sheet forming," International Journal of Machine Tools and Manufacture, Vol. 59, pp. 46-54, 2012.
8. Dejardin, S., Thibaud, S., Gelin, J. C., and Michel, G., "Experimental investigations and numerical analysis for improving knowledge of incremental sheet forming process for sheet metal parts," Journal of Materials Processing Technology, Vol. 210, No. 2, pp. 363-369, 2010.
9. Jeswiet, J., Micari, F., Hirt, G., Bramley, A., Duflou, J., and Allwood, J., "Asymmetric single point incremental forming of sheet metal," CIRP Annals - Manufacturing Technology, Vol. 54, No. 2, pp. 88-114, 2005.
10. Emmens, W. C., Sebastiani, G., and Van den Boogaard, A. H., "The technology of Incremental Sheet Forming-A brief review of the history," Journal of Materials Processing Technology, Vol. 210, No. 8, pp. 981-997, 2010.
11. Filice, L., Fratini, L., and Micari, F., "Analysis of material formability in incremental forming," CIRP Annals- Manufacturing Technology, Vol. 51, No. 1, pp. 199-202, 2002.
12. Young, D. and Jeswiet, J., "Forming limit diagrams for single point incremental forming of aluminum sheet," Proc. of the Institution of Mechanical Engineers Part B: Journal of Engineering Manufacture, Vol. 219, No. 4, pp. 359-364, 2005.
13. Durante, M., Formisano, A., and Langella, A., "Observations on the influence of tool-sheet contact conditions on an incremental forming process," Journal of Materials Engineering and Performance, Vol. 20, No. 6, pp. 941-946, 2011.
14. Duflou, J. R., Tunçkol, Y., Szekeres, A., and Vanherck, P., "Experimental study on force measurements for single point incremental forming," Journal of Materials Processing Technology, Vol. 189, No. 1-3, pp. 65-72, 2007.
15. Jackson, K. P., Allwood, J. M., and Landert, M., "Incremental forming of sandwich panels," Journal of Materials Processing Technology, Vol. 204, No. 1-3, pp. 290-303, 2008.
16. Jeswiet, J., Duflou, J. R., and Szekeres, A., "Forces in single point and two point incremental forming," Advanced Materials Research, Vol. 6-8, pp. 449-456, 2005.
17. Folle, L. F., Netto, S. E. S., and Schaeffer, L., "Analysis of the manufacturing process of beverage cans using aluminum alloy," Journal of Materials Processing Technology, Vol. 205, No. 1-3, pp. 347-352, 2008.

4.3 The Papers

Paper 7

Investigation and optimisation of energy consumption and geometric accuracy in the incremental sheet forming process using response surface methodology

Li, Y.L., Lu, H.B., William J.T. Daniel and Meehan, P. A.

The International Journal of Advanced Manufacturing Technology

2015, DOI: 10.1007/s00170-015-6986-5.

Int J Adv Manuf Technol
DOI 10.1007/s00170-015-6986-5

ORIGINAL ARTICLE

Investigation and optimization of deformation energy and geometric accuracy in the incremental sheet forming process using response surface methodology

Yanle Li · Haibo Lu · William J. T. Daniel · Paul A. Meehan

Received: 20 January 2015 / Accepted: 2 March 2015

Abstract Incremental sheet forming (ISF) is a promising manufacturing process that features benefits of reduced forming forces, enhanced formability and greater process flexibility. It also has a great potential to achieve economic payoff for rapid prototyping applications and for small quantity production in various applications. However, limited research has been conducted from the sustainability point of view, particularly for energy consumption. More consumed energy will generate more heat and affect tool and product wear. Also, geometric accuracy is still one of the dominant limits for the further development and commercialization of the ISF technology. Therefore, the aim of this study is to investigate how different process parameters affect the consumed energy during the forming process and also find the optimal working condition for lower deformation energy with higher geometric accuracy. A Box-Behnken design of 27 tests for pyramid-forming processes have been performed for a multi-objective optimisation that considers four factors: step down, sheet thickness, tool diameter and wall angle at three levels. The deformation energy during the forming process was calculated based on the measured forming forces. It was found that the deformation energy heavily depends on the sheet thickness because of higher plastic energy required to deform the material. Increasing step-down size within a limited range or decreasing the wall angle is also an effective approach to reduce the deformation energy. Moreover, the effects of various process parameters on the global geometric accuracy have also been investigated. The geometric error has been empirically predicted by quadratic equations giving the influence of the most influential forming parameters. It was concluded that the geometric quality is largely determined by the quadratic effect of wall angle, the linear effect of sheet thickness and the interaction effect of thickness and step down. Finally, the optimal working conditions for both independent and simultaneous minimisation of deformation energy and geometric error during the pyramid-forming process are provided.

Keywords Incremental sheet forming · Box-Behnken design · Response surface methodology · Energy consumption · Geometric accuracy · Optimisation

1 Introduction

In recent years, environmental and sustainability concerns for metal forming processes have brought considerable attention in the academic world. As for the incremental sheet forming (ISF) process, particular interest has focussed on the investigation of the forming efficiency and energy consumption under various process parameters and different machine facilities. ISF technology is an emerging sheet forming process ideal for rapid prototype and small batch production. In the process, a flat metal sheet is gradually formed into the designed 3D shape using computer numerical control (CNC)-controlled generic forming tool. The process is characterized by the fact that at any time, only a small part of the product is formed and the local deformation area moves over the sheet until the desired shape is achieved. By using this process, useable parts can be formed directly from computer-aided design (CAD) data without the use of specialized tooling. Therefore, ISF is widely accepted as a promising forming

Y. Li (✉) · H. Lu · W. J. T. Daniel · P. A. Meehan
School of Mechanical & Mining Engineering, The University of Queensland, St Lucia, Brisbane, QLD 4072, Australia
e-mail: yanle.li@uq.edu.au

Published online: 14 March 2015

process over conventional processes such as deep drawing and stamping for small batch production and custom manufactured products [1, 2].

1.1 Energy consumption

Duflou et al. [3] provided a systematic overview of the energy and resource efficiency improvement methods in the domain of discrete part manufacturing. In terms of the ISF process, three strategies were concluded to reduce the energy usage and improve resource efficiency: (a) redesign of machine tools and selective control, (b) allocating the machine tool at its nominal capacity level and (c) optimising the process parameter settings. Dittrich et al. [4] proposed the concept of exergy analysis (the maximum useful work that can be obtained from a system at a given state in a given environment) in the ISF process and concluded that the exergy of the sheet material contributed a significant fraction to the total exergy input. Also, compared with conventional forming and hydroforming processes, ISF is advantageous for prototyping and small production runs up to 300 parts from an environmental point of view. Branker et al. [5] firstly analysed the cost, energy and carbon dioxide emissions in a single point incremental forming (SPIF) process for manufacturing a custom-designed aluminium hat. By doubling the feed rate and step-down size, as well as using an eco-benign lubricant, it was found that the cost and energy used during the process without labour reduced from $4.48 to $4.10 and 4580 to 1420 kJ, respectively.

Ingarao et al. [6] analysed the energy consumption during both the traditional stamping and the ISF process based on the measured forming forces. The focus was to investigate both the efficient use of materials and process energy saving. It should be noted that the energy consumption was calculated from the recorded forces in all three orthogonal directions multiplied by the corresponding travel distance of the forming tool in that direction. One conclusion has been drawn that the required deformation energy in the ISF process is always higher than that for stamping for all the considered cases, although the ISF process allows a certain material saving. Also, it is suggested that the energy reduction could be obtained through varying the material type, part shape as well as thickness. The empirical evidence presented in this paper provides useful comparison guidelines for materials saving and energy consumption but the optimal solution is not discussed. Recently, Ingarao et al. [7] comprehensively analysed and compared the electric energy consumption of the ISF process by using three different machines: a CNC milling machine, a six-axis robot as well as the dedicated AMINO machine tool. Working cycle time and power studies were conducted for all three setups. In terms of the effect of material type of the workpiece, no difference in power demand was observed for CNC milling machine but the six-axis robot was proved to be sensitive to the material type. The AMINO setup is the most efficient machine tool in terms of instantaneous power but requires higher total electric energy due to the lower forming speed compared with the six-axis robot. As far as the process parameters are regarded, the strategy to reduce the forming time by increasing feed rate and step-size within the admissible range was recommended as the most effective approach to reduce the energy consumption. In addition, the authors also presented a parametric model to predict the energy consumption for the robot-based ISF operations by simply considering the ultimate tensile strength of the material and the processing time. It should be noted that this model highly depends on the predicting accuracy of the steady vertical force from previous work [8].

Ambrogio et al. [9] compared the power consumption of the SPIF process with two setups: a CNC milling machine and a CNC turning machine. A constant power trend was recorded during the forming step for all the tests due to the fact that loads required to deform the material are much lower than the ones required for the normal operation of machining. It is suggested that the forming time is the dominant factor for energy consumption in the SPIF process. Using the same setup, by reducing the forming time from 144 to 12 s, the energy consumption can be effectively reduced from 838 to 103 kJ. Also, a proper selection and use of machine setup could lead to further saving of energy consumption. Bagudanch et al. [10] studied the effect of process parameters on the energy consumption in the ISF process. A series of experiments were conducted by considering sheet material, step down as well as the tool rotation speed while keeping feed rate as constant. Interestingly, it was concluded that the variation of tool rotation speed is the most significant parameter, followed by the material of the workpiece and incremental step size. It is explained that the lower rotation speed greatly reduced the friction between the sheet and the tool and also decreased the processing time since the rotation has to be stopped when the tool descends to the next contour for the machine setup. Unfortunately, the investigated process parameters were only varied at two levels which should be further extended to provide more comprehensive conclusions.

1.2 Geometric accuracy

Presently, the geometric accuracy for ISF products is still one of the biggest challenges for both academic researchers and industrial users. Allwood et al. [11] reported that the specification of geometric accuracy from industrial users for metal sheet components are typically within ±0.2 mm over the whole surface of a part, while the geometric error for ISF currently only achieved around ±3 mm. They [12] also summarized the geometric accuracy in the ISF process into three definitions, i.e. (a) clamped accuracy, (b) unclamped accuracy

and (c) final accuracy. Research is mainly aimed at improving the clamped accuracy. Micari et al. [13] further categorized the shape accuracy of ISF into three different typologies as shown in Fig. 1: (a) sheet bending close to the major base of the part where plastic deformation starts, (b) sheet springback after the forming tool is lifted after forming and (c) pillow effect on the minor base of the product.

The effects of process parameters on geometric accuracy have been investigated through both numerical modelling and experimental methodology. Essa and Hartley [14] found that the sheet bending near the initial tool contact location can be minimised by the backing plate; the springback can be reduced by the kinematic tool; and the pillow effect can be eliminated by extending the tool path across the base of the sheet. Guzmán et al. [15] simulated a two-slope SPIF pyramid with two different depths using the FEM to investigate the geometric deviation at the slope transition zone. It is concluded that elastic strains due to structural elastic bending were the main causes of the shape deviations. The localized springback has only minor contribution because no plastic deformation is observed in the angle transition zone.

Ambrogio et al. [16] statistically analysed the effects of process parameters of tool diameter, depth step, wall angle, final product depth and the sheet thickness on geometric accuracy of the formed truncated cone. It was suggested that the geometric error measured at the corner was largely influenced by sheet thickness and total part depth. On the other hand, the pillow effect at the middle of the base was strongly affected by the tool diameter and product height. Ham [17] performed a Box-Behnken design with 46 experimental tests considering 5 factors (material type, sheet thickness, tool size, step size and formed shape) varied at 3 levels to study their effects on dimensional accuracy. It is observed that the geometric deviation at the bottom of the formed shape is small compared with the remaining area, and the overall geometric error for most of the parts is within 1 mm after a user-defined scale. However, only qualitative comparisons were provided based on several contour plots of geometric deviations in this study, and further qualitative investigation is required.

The above literature suggests that the total energy consumption in an ISF process includes machine standby energy, positioning energy and deformation energy. The machine standby energy and positioning energy highly depend on the type of machine used for the process and have no direct relation with the process parameters. The deformation energy is directly related to the heat generation and also wear to the tool and the formed material. Therefore, deformation energy is focused on for investigation in the present work. Although substantial research work has been conducted on the clamped accuracy, the degradation in unclamped and final accuracy due to residual stresses in the sheet has had very little attention in the literature. Therefore, the effects of process parameters on the unclamped accuracy should be further investigated. Additionally, there is still a lack of comprehensive research on the simultaneous optimization of energy consumption together with other process quality outputs such as geometric accuracy taking into account the effects of the most relevant process parameters. Based on the extensive review of the current status of ISF, the aims of the present work are set as follows:

- To perform a series of systematic tests using response surface methodology (RSM) with Box-Behnken design to study the effects of the most relevant process parameters (step down, sheet thickness, tool diameter and wall angle) on both deformation energy and geometric accuracy by forming the shape of truncated pyramid.
- To develop empirical models for predicting consumed energy and geometric error individually using response surface methodology based on the experimental results obtained. The effect of each factor on these two responses will be analysed in detail.
- To optimise the deformation energy and geometric error independently and simultaneously using the desirability function. The optimal working conditions for these optimisations will be provided.

2 Methodology

The details of experimental facilities, determination of deformation energy and geometric error and the experimental design procedure adopted for the study are described in this section.

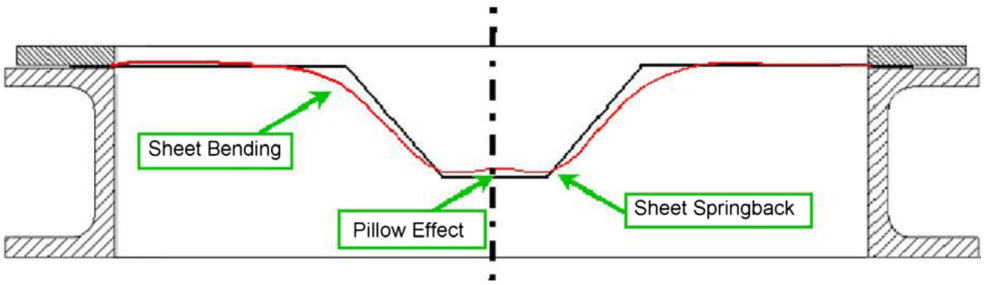

Fig. 1 Geometrical errors during the SPIF process [13]

2.1 Experimental setup

The forming tests were performed on a state-of-the-art AMINO machine dedicated for the ISF process as shown in Fig. 2. The machine allows mould-based forming for a maximum size of 2100 mm×1450 mm×550 mm with a FANUC controller for precise control. The movement of the two horizontal axes (*X* and *Y*) can have a maximum speed of 60 m/min with a repeatability of ±0.05 mm. The vertical (*Z*) axis is driven by an AC servo motor with the power of 1 kW that allows a maximum acting force of 3 kN. Hemispherical tools with the diameters of 10, 20 and 30 mm were used to deform the material. The tip of each tool is tungsten carbide and the body is made of K110 steel which was hardened and tempered to HRC60. The forming tool was set not to rotate in this study for all the tests. The material used in the present study was aluminium alloy 7075-O sheets with three different thicknesses which were cut into 300 mm×300 mm-sized samples.

The geometry of a truncated pyramid was selected as the targeted shape to facilitate the calculation of consumed energy and evaluation of geometric accuracy. The four investigated process parameters are step down, sheet thickness, tool diameter and wall angle. The definition of these parameters and the configuration of the forming process are illustrated in Fig. 3. The vertical distance between each neighbouring contour is defined as step down, and the angle between the deformed sheets to the horizontal plane is defined as wall angle. Before forming, the sheet was clamped on the frame with 12 evenly distributed blank holders. During the forming process, the forming tool was numerically controlled by a FANUC controller which follows the previously designed tool path. The contact between forming tool and metal sheet was lubricated by Shell Tellus Oil 68 to reduce friction and avoid excessive wear of the tool surface.

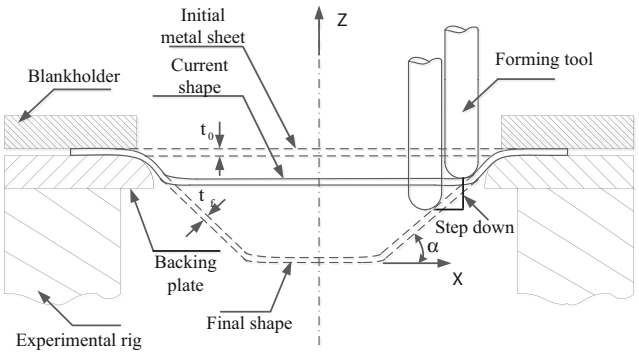

Fig. 3 Sketch of ISF experimental configuration and associated parameters [18]

2.2 Calculation of deformation energy

The deformation energy was calculated based on the measured force components [6]. It should be noted that the deformation energy investigated in the present study is only the theoretical one that is different from the actual electric energy consumed by the machine. Although the deformation energy is only part of the total electric energy, it is directly related to the change of process parameters. Therefore, the study of deformation energy is critically helpful for the understanding of the actual deformation behaviour of the material under different process conditions during the forming process. The total deformation energy is constituted by three components E_x, E_y and E_z corresponding to three orthogonal forming forces *Fx*, *Fy* and *Fz*, respectively. As shown in Fig. 2b, a multiple-axis force sensor K6D175-50 was used to measure the forces between the tool and workpiece during the forming process. The force sensor was manufactured by ME-Meßsysteme GmbH which allows measurement of the three orthogonal forces and three torque components at the same time. To alleviate the possible deflection from other structures, the force sensor

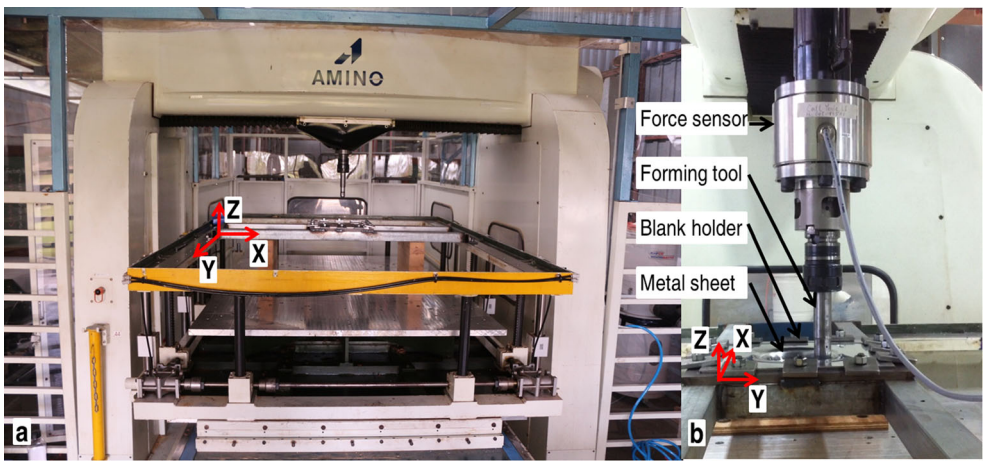

Fig. 2 The AMINO incremental forming machine and the implemented force sensor: **a** front view; **b** detailed side view

was mounted directly between the spindle and the tool holder. The six-channel output signals were recorded with two NI 9237 data loggers and post-processed with the LabVIEW SignalExpress software.

Figure 4 presents typical measured force components for a pyramid-forming process. It is noted that, during the *i*th contour, forming forces during forming of the four straight sides are steady and with only sudden peaks at corners (as marked in Fig. 4). Therefore, the work done by two horizontal force components can be estimated by the average force at each contour multiplied by the travel distance at the corresponding direction of the forming tool. For the vertical component, the energy is only produced when the tool increments to the next contour. As a result, the deformation energy at the *i*th contour can be calculated as follows:

$$E_i = 2F_{xi} \cdot f \cdot t_{xi} + 2F_{yi} \cdot f \cdot t_{yi} + F_{zi}\Delta z, \quad (1)$$

where f is the feed rate of the forming tool, t_{xi} and t_{yi} are the forming time in x and y directions at the ith contour and Δz is the step-down size. Then the total energy to the nth contour can be obtained as follows:

$$E_{total} = \sum_{i=0}^{n} E_i, \quad (2)$$

where n is determined by the formed depth H and step-down size as $H/\Delta z$.

2.3 Measurement of geometric error

To evaluate the geometric accuracy, the 3D geometry of formed parts in an unclamped condition was measured using a noncontact 3D digitiser (VIVID 9i), as shown in Fig. 5. The scanning accuracy is within ±50 μm, which was used in the literature for geometric accuracy previously [19]. GEOMAGIC Qualify was used to process the 3D geometry data from the scanned shape and analyse the dimensional error between deformed test parts and designed CAD models. Specifically, both produced and designed profiles were represented in large sets of points in the same Cartesian coordinate system. In this work, the shape of truncated pyramid is selected as the target shape, and the four investigated process parameters of step down, sheet thickness, tool diameter and wall angle are presented in Fig. 3. The cross-sectional profile through the pyramid centre and perpendicular to the edges was used to evaluate the geometric accuracy. The deviation in vertical direction (Z) between the designed and fabricated profiles as shown in Fig. 9 was calculated as the global geometric error for subsequent investigation. Before scanning, the surface of the parts needs to be sprayed with white powder to avoid light refection as shown in the marked sample in Fig. 6.

2.4 Response surface methodology with Box-Behnken design

Response surface methodology (RSM) was employed in the present work to model and optimise the effects of four independent variables on deformation energy and geometric error during the ISF forming process. RSM is an empirical modelling technique that can help to investigate the interactive effects of process variables and to build a

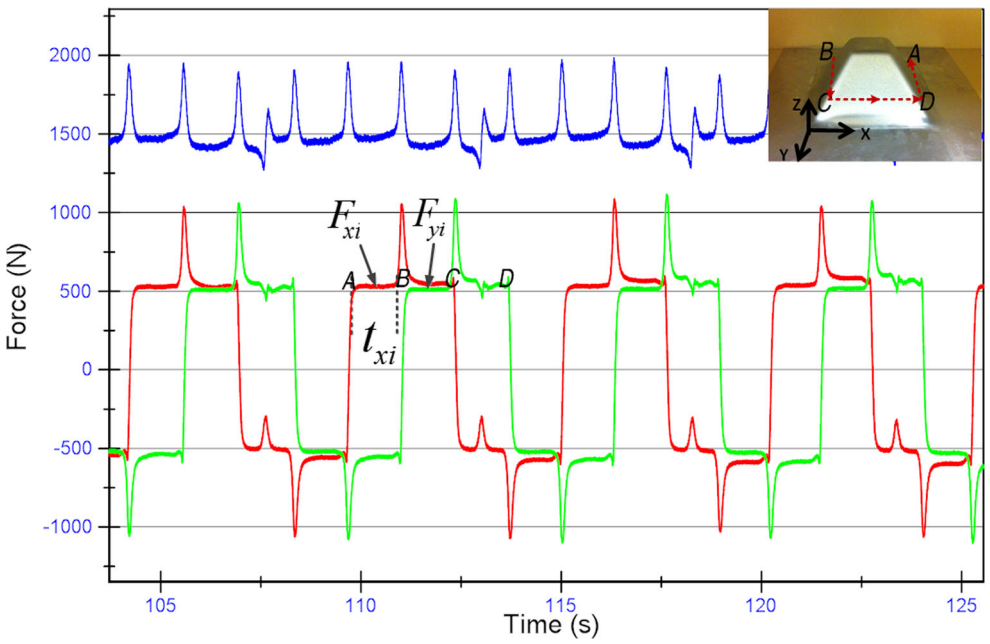

Fig. 4 Typical force components during the pyramid-forming process

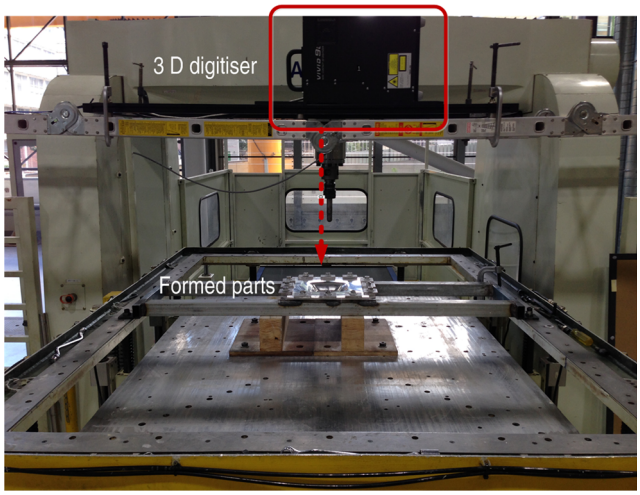

Fig. 5 Set-up of the 3D digitiser

mathematical model that accurately describes the overall process [20]. This optimisation process involves three major steps: (i) performing statistically designed experiments, (ii) estimating the coefficients in a mathematical model and (iii) predicting the response and checking the adequacy of the model [21]. The most common and efficient design used in response surface modelling is the Box-Behnken design. This design allows efficient estimation of the first- and second-order coefficients between the response and selected factors. Since Box-Behnken designs have fewer design points, they are less expensive to run than other designs with the same number of factors. This design was also proved to be feasible for ISF process by many researchers [17, 22, 23]. Hence, a Box-Behnken experimental design was conducted to evaluate the effects of process parameters on deformation energy and geometric accuracy. The steps in this research work for the experimental investigation include the following [24]:

Fig. 6 Truncated pyramids by incremental sheet forming

- Identifying the important process control variables. In this case, based on previous experimental work, four process parameters of step down, sheet thickness, tool diameter and wall angle were selected as the most relevant factors. Previous research has found that increasing the feed rate (forming speed) can effectively reduce the total energy [9] and has no considerable effect on the part quality regarding the formability and surface roughness [25]. To emphasize the effects of other factors, the feed rate has been set as constant at 4000 mm/min in the present study. Although sheet thickness and wall angle may not be changeable according to the manufacturing requirement, they directly influence the contact condition during the process so the investigation of these factors will benefit the understanding of the deformation mechanics in ISF.
- Finding the upper and lower limits of the control variables. Three levels of each factor were considered and their upper and lower values were set as listed in Table 1.
- Development of the design matrix using Box-Behnken design and conducting the corresponding experiments. A total of 27 experimental tests were designed using Minitab Version 16.2.4 in the presented study.

3 Results and discussion

This section first provides the experimental results of deformation energy and geometric error for each test according to the Box-Behnken design. Then, the effect of each factor on both energy and geometric error are discussed in detail followed by the optimisation of these two design responses during the pyramid-forming processes.

3.1 Design of experiments

The Box-Behnken design was applied using Minitab software based on the selected factors and values in Table 1. A design matrix with 27 experimental runs was generated as listed in Table 2. Experiments were conducted in sequence to mitigate the influence of non-considered factors. Due to the fact that parts with

Table 1 Process parameters and their levels

Symbols	Factors	Levels			Units
		−1	0	1	
A	Step down	0.5	1.0	2.0	mm
B	Sheet thickness	1.27	1.80	2.54	mm
C	Tool diameter	10	20	30	mm
D	Wall angle	50	60	70	degree

70° wall angle were not successfully formed to the designed depth of 65 mm, the deformation energy for forming until a depth of 24 mm was calculated and analysed for all the cases. In terms of the geometric accuracy, the successfully formed parts were compared with the designed shape, while the fractured parts were compared with the supposed intermediate shapes corresponding to the final formed tool path. Deformation energy and geometric error are the design responses and their calculated values for each test are presented in Table 2. Figure 6 shows the formed pyramid parts according to the Box-Behnken design matrix, with the last sample sprayed with white powder for geometric scanning.

3.2 Deformation energy

An empirical relationship between deformation energy and the four studied factors was obtained from the Box-Behnken design results. In the following analysis, factors are considered as their coded values as given in Table 1. This is because coding eliminates any spurious statistical results due to different measurement scales from factors (e.g. step down versus degrees). Additionally, using uncoded units often leads to co-linearity among the terms in the model. This inflates the variability in the coefficient estimates and makes them difficult to interpret. Consequently, the statistical equation for the relation between deformation energy and selected coded parameters was derived as follows:

$$E = 4205.32 - 1652.69A + 2018.26B - 568.51C + 701.54D + 1030.47A^2 + 624.27C^2 - 637.57AB - 269.23AC - 207.26AD + 338.38BD, \quad (3)$$

Table 2 Box-Behnken design for four factors and observed responses

Test run no.	Step down (mm)	Sheet thickness (mm)	Tool diameter (mm)	Wall angle (°)	Formed depth (designed) (mm)	Deformation energy (J)	Global geometric error (mm)
1	0.5	1.27	20	60	65	4273.85	2.749
2	2	1.27	20	60	65	2169.40	2.635
3	0.5	2.54	20	60	65	9801.50	4.137
4	2	2.54	20	60	65	5065.90	4.947
5	1	1.8	10	50	65	5099.50	2.204
6	1	1.8	30	50	65	3991.70	3.049
7	1	1.8	10	70	27	6286.40	1.620
8	1	1.8	30	70	31	5346.70	1.938
9	0.5	1.8	20	50	65	5574.40	2.818
10	2	1.8	20	50	65	2887.50	3.239
11	0.5	1.8	20	70	26	7414.20	1.218
12	2	1.8	20	70	30	3831.20	2.233
13	1	1.27	10	60	65	3550.60	2.639
14	1	2.54	10	60	33	8500.00	2.743
15	1	1.27	30	60	65	2904.50	2.676
16	1	2.54	30	60	65	7271.50	4.672
17	0.5	1.8	10	60	65	7225.80	2.860
18	2	1.8	10	60	65	4856.00	3.584
19	0.5	1.8	30	60	65	6799.60	3.187
20	2	1.8	30	60	65	3290.50	3.756
21	1	1.27	20	50	65	2503.10	2.491
22	1	2.54	20	50	65	5925.30	3.787
23	1	1.27	20	70	24	3435.00	2.391
24	1	2.54	20	70	33	8191.60	2.825
25	1	1.8	20	60	65	4492.20	3.699
26	1	1.8	20	60	65	4450.50	3.516
27	1	1.8	20	60	65	4569.70	3.7977

where variables A to D are defined in Table 1. The significance of the developed response function is examined from the following aspects. First, the analysis of variance (ANOVA) is adopted to evaluate the fitness of the established model and also the importance of factors to the response. Table 3 presents the results of ANOVA of the response function surface. The present analysis is carried out at a level of confidence of 95 %. Accordingly, if the *P* value is less than or equal to 0.05, then the effect of the corresponding factor on the response is considered significant. As shown in Table 3, with a probability *P* value less than 0.0001 for the established model, it is indicated that the developed second-order response function is sufficiently adequate. Second, the residuals versus their expected percentiles are plotted in Fig. 7 to examine if the distribution is normal. In this figure, the abscissa represents the residuals between the measured and predicted values and the ordinate stands for the percentage of the measurements that fall below the residuals. If the data is distributed normally, the plot of the residuals should be linear. Since the experimental results are approximately a straight line in Fig. 7, it is confirmed that the model is effective. Moreover, the value of predicted R^2 is used to measure the prediction ability of the developed model. In this analysis, a value of 0.996 of predicted R^2 suggests that the model can be reasonably used for future prediction.

According to the *P* values in Table 3 and coefficients in Eq. (3), all four parameters, especially the sheet thickness, are found to have significant linear effect on the energy consumed for forming the pyramids. Additionally, the quadratic effects of the step down (A^2) and tool diameter (C^2) are also compelling as well as two-level interaction effect of step down and thickness (*AB*). The response surface plots of deformation energy with different factors are presented in Fig. 8 to facilitate the investigation of their individual influences. In each sub-figure, the response is constructed by two experimental factors while holding the remaining two at the middle level. Since further examinations show that the response trends for holding at different levels are similar, it is reasonable to analyse the effect of each factor by the figures given below.

Table 3 Results of ANOVA for global deformation energy (from Minitab)

Source	SS	DOF	MS	*F* value	*P* value	Remarks
Model		14		265.91	<0.0001	Significant
A		1		1172.02	<0.0001	Significant
B		1		1590.61	<0.0001	Significant
C		1		121.84	<0.0001	Significant
D		1		185.53	<0.0001	Significant
A^2		1		157.56	<0.0001	Significant
B^2		1		1.3	0.277	
C^2		1		76.79	<0.0001	Significant
D^2		1		0.39	0.542	
AB		1		65.69	<0.0001	Significant
AC		1		11.5	0.005	Significant
AD		1		6.82	0.023	Significant
BC		1		3.12	0.103	
BD		1		17.23	0.001	Significant
CD		1		0.26	0.619	
Residual		12				
Lack of fit		10		8.68	0.108	
Total		26				

In Fig. 8, it can be seen that the deformation energy under different working conditions are varied over a large range from 2000 J to more than 9000 J, so the investigation of how different process factors affect the required energy is critical for the sustainable development of the ISF technology. The effect of sheet thickness (*B*) is analysed as the most significant factor associated with deformation energy during the pyramid-forming process. Figure 8a, d, e show the response surface of deformation energy with the variation of sheet thickness with step down, tool diameter and wall angle, respectively. All these figures have clearly confirmed that the required deformation energy increases with the increase of the sheet thickness. This is because thicker sheets require larger forming forces to achieve the same amount of plastic deformation. More specifically, the increase of deformation energy appears to be linearly proportional to the rise of the sheet thickness. This was confirmed by both experimental measurements and theoretical analysis. Previous experimental results [26] showed that the tangential forming force is linearly proportional to the sheet thickness in the forming of the truncated cone. Moreover, according to the calculation of plastic deformation power in [27], the power has a linear relation with the sheet thickness under both shear and stretching deformation modes. Therefore, when the shear and stretching deformation modes are dominant, it is reasonable to observe a linear response of deformation energy with varying sheet thickness.

The effect of wall angle on the deformation energy can be approximately treated as a linear effect based on the observation from Fig. 8c, e, f. Parts with larger wall angles require more energy to produce. However, due to the interaction effects of *AD* and *BD*, the slope of the response surface with the change of wall angle in these three conditions are varied, but the most evident cases occur with lower values of step down in Fig. 8c and thicker sheet thickness in Fig. 8e.

It is clearly illustrated from Fig. 8a to c that the increase of the step-down size (*A*) will result in a substantial reduction of deformation energy, which is evidenced in both Eq. (3) and *F* value in Table 3. Although the quadratic term of step down has a positive influence on the required energy, it is counteracted by a more significant negative effect from the linear term. This is explained by the fact that reduction of the number of forming contours

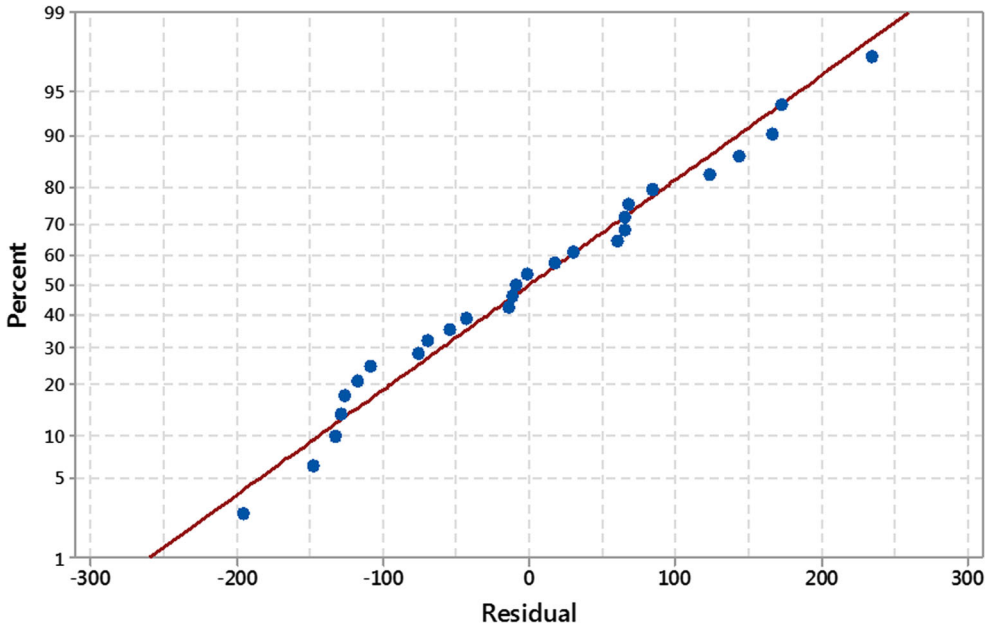

Fig. 7 Normal probability plot of the residuals for the response of deformation energy

also reduces the forming distance due to the increased step down, and leads to the decline of the deformation energy. The increased forming length is associated with the increased friction and heat dissipation. In terms of tool diameter, no obvious effect has been found on deformation energy since contributions from first-order, second-order and interaction effects may be counteracted among each other. Therefore, the optimum selection of tool size to minimise deformation energy depends on the values of other forming parameters.

3.3 Geometric accuracy

The formed components were scanned in the unclamped condition using a MINOLTA VIVID laser scanner, and their profiles were represented by a mass of point clouds. These profiles were then sectioned in the plane across the middle of the pyramid. For each test, the scanned profile was aligned with the designed shape at the outer undeformed region in the vertical direction. A comparison of the formed profile with the designed component shape is shown in Fig. 9.

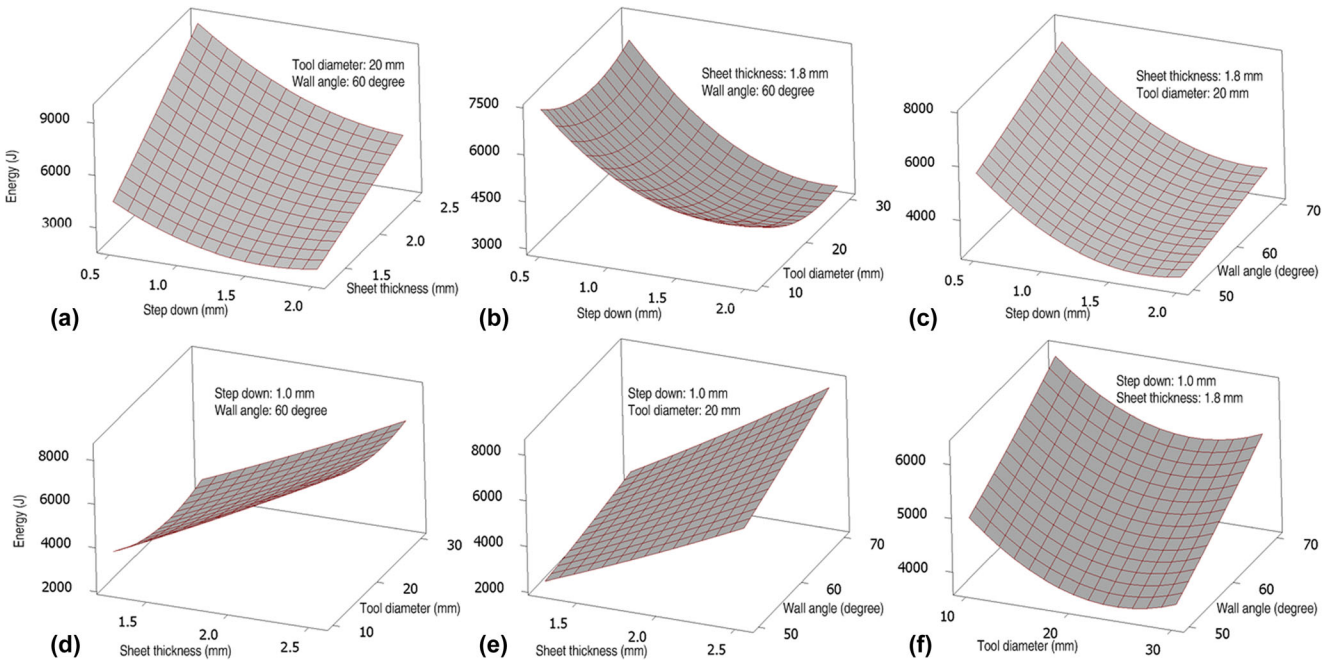

Fig. 8 Response surface plots of deformation energy by varying process parameters

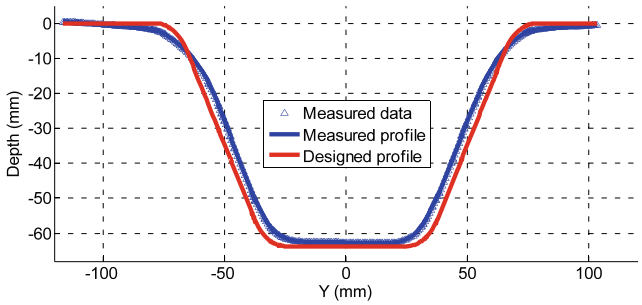

Fig. 9 Comparison between the measured and designed profiles

The global geometric error is defined by the average vertical deviation between the measured and designed profiles for all the points along the cross-section, and this global error is used for evaluating the geometric quality of the formed parts. In particular, the geometric error for the fractured parts (α=70°) is calculated as the vertical difference between the formed parts at the onset of material fracture to the intermediate shape corresponding the current tool path. It can be seen from Fig. 9 that although all the remaining regions were not formed to the targeted positions, the sheet was overformed at the transition area around the major diameter. The largest deviation was obtained at the side wall while good geometric accuracy was obtained for the bottom of the truncated pyramid.

A similar analysis procedure used for deformation energy was also performed. First, an empirical model described by a second-order response surface was obtained for the global geometric error,

$$\varepsilon_g = 3.671 + 0.285A + 0.627B + 0.302C - 0.447D - 0.403C^2 - 1.042D^2 + 0.473BC. \quad (4)$$

Table 4 presents the results of ANOVA for the response function surface and a probability P value less than 0.0001 indicates that the developed response function is adequate. Figure 10 shows a linear relation between the residuals and the percentage of the measurements that fall below these residuals, confirming that the experimental results are effective. Moreover, a value of 0.914 for predicted R^2 also suggests that the model can be reasonably used for future prediction.

According to the P value in Table 4 and the coefficients in Eq. (4), it can be seen that the quadratic effect of wall angle (D) is the most influential factor on the global error followed by the linear effect of sheet thickness (B), wall angle (D) and tool diameter (C) as well as step down (A). Furthermore, the interaction effect of sheet thickness and tool diameter (BC) also has considerable effect on global geometric error. To investigate the effect of each factor on the global geometric error in detail, response surfaces by varying the values of process parameters are plotted in Figs. 11 and 12. Overall, the

Table 4 Results of ANOVA for global geometric error (from Minitab)

Source	SS	DOF	MS	F value	P-value	Remarks
Model		14		9.11	<0.0001	Significant
A		1		6.99	0.021	Significant
B		1		33.77	<0.0001	Significant
C		1		7.84	0.016	Significant
D		1		17.13	0.001	Significant
A^2		1		0.37	0.556	
B^2		1		0.18	0.683	
C^2		1		6.19	0.029	Significant
D^2		1		41.40	<0.0001	Significant
AB		1		1.53	0.24	
AC		1		0.04	0.84	
AD		1		0.63	0.442	
BC		1		6.39	0.027	Significant
BD		1		1.33	0.272	
CD		1		0.50	0.495	
Residual		12				
Lack of fit		10		8.05		
Total		26				

geometric errors fall into the range from 1.5 to 4.5 mm for most of the cases.

As shown in Fig. 11, the response surfaces of global geometric error are constructed with sheet thickness and wall angle with different settings of step down and tool radius ranging from the lowest to highest levels. In all levels, the response of geometric error has the largest value when the pyramids with the wall angle of 60° are formed. By either reducing or increasing the wall angle, a better geometric accuracy can be achieved especially when the step down and tool radius are set as lower values as demonstrated in Fig. 11a. However, the following aspects need to be clarified in terms of the effect of wall angle. The difference of wall angles leads to the variation of the area ratio between the side wall and the bottom region of the formed parts. Considering that the average geometric error at the bottom region is smaller than that at the side wall, the calculation of the global error would be affected. Specifically, with larger wall angles, the side wall is steeper so the area ratio between bottom regions to side wall is increased under the same formed depth. Additionally, for the parts of 70° wall, sheets are not formed successfully to the designed depth of 65 mm but fracture earlier at a depth between 25 and 30 mm. This could also result in a higher area ratio between bottom region to side wall hence further reduce the geometric deviation due to the better geometric accuracy at the bottom region.

The sheet thickness also has a significant effect on the overall geometric accuracy. As shown in Fig. 11, greater global geometric accuracy can be attained with thinner sheets in

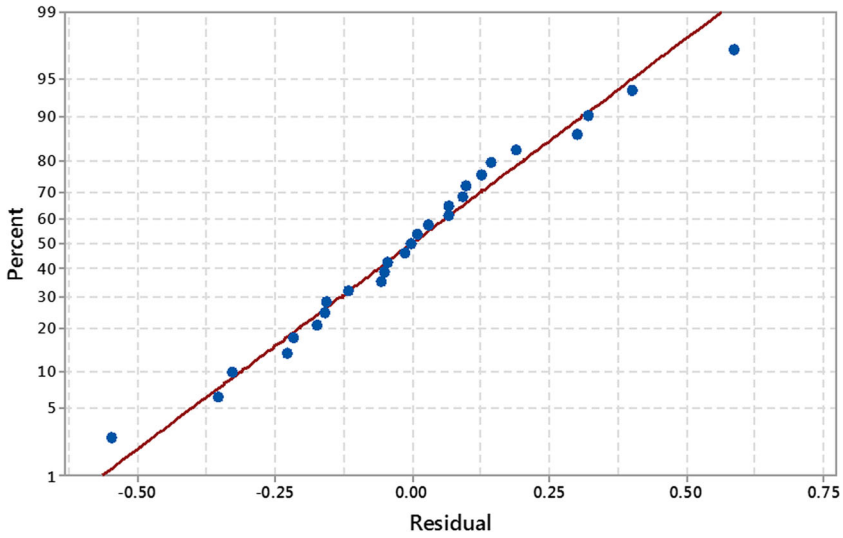

Fig. 10 Normal probability plot of the residuals for the response of global error

most of the conditions. This effect is evident especially when the step down and tool diameter were set as higher levels. This confirms the previous reported conclusion that the increase of the sheet thickness will result in higher geometric error at the bottom corner of the formed cone [16]. However, with small step-down value, small tool size but large wall angle (see Fig. 11a), increase of the thickness will contribute to a better geometric quality.

The selections of step down and tool diameter also have considerable effects on global geometric error according to *P* values in Table 4. Response surface plots with step down and tool diameter are presented in Fig. 12. For parts with thicker sheets and large wall angles, reducing the step-down size can be considered as an effective strategy to improve the geometric accuracy as also suggested in previous experimental work [19]. The reduced step-down size would result in a smaller transition zone between two adjacent contours which allows for a better control of the material deformation towards the targeted profile. However, the effect is not evident under smaller wall angle with thin sheets.

From Fig. 12, it can be seen that cases with medium step-down size and tool diameter tend to have poor geometric

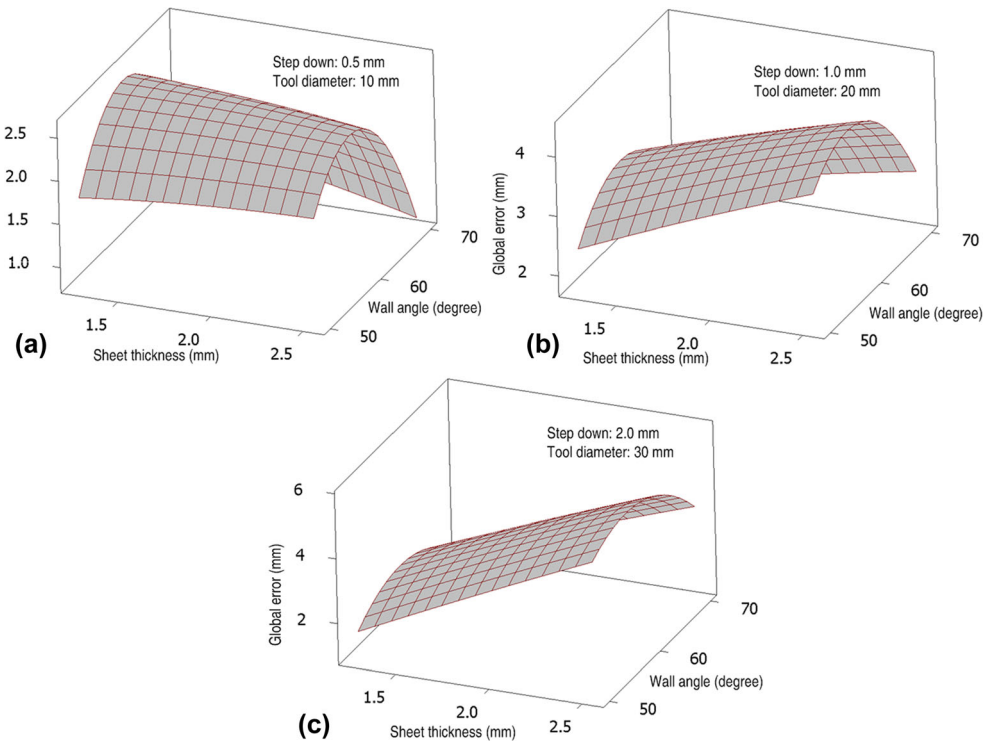

Fig. 11 Response surface plots of global geometric error in sheet thickness and wall angle

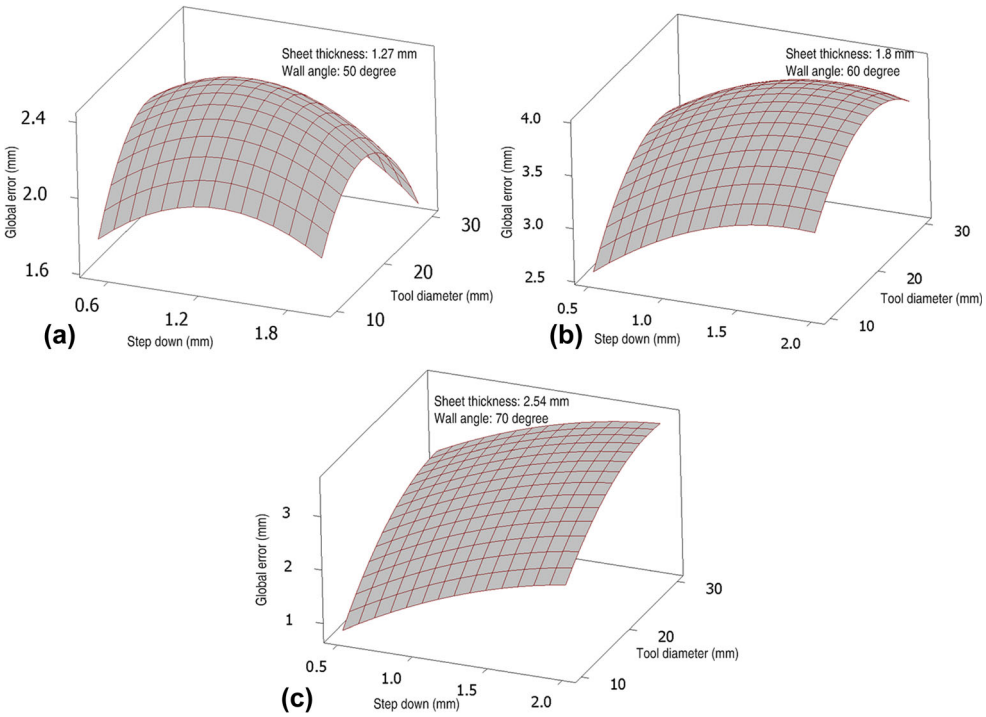

Fig. 12 Response surface plots of global geometric error in step down and tool diameter

accuracy. This was indicated in Eq. (4) by an extra quadratic term of tool diameter which leads to a non-linear effect on geometric error. Since the geometric error was measured under unclamped condition, the springback of the material plays a vital role in part inaccuracy after releasing forming load and boundary constraints. The membrane analysis by Silva etc. [28] suggested that the membrane stress is closely related with the ratio between thickness and tool radius. Due to the fact that the springback is caused by the release of residual stress, geometric accuracy is also affected by this ratio (as presented by the response surface from Fig. 12a to c). Furthermore, the interaction between thickness and tool diameter also has a non-ignorable effect as suggested by a low *P* value in Table 4. This is consistent with published work by Hussain et al. [29] that the ratio between tool diameter and sheet thickness has great influence on the ISF process in terms geometric accuracy and formability.

3.4 Optimisation

This section provides the optimisation results of both individual and simultaneous minimisation of deformation energy and geometric error during pyramid-forming processes. The desirability function in Minitab has been used to find the optimal setting. The desirability has a range of 0 to 1 and was used to evaluate how the settings optimise a response. First, an optimal setting condition for minimising the deformation energy was obtained. According to the range of the measured experimental results, the target value for the minimum deformation energy was set as 1000 J and the upper bound was set as 20, 000 J. Figure 13a presents the optimised condition for achieving minimum deformation energy. In this figure, the trend of the desirability with the changing of each parameter over its defined range is plotted in the first row. The second row illustrates the trend of the value of predicted deformation energy over the whole defined range for all four parameters. Since the purpose of this optimisation is to determine the lowest energy, a lower value of deformation energy corresponds to a higher value of desirability as presented in the figure. In particular, the values of the parameters for the optimal condition are indicated at the vertical lines and also presented within the square brackets. Accordingly, as shown in Fig. 13a, the optimal condition was determined as step down (1.59 mm), sheet thickness (1.27 mm), tool diameter (24.75 mm) and wall angle (50°), obtaining a minimum deformation energy of 1659 J. Similarly, with the setting of target value for geometric error at 0.1 mm and upper bound at 10 mm, the optimal condition was found to be (Fig. 13b) at a step down of 0.5 mm, sheet thickness of 2.54 mm, tool diameter of 10 mm and wall angle of 70°. Since all the parameters are set at their boundary values, it seems that only a local optimisation solution is obtained. The predicted minimum geometric error is 0.81 mm with a desirability of 0.931.

Finally, the optimal combination of process parameters for simultaneously minimisation of both deformation energy and geometric error has been studied by using the multi-response optimisation approach. In this approach, each of the response value is transformed using a specific desirability function. The

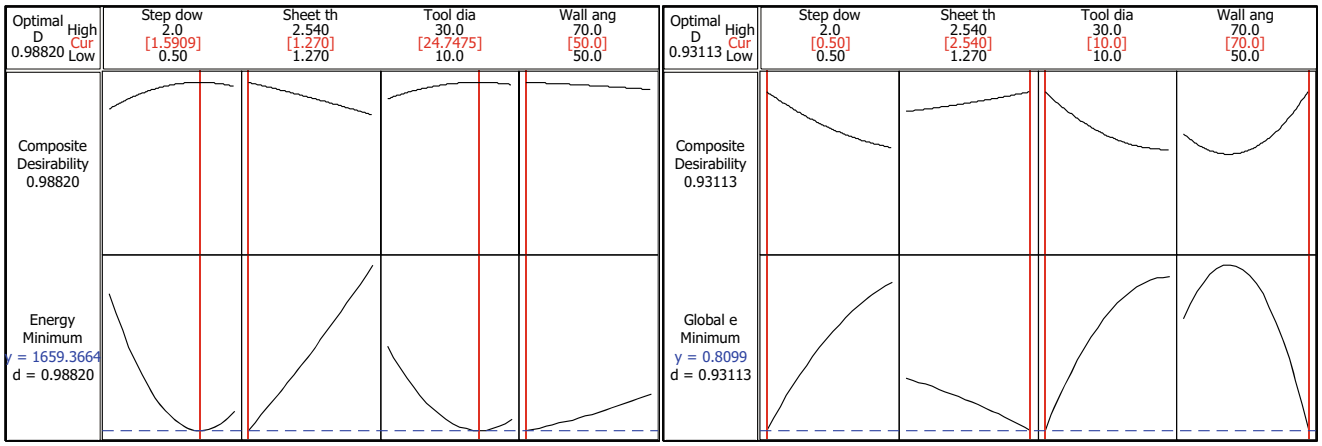

Fig. 13 Single response optimisation results for **a** deformation energy and **b** global geometric error (optimal parameters are indicated with *vertical lines*)

weight of each response can be determined by the user with the value from 0 to 1. This method includes three steps: (i) obtaining the individual desirability for each response, (ii) combining the individual desirability to obtain the combined or composite desirability and (iii) maximizing the composite desirability and identifying the optimal input variable settings [30]. The importance of these two responses is set as equal in the present study. As presented in Fig. 14, the trend of the composite desirability that combines geometric error and deformation energy is plotted in the first row. The trends of the predicted global geometric error and deformation energy over their whole defined range for all four parameters are illustrated in the second and third row, respectively. As indicated at the vertical lines, under the working condition with high step down of 2 mm, low sheet thickness of 1.27 mm, high tool diameter of 30 mm and large wall angle of 70°, a highest composite desirability of 0.917 can be achieved. The corresponding deformation energy and global geometric error are predicted to be 2459 J and 0.98 mm, respectively. The response surface method presented provides a useful guidance for optimal process design in terms of deformation energy and geometric error.

Under the actual forming condition, sheet thickness may need to be defined by other design parameters rather than optimisation. Therefore, the optimisation of both deformation energy and geometric error for a range of sheet thicknesses has been performed and tabulated in Table 5. It can be seen that, in the tested range, the selection of sheet thickness has no effect on the optimum setting of step down, tool diameter and wall angle, but greatly influences the required deformation energy and part geometric accuracy. Both the energy and geometric error increase largely with the increase of original sheet

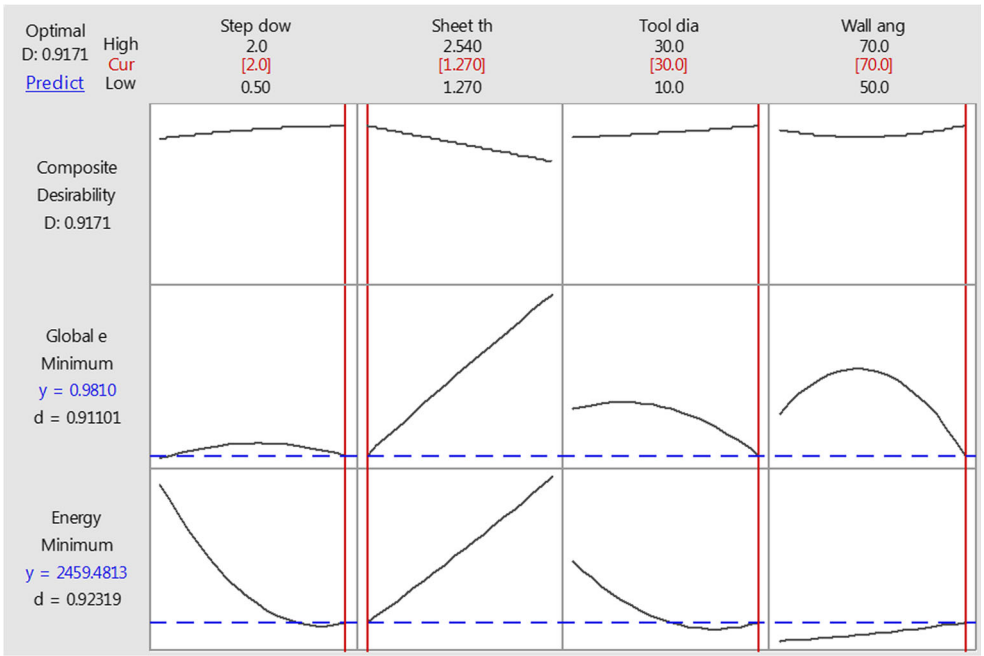

Fig. 14 Multi-responses optimisation result for both deformation energy and global geometric error (optimal parameters are indicated with *vertical lines*)

Table 5 Optimised results for deformation and geometric error under different sheet thickness

Sheet thickness (mm)	Optimised results					
	Step down (mm)	Tool diameter (mm)	Wall angle (°)	Composite desirability	Minimum energy (J)	Minimum error (mm)
1.27	2.0	30	70	0.917	2459	0.98
1.8	2.0	30	70	0.828	3693	2.09
2.54	2.0	30	70	0.702	5610	3.56

thickness. Consequently, reducing the sheet thickness will not only save the cost of material and energy consumption but also improve the part geometric quality in the ISF process.

4 Conclusions and future work

In this study, the effects of the four key process parameters on deformation energy and geometric accuracy in ISF have been investigated by performing a Box-Behnken design. Quadratic statistical models have been developed to predict the values of deformation energy and geometric error under different settings of the process parameters. Moreover, the optimum working conditions are determined to achieve minimum energy and geometric error using response surface methodology with desirability functions. The main conclusions from this study are drawn as follows:

- Response surface methodology with Box-Behnken design was successfully applied to investigate the effects of step down, sheet thickness, wall angle and tool diameter on both deformation energy and geometric accuracy during pyramid-forming processes. Statistical models have been established considering both quadratic and linear effects of most influential forming parameters.
- The deformation energy during the forming process was calculated based on measured forming forces. It was found that the deformation energy heavily depends on the sheet thickness because of higher plastic energy required to deform the material. Increasing step-down size with a limited range or decreasing the wall angle is an effective approach to reduce the deformation energy.
- The global geometry error defined by the vertical distance between the formed and designed profiles is selected as the measure of the geometric accuracy. It was concluded that the accuracy is largely determined by the quadratic effect of wall angle, the linear effect of sheet thickness and the interaction effect of thickness and step down. Decreasing the step-down size was found always helpful to improve the geometric accuracy.
- The optimisation results for both independent and simultaneous minimisation of deformation energy and geometric error during the pyramid-forming process are provided. Under the working condition with high step down of 2 mm, low sheet thickness of 1.27 mm, high tool diameter of 30 mm and large wall angle of 70°, the deformation energy and global geometric error are expected to be minimised to 2459 J and 0.98 mm, respectively.

Some suggestions for future investigation are provided,

- The deformation energy was calculated from forming forces during the forming operations. Actually, the total process energy may include the components related to idle times and relevant auxiliary operations and also machine tool inefficiencies during production mode: electrical losses, mechanical losses, etc. A comprehensive evaluation for the total consumed energy could be employed in further study.
- In this study, the global geometric error was used as the indicator for evaluating the geometric quality while in some cases the tolerances at some particular positions may be of interest instead.
- It is known that increasing the feed rate (forming speed) will save the required energy due to the reduced forming time, but this may affect the part accuracy as reported in [25]. An optimum value for the feed rate needs to be found so that the energy can be greatly saved without sacrificing part quality.

Acknowledgments The present work was supported by the Australian Research Council (ARC) Linkage project, Boeing Research and Technology Australia (BRTA) and QMI Solutions. China Scholarship Council (CSC) is also acknowledged for the scholarship support.

Funding This study was funded by Australian Research Council (ARC) Linkage project (grant number LP100200689).

Conflict of interest Yanle Li has received scholarship from China Scholarship Council (CSC). Haibo Lu has received scholarship from China Scholarship Council (CSC).

Ethical statement The authors declare that the manuscript follows the ethical statement of the International Journal of Advanced Manufacturing Technology. The manuscript has not been submitted to more than one journal for simultaneous consideration and has not been published partly or full previously.

References

1. Jeswiet J, Micari F, Hirt G, Bramley A, Duflou J, Allwood J (2005) Asymmetric single point incremental forming of sheet metal. Annal Manuf Technol 54(2):623–649
2. Echrif SBM, Hrairi M (2011) Research and progress in incremental sheet forming processes. Mater Manuf Process 26(11):1404–1414. doi:10.1080/10426914.2010.544817
3. Duflou JR, Sutherland JW, Dornfeld D, Herrmann C, Jeswiet J, Kara S, Hauschild M, Kellens K (2012) Towards energy and resource efficient manufacturing: a processes and systems approach. CIRP Ann Manuf Technol 61(2):587–609. doi:10.1016/j.cirp.2012.05.002
4. Dittrich MA, Gutowski TG, Cao J, Roth JT, Xia ZC, Kiridena V, Ren F, Henning H (2012) Exergy analysis of incremental sheet forming. Prod Eng 6(2):169–177. doi:10.1007/s11740-012-0375-9
5. Branker K, Adams D, Jeswiet J (2012) Initial analysis of cost, energy and carbon dioxide emissions in single point incremental forming - producing an aluminium hat. Int J Sustain Eng 5(3):188. doi:10.1080/19397038.2011.634033
6. Ingarao G, Ambrogio G, Gagliardi F, Di Lorenzo R (2012) A sustainability point of view on sheet metal forming operations: material wasting and energy consumption in incremental forming and stamping processes. J Clean Prod 29–30:255–268. doi:10.1016/j.jclepro.2012.01.012
7. Ingarao G, Vanhove H, Kellens K, Duflou JR (2014) A comprehensive analysis of electric energy consumption of single point incremental forming processes. J Clean Prod 67:173–186. doi:10.1016/j.jclepro.2013.12.022
8. Aerens R, Eyckens PV, Bael A, Duflou JR (2010) Force prediction for single point incremental forming deduced from experimental and FEM observations. Int J Adv Manuf Technol 46(9):969–982
9. Ambrogio G, Ingarao G, Gagliardia F, Di Lorenzo R (2014) Analysis of energy efficiency of different setups able to perform single point incremental forming (SPIF) processes. Procedia CIRP 15:111–116. doi:10.1016/j.procir.2014.06.055
10. Bagudanch I, Garcia-Romeu ML, Ferrer I, Lupiañez J (2013) The effect of process parameters on the energy consumption in single point incremental forming. Procedia Eng 63:346–353. doi:10.1016/j.proeng.2013.08.208
11. King JM, Allwood GPF, Duflou J (2005) A structured search for applications of the incremental sheet-forming process by product segmentation. Proc Inst Mech Eng B J Eng Manuf 219(2):239–244. doi:10.1243/095440505x8145
12. Braun JM, Allwood D, Music O (2010) The effect of partially cut-out blanks on geometric accuracy in incremental sheet forming. J Mater Process Technol 210(11):1501–1510. doi:10.1016/j.jmatprotec.2010.04.008
13. Micari F, Ambrogio G, Filice L (2007) Shape and dimensional accuracy in Single Point Incremental Forming: state of the art and future trends. J Mater Process Technol 191(1–3):390–395. doi:10.1016/j.jmatprotec.2007.03.066
14. Essa K, Hartley P (2011) An assessment of various process strategies for improving precision in single point incremental forming. Int J Mater Form 4(4):401–412. doi:10.1007/s12289-010-1004-9
15. Guzmán CF, Gu J, Duflou J, Vanhove H, Flores P, Habraken AM (2012) Study of the geometrical inaccuracy on a SPIF two-slope pyramid by finite element simulations. Int J Solids Struct 49(25):3594–3604. doi:10.1016/j.ijsolstr.2012.07.016
16. Ambrogio G, Cozza V, Filice L, Micari F (2007) An analytical model for improving precision in single point incremental forming. J Mater Process Technol 191(1–3):92–95. doi:10.1016/j.jmatprotec.2007.03.079
17. Ham MEJ (2007) Single point incremental forming of aluminum sheet metal: the development of maximum forming angle forming limits, measured strains, surface roughness and dimensional accuracy. Ph.D., Queen's University (Canada), Ann Arbor
18. Skjoedt MB, Silva M, Martins PAF, Bay N (2008) Revisiting the fundamentals of single point incremental forming by means of membrane analysis. Int J Mach Tools Manuf 48(1):73–83. doi:10.1016/j.ijmachtools.2007.07.004
19. Lu H, Li Y, Liu Z, Liu S, Meehan PA (2014) Study on step depth for part accuracy improvement in incremental sheet forming process. Adv Mater Res 939:274–280. doi:10.4028/www.scientific.net/AMR.939.274
20. Mourabet M, El Rhilassi A, El Boujaady H, Bennani-Ziatni M, Taitai A (2013) Use of response surface methodology for optimization of fluoride adsorption in an aqueous solution by Brushite. Arab J Chem. doi:10.1016/j.arabjc.2013.12.028
21. Mourabet M, El Rhilassi A, El Boujaady H, Bennani-Ziatni M, El Hamri R, Taitai A (2012) Removal of fluoride from aqueous solution by adsorption on Apatitic tricalcium phosphate using Box–Behnken design and desirability function. Appl Surf Sci 258(10):4402–4410. doi:10.1016/j.apsusc.2011.12.125
22. Liu Z, Liu S, Li Y, Meehan PA (2014) Modeling and optimization of surface roughness in incremental sheet forming using a multi-objective function. Mater Manuf Process 29(7):808–818. doi:10.1080/10426914.2013.864405
23. Bhattacharya A, Maneesh K, Venkata Reddy N, Cao J (2011) Formability and surface finish studies in single point incremental forming. J Manuf Sci Eng 133(6):61020. doi:10.1115/1.4005458
24. Natarajan U, Periyanan P, Yang S (2011) Multiple-response optimization for micro-endmilling process using response surface methodology. Int J Adv Manuf Technol 56(1–4):177–185
25. Ambrogio G, Filice L, Gagliardi F (2012) Improving industrial suitability of incremental sheet forming process. Int J Adv Manuf Technol 58(9–12):941–947. doi:10.1007/s00170-011-3448-6
26. Li Y, Daniel WJT, Liu Z, Lu H, Meehan PA (2015) Deformation mechanics and efficient force prediction in single point incremental forming. J Mater Process Technol. doi:10.1016/j.jmatprotec.2015.02.009
27. Li Y, Liu Z, Lu H, Daniel WJT, Liu S, Meehan P (2014) Efficient force prediction for incremental sheet forming and experimental validation. Int J Adv Manuf Technol 73(1–4):571–587. doi:10.1007/s00170-014-5665-2
28. Silva MB, Nielsen PS, Bay N, Martins PAF (2011) Failure mechanisms in single-point incremental forming of metals. Int J Adv Manuf Technol 56(9):893–903. doi:10.1007/s00170-011-3254-1
29. Hussain G, Khan HR, Gao L, Hayat N (2012) Guidelines for tool-size selection for single-point incremental forming of an aerospace alloy. Mater Manuf Process 28(3):324–329. doi:10.1080/10426914.2012.700151
30. What is response optimization. (2014). http://support.minitab.com/

4.3 The Papers

Paper 8

Study on Step Depth for Part Accuracy Improvement in Incremental Sheet Forming Process

Lu, H.B., **Li, Y.L.**, Liu, Z.B., Liu, S. and Meehan, P. A.

Advanced Materials Research

2014, Volume: 939, Pages: 274-280.

Advanced Materials Research Vol. 939 (2014) pp 274-280
© (2014) Trans Tech Publications, Switzerland
doi:10.4028/www.scientific.net/AMR.939.274

Study on step depth for part accuracy improvement in incremental sheet forming process

Haibo Lu[1, a], Yanle Li[1,b], Zhaobing Liu[1,c], Sheng Liu[1,d] and Paul A. Meehan[1,e]

[1]School of Mechanical & Mining Engineering, University of Queensland, St Lucia, Brisbane, QLD 4072, Australia

[a]h.lu2@uq.edu.au, [b]yanle.li@uq.edu.au, [c]z.liu7@uq.edu.au, [d]s.liu3@uq.edu.au, [e]meehan@uq.edu.au

Keywords: incremental sheet forming, step depth, part accuracy

Abstract. Incremental Sheet Forming (ISF) is a new-emerging sheet forming process well suited for small batch production or prototyping because it does not need any dedicated dies or punches. In this forming process, sheet metal parts are formed by a smooth-end tool in a stepwise way, during which plastic deformation is highly localized around the tool end. The part geometric accuracy obtained in the current ISF process, however, has not met the industry specification for precise part fabrication. This paper deals with a study on step depth, a critical parameter in ISF, for improving the geometric accuracy, surface quality and formability. Two sets of experiments were conducted to investigate the influence of step depth on part quality. Dimensional accuracy, surface morphology and material fracture of deformed parts were compared and analysed. An optimum value of step depth was suggested for forming a truncated cone. The present work provided significant fundamental information for the development of an advanced ISF control system on tool path control and optimization.

Introduction

Sheet metal forming is a widely used manufacturing process and plays a significant role in industry. There is a wide range of sheet metal forming processes, including stamping, pressing, etc. These require dedicated dies and punches to manufacture sheet-metal components with complex shapes. Due to the high cost in realizing such process and the lack of flexibility, conventional manufacturing methods are efficient for large scale production but less competitive for small scale fabrication of customised parts [1]. As market demand in the sheet forming area is becoming increasingly customer-oriented and sophisticated, more flexible manufacturing technologies for custom parts fabrication are demanded to be introduced and developed [2]. Incremental sheet forming (ISF) is a flexible process well suited for small batch production or prototyping because expensive dies and tools are not required, which makes it a promising alternative to meet the new market requests [3, 4].

In ISF, sheet metal parts are formed by a smooth-end tool, generally mounted on a three-axis CNC milling machine, in a stepwise way. Fig. 1 schematically illustrates the single point incremental forming (SPIF) process. The simple tool moves over the surface of the clamped metal sheet along a tool path directly generated from a 3D CAD file, during which plastic deformation is highly localized around the tool end. ISF is a dieless forming process and possesses a high degree of flexibility because specialised tooling is not required. The product design can be modified or changed easily and quickly. Additionally, the formability in ISF is higher than conventional processes due to the small plastic zone and incremental nature of the process, making it easier to deform sheet metal with low formability [5]. The small contact zone and incremental step size also contributes to small forces within the material. Therefore, the lead-time and cost of tooling in ISF can be greatly minimized. This forming technique makes rapid prototypes or small serial production of sheet metal parts relatively fast and economical [6].

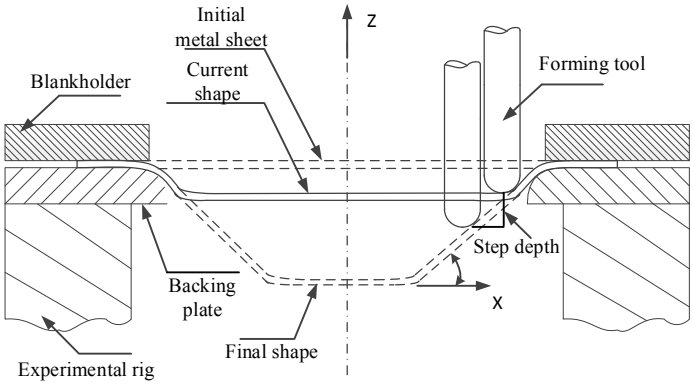

Fig.1 Process principle of SPIF: step depth (ΔZ) is the vertical distance between two neighbouring contours.

Nevertheless, the major limitation of ISF is that the geometric accuracy obtained currently is lower compared with conventional forming processes and cannot reliably reach suitable levels specified by industrial users. Hence, the ISF process is still in the embryonic stage with no widespread industrial applications although rapid advances have been achieved recently. Additionally, the forming process is slow due to its point-to-point forming nature.

Recently, the improvement of part accuracy and process optimization in ISF has been a key issue for researchers. During the ISF process, the tool path directly affects the forming accuracy since the shape is formed by a simple tool following a designed tool path. Regarding the generation of tool path, the most common method is a contour parallel method by which the tool path is generated in commercial CAM software and consists of a series of contours, with the step depth constant, parallel to the sheet plane. However, this method fails to fabricate complex parts with high precision. Many studies on the design, optimization and control of forming tool path have been carried out to overcome the limitations. Hirt et al. [7] proposed a tool path optimization method based on experiments and the modification of the tool path by a correction algorithm in the second run. Attanasio et al. [8] conducted a study on tool path optimization in TPIF and concluded that tool path with a small scallop height and variable step depth sizes contribute to better part quality. As reported in [9], a closed loop control scheme was used to modify the step depth during the forming process for tool trajectory control. Malhotra et al. [10] presented an automatic spiral tool path generation algorithm for SPIF, in which the incremental depth is controlled by the geometrical error between CAD model and formed parts.

According to the previous research, step depth has been considered as a critical parameter in the design, optimization and control of tool paths. At present, comprehensive research work on step depth is required to further study the relationship between step depth and part quality, especially for improving part accuracy via tool path control and optimization. This paper focuses on the investigation of step depth to fully understand its influence on the formability and part quality, including geometric accuracy and surface finish. This would be of great significance for ISF tool path control and optimization to address the limitation of low geometric accuracy.

Experiments

Experiments were carried out on an AMINO® DLNC-PC ISF machine (Fig. 2). The sheet blank is clamped between a blank holder and a steel backing plate to prevent any movement of the blank during forming process. The metal blank, with 1.6 mm in thickness and 300 mm × 300 mm in size, is made of aluminium (7075-O), commonly utilized for forming automotive and aviation components. A 30 mm diameter cylindrical steel tool with a hemispherical end was used to deform the blank; the tip of the tool is tungsten carbide and the body is made of K110 steel which was

hardened and tempered to HRC60. Lubricant (oil-Shell Tellus Oil 68) was used to reduce the wear of the tool and friction between the tool and the blank.

Fig. 2 AMINO® DLNC-PC ISF Machine

Two sets of tests were performed by varying the ΔZ values to study this parameter, focusing on geometric accuracy and surface quality and on material formability, respectively. CAD models of truncated cones with two different wall angles were designed in SOLIDWORKS. A laser scanner (Non-contact 3D Digitizer VIVID 9i) was used to measure the geometry of the deformed components. Surface morphology of machined faces on produced truncated cones was analysed as well. The parameter settings of experiments are shown in Tables 1, as follows.

Table 1 Parameter settings of experiments on step depth

Parameter	Geometric accuracy and surface quality test	Formability test
Shape design	Truncated cone	Truncated Cone
Wall angle (°)	50	60
Feed rate (mm/min)	4000	4000
Sheet thickness (mm)	1.6	1.6
Tool diameter (mm)	30	30
Step depth/ΔZ (mm)	0.1, 0.6, 1.1	0.1, 0.2, 0.3, 0.4, 0.5, 0.7, 1.0

Results and Discussion

This section presents experimental results obtained in the tests to analyse the influence of step depth in ISF process in terms of geometric accuracy, surface morphology and material fracture.

Geometric accuracy. GEOMAGIC Qualify was used to produce 3D geometry data of the scanned shape and analyse the dimensional error between deformed test parts and designed CAD models. Specifically, both produced and designed profiles were given in large sets of points in the same Cartesian coordinate system. In this work, cross-sectional comparison along a defined section plane was used to evaluate the geometric accuracy since the truncated cone is symmetric. A system plane (plane XOZ) across the symmetry axis of the cone was set as the section plane. The deviation in Z direction between the designed and fabricated profiles was calculated as the geometric error in cross-sectional comparison.

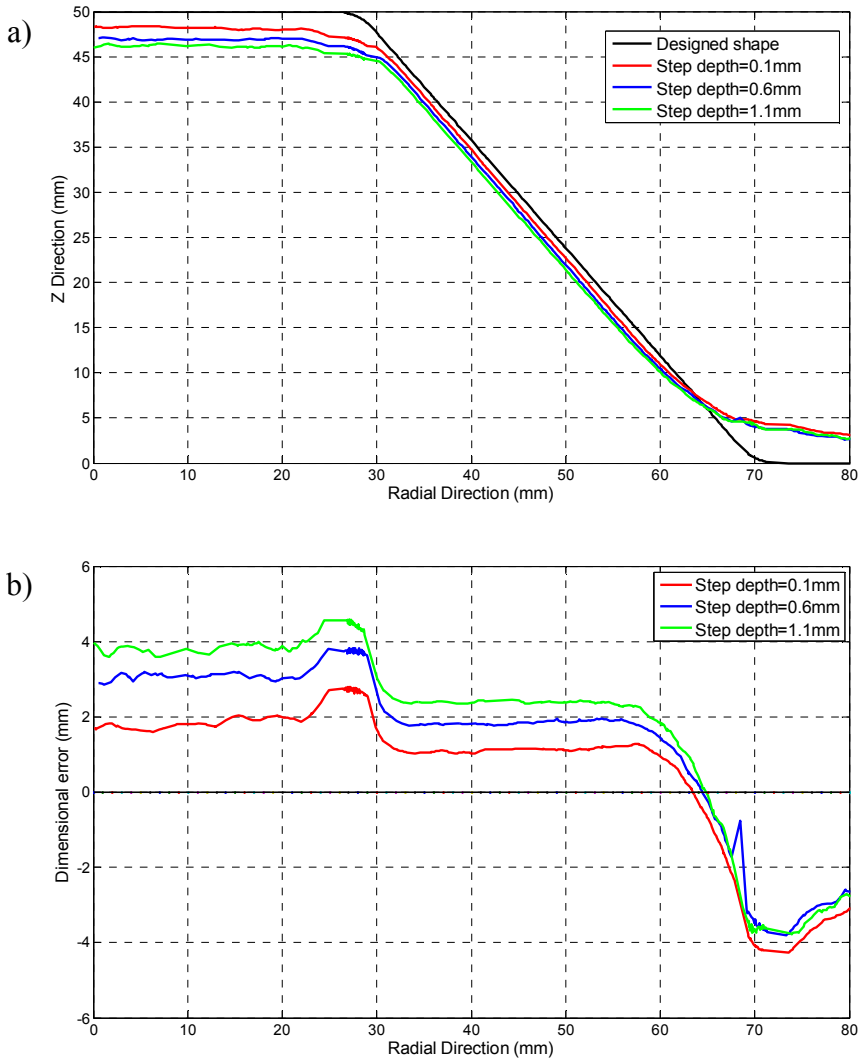

Fig.3: (a) Cross-sectional comparison among deformed profiles and the target profile; (b) Error distribution of deformed parts

The comparison among profiles of formed parts and the designed shape in geometric accuracy test is illustrated in the Fig. 3a), while detailed error distributions are correspondingly shown in Fig. 3b). According to the curves in Fig. 3, the profile with 0.1 mm step depth has the best dimensional accuracy in the test compared with the target profile. Therefore, step depth can significantly affect the geometric accuracy. Specifically, the geometric accuracy increases when decreasing the step depth size. This can be due to the fact that the generated forming contours are more intensive when setting step depth at a small value. Consequently, the movement of the forming tool would be smaller between two adjacent parallel contours, providing more homogeneous material distribution and deformation as well as the reduction of the spring-back effect.

Surface morphology. Surface morphology of inner faces, namely the machined faces, of deformed cones was shown in Fig. 5. Obviously, in the comparison of surface waviness among three produced parts, step depth has a great influence on the surface finish quality. As can be seen in Fig. 5a) and 5b), there are obvious tool marks left on the machined surfaces when using large step depth sizes (0.6mm and 1.1mm). The distance between two adjacent tool marks on the formed surface, d, illustrated in Fig. 4, increases with the increase of step depth value. The relationship between d and ΔZ coincides with the sine law, as shown in Equation 1.

$$d = \Delta Z / sin\alpha \ . \quad (1)$$

Where α is the wall angle of the truncated cone.

Due to the geometric error, the measured *d* values (1.406mm and 0.751mm with *ΔZ* at 1.1mm and 0.6mm, respectively) are a little smaller than calculated ones (1.436mm and 0.783mm). On the contrary, as for small step depth (0.1mm), the formed surface shown in Fig. 5c) is much smoother than the two surfaces above, with no visible tool marks on the surface. Thus, it can be concluded that the surface quality can be improved by choosing small step depth in the ISF process.

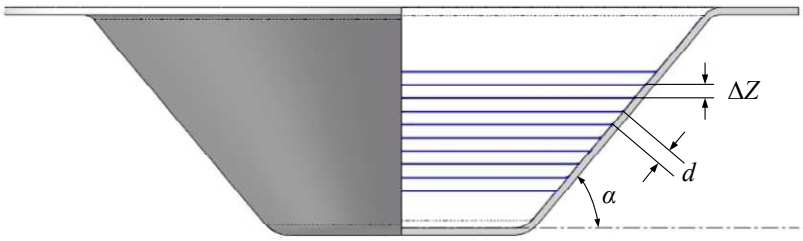

Fig. 4 Diagram of tool marks on the inner part face

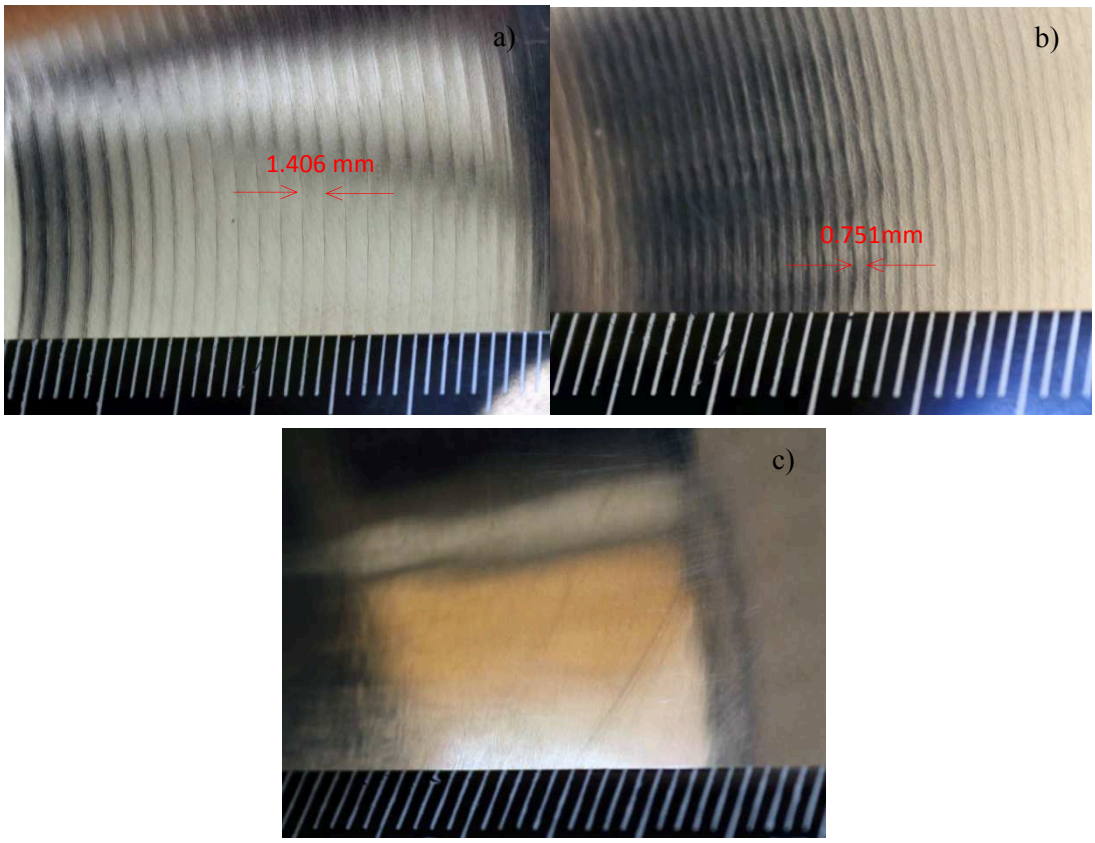

Fig. 5 Surface morphology of deformed parts in surface quality test: (a) *ΔZ*=1.1mm; (b) *ΔZ*=0.6mm; (c) *ΔZ*=0.1mm

Fracture analysis. Based on the analysis above, smaller step depth contributes to better geometric accuracy and part surface quality but lower efficiency due to the increase of forming time. More importantly, small step depth also adversely affects the forming process in terms of material formability, especially when the forming wall angle gets close to the forming wall angle limit. In the formability test, a truncated cone with a 60° wall angle (close to the wall angle limit) was used to evaluate the formability at different step depth sizes, with *ΔZ* ranging from 0.1 to 1.0 mm. The sheet fractured during the forming process with small step depth below 0.5 mm while only the parts with *ΔZ* over 0.7mm were successfully produced. Fig. 6a) shows the material fracture of a deformed cone with *ΔZ* being 0.1mm. Furthermore, the material facture occurs at smaller forming depth in Z direction when the step depth is smaller, which is illustrated in Fig. 6b). This can be due to the fact that a smaller step depth size means a smaller tool contour distance between two neighbouring contours. Thus, more intensive contact between sheet material and tool end will happen in the ISF

process, during which material in the contact zone of the metal sheet is pressed and hardened by the tool end in each forming contour. More already hardened material would be deformed again by the tool in the following several contours when using a tool path with smaller step depth. This leads to a great increase in the contact stress required to reach the target deformation. Consequently, sheet formability will be reduced due to higher stress state induced in the material. Therefore, too small step depth values should be avoided in consideration of material failure. In this case, 0.7 mm step depth was suggested to be the optimum value for the forming of the truncated cone with 60° wall angle.

(a)

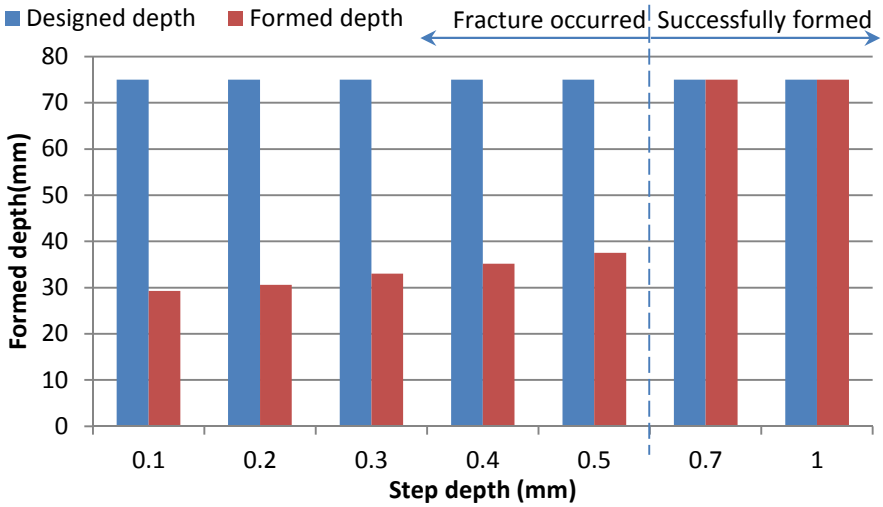

Fig. 6: (a) Part fracture in formability test (ΔZ=0.1mm); (b) Formed depth of parts in formability test

Conclusion and future work

This research aimed to provide a comprehensive investigation on step depth, as a critical process variable in ISF process, and to demonstrate that this variable is of great importance in design and control of tool path. Several experiments were conducted to investigate its influence on the part quality of the formed parts, including geometric accuracy, part surface quality and material formability. According to the results, smaller step depth leads to better geometric accuracy and part surface quality in ISF process. Parts deformed with large step depth cannot reach the required level both in geometric accuracy and surface quality but too small a step depth value should also be avoided with regard to the material fracture, especially when producing parts with large wall angles. Also, the forming time will increase as the step depth decreases. Even so, smaller step depth should be used within a reasonable range in tool path control and optimization. A trade-off among geometric accuracy, part surface quality, material failure and forming time should be made in the design and control of tool paths and the first two aspects should be considered as priorities. It is clearly suggested that there is an optimum value of step depth in the ISF path design; for instance

0.7mm in the case presented. Further research on the optimization of step depth should be included in the design of an advanced ISF control system. The presented work is a foundation, which offers significant information for tool path control and optimization, and needs to be developed to further determine the constraints in tool path control system. The inaccuracy of parts is still obvious in using contour tool paths with constant step depth. For the future, control of tool path will be developed for part accuracy improvement and to reduce design time for new parts in the ISF process.

Acknowledgements The present work was supported by China Scholarship Council (CSC) scholarship.

References

[1] L. Filice, L. Fratini, F. Micari, Analysis of material formability in incremental forming, CIRP Ann. Manuf. Technol. 51 (2002) 199-202.

[2] Y. H. Kim, J. J. Park, Effect of process parameters on formability in incremental forming of sheet metal, J. Mater. Process. Technol. 130 (2002) 42-46.

[3] E. Hagan, J. Jeswiet, A review of conventional and modern single-point sheet metal forming methods, Proc. Inst. Mech. Eng. Pt. B J. Eng. Manufact. 217 (2003) 213-225.

[4] S. B. M. Echrif, M. Hrairi, Research and Progress in Incremental Sheet Forming Processes, Mater. Manuf. Processes 26 (2011) 1404-1414.

[5] J. Jeswiet, F. Micari, G. Hirt, A. Bramley, J. Duflou, J. Allwood, Asymmetric single point incremental forming of sheet metal, CIRP Ann. Manuf. Technol. 54 (2005) 88-114.

[6] J.R. Duflou, J. Verbert, B. Belkassem, J. Gub, H. Sol, C.A.M Henrard, A.M. Habraken, Process window enhancement for single point incremental forming through multi-step toolpaths, CIRP Ann. Manuf. Technol. 57 (2008) 253-256.

[7] G. Hirt, J. Ames, M. Bambach, R. Kopp, Forming strategies and process modelling for CNC incremental sheet forming, CIRP Ann. Manuf. Technol. 53 (2004) 203-206.

[8] A. Attanasio, E. Ceretti, C. Giardini, L. Mazzoni, Asymmetric two points incremental forming: improving surface quality and geometric accuracy by tool path optimization, J. Mater. Process. Technol. 197 (2008) 59-67.

[9] W. Hao, S. Duncan, Optimization of tool trajectory for Incremental Sheet Forming using closed loop control, In CASE, IEEE Int Conf, (2011) 779-784.

[10] R. Malhotra, N.V. Reddy, J. Cao, Automatic 3D spiral toolpath generation for single point incremental forming, J. Manuf. Sci. Eng. 132 (2010).

4.3 The Papers

Paper 9

Taguchi Optimization of Process Parameters for Forming Time in Incremental Sheet Forming Process

Liu, Z.B., **Li, Y.L.**, Daniel, W. J. T. and Meehan, P. A.

Materials Science Forum

2013, Volume: 773, Pages: 137-143.

Materials Science Forum Vols. 773-774 (2014) pp 137-143

doi:10.4028/www.scientific.net/MSF.773-774.137

Taguchi Optimization of Process Parameters for Forming Time in Incremental Sheet Forming Process

Zhaobing Liu[1, a], Yanle Li[1,b], Bill Daniel[1,b] and Paul Meehan[1,c]

[1]School of Mechanical and Mining Engineering, The University of Queensland, St Lucia, Brisbane, QLD 4072, Australia

[a]z.liu7@uq.edu.au, [b]yanle.li@uq.edu.au, [c]Billd@uq.edu.au, [d]meehan@uq.edu.au

Keywords: Incremental sheet forming, Optimization, Taguchi method, Orthogonal array

Abstract: Incremental sheet forming (ISF) is a new promising technology due to its flexibility and low-cost tooling properties compared with conventional forming processes. However, it is only suitable for small-batch production because of its incremental feature inducing relative long forming time. Presently, widespread usage of the process is restricted by a lack of predictive understanding of the process due to its complexity. In this paper, the aspect of forming time is studied by investigating the effects of four distinctive process parameters (step over, feed rate, sheet thickness and tool diameter). An effective analysis tool, Taguchi method together with design of experiment (DOE) and analysis of variance (ANVOA) is utilized to study the effects of the four process parameters on forming time and further to optimize parameter combinations in order to minimize forming time. Using these techniques, experimental results show that the step over of spiral tool path is the most important process parameter affecting forming time followed by feed rate. Sheet thickness and tool diameter have little effect on forming time. The comparison between the prediction of optimized parameter combination and the confirmation test result has further demonstrated the effectiveness of the proposed method. It is worth noting that the results of this study will indicate a further direction on how to optimize process parameters to find a balance between forming efficiency (forming time) and forming quality (forming accuracy and surface roughness).

Introduction

With the demands of niche markets and individual preferences on sheet metal products, incremental sheet forming (ISF), as a new promising technology, has received considerable attentions since its inception[1-3]. In the incremental forming process, a simple forming tool is controlled by a computer numerically controlled (CNC) machine following a prescribed tool path which plastically deforms the sheet metal into the desired shape. Basically, there are two variations of incremental sheet forming, single point incremental forming (SPIF) and two point incremental forming (TPIF). In single point incremental forming, the tool deforms the sheet metal into the concave shape without any dies while in two point incremental forming, the tool moves on the convex sheet surface with a positive die. The blank holder should be moved by the hydraulic actuator in order to firmly maintain the sheet metal in the proper working position. One of the advantages of this technology is the cost reduction compared with traditional forming processes such as stamping and deep drawing processes because punches or expensive dies are avoided. However, it is only suitable for small-batch production due to the slowness of the manufacturing process[4,5]. There is thus the challenge of improving forming time in ISF. Although numerous researches in ISF during the last decade has focused on deformation mechanism and the effects of different process parameters on forming process[6,7], proper combination and optimization of process parameters to improve forming efficiency and quality is still an active topic in ISF process and needs to be further investigated. In fact, the lack of forming process knowledge is the main reason behind difficulty of improvement of forming efficiency and quality. In this study, Taguchi-based optimization technique is utilized to investigate the effects of four process parameters, namely step over (S), feed rate (V), sheet thickness (T) and tool diameter (D), on forming

efficiency. It is noted that these four process parameters have the most relevant influence on SPIF process and have been mentioned in many ISF papers. Presently optimal values of these process parameters have been investigated experimentally

Experimental work

Equipment: The experiments were performed on an Amino ISF machine (Model DLNC-PC for industrial use) using steel tools with a tungsten carbide hemispherical head as shown in Fig.1. Shell Tellus Oil 68 was used in the tests as forming oil.

Fig.1. Amino ISF machine.

Material and testing geometry: The material used for the present investigation is AA7075-0 alloy. 7075 is the highest strength alloy of the commercially available aluminum, and is typically used as aircraft structures. The mechanical properties for AA7075-0 are shown in Table 1.

Table 1. Mechanical properties for AA7075-0.

Material Property	Value
Density (kg/m^3)	2,800
Young's modulus (MPa)	75,000
Poisson's ratio	0.33
Yield strength (MPa)	100
Ultimate tensile strength (MPa)	200
Strain hardening coefficient (MPa)	330
Power law coefficient	0.19

A truncated cone (frustum) with a slope angle of 45 degrees was selected as the shape to be optimized, beginning from a square sheet with a side of 300mm. The major base of the cone is 140mm and the height is 50mm. This slope angle for the truncated cone is safe in that fracture of the sheet has not occured[8]. Fig.2 shows a truncated cone with a curvature generatrix and draw angle changing from 59˚ to 73˚. This shape was successfully made and no fracture has been observed experimentally.

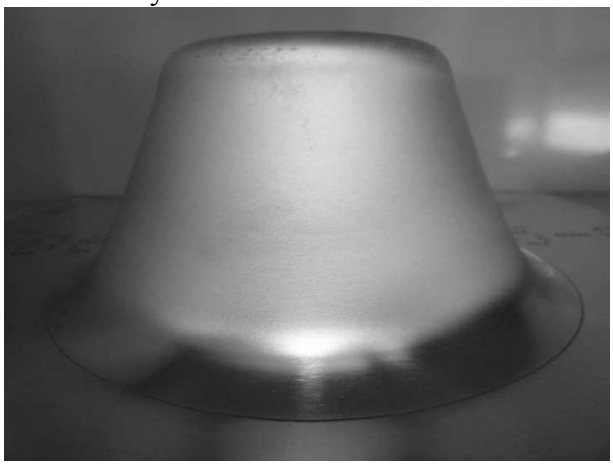

Fig.2. The formability test-a truncated cone with curvature generatrix.

Experimental design tool-Taguchi method

The present investigation utilizes the Taguchi method[7,9-10], which aims to optimize processes in order to minimize quality loss with one of the objective functions of "the-nominal-the-best", "the-larger-the-better", or "the-smaller-the-better" depending on the experimental objective. Taguchi method uses an orthogonal array to organize the parameters affecting the process and the levels at which they should be varies. Instead of having to test all possible combinations like the factorial design, the Taguchi method tests pairs of combinations. This allows for the efficient collection of the necessary data to determine which factors most affect product quality with a minimum amount of experimentation. The general design steps involved in Taguchi method are as follows:

1. Define the process objective, or more specifically, a target value for a performance measure of the process.
2. Determine the design parameters affecting the process. Parameters are variables within the process that affect the performance measure set above.
3. Create orthogonal arrays for the parameter design indicating the number of and conditions for each experiment.
4. Conduct the experiments and select the optimum level of process parameters through ANVOA analysis.
5. Perform a confirmation test to verify the optimal process parameters.

The Taguchi optimization procedure starts with selection of orthogonal array. The minimum number of runs in the array is

$$N_{\min} = (L-1)F + 1 \tag{1}$$

where L and F is number of levels and number of factors, respectively. In this study, four process parameters (step over, feed rate, sheet thickness, tool diameter) are chosen as factors to study the effect on forming time. Three levels are defined for each of the factors as summarized in Table 2. Calculated by Eq.(1), L_9 orthogonal array is selected as described in Table 3. The signal-to-noise ratio (S/N) is originally defined as the ratio of the signal to random noise. In Taguchi designs, the S/N ratio represents a measure of robustness used to identify controllable factors (step over, feed rate, sheet thickness and tool diameter) that reduce variability in a product or process by minimizing the effects of uncontrollable factors (loading and unloading time which refer to the time for movement of machine table with workpiece or deformed product to or away from the machine working zone). Higher values of the S/N ratio indicate controllable factor settings that minimize the effects of the uncontrollable factors. Therefore, the S/N ratio is a quality control indicator in which it reflects the influence of changing any process parameters on the performance of the process. Different S/N ratios can be chosen depending on the goal of the experiment. An S/N ratio of the-smaller-the-better as defined in [13] is chosen because the objective is to minimize the output value (forming time) and the target is zero. This is calculated as

$$\eta = -10\log\left(\frac{1}{n}\sum_{i=1}^{n} y_i^2\right) \tag{2}$$

where η is the S/N ratio, n is the number of experiments taken in one test run, y_i indicates the dimensionless output at the ith experiment with respect to one unit measure.

Table 2. Process parameters and their levels studied.

Factors	Description	Level 1	Level 2	Level 3
A	Step-over (Spiral path), S (mm)	0.5	1.0	2.0
B	Feed rate, V (mm/min)	1000	2000	3000
C	Sheet thickness, T (mm)	1.02	1.60	2.54
D	Tool diameter, D (mm)	10	12	15

Table 3. Orthogonal array L9 (3^4) of the experimental runs.

Factors/Run no.	A Step over(mm)	B Feed rate(mm/min)	C Sheet thickness(mm)	D Tool diameter(mm)
1	1(0.5)	1(1000)	1(1.02)	1(10)
2	1(0.5)	2(2000)	2(1.60)	2(12)
3	1(0.5)	3(3000)	3(2.54)	3(15)
4	2(1.0)	1(1000)	2(1.60)	3(15)
5	2(1.0)	2(2000)	3(2.54)	1(10)
6	2(1.0)	3(3000)	1(1.02)	2(12)
7	3(2.0)	1(1000)	3(2.54)	2(12)
8	3(2.0)	2(2000)	1(1.02)	3(15)
9	3(2.0)	3(3000)	2(1.60)	1(10)

Experimental results and analysis

In this experiment, the forming time includes the loading and unloading time and can be measured accurately using the Fanuc controller in the Amino ISF machine. Fig.3 shows the formed truncated cones based on Taguchi design. The results of the nine experiments are listed in Table 4 and corresponding S/N ratio are calculated.

Fig.3. The nine formed truncated cones according to Taguchi design.

Table 4. Experimental results for forming time and S/N ratio.

Experimental run no.	Process parameter level Step over (S)	Feed rate (V)	Sheet thickness (T)	Tool diameter (D)	Measured forming time (s)	Calculated S/N ratio (dB)
1	1(0.5)	1(1000)	1(1.02)	1(10)	1872	-65.446
2	1(0.5)	2(2000)	2(1.60)	2(12)	1008	-60.069
3	1(0.5)	3(3000)	3(2.54)	3(15)	717	-57.110
4	2(1.0)	1(1000)	2(1.60)	3(15)	967	-59.709
5	2(1.0)	2(2000)	3(2.54)	1(10)	525	-54.403
6	2(1.0)	3(3000)	1(1.02)	2(12)	380	-51.596
7	3(2.0)	1(1000)	3(2.54)	2(12)	512	-54.185
8	3(2.0)	2(2000)	1(1.02)	3(15)	292	-49.308
9	3(2.0)	3(3000)	2(1.60)	1(10)	217	-46.729

The process of estimating the main effects of each factor is called the analysis of means (ANOM) and the effect of a factor level is the deviation it causes from the overall mean response. The analysis of variance (ANOVA) establishes the relative significance of factors in terms of their percentage contribution to the response. ANOVA is also needed for estimating the error variance for the effects

and variance of the prediction error[11]. The results of the ANOM and ANOVA for four process parameters are presented in Tables 5 and 6 and Fig.4.

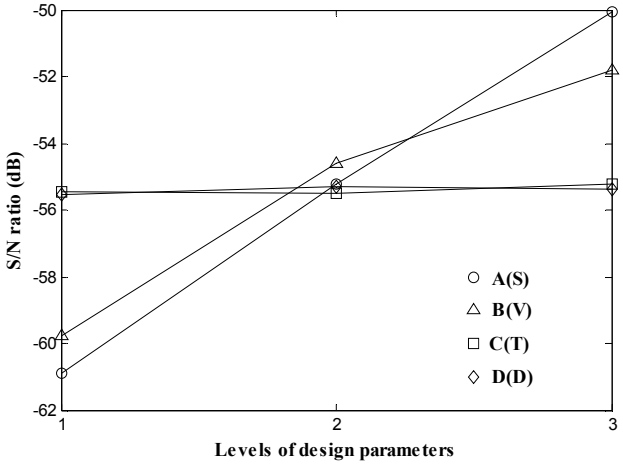

Fig. 4 Graph showing factor effects for S/N ratio.

Table 5. S/N response table for forming time.

		Mean S/N radio (dB)			
Factors	Description	Level 1	Level 2	Level 3	Max-min
A	Step over, S	-60.875	-55.236	-50.074*	10.801
B	Feed rate, V	-59.780	-54.593	-51.812*	7.968
C	Sheet thickness, T	-55.450	-55.502	-55.233*	0.269
D	Tool diameter, D	-55.526	-55.283*	-55.376	0.243

The total mean S/N ratio=-55.395 dB and * indicates the optimum level.

Table 6. ANOVA table for effect of different forming time.

Factors	Description	Degrees of freedom	Sum of squares	Mean square	Contribution(%)
A	Step over, S	2	175.106	87.553	64.04
B	Feed rate, V	2	98.128	49.064	35.89
C	Sheet thickness, T	2	0.122	0.061	0.04
D	Tool diameter, D	2	0.090	0.045	0.03
Error		0	0	-	-
Total		8	273.446	136.723	100

Those results revealed that the step over (S), which reached 64.04%, made the major contribution to the forming time. While the contribution percentages of the feed rate (V), sheet thickness (T) and tool diameter (D) were at 35.89%, 0.04% and 0.03%, respectively. It can be concluded that the step over had the most significant effect on the forming time followed by feed rate, whereas the influence of sheet thickness and tool diameter can be ignored. Since the ANOVA has resulted in zero degree of freedom for error term, it is necessary to pool the factor having less influence on forming time.

According to the Taguchi method, the higher the η value is, the better the overall performance is. This means that the factor with the highest signal-to-noise ratio should be selected as the optimal level. The average value for each experimental level was calculated using the highest η value for each factor to establish Table 5 and Fig.4. As can be seen in Table 5 and Fig.4, the optimal condition is described as $A_3B_3C_3D_2$, which means step over $S = 2.0$ mm, feed rate $V = 3000$ mm/min, sheet thickness $T = 2.54$ mm and tool diameter $D = 12$ mm. This optimal condition provides minimum forming time to be calculated in the subsequent section.

Confirmation test

Once the optimal level of the design parameters has been selected, a confirmation experiment is needed to validate the results with the predicted optimal conditions in Table 5 and Fig.4. The estimated S/N ratio $\hat{\eta}$ using the optimal level of the design parameters can be calculated as:

$$\hat{\eta} = \eta_m + \sum_{i=1}^{k} (\overline{\eta}_i - \eta_m) \tag{3}$$

where η_m is the total mean S/N ratio, $\overline{\eta}_i$ is the mean S/N ratio ate the optimal level, and k is the number of the main process parameters that affect the quality of the process. Table 7 shows the results of confirmatory tests at optimal level $A_3B_3C_3D_2$.

Table 7. Results of confirmatory tests at optimal level $A_3B_3C_3D_2$

	Predicted	Observed	|Error|
Forming time (s)	205	217	12
S/N ratio (dB)	-46.2	**-46.7**	0.5

As can be seen in Table 7, the optimal conditions provide a minimum forming time of 205s calculated by Eq.(3). The observed experimental forming time is higher than the predicted value (205s), but the error between them is only 5.9%. The deviation of S/N ratio is also only 1.1%, confirming a good agreement between predicted and observed S/N ratio values.

In order to verify the closeness of predicted S/N ratio with that of observed S/N ratio, confidence interval (CI) value of predicted S/N ratio for the optimum factor level combination at 95% CI is determined [12]. The prediction error, i.e., the difference between predicted S/N ratio and observed S/N ratio is within the CI value (±0.80 dB), so the choice of optimal combination of process parameters for minimizing forming time is statistically confirmed.

Conclusions

In this paper, the process parameters influencing forming time in ISF process has been investigated. The Taguchi method, a powerful analysis tool, together with DOE and ANOVA is utilized to determine the best combination of process parameters in order to minimize forming time. Further, the best combination values were confirmed by the experimental verification. The conclusions drawn from the results are as follows:

1. The most significant process parameter influencing forming time is the step over followed by the feed rate. The sheet thickness and tool diameter have little effect on forming time, so in this study their influence can be ignored.

2. Using Taguchi method, the optimal combination of process parameters has been determined and minimum forming time has been predicted as 205 s based on optimal values of step over, feed rate, sheet thickness and tool diameter.

3. Additional confirmation experiments at these optimal conditions have been carried out. The experimental results have shown a very good agreement with the prediction results for forming time obtained by Taguchi analysis. Confidence interval was calculated as ± 0.80 dB to statistically confirm the good agreement between prediction and experimental results.

The contribution of this work is to clarify the most influential process factors influencing forming time and determine the best combination in order to improve forming efficiency. The next step is to investigate process parameter values to optimize the forming quality while simultaneously minimizing forming time.

Acknowledgments

This work was financially supported by the ARC Linkage Program, Boeing Research Technology and QMI Solutions. Many thanks to Michael Elford, Paul Bellette and Prasad Gudimetla for their support and useful comments.

References

[1] J. Jeswiet, F. Micari, G. Hirt, A. Bramley, J. Duflou and J. Allwood, CIRP Ann. – Manuf. Techn. 54, 623(2005)
[2] W.C. Emmens and A.H. van den Boogaard, J. Mater. Process. Technol. 209, 3688 (2009)
[3] Z.B. Liu, P. Meehan and P. Bellette, Adv. Mater. Res. 337,452 (2011)
[4] W.K.H. Sarraji, J. Hussain and W.X. Ren, Mater. Manuf. Process. 27, 499 (2012)
[5] R. Malhotra, N.V.Reddy and J. Cao, J. Manuf. Sci. E.-T. ASME, 132, 061003-1 (2010)
[6] K. Jackson and J. Allwood, J. Mater. Process. Technol., 209, 1158 (2009)
[7] D.T. Nguyen, J.G. Park, H.J Lee and Y.S. Kim, P. I. Mech. Eng. B- J. Eng. 224, 913 (2009)
[8] G. Hussain, L. Gao, N. Hayat and L. Qijian, Int. J. Mach. Tools Manuf. 47, 2177 (2007)
[9] V.N. Gaitonde, S.R. Karnik, B.T. Achyutha and B. Siddeswarappa, J. Mater. Process. Technol. 202, 374 (2008)
[10] C. Gologlu and N. Sakarya, J. Mater. Process. Technol. 206, 7 (2008)
[11] M.S. Phadke, Editor, Quality Engineering using Robust Design, Prentice Hall, Englewood Cliffs, New Jersey (1989)
[12] P.J. Ross, Editor, Taguchi Techniques for Quality Engineering, McGraw-Hill, New York (1996)
[13] G. Taguchi, S. Chowdhury and Y.I. Wu, Editor, Taguchi's Quality Engineering Handbook, Wiley, Michigan (2005)

4.3 The Papers

Paper 10

Modeling and Optimization of Surface Roughness in Incremental Sheet Forming using a Multi-objective Function

Liu, Z.B., Liu, S., **Li, Y.L.** and Meehan, P. A.

Materials and Manufacturing Processes

2014, Volume: 29, Pages: 808-818.

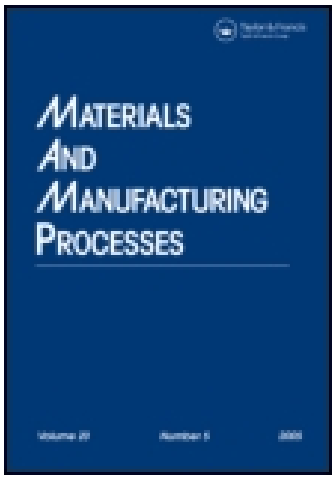

Materials and Manufacturing Processes
Publication details, including instructions for authors and subscription information:
http://www.tandfonline.com/loi/lmmp20

Modeling and Optimization of Surface Roughness in Incremental Sheet Forming using a Multi-objective Function

Zhaobing Liu [a] , Sheng Liu [a] , Yanle Li [a] & Paul Anthony Meehan [a]
[a] Department of Mechanical Engineering, School of Mechanical and Mining Engineering , The University of Queensland , Brisbane , Australia
Accepted author version posted online: 02 Jan 2014.Published online: 07 Jul 2014.

Materials and Manufacturing Processes, 29: 808–818, 2014

ISSN: 1042-6914 print/1532-2475 online
DOI: 10.1080/10426914.2013.864405

Taylor & Francis
Taylor & Francis Group

Modeling and Optimization of Surface Roughness in Incremental Sheet Forming using a Multi-objective Function

Zhaobing Liu, Sheng Liu, Yanle Li, and Paul Anthony Meehan

Department of Mechanical Engineering, School of Mechanical and Mining Engineering, The University of Queensland, Brisbane, Australia

As a critical product quality constraint, surface roughness is regarded as a weak point in incremental sheet forming (ISF). It is of great importance to identify the impact of forming parameters on the surface roughness and optimize the surface finish at the production stage. This paper proposes a systematic approach to modeling and optimizing surface roughness in ISF. The quantitative effects of four parameters (step down, feed rate, sheet thickness, and tool diameter) on surface roughness are analyzed using the response surface methodology with Box–Behnken design. The multi-objective function is used to evaluate the overall surface roughness in terms of the tool-sheet contact surface roughness, i.e., internal surface roughness and the noncontact surface roughness, i.e., external surface roughness. Additionally, the average surface roughness (R_a) on each surface is measured along the tool-path step-down direction taking the impact of sheet roll marks into account. The optimal conditions for the minimization of overall surface roughness are determined as step down (0.39 mm), feed rate (6000 mm/min), sheet thickness (1.60 mm), and tool diameter (25 mm). This study shows that Box–Behnken design with a multi-objective function can be efficiently applied for modeling and optimization of the overall surface roughness in ISF.

Keywords Aluminum; Box–Behnken; Deformation; Forming; Incremental; Objective; Optimization; Response; Roughness; Surface.

Introduction

New trends in sheet metal forming are rapidly developing to meet various demands in the niche market. Incremental sheet forming (ISF), as a promising technology, has demonstrated its high potential to shape complex three-dimensional parts without using specific tooling [1–6]. However, the forming accuracy, including the geometric accuracy at the macroscopic level and the surface finish at the microscopic level, is still one of the major concerns for industrial applications. Extensive research has been steered into the improvement of forming accuracy on a macro scale [3, 5, 6]. However, relatively high surface roughness is considered as a significant issue in ISF, which has gained research interest in the past few years [7–10]. Of particular interest, Hagan and Jeswiet [7] performed surface roughness tests and analyzed the influence of several forming variables, such as step-down size and spindle speed, on surface roughness. They concluded that the surface finish can be viewed as a resultant of large-scale waviness created by the tool path and small-scale roughness induced by large surface strains. With step-down sizes decreasing, the morphology of surfaces transforms from waviness to strict roughness without waviness. In Ref. [8], analytical and experimental results were compared in terms of surface roughness in single point incremental forming (SPIF). Three process parameters – tool radius, step-down size, and slope angle were selected to establish the analytical model by means of considering geometrical relations. The roughness values R_a, R_z, and the mean spacing between profile peaks were evaluated as the output of the models. The prediction and experimental results showed that a good agreement can be achieved with an error below 10%. Hamilton et al. [9] investigated the influences of tool feed rates and spindle rotation at high speeds during forming on the noncontact side roughness (i.e., orange peel effect). A model for the orange peel prediction in SPIF was established, which provided some guidelines for the improvement of external surface quality by choosing desirable process parameters during forming. Powers et al. [10] investigated the surface metrology through a SPIF case analysis. The effect of sheet rolling mark direction and analysis direction on surface topology in SPIF considering two process variables (feed rate and forming direction) was first studied. The results showed that surface roughness R_z is greater with rolling marks perpendicular to forming orientation. Lasunon et al. [11] assessed the effects of three process parameters on the surface roughness in SPIF by a factorial design. The results showed that wall angle, depth increment, and its interaction play an important role on the surface roughness, while feed rate has little effect.

The previous studies have shown that focus was given to tool-sheet contact surface roughness, i.e., internal surface roughness and noncontact surface roughness, i.e., external surface roughness independently with

Received August 6, 2013; Accepted November 6, 2013

Address correspondence to Zhaobing Liu, Department of Mechanical Engineering, School of Mechanical and Mining Engineering, The University of Queensland, Brisbane, Australia; E-mail: zhaobing.liu@uqconnect.edu.au, z.liu7@uq.edu.au

Color versions of one or more of the figures in the article can be found online at www.tandfonline.com/lmmp.

respect to the influence of specific process parameters. However, in most applications, the surface quality of both internal and external surfaces of formed parts requires to be maximized with the aim of reaching a desired design level. An efficient forming process should be modeled and optimized to guarantee a steady manufacturing process with the aim of achieving the required surface roughness. Therefore, an efficient predictive modeling for surface roughness in ISF is needed to assist ISF designers to better understand and control the surface quality at the production stage. In this paper, a systematic approach to modeling and optimizing of the overall surface roughness in ISF has been developed considering the effect of four main process factors (step down, feed rate, sheet thickness, and tool diameter). The major work and contributions are briefly summarized as follows:

- The efficient surface roughness modeling is implemented using response surface methodology (RSM) with Box–Behnken design, which is widely employed to develop, improve, and optimize a production process and evaluate the corresponding importance of several process parameters considering complex interactions [12–15]. A similar research on modeling and optimization of thinning rate and forming force in SPIF can be found in Ref. [15]. However, as discussed above, little research has been focused on the evaluation of overall surface roughness.
- A multi-objective function [16], as a simple efficient approach to converting multiple responses to a single response, is used to evaluate the overall surface roughness associated with both the internal contact and the external noncontact surface roughness. Then, the overall surface roughness, as a single response, is minimized using a single-objective desirability function [13]. The predicted optimal forming conditions are determined and compared with the predicted values using a desirability function with multiple responses [14, 17].
- The impact of roll mark orientation of 7075-O aluminum sheets on surface roughness (R_a) is hypothesized and clarified when the surface roughness measurement is carried out along the step-down direction. Although this aspect has been considered in Ref. [10], the effect of only two process factors and the internal contact surface roughness was taken into account, which may limit the findings. This study has further investigated and clarified this aspect by taking more process factors and both internal and external surfaces into consideration.

Methodology

Surface Roughness Characterization in ISF

Throughout this study, surface roughness characterization is analyzed using SPIF. However, the analysis methodology can be easily applied to other types of ISF process, such as two point incremental forming. In SPIF, surface finish on the internal surface can be characterized as a resultant of large-scale waviness created by the forming path and small-scale roughness induced by large surface strains (Fig. 1(a)). As for the external surface, roughness is mainly caused by large surface strains, which usually leads to an orange peel phenomenon (Fig. 1(b)). In addition, as the step-down size decreases, the internal tool-sheet contact surface will change from a waviness look to a strict roughness look as seen in Fig. 2, which describes the evolution of internal tool-sheet contact surface look.

As discussed above, a typical internal surface in SPIF exhibits both roughness and waviness. A detailed illustration can be described in Fig. 3. It is noted that the measurement of surface irregularities due to roughness is carried out without considering the more widely spaced irregularities caused by waviness. In addition, in order to clarify the surface characterization created by SPIF, the roughness measurement on the internal and external surfaces is performed along the step-down direction perpendicular to tool-path direction.

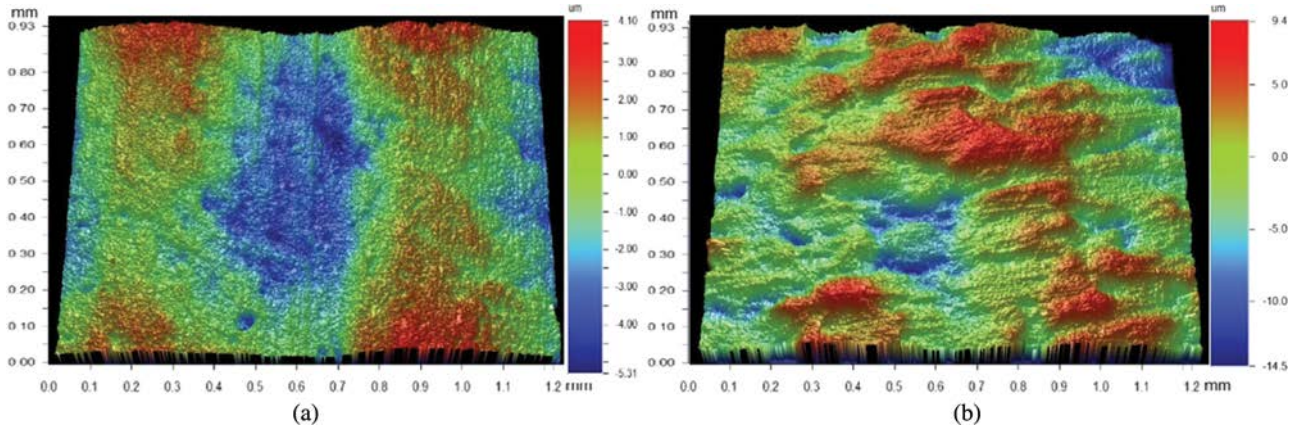

FIGURE 1.—Surface topography in SPIF: (a) internal tool-sheet contact surface; (b) external noncontact surface (shape: a 45° cone, step down: 0.5 mm, feed rate: 1000 mm/min, tool diameter: 10 mm, sheet thickness (AA7075-O): 1.02 mm).

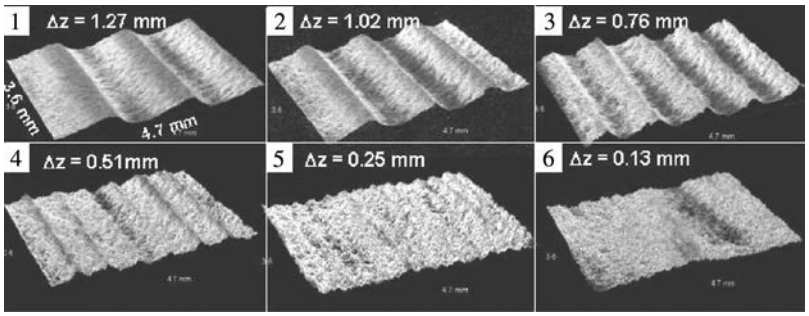

FIGURE 2.—Evolution of internal tool-sheet contact surface roughness with a tool diameter of 12.7 mm influenced by different step-down sizes [7].

Another focus of surface quality in ISF is to examine how much roll marks can influence the surface roughness. Roll marks on metal sheets are a kind of shallow marks created during the manufacture of the sheets (see the lines from top to bottom in Fig. 4). Roughness measurement direction relative to roll mark orientation is taken into account. In this research, a pyramidal shape with 55° draw angle is designed as a test benchmark, see Fig. 5. For this investigated pyramidal shape, the *z*-level tool path will travel parallel and perpendicular to the roll mark direction during forming. Figure 5 shows an example of tested pyramidal shapes, which illustrates that two squared samples with a size of 30 mm × 30 mm are taken from each side of the wall in regions A and B and used for the surface roughness measurement. The two samples in region A are measured parallel to the roll mark direction, and the other two samples in region B are measured perpendicular to the roll mark direction. Ten measurements are implemented on each sample, and then the arithmetic average is taken to represent the surface roughness values for each sample in regions A and B, respectively.

R_a is chosen as the studied quantity of surface roughness, which is the universally recognized, and most used, international parameter of roughness (ISO 4287:1997 standard). It is the arithmetic mean of the profile departures from the mean line within the measuring distance l (Fig. 6) [13].

Modeling Methodology – Response Surface Methodology with Box–Behnken Design

The surface roughness modeling employs the RSM based on design of experiments along with a statistical analysis. As an empirical modeling technique, RSM can be used to evaluate the relationship between controllable process variables and experimental results. Three main procedures are involved in the optimization process: (i) performing a statistical experimental design;

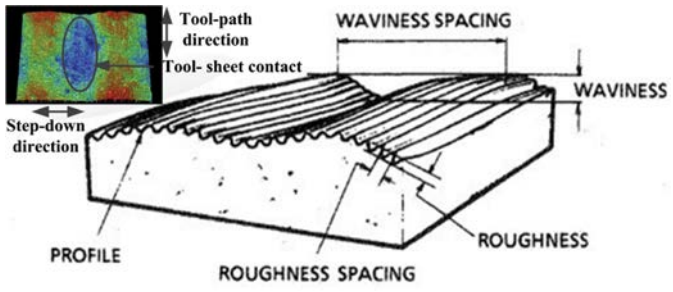

FIGURE 3.—Illustration of surface characteristics in detail.

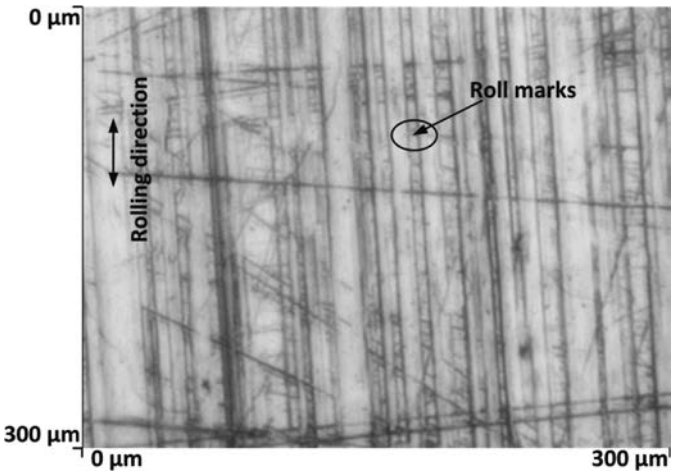

FIGURE 4.—Optical image for roll marks on AA7075-O sheets with a thickness of 1.02 mm.

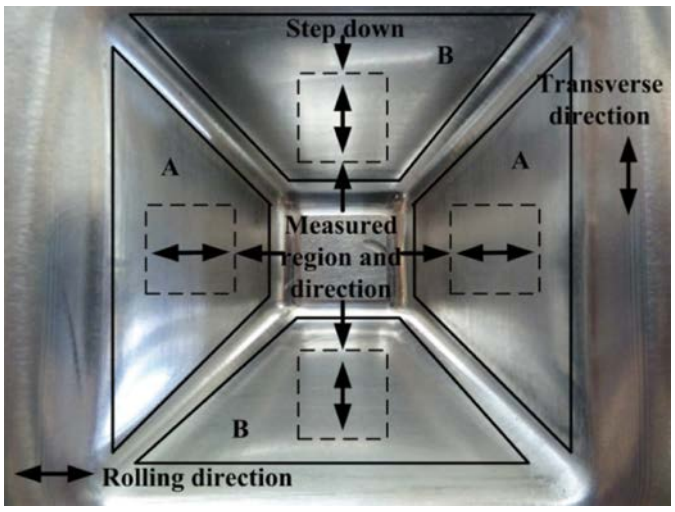

FIGURE 5.—An example of tested pyramidal shapes with 55° draw angle illustrating measured regions and directions parallel and perpendicular to roll mark direction.

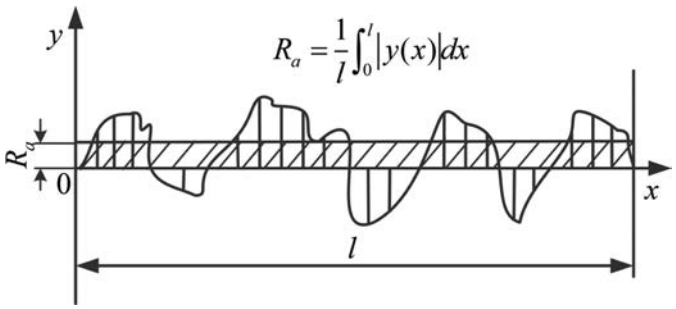

FIGURE 6.—Definition of R_a.

(ii) determining the coefficients in a mathematical model; (iii) predicting the response and checking the adequacy of the developed model [14]. Based on the developed model, surface roughness can be predicted under different process conditions over a wide range of forming process factors. In this study, a quadratic mathematical model with a four-factor, three-level design was constructed to explore quadratic response surfaces.

Twenty-seven experiments have been performed to evaluate the effects of four main independent factors on surface roughness. Using a nonlinear regression method, the quadratic mathematical model can be fit to the experimental results. The corresponding model terms can also be identified. Taking linear terms, square terms and linear by linear interaction terms into consideration, the quadratic response model can be established as

$$Y = \beta_0 + \sum_{i=1}^{4} \beta_i X_i + \sum_{i=1}^{4} \beta_{ii} X_i^2 + \sum_{i=1}^{4} \sum_{j=2,i<j}^{4} \beta_{ij} X_i X_j \qquad (1)$$

where Y is the predicted response surface function, β_0 is the model constant, β_i is the slope or linear effect of the input factor X_i, β_{ii} is the quadratic effect of input factor X_i, and β_{ij} is the linear by linear interaction effect between the input factor X_i and factor X_j. In this work, the experimental design software Minitab 16 is used for data analysis and result plotting.

Multi-Objective Function

The original RSM is only limited to single response optimization. To minimize the internal surface roughness SR_i and the external surface roughness SR_e simultaneously, a simple modification to evaluate the overall surface response for multi-objective performance has been adopted [16]. As described in Fig. 7, this approach utilizes the membership functions μ_α and μ_β as weighting factors, which can be used to calculate the corresponding objective functions.

$$\mu_\alpha = 1 - \frac{SR_i}{SR_{i,max}} \qquad (2)$$

$$\mu_\beta = 1 - \frac{SR_e}{SR_{e,max}} \qquad (3)$$

where $SR_{i,max}$ and $SR_{e,max}$ are the maximum values of internal surface roughness SR_i and external surface roughness SR_e, respectively, assumed according to experimental measurements. The simultaneous optimization of SR_i and SR_e requires the minimization of the shaded area as depicted in Fig. 7. Therefore, the multi-objective function for the overall surface roughness $SR_{overall}$ is defined as

$$SR_{overall} = \frac{1}{2} SR_i(1 - \mu_\alpha) + \frac{1}{2} SR_e(1 - \mu_\beta) \qquad (4)$$

EXPERIMENTAL WORK

Sheet Material

AA 7075 O-temper aluminum alloy sheets with thicknesses of 1.02, 1.60 and 2.54 mm are used, which have practical and wide industrial applications, such as aircraft structures due to their higher formability compared with the other temper conditions.

Experimental Equipment

Experimental investigations are performed on the AMINO® DLNC-PC incremental forming machine in

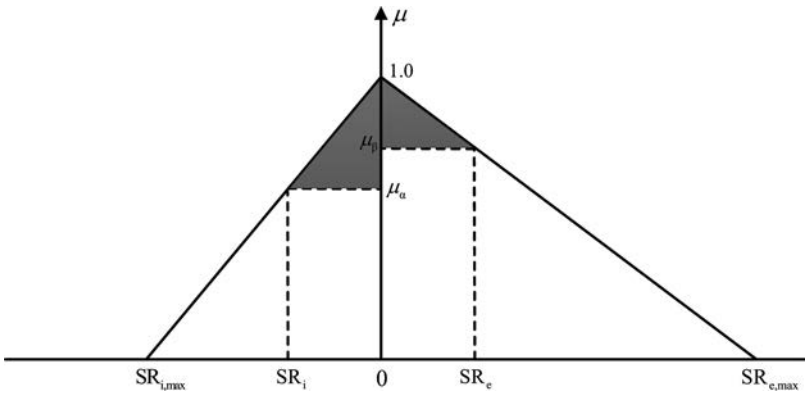

FIGURE 7.—Membership functions for internal tool-sheet contact surface roughness SR_i and external noncontact surface roughness SR_e [16].

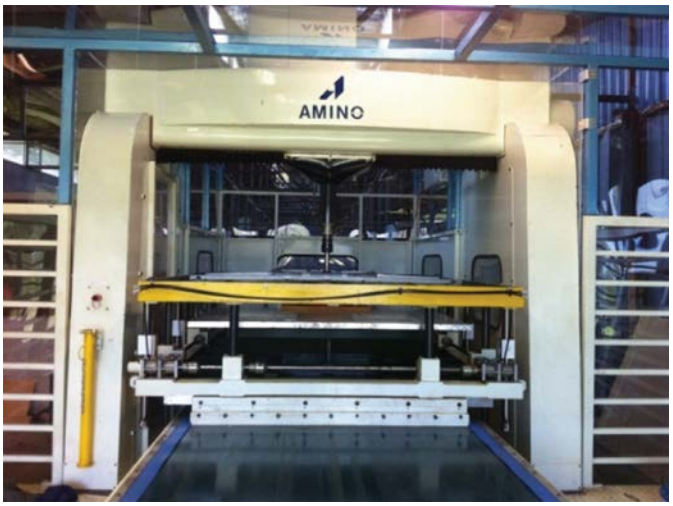

FIGURE 8.—The Amino ISF machine for experiments.

Fig. 8. The machine is a three-axis CNC machine with a maximum workspace of $2100 \times 1450 \times 500\,\text{mm}^3$ and can exert maximum forces of 3.0 kN in vertical axis and 1.5 kN in X- and Y-axis. The maximum feed rates in X- and Y-axes are 6000 mm/min and 1000 mm/min, respectively, in the Z-axis. In the experiments, the forming tools with diameters of 15, 20, and 25 mm are used. The applied forming feed rates are 4000, 5000, and 6000 mm/min. The step-down sizes of z-level tool path are set to be 0.2, 0.5 and 0.8 mm. Before forming, lubricant oil-Shell Tellus Oil 68 is sprayed on the blank.

Measuring Equipment for Surface Roughness

The surface roughness measurements are implemented using a portable, self-contained instrument (Taylor-Hobson Surtronic 3+ Profilometer [Leicester, United Kingdom] in Fig. 9). According to ISO standard, nonperiodic roughness profile evaluation has been conducted with a high-pass Gaussian filter. In this work, the sampling length, evaluation length, and calculated resolution are set to be 0.8, 4, and 0.01 μm, respectively.

FIGURE 9.—Taylor-Hobson Surtronic 3+ Profilometer.

RESULTS AND DISCUSSION

Design of Experiments

The coded four main independent factors are described in Table 1. It is worth noting that the main purpose of this study is to provide a modeling and analysis methodology for surface roughness, therefore the selection of range of parameters is based on the feasibility and efficiency of actual forming (other choices could be chosen) and is not specifically optimized. The design matrix generated for Box–Behnken design is provided in Table 2.

As discussed in Section 2, surface roughness for the final part may be influenced by roll marks, which needs to be examined and clarified by measurements. Figure 10 shows the measured results, showing the influence of roll marks on surface roughness (internal surface and external surface) in regions A and B. For the internal tool-sheet contact surface, the surface roughness measured parallel (region A) and perpendicular (region B) to the roll mark direction is nearly the same in all cases, indicating that roll marks have little influence on the internal surface roughness for all experimental combinations in terms of R_a. As for the external noncontact surface, the biggest variation of the measured data is approximately 15.2%, which demonstrates the roughness of external noncontact surface is affected by the roll marks to some extent especially for experimental combinations (no. 5–8, 13–20) with sheet thicknesses of 1.02 and 2.54 mm. Furthermore, Fig. 10 shows that the trend of surface roughness can be compared in terms of different data group with only one factor changing.

In addition, the roughness (R_a) measured perpendicular to the roll mark direction is slightly greater than that measured parallel to the roll mark direction. In Fig. 11, optical images for experimental sample 17 are provided to further examine the hypothesis and analyze the impact of roll marks on surface measurements. From Fig. 11(a) and (b), it is noted that roll marks cannot be clearly observed after forming, which means the internal surface quality is mainly influenced by forming tool paths. The influence of roll marks can be neglected on internal tool-sheet contact surfaces. This conclusion consists with the roughness measurements depicted in Fig. 10. In contrast, the external noncontact surface

TABLE 1.—Independent factors and coded levels for response surface.

		Levels		
Independent factors	Coded symbols	−1	0	1
Step down – Sd (mm)	X_1	0.2	0.5	0.8
Feed rate – Fr (mm/min)	X_2	4000	5000	6000
Sheet thickness – St (mm)	X_3	1.02	1.60	2.54
Tool diameter – Td (mm)	X_4	15	20	25

TABLE 2.—Box–Behnken design for four factors and observed responses.

No.	X_1	X_2	X_3	X_4	SR_i (μm)	SR_e (μm)	$SR_{overall}$ (μm)
1	−1(0.2)	−1(4000)	0(1.60)	0(20)	0.53	1.68	0.43
2	−1(0.2)	1(6000)	0(1.60)	0(20)	0.53	1.66	0.42
3	1(0.8)	−1(4000)	0(1.60)	0(20)	1.09	1.67	0.70
4	1(0.8)	1(6000)	0(1.60)	0(20)	1.03	1.69	0.67
5	0(0.5)	0(5000)	−1(1.02)	−1(15)	0.72	3.25	1.45
6	0(0.5)	0(5000)	−1(1.02)	1(25)	0.64	3.42	1.55
7	0(0.5)	0(5000)	1(2.54)	−1(15)	0.87	3.83	2.02
8	0(0.5)	0(5000)	1(2.54)	1(25)	0.68	3.77	1.87
9	−1(0.2)	0(5000)	0(1.60)	−1(15)	0.47	1.72	0.43
10	1(0.8)	0(5000)	0(1.60)	−1(15)	1.28	1.65	0.83
11	−1(0.2)	0(5000)	0(1.60)	1(25)	0.32	1.66	0.37
12	1(0.8)	0(5000)	0(1.60)	1(25)	0.71	1.76	0.53
13	0(0.5)	−1(4000)	−1(1.02)	0(20)	0.68	3.34	1.50
14	0(0.5)	−1(4000)	1(2.54)	0(20)	0.70	4.04	2.14
15	0(0.5)	1(6000)	−1(1.02)	0(20)	0.66	3.51	1.63
16	0(0.5)	1(6000)	1(2.54)	0(20)	0.73	3.75	1.88
17	−1(0.2)	0(5000)	−1(1.02)	0(20)	0.65	3.54	1.66
18	−1(0.2)	0(5000)	1(2.54)	0(20)	0.48	3.84	1.87
19	1(0.8)	0(5000)	−1(1.02)	0(20)	0.94	3.74	1.98
20	1(0.8)	0(5000)	1(2.54)	0(20)	1.61	3.86	2.61
21	0(0.5)	−1(4000)	0(1.60)	−1(15)	0.74	1.75	0.54
22	0(0.5)	−1(4000)	0(1.60)	1(25)	0.46	1.69	0.41
23	0(0.5)	1(6000)	0(1.60)	−1(15)	0.78	1.71	0.54
24	0(0.5)	1(6000)	0(1.60)	1(25)	0.42	1.72	0.42
25	0(0.5)	0(5000)	0(1.60)	0(20)	0.58	1.65	0.43
26	0(0.5)	0(5000)	0(1.60)	0(20)	0.57	1.69	0.45
27	0(0.5)	0(5000)	0(1.60)	0(20)	0.59	1.68	0.45

roughness is affected by roll marks to a small extent, which can be clearly distinguished in Fig. 11(c) and (d). The external surface quality in Fig. 11(c) along the roll mark orientation seems better than that in Fig. 11(d) perpendicular to the roll mark orientation. The possible reason is the external surface roughness perpendicular to the roll mark orientation is mainly induced by large surface strains during forming together with initial roll marks compared with the roughness mainly caused by large surface strains along the roll mark direction. This finding is also verified by the roughness measurements as shown in Fig. 10, especially for the experimental combinations with sheet thicknesses of 1.02 and 2.54 mm.

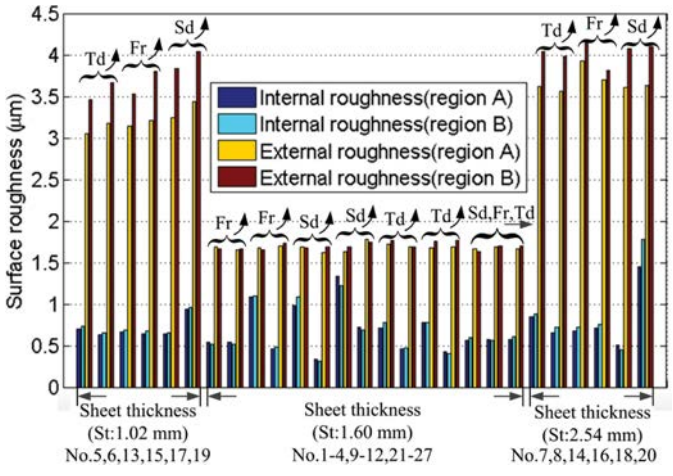

FIGURE 10.—Measured results of internal and external surface roughness. *Note*: Sd, Fr, St, and Td are defined as step down, feed rate, sheet thickness, and tool diameter, respectively.

In Table 2, the corresponding surface roughness results are also provided in the last three columns. To simplify the modeling process in terms of the observed experimental data, the average of the surface roughness values in regions A and B can be taken with the aim of representing the overall internal surface roughness and the overall external surface roughness, as seen in Table 2 (columns SR_i and SR_e). Furthermore, based on the roughness values (SR_i and SR_e), $SR_{i,max}$ and $SR_{e,max}$ in the membership functions (Eqs. (2) and (3)) can be assumed as 1.65 and 4.10 μm, respectively. The calculated overall surface roughness $SR_{overall}$ in Eq. (4) is shown in Table 2 (see the last column). Therefore, the simultaneous minimization of SR_i and SR_e involves the minimization of multi-objective function $SR_{overall}$.

Estimated RSM Model

An empirical relationship described by a quadratic mathematical model (Eq. (1)) was fitted in terms of the experimental results derived from Box–Behnken design and multi-objective function. The empirical model with the coded factors is given as follows:

$$\begin{aligned} SR_{overall} = {} & 0.4425 + 0.1787X_1 - 0.0126X_2 + 0.2181X_3 \\ & - 0.0547X_4 + 0.1539X_1^2 + 0.0036X_2^2 \\ & + 1.3629X_3^2 - 0.0369X_4^2 - 0.0052X_1X_2 \\ & + 0.1043X_1X_3 - 0.0605X_1X_4 - 0.0985X_2X_3 \\ & + 0.0004X_2X_4 - 0.0616X_3X_4 \end{aligned} \quad (5)$$

Analysis of variance (ANOVA) is adopted in order to examine the test for the importance and fitness of the established model [12–14, 17]. The results of ANOVA for the overall surface roughness are given in Table 3. Usually, *P*-values less than 0.05 indicate that the model terms have an important impact on the response. As shown in Table 3, the model *F*-value of 94.80 with a probability *P*-value of less than 0.0001 implies the model is significant. In addition, it can be seen that sheet thickness (X_3) is the most influential factor on the overall surface roughness followed by step down (X_1) by examining the *F*-value and the *P*-value. The coefficients in Eq. (5) indicate the relative influence of each factor to the response, in which the positive sign means the ability to increase the response and vice versa. The value of predicted R^2 is used to measure the prediction ability of the established model. To achieve a reasonable agreement, the values of predicted R^2 and adjusted R^2 should be within approximately 0.20. Otherwise, a problem possibly exists in the experimental data or the fitted model. In this case, the predicted R^2 is 0.9484, which reasonably

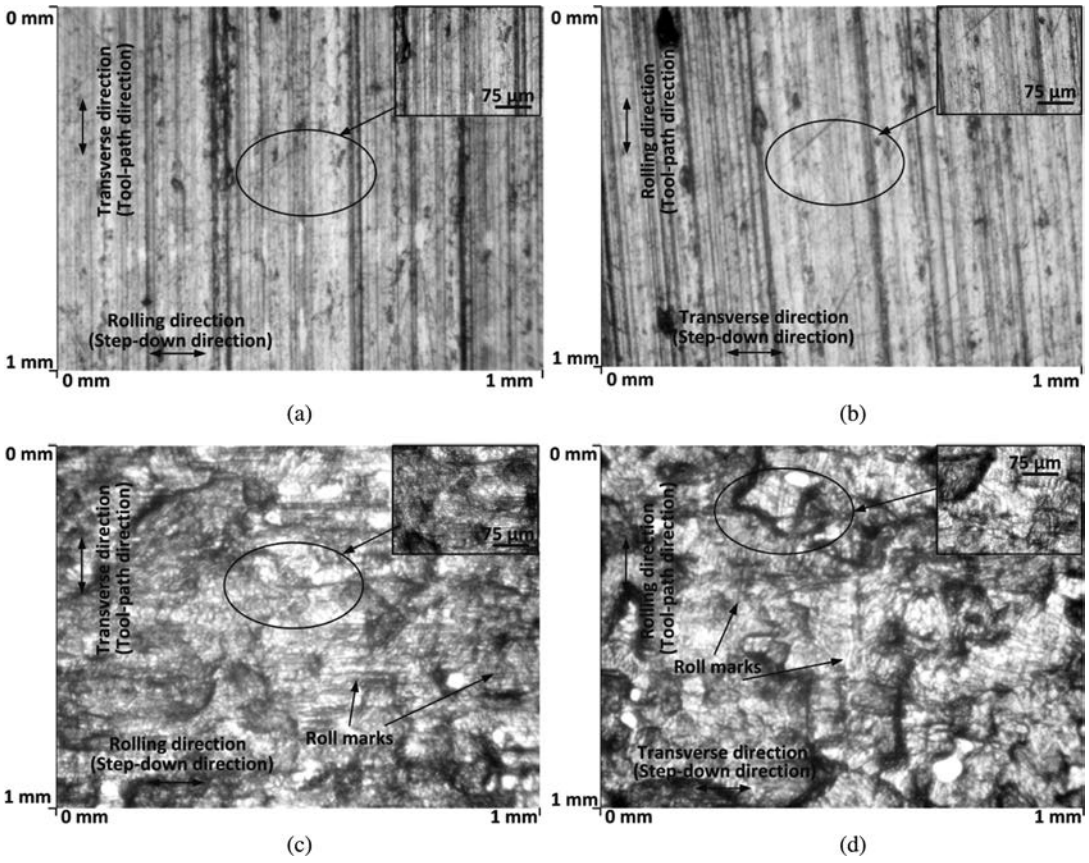

FIGURE 11.—Optical images for experimental sample 17: (a) internal roughness–region A; (b) internal roughness–region B; (c) external roughness–region A; (d) external roughness–region B.

consists with the adjusted R^2 of 0.9806. As some of the square and interaction terms presented little effect on the model (have a very high P-value), these less significant sources can be excluded from the regression analysis. Therefore, the empirical model in Eq. (5) can be simplified as

TABLE 3.—Results of ANOVA for overall surface roughness (from Minitab).

Source	SS	DF	MS	F-value	P-value
Model	13.2306	14	0.9450	94.80	0.0000
X_1 (Step down)	0.3831	1	0.3831	38.43	0.0000
X_2 (Feed rate)	0.0019	1	0.0019	0.19	0.6690
X_3 (Sheet thickness)	0.5705	1	0.5705	57.23	0.0000
X_4 (Tool diameter)	0.0359	1	0.0359	3.60	0.0820
X_1^2 (Step down^2)	0.1262	1	0.1263	12.66	0.0040
X_2^2 (Feed rate^2)	0.0001	1	0.0001	0.01	0.9350
X_3^2 (Sheet thickness^2)	9.9072	1	9.9072	993.86	0.0000
X_4^2 (Tool diameter^2)	0.0073	1	0.0073	0.73	0.4100
X_1X_2 (Step down * Feed rate)	0.0001	1	0.0001	0.01	0.9180
X_1X_3 (Step down * Sheet thickness)	0.0435	1	0.0435	4.37	0.0590
X_1X_4 (Step down * Tool diameter)	0.0146	1	0.0146	1.47	0.2490
X_2X_3 (Feed rate * Sheet thickness)	0.0388	1	0.0388	3.89	0.0720
X_2X_4 (Feed rate * Tool diameter)	0.0000	1	0.0000	0.00	0.9940
X_3X_4 (Sheet thickness * Tool diameter)	0.0152	1	0.0152	1.52	0.2410
Residual	0.1196	12	0.0100		
Lack of Fit	0.1195	10	0.0120	147.99	0.0070
Cor total	13.3502	26			

Note: SS, DF, and MS denote sum of squares, degree of freedom, and mean square, respectively.

$$SR_{overall} = 0.4425 + 0.1787X_1 - 0.0126X_2 + 0.2181X_3 - 0.0547X_4 + 0.1539X_1^2 + 1.3629X_3^2 - 0.0369X_4^2 + 0.1043X_1X_3 - 0.0605X_1X_4 - 0.0985X_2X_3 - 0.0616X_3X_4 \quad (6)$$

Analysis of Response Surface

The three-dimensional graphs are provided to illustrate the relationships between experimental factors and responses. In Fig. 12, the response surfaces are built by step down (X_1) and sheet thickness (X_3). To be more specific, Fig. 12(a) shows the changes of the overall surface roughness when feed rate (X_2) and tool diameter (X_4) are set as 4000 mm/min and 15 mm, respectively. The overall surface roughness slightly rises as step down (X_1) increases. However, as sheet thickness (X_3) becomes bigger, the overall surface roughness first decreases and then increases again. The big change shows that sheet thickness (X_3) is the most significant forming variable influencing the overall surface roughness, which is consistent with the analysis in the ANOVA table. The possible reason is the sheets with different thicknesses can lead to different surface strains during forming, which have a significant influence on surface finish. The evolution of the overall surface roughness in Fig. 12(b) and (c) represents a similar trend as that in Fig. 12(a), which illustrates that the factors of feed rate (X_2) and tool diameter (X_4) have little influence on the overall surface roughness.

The response surfaces are constructed by feed rate (X_2) and tool diameter (X_4) in Fig. 13, in which step down (X_1) is kept as a constant 0.5 mm, and the factor sheet thickness (X_3) is changed from 1.02 to 2.54 mm. It is observed that as sheet thickness (X_3) increases, a large difference can be found in terms of the overall surface roughness between Fig. 13(a), (b), and (c). In Fig. 13(a), it can be noted that the trend of the overall surface roughness goes up as feed rate (X_2) and tool diameter (X_4) increase. On the contrary, in Fig. 13(b) and (c), the values of overall surface roughness go down as feed rate (X_2) and tool diameter (X_4) increases. This further illustrates that sheet thickness (X_3) has a significant impact on the overall surface roughness. The middle level with sheet thickness ($X_3 = 1.6$ mm) appears to be the turning point of the overall surface roughness, having the least range of overall surface roughness.

Figure 14 shows the response surfaces constructed by feed rate (X_2) and tool diameter (X_4) but with constant sheet thickness (X_3) of 1.60 mm and step down (X_1) changing from 0.2 to 0.8 mm. The trend of the overall surface roughness rises and then goes downwards as tool diameter (X_4) increases. As for the situations in Fig. 14(b) and (c), a descending trend of the overall

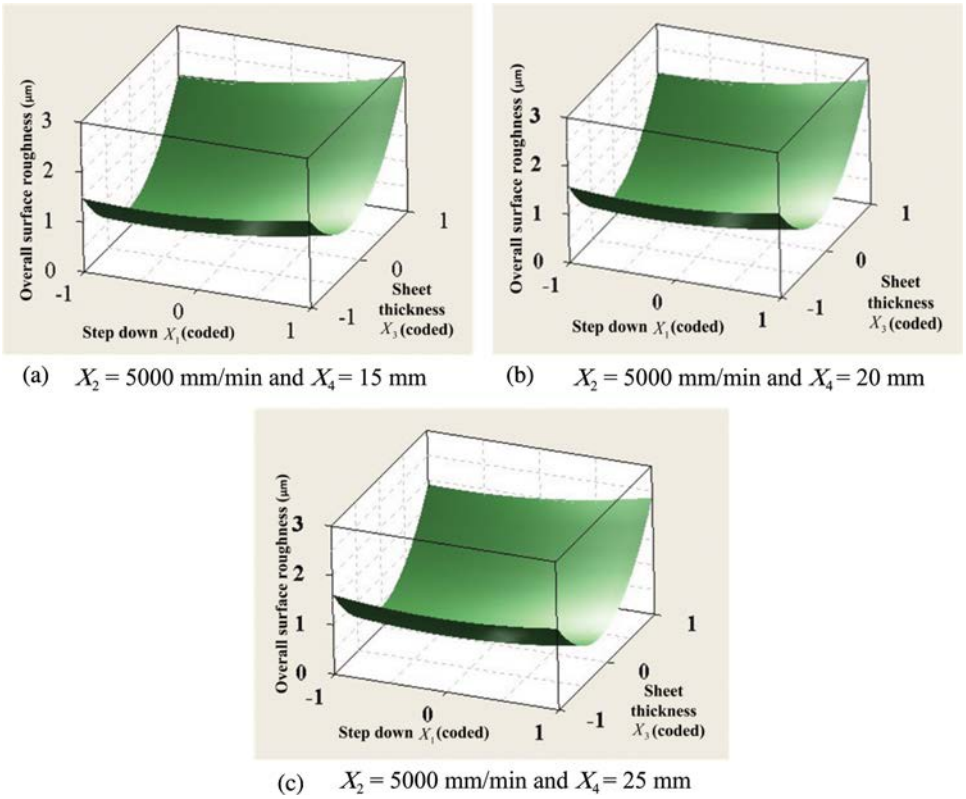

FIGURE 12.—Three-dimensional response surface showing the effect of factors step down (X_1) and sheet thickness (X_3) on the overall surface roughness with the constant feed rate (X_2) of 5000 mm/min: (a) tool diameter (X_4) = 15 mm; (b) tool diameter (X_4) = 20 mm; (c) tool diameter (X_4) = 25 mm.

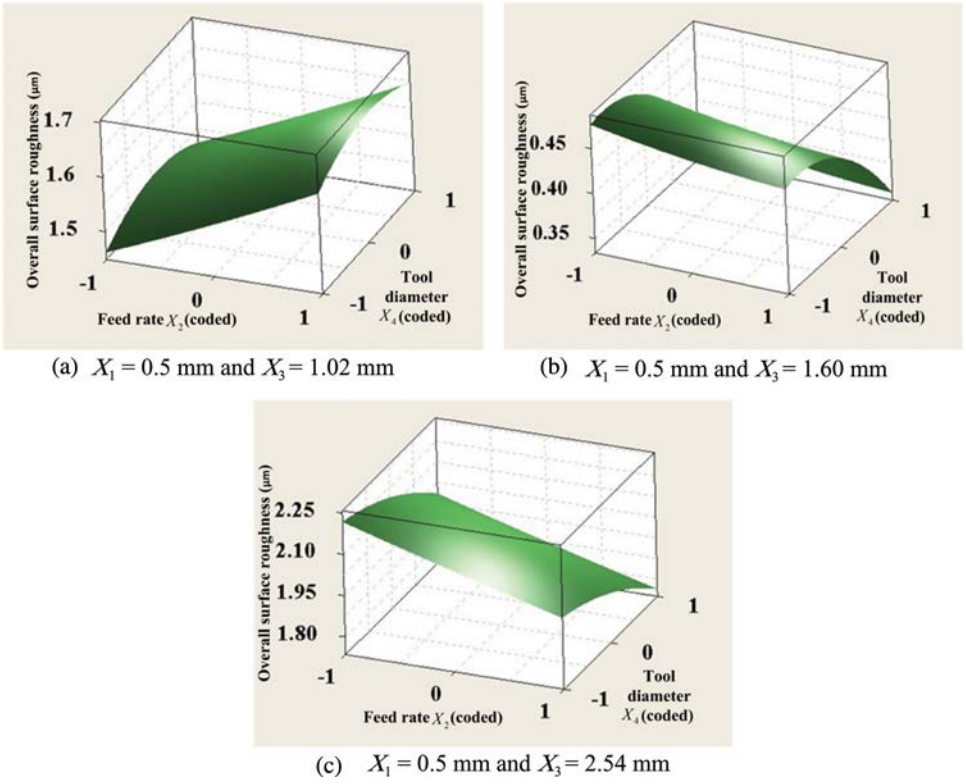

FIGURE 13.—Three-dimensional response surface showing the effect of factors feed rate (X_2) and tool diameter (X_4) on the overall surface roughness with the constant step down (X_1) of 0.5 mm: (a) sheet thickness (X_3) = 1.02 mm; (b) sheet thickness (X_3) = 1.60 mm; (c) sheet thickness (X_3) = 2.54 mm.

surface roughness can be observed. Feed rate (X_2) has little effect on the overall surface roughness in all these figures. As discussed in Ref. [4], the surface finish can be viewed as a resultant of large-scale waviness created by the tool path and small-scale roughness induced by large surface strains, which is less likely affected by feed rate (X_2). This is the possible reason why feed rate (X_2) represents little influence on the surface roughness. In addition, the magnitude of the overall surface roughness increases dramatically from Fig. 14(a) to (c), indicating that step down (X_1) is another important influential process factor on the overall surface roughness. The reason is step down (X_1) can cause waviness marks on the internal contact surface as shown in Figs. 1(a) and 2. This is also identified by the high *F*-value and low *P*-value in the ANOVA table.

Optimization

This section discusses the optimization method to minimize the overall surface roughness obtained from the multi-objective function with the aim of simultaneous minimization of both internal and external surface roughness. Two methods have been used. One is the proposed multi-objective function with single-response desirability function, which can simplify the optimization process. The other is the direct desirability function with multiple responses for a comparison purpose. The numerical optimization process in Minitab has been performed with the aim of finding the specific optimal experimental conditions. The difference between the multi-objective function method and the direct desirability function method with multiple responses is that the multi-objective function method first converts the multiple observed values to a single observed value, and then the nonlinear programming approach (single-objective desirability function) is employed to find the optimal values [13]. In contrast, the direct desirability function method includes two stages: (i) determining levels of the independent factors in order to simultaneously produce the most desirable predicted responses on the dependent factors and (ii) maximizing the overall desirability in terms of the controllable factors [14].

Figure 15(a) shows the optimization results using the multi-objective function. As can be seen, the optimal conditions are determined as step down (0.39 mm), feed rate (6000 mm/min), sheet thickness (1.60 mm), and tool diameter (25 mm), obtaining a minimum overall surface roughness 0.32 μm. Figure 15(b) shows the optimization results using the desirability function with multiple responses. The calculated minimum overall surface roughness is 0.37 μm under the optimal conditions of step down (0.33 mm), feed rate (5333 mm/min), sheet thickness (1.60 mm), and tool diameter (25 mm). The predicted error between these two methods is 12.8%, showing that the proposed multi-objective function method is reliable.

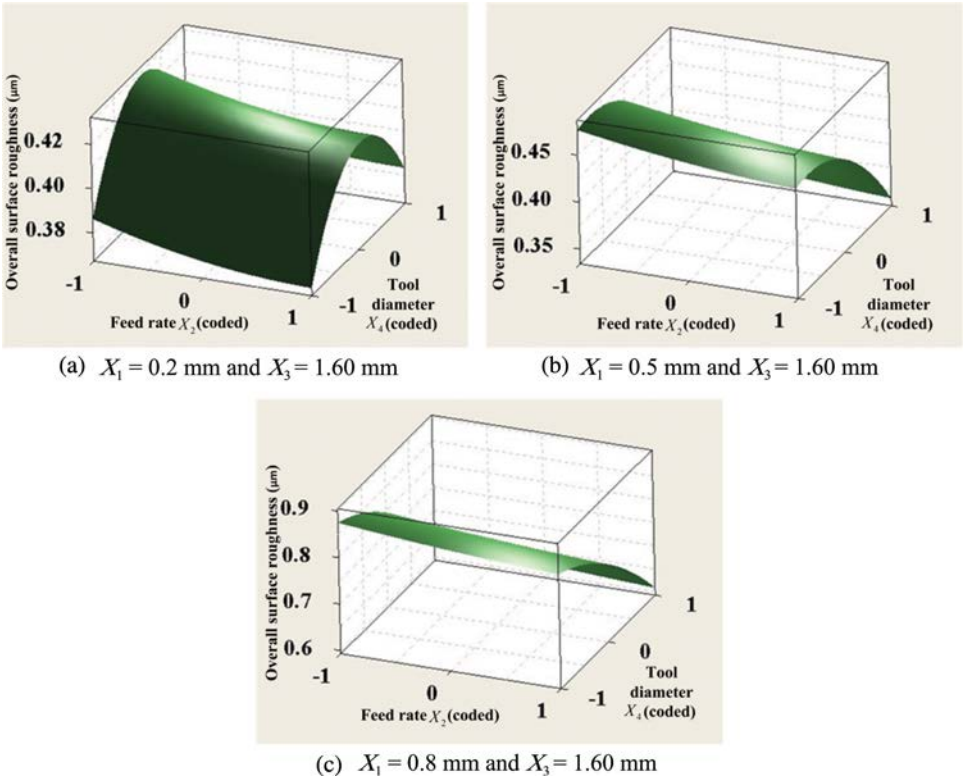

FIGURE 14.—Three-dimensional response surface showing the effect of factors feed rate (X_2) and tool diameter (X_4) on the overall surface roughness with the constant sheet thickness (X_3) of 1.60 mm: (a) step down (X_1) = 0.2 mm; (b) step down (X_1) = 0.5 mm; (c) step down (X_1) = 0.8 mm.

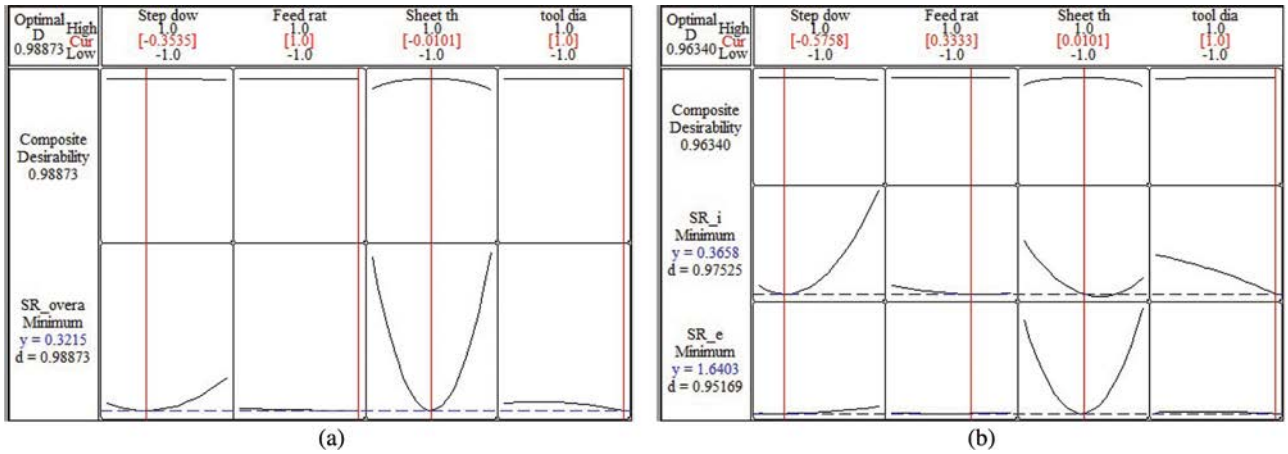

FIGURE 15.—Optimization results: (a) multi-objective function with single-objective desirability function; (b) desirability function with multiple responses.

Finally, for experimental validation, a duplicate confirmatory experiment on the ISF machine was conducted using the optimal parameters. The internal and external surface roughness was measured as 0.38 and 1.69 μm, respectively. This gives an overall surface roughness of 0.39 μm compared with 0.32 μm for the optimization analysis using the multi-objective function approach. It indicates that Box–Behnken design in conjunction with the multi-objective function can be used as a modeling methodology to optimize the overall surface roughness in SPIF.

CONCLUSION

In this study, empirical modeling and optimization of the overall surface roughness in ISF have been investigated. RSM with Box–Behnken design and multi-objective function was employed to establish the

prediction model and examine the impact of four forming variables on the overall surface roughness. The conclusions can be drawn as follows:

- As an efficient and reliable approach, the proposed multi-objective method can be used to evaluate the overall surface roughness in SPIF compared with those of simultaneous optimization of multiple responses using a desirability function.
- Sheet thickness is the most influential forming variable on the overall surface finish, followed by step down. In contrast, feed rate and tool diameter have little influence on the overall surface roughness. Furthermore, the optimal experimental conditions were determined as step down (0.39 mm), feed rate (6000 mm/min), sheet thickness (1.60 mm), and tool diameter (25 mm) with a minimum overall surface roughness 0.32 μm, which is effectively confirmed by a validation experiment.
- Roll marks have small influences on the external surface roughness with respect to R_a for AA7075-O sheets with thicknesses of 1.02 and 2.54 mm. As for the internal surface, tool paths have dominant effects on the surface quality with little influence of roll marks. Surface roughness on the external noncontact surface is always higher than that of the internal tool-sheet contact surface in the range of investigated factor values.

This research provided a systematic insight into the impact of forming variables on the surface finish in ISF. This information could be extensively applied to a further design of process control system to predict and control the surface quality of final parts manufactured by ISF.

Funding

The authors would like to thank the ARC Linkage Program, Boeing Research and Technology Australia (BRTA) and QMI Solutions in Australia for the funding and assistance in undertaking this work.

References

1. Jeswiet, J.; Micari, F.; Hirt, G.; Bramley, A.; Duflou, J.; Allwood, J. Asymmetric single point incremental forming of sheet metal. *CIRP Annals – Manufacturing Technology* **2005**, *54* (2), 88–114.
2. Liu, Z.B.; Li, Y.L.; Meehan, P.A. Vertical wall formation and material flow control for incremental sheet forming by revisiting multistage deformation path strategies. *Materials and Manufacturing Processes* **2013**, *28* (5), 562–571.
3. Radu, C.; Tampu, C.; Cristea, I.; Chirita, B. The effect of residual stresses on the accuracy of parts processed by SPIF. *Materials and Manufacturing Processes* **2013**, *28* (5), 572–576.
4. Silva, M.B.; Martinho, T.M.; Martins, P.A.F. Incremental forming of hole-flanges in polymer sheets. *Materials and Manufacturing Processes* **2013**, *28* (3), 330–335.
5. Dejardin, S.; Thibaud, S.; Gelin, J.C.; Michel, G. Experimental investigations and numerical analysis for improving knowledge of incremental sheet forming process for sheet metal parts. *Journal of Materials Processing Technology* **2010**, *210* (2), 363–369.
6. Allwood, J.M.; Braun, D.; Music, O. The effect of partially cut-out blanks on geometric accuracy in incremental sheet forming. *Journal of Materials Processing Technology* **2010**, *210* (11), 1501–1510.
7. Hagan, E.; Jeswiet, J. Analysis of surface roughness for parts formed by computer numerical controlled incremental forming. *Proceedings of the Institution of Mechanical Engineers, Part B: Journal of Engineering Manufacture* **2004**, *218* (10), 1307–1312.
8. Durante, M.; Formisano, A.; Langella, A. Comparison between analytical and experimental roughness values of components created by incremental forming. *Journal of Materials Processing Technology* **2010**, *210* (14), 1934–1941.
9. Hamilton, K.; Jeswiet, J. Single point incremental forming at high feed rates and rotational speeds: Surface and structural consequences. *CIRP Annals – Manufacturing Technology* **2010**, *59* (1), 311–314.
10. Powers, B.M.; Ham, M.; Wilkinson, M.G. Small data set analysis in surface metrology: An investigation using a single point incremental forming case study. *Scanning* **2010**, *32* (4), 199–211.
11. Lasunon, O.U. Surface roughness in incremental sheet metal forming of AA5052. *Advanced Materials Research* **2013**, *753–755*, 203–206.
12. Wang, W.; Kweon, S.H.; Yang, S.H. A study on roughness of the micro-end milled surface produced by a miniature machine tool. *Journal of Materials Processing Technology* **2005**, *162–163*, 702–708.
13. Krajnik, P.; Kopac, J.; Sluga, A. Design of grinding factors based on response surface methodology. *Journal of Materials Processing Technology* **2005**, *162–163*, 629–636.
14. Mourabet, M.; El Rhilassi, A.; El Boujaady, H.; Bennani-Ziatni, M.; El Hamri, R.; Taitai, A. Removal of fluoride from aqueous solution by adsorption on apatitic tricalcium phosphate using Box–Behnken design and desirability function. *Applied Surface Science* **2012**, *258*, 4402–4410.
15. Bahloul, R.; Arfa, H.; Belhadjsalah, H. Application of response surface analysis and generic algorithm for the optimization of single point incremental forming process. *Key Engineering Materials* **2013**, *554–557*, 1265–1272.
16. Gaitonde, V.N.; Karnik, S.R.; Achyutha, B.T.; Siddeswarappa, B. Taguchi optimization in drilling of AISI 316 L stainless steel to minimize burr size using multi-performance objective based on membership function. *Journal of Materials Processing Technology* **2008**, *202* (1–3), 374–379.
17. Li, M.; Feng, C.Q.; Zhang Z.Y.; Liu, X.; Ma, W.F.; Xue, Q.; Sugiura, N. Optimization of electrochemical ammonia removal using Box–Behnken design. *Journal of Electroanalytical Chemistry* **2011**, *657*, 66–73.

Chapter 5 Conclusions and Future Work

This chapter provides a summary of the conducted work in this thesis which mainly includes two aspects: forming force prediction and process investigation. Then the contributions to the field of research and some suggestions for future work based on the current study are outlined.

Two types of FE modes have been developed to investigate the deformation mechanism in ISF. A groove forming process has been simulated with FE models to study the strain behaviour and thickness distribution. The simulated results suggested that the level of strain decreases as the tool size increases. It was also noticed that the maximum effective strain occurs before the corner of the groove with a distance of 6 mm, suggesting that the crack initially occurs just prior to the end of the groove. In terms of thickness distribution after forming, it was found that thickness at the middle of the groove is thicker than that near the ends which further explains why the failure always occurs near the ends. According to both FE simulations and experimental results, the 30 mm tool can provide with a higher formability than 20 mm and 10 mm forming tools in the groove forming test. Moreover, FE models with fine solid elements for the cone-forming process have been established to further investigate the role of different deformation modes. These models were proven to be reliable by experimental validation with forming forces. The FE simulation confirmed that the deformation behaviour in the cone-forming process is a combination of stretching, bending and shearing. In addition, it was found that direct strain perpendicular to the tool motion is the major deformation mode in the cone-forming process. Shear strain in the forming direction (ε_{23}) prevails greatly among the three shear components with the maximum value occurring in the middle of the sheet. It was also found that the in-plane shear strain is not negligible, especially at the upper surface.

Based on the understanding of the deformation mechanism during the forming process, an efficient analytical model for tangential force prediction has been developed. Initially, two analytical sub-models have been developed to consider shear and bending with stretching deformation modes separately, but it was found neither of these two sub-models alone can reasonably predict the force with varying forming parameters in a wide range. Therefore, an empirical combination of these two modules has been constructed to balance the contribution of shear and bending on the prediction of tangential force. The combined force prediction model was validated through a comprehensive experimental campaign with two geometric shapes (truncated cone and pyramid) and various process parameters (step down, wall angle, tool radius and thickness). Finally, the analytical model was further extended to capture the changing of local curvature and wall angle during forming to

address more complex shapes. The truncated ellipsoidal cup was selected as the target shape which has local curvature and wall angle variations in each contour. The extended model is able to predict reasonably accurate tangential force variation in each contour compared to experiments.

The work in the second part of this thesis is the process investigation and improvement of forming forces, geometric accuracy, forming efficiency and surface roughness. **(i) Forming forces.** The influence of different process parameters (i.e. wall angles, sheet thicknesses, step-down sizes, tool radius, tool-path types and sheet orientation) on forming forces were investigated in detail by forming various shapes including straight groove, truncated cone, truncated pyramid and truncated ellipsoidal cup. Particular attention has been paid to the relationship between converted tangential forces and forming parameters. Tangential forces were nearly constant during the second stage of the process and the steady values demonstrate a growing trend with the increase of step-down size and wall angle. However, the steady tangential force varies in a concave manner with the variation of tool diameter from 10 to 30 mm with a minimum occurring between 20-25mm. **(ii) Geometric accuracy.** It was concluded that the accuracy is largely determined by the quadratic effect of wall angle, the linear effect of sheet thickness and the interaction effect of thickness and step down. Decreasing the step-down size was found helpful to improve the geometric accuracy. **(iii) Forming efficiency.** It was found that the step over (spiral tool path) is the most significant process parameter influencing forming time followed by the feed rate. It was concluded that the deformation energy heavily depends on the sheet thickness because of higher plastic energy required to deform the material. Increasing step-down size and decreasing the wall angle with a limited range are effective approaches to reduce the energy consumption. **(iv) Surface roughness.** Microscopic observations of the surface topography revealed that a rolling tool tip produced better surface integrity as compared with a sliding tool tip, wherein, distinct scratch patterns in the tool traverse direction were evident. Furthermore, the empirical model developed using the design of experiments (DOE) together with response surface methodology (RSM) suggested that sheet thickness has the most influential effect on overall surface roughness followed by the step-down size.

5.1 Thesis contributions

The following results from this thesis are believed to be the novel contributions to the existing literature:

- The development of both simplified FE models with shell elements and comprehensive FE models with fine solid elements for ISF. The models can simulate actual SPIF processes and

derive reliable predicted results in terms of forming forces, material strain behaviours and thickness distributions. The results show that the cone-forming process involves a combination of shearing, bending and stretching deformation modes and allow an extensive discussion of the evolution trend and the contribution of each mode.

- The development of analytical sub-models for tangential force prediction in which major deformation modes including shearing and bending with stretching are considered separately. These modes can be efficiently solved within several minutes compared with FE models which normally take several days.

- The construction of a combined model in which the weight of each sub-model is determined by values of the wall angle and step-down size to reflect the actual deformation mechanism. This is the first reported efficient force prediction model considering all the main deformation modes in ISF.

- The validation of the combined force prediction model through a comprehensive experimental campaign with two geometric shapes (truncated cone and truncated pyramid) and various process parameters (step down, wall angle, tool radius and thickness).

- The further extension of the force prediction model to capture the changing of local curvature and wall angle during forming to suit more complex shapes. This is believed to be the first attempt to predict the variation of forces for complex shapes in ISF.

- Extensive and in-depth experimental studies for the effects of process parameters on forming forces, geometric accuracy, forming efficiency and surface finish. The experimental results not only clarified some divergent arguments in literature, but also provide additional insight into the further understanding and improvement of ISF technology.

5.2 Suggested future work

Although this PhD project has made some progress in understanding and promoting the ISF technology towards its industrial application, the research also raises a number of questions and issues which remain unsolved and further studies are needed. They are summarised as follows:

- Although it is widely accepted that different types of deformation modes are involved during the ISF process, there is still uncertainty as to how different process parameters affect

the contribution of each deformation mode. Experimental strategies that allow tracking the deformation of the material would benefit the quantitative studies.

- The proposed devisable model could be further developed to predict both vertical and radial force components. Only tangential force is predicted in the proposed force prediction model.

- The extension of the force prediction model to be capable of more complex geometrical cases. The mechanism of how does the change of the local curvature affect the plastic deformation of the sheet and hence influence the forming force could be further explained.

- Forming forces for two point incremental forming could be investigated since current force study is mainly based on SPIF configuration. In what way does forming over a backing die influence the forming force and its prediction?

- Forming forces can be used for feedback control systems to prevent failure and improve the product quality. How the force trend can be characterized as an effective indicator for material failure could be further investigated.

References

1. Jeswiet, J., et al., *Asymmetric single point incremental forming of sheet metal.* Annals of CIRP—Manufacturing Technology, 2005. **54**(2): p. 623-649.
2. Echrif, S.B.M. and M. Hrairi, *Research and Progress in Incremental Sheet Forming Processes.* Materials and Manufacturing Processes, 2011. **26**(11): p. 1404-1414.
3. Leszak, E., *Apparatus and process for incremental dieless forming*, U. Pat.3342051A, Editor. 1967: USA.
4. Kitazawa, K., et al., *Metal-flow phenomena in computerized numerically controlled incremental stretch-expanding of aluminum sheets*. Vol. 46. 1996, Tokyo, JAPAN: Keikinzoku
5. Jeswiet, J., *Incremental single point forming.* Transaction of the North American Manufacturing Research INstitution of SME, 2001. **29**: p. 75-79.
6. Filice, L., L. Fratini, and F. Micari, *Analysis of Material Formability in Incremental Forming.* CIRP Annals - Manufacturing Technology, 2002. **51**(1): p. 199-202.
7. Smith, J., et al., *Deformation mechanics in single-point and accumulative double-sided incremental forming.* The International Journal of Advanced Manufacturing Technology, 2013. **69**(5-8): p. 1185-1201.
8. Amino, M., et al., *Current Status of "Dieless" Amino's Incremental Forming.* Procedia Engineering, 2014. **81**(0): p. 54-62.
9. Ceretti, E., C. Giardini, and A. Attanasio, *Experimental and simulative results in sheet incremental forming on CNC machines.* Journal of Materials Processing Tech, 2004. **152**(2): p. 176-184.
10. Duflou, J.R., et al., *Laser Assisted Incremental Forming: Formability and Accuracy Improvement.* CIRP Annals - Manufacturing Technology, 2007. **56**(1): p. 273-276.
11. Otsu, M., et al., *Friction Stir Incremental Forming of A2017 Aluminum Sheets.* Procedia Engineering, 2014. **81**(0): p. 2318-2323.
12. Fan, G., et al., *Electric hot incremental forming: A novel technique.* International Journal of Machine Tools and Manufacture, 2008. **48**(15): p. 1688-1692.
13. Xu, D., et al., *A Comparative Study on Process Potentials for Frictional Stir- and Electric Hot-assisted Incremental Sheet Forming.* Procedia Engineering, 2014. **81**(0): p. 2324-2329.
14. Ambrogio, G., et al., *Application of Incremental Forming process for high customised medical product manufacturing.* Journal of Materials Processing Technology, 2005. **162–163**(0): p. 156-162.
15. Ambrogio, G., L. Filice, and F. Micari, *A force measuring based strategy for failure prevention in incremental forming.* Journal of Materials Processing Technology, 2006. **177**(1-3): p. 413-416.
16. Filice, L., G. Ambrogio, and F. Micari, *On-Line Control of Single Point Incremental Forming Operations through Punch Force Monitoring.* CIRP Annals - Manufacturing Technology, 2006. **55**(1): p. 245-248.
17. Petek, A., K. Kuzman, and B. Suhač, *Autonomous on-line system for fracture identification at incremental sheet forming.* CIRP Annals - Manufacturing Technology, 2009. **58**(1): p. 283-286.
18. Fiorentino, A., *Force-based failure criterion in incremental sheet forming.* The International Journal of Advanced Manufacturing Technology, 2013. **68**(1-4): p. 557-563.
19. Nallagundla, V., R. Lingam, and J. Cao, *Incremental Sheet Metal Forming Processes*, in *Handbook of Manufacturing Engineering and Technology*, A.Y.C. Nee, Editor. 2014, Springer London. p. 411-452.
20. Adams, D.W., *Improvements on single point incremental forming through electrically assisted forming, contact area prediction and tool development*. 2014, ProQuest, UMI Dissertations Publishing.
21. Liu, Z., Y. Li, and P. Meehan, *Experimental investigation of mechanical properties, formability and force measurement for AA7075-O aluminum alloy sheets formed by incremental forming.* International Journal of Precision Engineering and Manufacturing, 2013. **14**(11): p. 1891-1899.

22. Vihtonen, L., A. Puzik, and T. Katajarinne, *Comparing two robot assisted incremental forming methods: incremental forming by pressing and incremental hammering.* International Journal of Material Forming, 2008. **1**(1): p. 1207-1210.
23. Malhotra, R., et al., *Improvement of Geometric Accuracy in Incremental Forming by Using a Squeezing Toolpath Strategy With Two Forming Tools.* Journal of Manufacturing Science and Engineering, 2011. **133**(6): p. 61019.
24. Kim, T.J. and D.Y. Yang, *Improvement of formability for the incremental sheet metal forming process.* International Journal of Mechanical Sciences, 2000. **42**(7): p. 1271-1286.
25. Jeswiet, J. and D. Young, *Forming limit diagrams for single-point incremental forming of aluminium sheet.* Proceedings of the Institution of Mechanical Engineers, Part B: Journal of Engineering Manufacture, 2005. **219**(4): p. 359-364.
26. Silva, M.B., et al., *Revisiting the fundamentals of single point incremental forming by means of membrane analysis.* International Journal of Machine Tools and Manufacture, 2008. **48**(1): p. 73-83.
27. Martins, P.A.F., et al., *Theory of single point incremental forming.* CIRP Annals - Manufacturing Technology, 2008. **57**(1): p. 247-252.
28. Jackson, K. and J. Allwood, *The mechanics of incremental sheet forming.* Journal of Materials Processing Tech, 2009. **209**(3): p. 1158-1174.
29. Silva, M.B., et al., *Failure mechanisms in single-point incremental forming of metals.* The International Journal of Advanced Manufacturing Technology, 2011. **56**(9): p. 893-903.
30. Silva, M.B., et al., *Single-point incremental forming and formability-failure diagrams.* Journal of Strain Analysis for Engineering Design, 2008. **43**(1): p. 15-35.
31. Allwood, J., D. Shouler, and A.E. Tekkaya, *The increased forming limits of incremental sheet forming processes.* Key Engineering Materials, 2007. **344**: p. 621-628.
32. Mirnia, M.J. and B.M. Dariani, *Analysis of incremental sheet metal forming using the upper-bound approach.* Proceedings of the Institution of Mechanical Engineers, Part B: Journal of Engineering Manufacture, 2012.
33. Malhotra, R., et al., *Mechanics of fracture in single point incremental forming.* Journal of Materials Processing Technology, 2012. **212**(7): p. 1573-1590.
34. Xue, L., *Damage accumulation and fracture initiation in uncracked ductile solids subject to triaxial loading.* International Journal of Solids and Structures, 2007. **44**(16): p. 5163-5181.
35. Lu, B., et al., *Mechanism investigation of friction-related effects in single point incremental forming using a developed oblique roller-ball tool.* International Journal of Machine Tools and Manufacture, 2014. **85**(0): p. 14-29.
36. Xu, D., et al., *Mechanism investigation for the influence of tool rotation and laser surface texturing (LST) on formability in single point incremental forming.* International Journal of Machine Tools and Manufacture, 2013. **73**(0): p. 37-46.
37. Eyckens, P., et al., *Strain evolution in the single point incremental forming process: digital image correlation measurement and finite element prediction.* International Journal of Material Forming, 2011. **4**(1): p. 55-71.
38. Smith, J., et al., *Deformation mechanics in single-point and accumulative double-sided incremental forming.* The International Journal of Advanced Manufacturing Technology, 2013: p. 1-17.
39. Emmens, W.C. and A.H. Boogaard, *Tensile tests with bending: a mechanism for incremental forming.* International Journal of Material Forming, 2008. **1**(1): p. 1155-1158.
40. Emmens, W.C. and A.H. van den Boogaard, *An overview of stabilizing deformation mechanisms in incremental sheet forming.* Journal of Materials Processing Technology, 2009. **209**(8): p. 3688-3695.
41. Fang, Y., et al., *Analytical and experimental investigations on deformation mechanism and fracture behavior in single point incremental forming.* Journal of Materials Processing Technology, 2014. **214**(8): p. 1503-1515.
42. Iseki, H., Kato, K., Sakamoto, S.,, *Forming limit of flexible and incremental sheet metal bulging with a spherical roller.* Proceedings of 4th ICTP, Beijing, China, 1993: p. 1635-1640.
43. Shim, M.-S. and J.-J. Park, *The formability of aluminum sheet in incremental forming.* Journal of Materials Processing Tech, 2001. **113**(1): p. 654-658.

44. Kim, Y.H. and J.J. Park, *Effect of process parameters on formability in incremental forming of sheet metal.* Journal of Materials Processing Technology, 2002. **130–131**(0): p. 42-46.
45. Park, J.-J. and Y.-H. Kim, *Fundamental studies on the incremental sheet metal forming technique.* Journal of Materials Processing Technology, 2003. **140**(1–3): p. 447-453.
46. Allwood, J.M. and D.R. Shouler, *Generalised forming limit diagrams showing increased forming limits with non-planar stress states.* International Journal of Plasticity, 2009. **25**(7): p. 1207-1230.
47. Ham, M. and J. Jeswiet, *Single Point Incremental Forming and the Forming Criteria for AA3003.* CIRP Annals - Manufacturing Technology, 2006. **55**(1): p. 241-244.
48. Minutolo, F.C., et al., *Evaluation of the maximum slope angle of simple geometries carried out by incremental forming process.* Journal of Materials Processing Technology, 2007. **194**(1–3): p. 145-150.
49. Bhattacharya, A., et al., *Formability and Surface Finish Studies in Single Point Incremental Forming.* Journal of Manufacturing Science and Engineering, 2011. **133**(6): p. 61020.
50. Fratini, L., et al., *Influence of mechanical properties of the sheet material on formability in single point incremental forming.* CIRP Annals - Manufacturing Technology, 2004. **53**(1): p. 207-210.
51. Hussain, G., et al., *A new formability indicator in single point incremental forming.* Journal of Materials Processing Technology, 2009. **209**(9): p. 4237-4242.
52. Li, Y., et al., *Experimental Study and Efficient Prediction on Forming Forces in Incremental Sheet Forming.* Advanced Materials Research, 2014. **939**: p. 313-321.
53. Fiorentino, A., et al., *Analysis of forces, accuracy and formability in positive die sheet incremental forming.* International Journal of Material Forming, 2009. **2**(1): p. 805-808.
54. Fiorentino, A., et al., *On forces, formability and geometrical error in metal incremental sheet forming.* INTERNATIONAL JOURNAL OF MATERIALS & PRODUCT TECHNOLOGY, 2011. **40**(3-4): p. 277-295.
55. Ambrogio, G., L. Filice, and F. Gagliardi, *Formability of lightweight alloys by hot incremental sheet forming.* Materials & Design, 2012. **34**(0): p. 501-508.
56. Jeswiet, J., et al., *Asymmetric Single Point Incremental Forming of Sheet Metal.* CIRP Annals - Manufacturing Technology, 2005. **54**(2): p. 88-114.
57. Petek, A., K. Kuzman, and J. Kopač, *Deformations and forces analysis of single point incremental sheet metal forming.* Archives of Materials Science and Engineering, 2009. **35**(2): p. 107-116.
58. Avitzur, B. and C.T. Yang, *Analysis of Power Spinning of Cones.* Journal of Engineering for Industry, 1960. **82**(3): p. 231.
59. Bambach, M., *A geometrical model of the kinematics of incremental sheet forming for the prediction of membrane strains and sheet thickness.* Journal of Materials Processing Tech, 2010. **210**(12): p. 1562-1573.
60. Iseki, H., *An approximate deformation analysis and FEM analysis for the incremental bulging of sheet metal using a spherical roller.* Journal of Materials Processing Technology, 2001. **111**(1): p. 150-154.
61. Young, D. and J. Jeswiet, *Wall thickness variations in single-point incremental forming.* Proceedings of the Institution of Mechanical Engineers, Part B: Journal of Engineering Manufacture, 2004. **218**(11): p. 1453-1459.
62. Chung, K. and O. Richmond, *Ideal forming-II. Sheet forming with optimum deformation.* International Journal of Mechanical Sciences, 1992. **34**(8): p. 617-633.
63. Ding, S., W.J.T. Daniel, and P.A. Meehan. *A new relaxation method for roll forming problems*. 2006. Springer.
64. Halmos, G.T., *Roll forming handbook*. Vol. 67. 2006, Boca Raton: CRC/Taylor & Francis.
65. Chung, K. and S. Alexandrov, *Ideal flow in plasticity.* APPLIED MECHANICS REVIEWS, 2007. **60**(1-6): p. 316-335.
66. Raithatha, A., et al. *Second order cone programming in modeling incremental deformation*. 2007. IEEE.
67. Raithatha, A. and S. Duncan, *Rigid plastic model of incremental sheet deformation using second‐order cone programming.* International journal for numerical methods in engineering, 2009. **78**(8): p. 955-979.

68. Henrard, C., et al., *Forming forces in single point incremental forming: prediction by finite element simulations, validation and sensitivity.* Computational Mechanics, 2011. **47**(5): p. 573-590.
69. Henrard, C., *Numerical Simulations of the Single Point Incremental Forming Process*. 2009.
70. Flores, P., et al., *Model identification and FE simulations: Effect of different yield loci and hardening laws in sheet forming.* International Journal of Plasticity, 2007. **23**(3): p. 420-449.
71. He., S., et al. *Effect of FEM choices in the modelling of incremental forming of aluminium sheets*. in *8th ESAFORM Conference on Material Forming*. 2005.
72. Eyckens, P., *Formability in incremental sheet forming: generalization of the Marciniak-Kuczynski model*. 2010, Katholieke Universiteit Leuven.
73. Lasunon, O. and W.A. Knight, *Comparative investigation of single-point and double-point incremental sheet metal forming processes.* Proceedings of the Institution of Mechanical Engineers, Part B: Journal of Engineering Manufacture, 2007. **221**(12): p. 1725-1732.
74. Yamashita, M., M. Gotoh, and S.-Y. Atsumi, *Numerical simulation of incremental forming of sheet metal.* Journal of Materials Processing Technology, 2008. **199**(1–3): p. 163-172.
75. Ma, L.W. and J.H. Mo, *Three-dimensional finite element method simulation of sheet metal single-point incremental forming and the deformation pattern analysis.* PROCEEDINGS OF THE INSTITUTION OF MECHANICAL ENGINEERS PART B-JOURNAL OF ENGINEERING MANUFACTURE, 2008. **222**(3): p. 373-380.
76. Dejardin, S., et al., *Experimental investigations and numerical analysis for improving knowledge of incremental sheet forming process for sheet metal parts.* Journal of Materials Processing Technology, 2010. **210**(2): p. 363-369.
77. Ambrogio., G., et al. *Process Mechanics Analysis in Single Point Incremental Forming*. in *Proceedings of the 8th International Conference on Numerical Methods in Industrial Forming Processes*. 2004. Columbus, Ohio (USA).
78. Kim, T.-J. and D.-Y. Yang, *FE-analysis of sheet metal forming processes using continuous contact treatment.* International Journal of Plasticity, 2007. **23**(3): p. 544-560.
79. Henrard, C., et al. *Development of a contact model adapted to incremental forming*. 2005. The publishing House of the Romanian Academy.
80. Robert, C., et al., *On some computational aspects for incremental sheet metal forming simulations.* International Journal of Material Forming, 2008. **1**(1): p. 1195-1198.
81. Robert, C., et al., *Comparison between incremental deformation theory and flow rule to simulate sheet-metal forming processes.* Journal of Materials Processing Tech, 2012. **212**(5): p. 1123-1131.
82. Johnson, K.L., *Contact mechanics*. 1987: Cambridge Univ Pr.
83. Nagatani, H. and A. Imou, *Contact Pressure and Shear Stress Analysis on Conforming Contact Problem.* JOURNAL OF ADVANCED MECHANICAL DESIGN SYSTEMS AND MANUFACTURING, 2008. **2**(6): p. 1055-1066.
84. Hamilton, K.A.S., *Friction and external surface roughness in single point incremental forming: A study of surface friction, contact area and the 'orange peel' effect*. 2010.
85. Eyckens, P., et al., *The significance of friction in the single point incremental forming process.* International Journal of Material Forming, 2010. **3**(S1): p. 947-950.
86. Eyckens, P., et al., *Small-scale Finite Element Modelling of the Plastic Deformation Zone in the Incremental Forming Process.* International Journal of Material Forming, 2008. **1**(1): p. 1159-1162.
87. Aerens, R., et al., *Force prediction for single point incremental forming deduced from experimental and FEM observations.* The International Journal of Advanced Manufacturing Technology, 2010. **46**(9): p. 969-982.
88. Minutolo, F.C., et al. *Forces analysis in sheet incremental forming and comparison of experimental and simulation results*. in *Intelligent production machines and systems-2nd IPROMS virtual internationl conference*. 2006.
89. Szekeres, A.J., *Three axis force measurement for computer numerical control single point incremental forming*. 2004, Queen's University at Kingston (Canada): Canada. p. 91 p.
90. Nyahumwa, C. and J. Jeswiet, *A Friction Sensor for Sheet-Metal Rolling.* CIRP Annals - Manufacturing Technology, 1991. **40**(1): p. 231-233.
91. Szekeres., A., M. Ham., and J. Jeswiet., *Force Measurement in Pyramid Shaped Parts with a Spindle Mounted Force Sensor.* Key Engineering Materials, 2007. **344**: p. 551-558.

92. J. Jeswiet, J.R.D., Alexander Szekeres, *Forces in Single Point and Two Point Incremental Forming.* Advanced Materials Research, 2005. **6-8**: p. 449-456.
93. Duflou, J.R., *Force Measurements for Single Point Incremental Forming: An Experimental Study.* Advanced Materials Research, 2005. **6-8**: p. 441-448.
94. Duflou, J., et al., *Experimental study on force measurements for single point incremental forming.* Journal of Materials Processing Tech, 2007. **189**(1): p. 65-72.
95. Bouffioux, C., et al., *Identification of material parameters to predict Single Point Incremental Forming forces.* International Journal of Material Forming, 2008. **1**(1): p. 1147-1150.
96. Cerro, I., et al., *Theoretical and experimental analysis of the dieless incremental sheet forming process.* Journal of Materials Processing Technology, 2006. **177**(1–3): p. 404-408.
97. Allwood, J.M., G.P.F. King, and J. Duflou, *A structured search for applications of the incremental sheet-forming process by product segmentation.* Proceedings of the Institution of Mechanical Engineers, Part B: Journal of Engineering Manufacture, 2005. **219**(2): p. 239-244.
98. Allwood, J.M., D. Braun, and O. Music, *The effect of partially cut-out blanks on geometric accuracy in incremental sheet forming.* Journal of Materials Processing Tech, 2010. **210**(11): p. 1501-1510.
99. Micari, F., G. Ambrogio, and L. Filice, *Shape and dimensional accuracy in Single Point Incremental Forming: State of the art and future trends.* Journal of Materials Processing Technology, 2007. **191**(1–3): p. 390-395.
100. Essa, K. and P. Hartley, *An assessment of various process strategies for improving precision in single point incremental forming.* International Journal of Material Forming, 2011. **4**(4): p. 401-412.
101. Guzmán, C.F., et al., *Study of the geometrical inaccuracy on a SPIF two-slope pyramid by finite element simulations.* International Journal of Solids and Structures, 2012. **49**(25): p. 3594-3604.
102. Ambrogio, G., et al., *An analytical model for improving precision in single point incremental forming.* Journal of Materials Processing Technology, 2007. **191**(1–3): p. 92-95.
103. Ham, M.E.J., *Single point incremental forming of aluminum sheet metal: The development of maximum forming angle forming limits, measured strains, surface roughness and dimensional accuracy*. 2007, Queen's University (Canada): Ann Arbor. p. 228.
104. Matsubara, S., *{Incremental Backward Bulge Forming of a Sheet Metal with a Hemispherical Head Tool}.* Journal of the J.S.T.P., 1994. **35**(406): p. 1311-1316.
105. Meier H, S.V., Dewald O, Zhang J. *Two Point Incremental Forming with Two Moving Forming Tools*. in *SheMet '07 Proceedings of the 12th International Conference on Sheet Metal*. 2007. Palermo, Sicily, Italy.
106. Meier, H., C. Magnus, and V. Smukala, *Impact of superimposed pressure on dieless incremental sheet metal forming with two moving tools.* CIRP Annals - Manufacturing Technology, 2011. **60**(1): p. 327-330.
107. Hirt, G., et al., *Forming strategies and Process Modelling for CNC Incremental Sheet Forming.* CIRP Annals - Manufacturing Technology, 2004. **53**(1): p. 203-206.
108. Attanasio, A., et al., *Asymmetric two points incremental forming: Improving surface quality and geometric accuracy by tool path optimization.* Journal of Materials Processing Technology, 2008. **197**(1–3): p. 59-67.
109. Malhotra, R., N.V. Reddy, and J. Cao, *Automatic 3D Spiral Toolpath Generation for Single Point Incremental Forming.* Journal of Manufacturing Science and Engineering, 2010. **132**(6): p. 061003-061003.
110. Ambrogio, G., F. Gagliardi, and L. Filice, *Robust Design of Incremental Sheet forming by Taguchi's Method.* Procedia CIRP, 2013. **12**(0): p. 270-275.
111. Wang, H. and S. Duncan. *Optimization of tool trajectory for Incremental Sheet Forming using closed loop control*. in *Automation Science and Engineering (CASE), 2011 IEEE Conference on*. 2011.
112. Bambach, M., B. Taleb Araghi, and G. Hirt, *Strategies to improve the geometric accuracy in asymmetric single point incremental forming.* Production Engineering, 2009. **3**(2): p. 145-156.

113. Sarraji, W.K.H., J. Hussain, and W.-X. Ren, *Experimental Investigations on Forming Time in Negative Incremental Sheet Metal Forming Process.* Materials and Manufacturing Processes, 2011. **27**(5): p. 499-506.
114. Ambrogio, G., L. Filice, and F. Gagliardi, *Improving industrial suitability of incremental sheet forming process.* The International Journal of Advanced Manufacturing Technology, 2012. **58**(9-12): p. 941-947.
115. Duflou, J.R., et al., *Towards energy and resource efficient manufacturing: A processes and systems approach.* CIRP Annals - Manufacturing Technology, 2012. **61**(2): p. 587-609.
116. Dittrich, M.A., et al., *Exergy analysis of incremental sheet forming.* Production Engineering, 2012. **6**(2): p. 169-177.
117. Branker, K., D. Adams, and J. Jeswiet, *Initial analysis of cost, energy and carbon dioxide emissions in single point incremental forming - producing an aluminium hat.* International Journal of Sustainable Engineering, 2012. **5**(3): p. 188.
118. Branker, K., et al., *Investigation of Energy, Carbon Dioxide Emissions and Costs in Single Point Incremental Forming*, in *Re-engineering Manufacturing for Sustainability*, A.Y.C. Nee, B. Song, and S.-K. Ong, Editors. 2013, Springer Singapore. p. 291-295.
119. Ingarao, G., et al., *A sustainability point of view on sheet metal forming operations: material wasting and energy consumption in incremental forming and stamping processes.* Journal of Cleaner Production, 2012. **29–30**(0): p. 255-268.
120. Ingarao, G., et al., *A comprehensive analysis of electric energy consumption of single point incremental forming processes.* Journal of Cleaner Production, 2014. **67**(0): p. 173-186.
121. Ambrogio, G., et al., *Analysis of Energy Efficiency of Different Setups Able to Perform Single Point Incremental Forming (SPIF) Processes.* Procedia CIRP, 2014. **15**(0): p. 111-116.
122. Bagudanch, I., et al., *The Effect of Process Parameters on the Energy Consumption in Single Point Incremental Forming.* Procedia Engineering, 2013. **63**(0): p. 346-353.
123. Hagan, E. and J. Jeswiet, *Analysis of surface roughness for parts formed by computer numerical controlled incremental forming.* PROCEEDINGS OF THE INSTITUTION OF MECHANICAL ENGINEERS PART B-JOURNAL OF ENGINEERING MANUFACTURE, 2004. **218**(10): p. 1307-1312.
124. Powers, B.M., M. Ham, and M.G. Wilkinson, *Small data set analysis in surface metrology: an investigation using a single point incremental forming case study.* Scanning, 2010. **32**(4): p. 199-211.
125. On Uma Lasunon, *Surface Roughness in Incremental Sheet Metal Forming of AA5052.* Advanced Materials Research, 2013. **753-755**: p. 203-206.
126. Durante, M., A. Formisano, and A. Langella, *Comparison between analytical and experimental roughness values of components created by incremental forming.* Journal of Materials Processing Technology, 2010. **210**(14): p. 1934-1941.
127. Hosford, W. and R. Caddell, *Metal Forming: Mechanics and Metallurgy*. 2007, Cambridge: Cambridge University Press.
128. Mirnia, M.J. and B.M. Dariani, *Analysis of incremental sheet metal forming using the upper-bound approach.* Proceedings of the Institution of Mechanical Engineers, Part B: Journal of Engineering Manufacture, 2012. **226**(8): p. 1309-1320.
129. Johnson, W. and P.B. Mellor, *Engineering plasticity*. 1983, Chichester, West Sussex, England: E. Horwood ; New York.
130. Li, Y., et al., *Efficient force prediction for incremental sheet forming and experimental validation.* The International Journal of Advanced Manufacturing Technology, 2014. **73**(1-4): p. 571-587.
131. Stephanie Fraley, M.O., Ben Terrien, John Zalewski. *Design of experiments via taguchi methods: orthogonal arrays*. 2006 [cited 2006; Available from: https://controls.engin.umich.edu/wiki/index.php/Design_of_experiments_via_taguchi_methods:_orthogonal_arrays.
132. Natarajan, U., P. Periyanan, and S. Yang, *Multiple-response optimization for micro-endmilling process using response surface methodology.* The International Journal of Advanced Manufacturing Technology, 2011. **56**(1-4): p. 177-185.